This Proceedings is dedicated
to the International Polar Year

Proceedings of the

16th NORTHERN RESEARCH BASINS INTERNATIONAL SYMPOSIUM AND WORKSHOP

27 August – 2 September, 2007
PETROZAVODSK, RUSSIA

EDITORS:

Nikolay Filatov

Yuri Salo

Tatjana Regerand

16th NRB
16th INTERNATIONAL NORTHERN RESEARCH BASINS
SYMPOSIUM AND WORKSHOP
PETROZAVODSK, RUSSIA, 27 AUG. - 2 SEPT. 2007

PETROZAVODSK
2007

ISBN 978-5-9274-0280-9

CONTENTS

PREFACE

Dear colleagues,

On behalf of the organizing committee we would like to express our pleasure to meet participants of 16th NRB Symposium, which takes place on 27 August – 2 September, 2007 in Petrozavodsk, capital of Republic of Karelia, Russia. The NRB Symposium was initiated in 1975 and eventually became a periodic event. The participants of NRB event have now an opportunity to visit Russia for the second time. First time it was a short visit to Murmansk during the 13th NRB Symposium in Saariselkaa, Finland (2001).

Karelia is extremely rich of rivers (more than 27000) and lakes (about 60000), including the Greatest European Lakes Ladoga and Onega. A part of its territory belongs to the watershed of the White [Beloe] Sea linked to the Arctic Ocean. It is a region that marches with the European Union, a total length of the border is about 1000 km.

The main theme of 16th Symposium is "Long-term and time-space changes in the northern hydrological systems: Features, consequences, prediction" accentuating problems of hydrology of polar regions in Northern America, Northern Europe (including Greenland, Finland, Sweden, Russia), and in northern Japan. Emphasis will be put on the effect of variations and variability of the regional climate on Arctic environments including taiga, tundra and boreal forest ecosystems. Some studies are devoted to the hydrological cycle of the high latitudes, which is dominated by snow and ice, including permafrost. The proceedings contain 20 full papers, which cover topics ranging from the broad aspects of Arctic hydrology. During the hydrological excursions, participants will acquaint themselves with wonderful nature of Karelia, including the wooden architecture museum on the Kizhi Archipelago, and will see the beauty of Lake Onego.

To my mind, the main idea of the workshop is to present the state of the art and get criticisms, to discuss results achieved and to formulate further steps in research, that is the most fruitful approach to get a better knowledge and understanding of problems in study. I do hope that the 16th NRB Symposium will be as productive as all previous, and you will find time to learn more about beautiful Karelia.

Nikolai Filatov – Head of organizing committee.

LIST OF PARTICIPANTS

CANADA

Abnizova, Anna	**York University** **Toronto, Ontario** anna_abnizova@yahoo.ca
Derksen, Chris	**Environment Canada,** **Toronto, Ontario** Chris.Derksen@ec.gc.ca
Duguay, Claude	**University of Waterloo** **Waterloo, Ontario** crduguay@fes.uwaterloo.ca
Janowicz, J. Richard	**Water Resources** **Yukon Department** **of Environment** **Whitehorse, Yukon** richard.janowicz@gov.yk.ca
Lafreniere, Melissa	**Queen's University** **Kingston, Ontario** Melissa.lafreniere@queensu.ca
Spence, Christopher	**Environment Canada** **11 Innovation Blvd.** **Saskatoon** chris.spence@ec.gc.ca
Woo, Ming-ko	**School of Geography** **and Earth Sciences,** **McMaster University,** **Hamilton, Ontario** woo@univmail.cis.mcmaster.ca
Young, Kathy L.	**York University** **Toronto, Ontario** klyoung@yorku.ca

DENMARK

Hasholt, Bent	**Institute of Geography** **University of Copenhagen** bh@geogr.ku.dk

FINLAND

Korhonen, Johanna	**Finnish Environment Institute** **Helsinki** Johanna.korhonen@ymparisto.fi
Lepparanta, Matti	**University of Helsinki** matti.lepparanta@helsinki.fi

JAPAN

Shirasawa, Kunio
Pan-Okhotsk Research Center
Institute of Low Temperature Science
Hokkaido University
kunio@lowtem.hokudai.ac.jp

Suzuki, Kazuyoshi
Cold Region Hydrological Cycle Group,
Hydrological Cycle Observational
Research Program, JAMSTEC, Yokosuka
skazu@jamstec.go.jp

RUSSIA

Efremova, Tatjana
Northern Water Problems Institute,
Russian Academy of Sciences
Petrozavodsk
efremova@nwpi.krc.karelia.ru

Filatov, Nikolay
Northern Water Problems Institute,
Russian Academy of Sciences
Petrozavodsk
nfilatov@nwpi.krc.karelia.ru

Nazarova, Larisa
Northern Water Problems Institute,
Russian Academy of Sciences
Petrozavodsk
nazarova@nwpi.krc.karelia.ru

Palshin, Nikolay
Northern Water Problems Institute,
Russian Academy of Sciences
Petrozavodsk
palshin@nwpi.krc.karelia.ru

Putyrsky, Vladimir
Water Research Institute,
Russian Academy of Sciences
Moscow
putyrsky1@yandex.ru

Regerand, Tatjana
Northern Water Problems
Russian Academy of Sciences
Petrozavodsk
regerand@nwpi.krc.karelia.ru

Salo, Yuri
Northern Water Problems Institute,
Russian Academy of Sciences
Petrozavodsk
yuris@nwpi.krc.karelia.ru

Shalina, Elena	**Scientific Foundation "Nansen International Environmental and Remote Sensing Centre", St. Petersburg** elena.shalina@niersc.spb.ru
Semenov, Anatoly	**Murmansk Hydrometeorology and Environmental Monitoring Administration Murmansk** leader@kolgimet.murman.ru
Shutov, Vladimir	**Valday Branch of the State Hydrological Institute Valday** vfggi@novgorod.net
Terzhevik, Arkady	**Northern Water Problems Institute, Russian Academy of Sciences Petrozavodsk** ark@nwpi.krc.karelia.ru

SWEDEN

Bengtsson, Lars	**Dept Water Resources Engineering Lund University** lars.bengtsson@tvrl.lth.se

UNITED STATES OF AMERICA

Berezovskaya, Sveta	**University of Alaska Fairbanks** ffslb2@uaf.edu
Liston, Glen E.	**Colorado State University Fort Collins** liston@cira.colostate.edu
Mernild, Sebastian H.	**University of Alaska Fairbanks International Arctic Research Center** fxsm@uaf.edu
Tidwell, Amy	**University of Alaska Fairbanks** fnact@uaf.edu

Hillslope Hydrological Linkages: Importance to Ponds within a Polar Desert High Arctic Wetland

Anna Abnizova* and Kathy L. Young,

Dept. of Geography, York University, 4700 Keele Street Toronto, Ontario, M3J 1P3 CANADA
**Corresponding author, e-mail: anna_abnizova@yahoo.ca*

ABSTRACT
Arctic wetland environments are considered to be sensitive to ongoing climate change (Hinzman *et al.* 2005) but they have received limited attention despite their ecological importance. To better understand and quantify the hydrologic processes which are leading to the sustainability and demise of High Arctic ponds, a water balance framework was employed on several ponds situated in two broad geomorphic areas near Creswell Bay, Somerset Island (72°43'N, 94°15'W). These ponds are also linked to an upland area through a range of linear features: stream, late-lying snowbeds and frost cracks. This study assesses the importance of these features with respect to the sustainability of these wetland ponds.
A pond's position in the moraine landscape was important in determining its connectivity to a nearby stream and late-lying snowbed. Close proximity to a stream draining a large upland snow-covered catchment ensures steady water levels during the snowmelt period. Once discharge slows, a late-lying snowbed continues to supply the pond and others with meltwater. The deeply thawed, sandy coastal zone is characterized by frost cracks which run both across and perpendicular within the wetland zone. These cracks function primarily as 'sinks' and serve to deprive small and medium-sized ponds of water during dry periods, often leading to their desiccation.

KEYWORDS
High Arctic wetland complexes; hydrologic linkages; permafrost landscape; polar desert environments; sustainability

1. INTRODUCTION

High Arctic wetlands are important ecosystems in Northern Canada with their ability to store, regulate and cleanse water flow. They provide homes and resting grounds for northern fauna and migratory birds. While, our understanding of small, patchy wetlands existing in polar desert environments has been improved recently (e.g. Woo and Young 2003), our understanding of extensive wetland systems existing within polar oasis and polar desert regimes is still limited (e.g. Woo and Guan 2006).
Various types of patchy wetlands exist and are governed by different aspects of topography, hydrology, vegetation, and frost conditions (Woo and Young 2006). Through surface depressions some wetlands are able to capture and maintain sufficient quantities of spring snowmelt maintaining a prolonged saturation long after snowmelt. Other wetlands have hydrologic linkages to late-lying snowbeds, streams and subsurface ground ice melt. These sources of water are critical in sustaining these wetlands during short-term shifts in climate (warm, dry summers) but are themselves vulnerable to shifting climatic conditions, particularly the loss of late-lying snowbeds and near-surface ground ice supplies during persistent warm summers. Woo and Guan (2006) recently investigated the hydrology of tundra ponds existing in a polar oasis environment (warm/dry). They found that meltwater inputs from the surrounding landscape was important in replenishing ponds during a high snow year but this role diminished during a year with little snow. The tundra thaw ponds instead relied on late summer rains to rejuvenate water levels to near snowmelt levels.

It has recently been suggested that climate change will influence numerous hydrological and ecological processes in wetlands (e.g. Bridgham *et al.* 1995; Rouse *et al.* 1997; Prowse *et al.* 2006). In fact, it has been documented that ponds and lakes are disappearing in Alaska and Siberia in response to recent climate warming (Fitzgerald *et al.* 2003; Smith *et al.* 2005). Alterations in water movement due to climate change will impact on the delivery of carbon and nutrients to ponds, ultimately influencing their productivity levels and ecology. Limited understanding about the hydrology of larger wetland complexes found in the High Arctic islands makes it difficult to predict how these systems will sustain themselves under a changing climate (Woo and Young 2006).
In this study we examine the role of different modes of lateral water inflow into a low-gradient wetland from adjacent hillslopes and uplands and discuss their importance in the sustainability of a suite of ponds situated here. These linear features can take a variety of forms: streams draining uplands, meltwater from late-lying snowbeds, and frost cracks which can channel water from hillslopes into wetlands and/or capture water back from ponds (reversal of flow), thereby depriving ponds of water during drought conditions. A sound understanding of the interactions between wetland ponds and upslope linkages is critical as we begin to anticipate how High Arctic wetland systems will respond to future climate warming.

2. STUDY AREA

The study occurred within an extensive, low-gradient wetland lying south of Creswell Bay on Somerset Island (72°42’N 94°15’W). The area can be described as having a polar desert climatic regime (cool/wet) comparable to Resolute Bay, Cornwallis Island about 100 km to the north. Here a government weather station exists. The study spanned two seasons: May to mid- August, 2005 and May to late-July, 2006. While three study sites were selected within this glacial till terrain, two are discussed here (Figure 1).

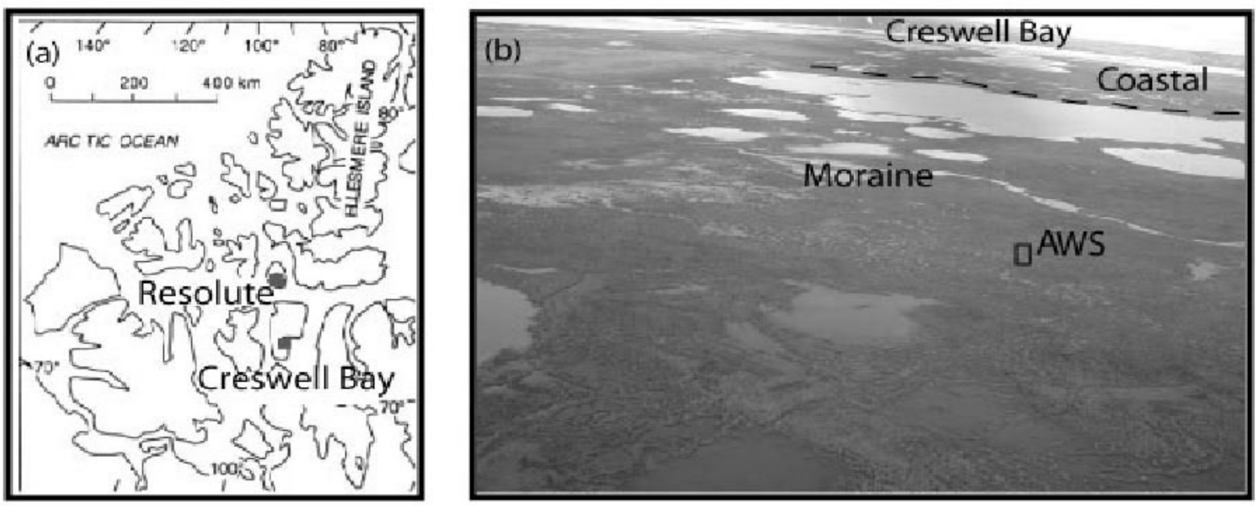

Figure 1. Location of the study area south of Creswell Bay (a) and a photograph of the general study area, August 2004 (b). The main Automatic Weather Station (AWS) is indicated and a dashed line approximately separates the Moraine wetland zone from the Coastal area.

The Moraine site contains lakes and ponds that formed as a result of glacial action, remnants of ponds formed behind an ancient lagoon and ponds likely created by thermokarst action (Brown and Young 2006). Here two ponds were selected, one fed by a late-lying snowbed and the other fed by a stream and a late-lying snowbed (Figure 2). The Coastal site with numerous ponds and lakes evolved over time being subjected to continual isostatic rebound. It contains very distinctive hydrological features, notably frost cracks, running both horizontally and linearly throughout the area. One medium-sized pond with a frost cracking running beside it is discussed in this study.

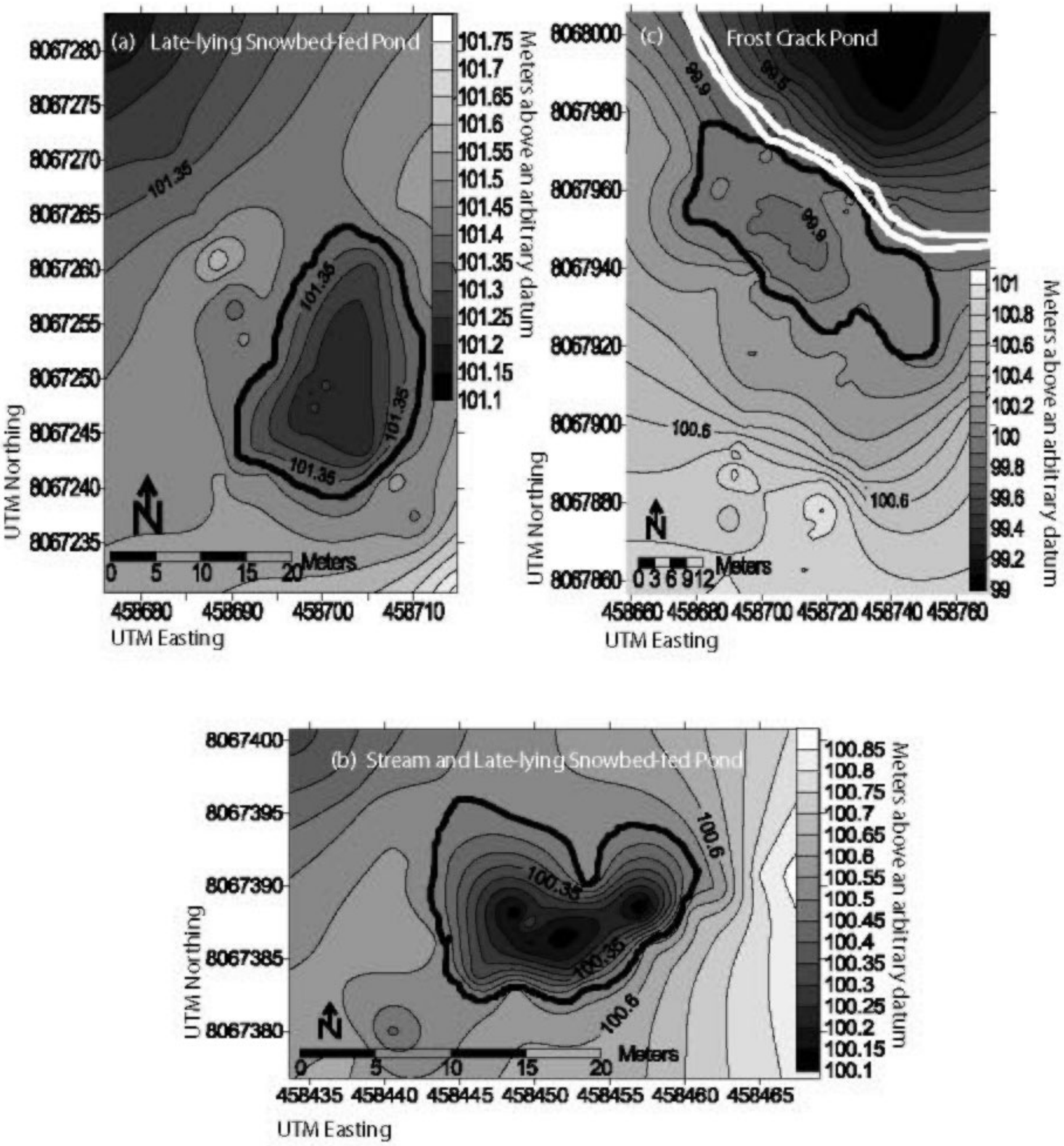

Figure 2. Topographic maps of the study ponds (a-c) and photographs of the linear features (d-f) described in the study.

3. METHODOLOGY

To better understand the hydrologic dynamics of ponds and their sustainability in a polar desert climatic setting, a detailed water balance framework was used during the summer seasons of 2005 and 2006. Here,

$$dS/dt = Sn + R - E \pm Q \quad (1)$$

where dS/dt is used to describe the change in storage (here we consider volume of water in the pond). The sum of Sn and R is precipitation input of snowfall (Sn) and rainfall (R), E is evaporation output, and Q is inflow to the pond or outflow (both surface and subsurface) (Woo *et al.* 1981). Owing to detailed data collection, water balance components are evaluated in more detail for the stream, snowbed-fed pond and the frost crack pond.

Snow comprises a large percentage of the annual precipitation in High Arctic regions and seasonal snowmelt remains one of the most important sources of water to wetland systems and consequently to ponds (Young and Woo 2004). At the end-of the winter period, a snow survey at each pond site (see Woo 1997) was conducted. A series of transects (n = 6) were laid across each pond and surrounding catchment and snow depth was taken every 2 m with a metric ruler or a longer snow rod if the snow depth > 1 m. Snow density was taken at 3 to 4 locations along each transect with a Meteorological Survey of Canada (MSC) snow corer and then averaged. Snowmelt was estimated directly (see Heron and Woo 1977) and indirectly with a snowmelt model described by Woo and Young (2003). Once the snowmelt season ceases, patches of late-lying snow often remain in lee of slopes, these features being common in these wind-swept environments (Young and Lewkowicz 1990). One of these late-lying snowbeds persisted adjacent to one of the study ponds and a detailed snow survey of it was made. Rate of retreat was monitored daily along 11 transects and photographs were taken twice weekly.

Summer precipitation (snow and rain) were measured with a tipping bucket raingauge geared into a CR10X datalogger at the main AWS (Figure 1). Manual raingauges were placed near each study site and regularly checked. Evaporation was evaluated using the Priestley-Taylor approach which has been found to work well in a range of arctic environments (e.g. Young and Woo 2003; Woo and Guan 2006). Its robustness was recently evaluated in a recent study where it was found to perform surprisingly well in comparison to other techniques (Rosenberry *et al*. 2004). In our study, an α=1.26 was applied. The AWS measured the following variables: Q*, K$\downarrow$, K$\uparrow$, U and direction, T_a, RH, T_s (1 cm, 10 cm), Q_g and PPT. An additional weather station monitoring: Q*, K$\uparrow$, U, T_a, T_w and Q_g rotated amongst the study sites every few days. Both stations provided climate data to estimate snowmelt, evaporation and ground thaw at the pond sites.

Groundwater inflow/outflow was evaluated using Darcy's law (e.g. Young and Woo 2003). A series of screened water wells dissected each pond site and the adjacent catchment. Wells were installed down to the permafrost table the previous year. In areas where water wells could not be easily inserted (e.g. frost cracks), dowels allowed surface water tables to be assessed. Water and frost tables were monitored regularly and hydraulic conductivity estimates (after Luthin 1966) were carried out at each site, at least once per season. Near-surface soil moisture (0-60 mm) in the pond catchment was measured with a Theta probe and confirmed with direct volumetric soil moisture measurements. These data quantified the degree of saturation in the pond catchment.

The stream draining the upland area (catchment size of 7 hectares, c.a. 45 m a.s.l) emptied into the moraine wetland area (c.a. 28 m a.s.l). The stream carved a well-defined channel for about 100 m within the wetland and then it spilled into a wet meadow zone. Stream discharge at the entry and exit of the wetland complex was monitored in both years using the area-velocity approach. Stage measurements together with current metering allowed discharge to be determined. In 2005, no water level recorder was available, so only 2 to 3 daily estimates of discharge were available. In 2006, water level in the stilling wells was monitored continuously with Ecotone water level recorders. During high flow periods, the floatation approach was used to determine stream velocity (Dunne and Leopold 1978). Again, 2 to 3 discharge measurements were made daily during the high flow period and less frequently during low flow.

To estimate the hydrological role played by frost cracks in pond sustainability, three frost cracks in the coastal zone were monitored during 2005 and 2006. The selection of the frost cracks was associated with their proximity to the observed ponds at the Coastal site and included both minor (1 m in width) and major-sized cracks (up to 2 m in width). Monitoring consisted primarily of regular measurements of water table and frost table. Finally all sites were surveyed in July 2005 with a Total Survey System.

4. RESULTS AND DISCUSSION

4.1 Climatology

Weather conditions near Creswell Bay in 2005 and 2006 are very similar to those of Resolute Bay (see Figure 3), confirming a polar desert climate designation (Woo and Young 2003). Mean temperature from Creswell Bay was slightly higher than Resolute Bay in 2005 (3.7^{o}C vs. 2.7^{o}C) and in 2006 (2.8^{o}C vs. 1.5^{o}C). Summer precipitation was slightly lower at Creswell Bay in 2005 (47 mm) than in 2006 (68 mm) and there was differences in the timing of rainfall. Rainfall was greater in July, 2005 but higher in June, 2006. Winds were generally from the west and averaged 3.6 m/s. End-of-winter snowcover at the AWS was 162 mm in 2005 and only 108 mm in 2006. Snowmelt was delayed in 2006 due to poor weather conditions and steady snowmelt did not commence until June 10 (JD 162) and lasted for 10 days. Growing degree-days were larger in 2005 (187) than in 2006 (102) when the same time period was compared.

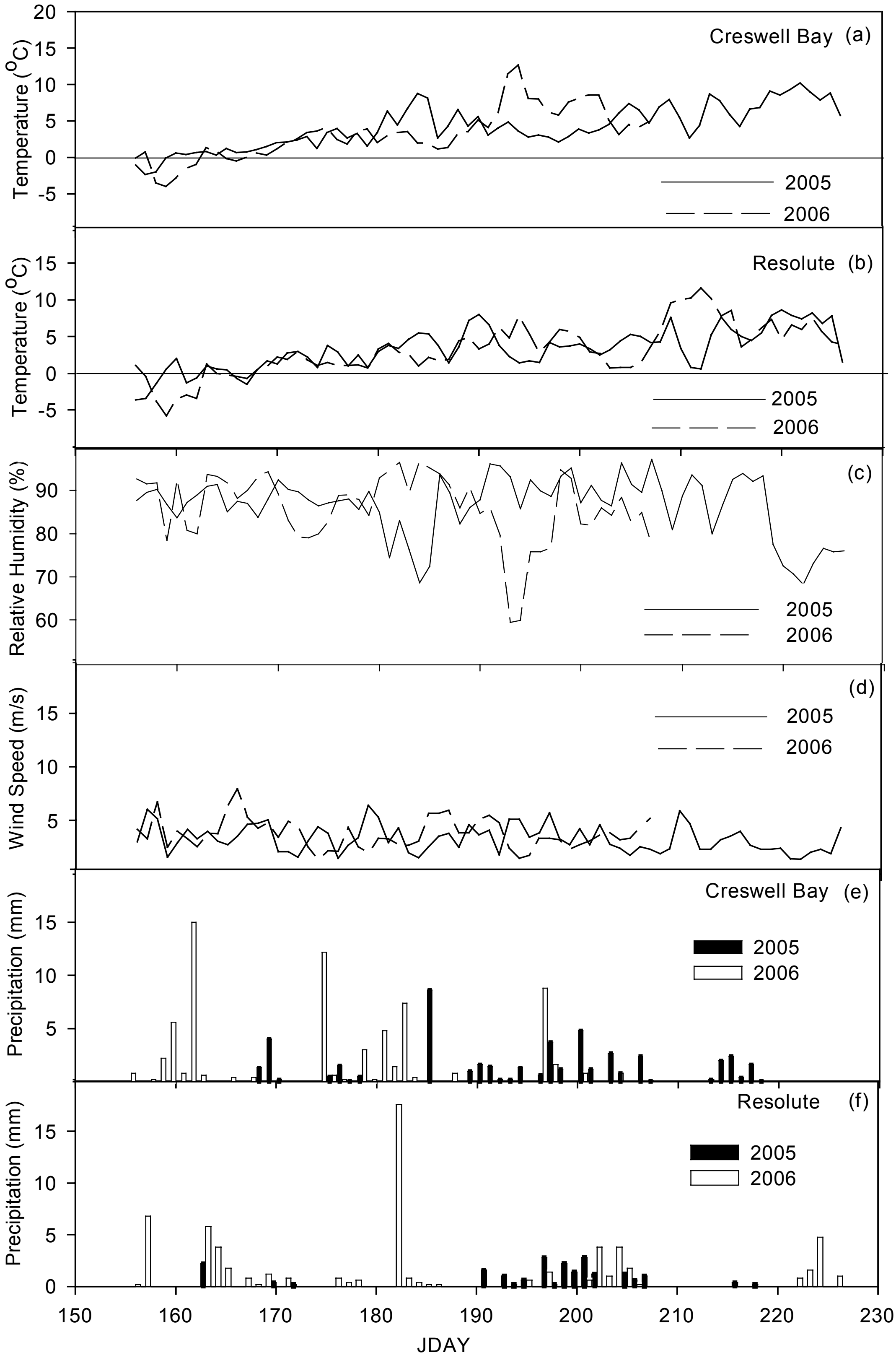

Figure 3. Seasonal pattern of mean daily air temperature at Creswell Bay (a) and Resolute Bay (b); mean daily relative humidity (c); mean daily wind speed (d); and daily total precipitation at Creswell Bay (e) and Resolute Bay (f). Note data collected at Creswell Bay was not complete in 2006 (only from June 1 to July 26).

4.2 Hillslope linkages

4.2.1 Single: Moraine zone-Late-lying snowbed-fed pond

This snow-bed fed pond is located near the lee of a slope and receives more snow than exposed ponds (280 mm in 2005 vs. 284 mm in 2006). Deeper snow here delayed snowmelt until June 21, 2005 (JD 173) and June 24, 2006 (JD 176) and snowmelt persisted here for 14 days in both years. Figure 4 indicates that water tables remained stable in both years (189±19 mm in 2005 and 175±35 mm in 2006) largely due to steady water contributions from the melting late-lying snowbed during favourable weather conditions (sunny, warm periods) and episodes of significant rainfalls (6.6 mm from JD 214 till JD 218 in 2005). Soil moisture in the adjacent catchment was also high varying between 55 to 60 % in both years due to prolonged meltwater contributions. However, some water loss from the pond did occur as the snowbank and water supplies diminished.

Young and Woo (2003) have previously shown the importance of late-lying snowbeds in providing meltwater to downslope patchy wetlands long after the seasonal snowmelt has disappeared. They note that these snow-beds buffer wetlands from variable climatic conditions, especially during warm, dry summers. However, snowbeds are also vulnerable to shifts in climate and can shrink dramatically during warm, dry summers (Woo and Young 2006). Future climate warming may see the disappearance of these features along with their ability to sustain near-by ponds and their adjacent wet meadows. Brown and Young (2006), using historical air photos showed that in the past ponds disappeared from this landscape when adjacent late-lying snowbeds also disappeared.

4.2.2 Multiple: Moraine zone-Stream-fed and Late-lying snowbed-fed pond

Evaluation of the water balance components of a second moraine pond demonstrated the importance of multiple water sources in this wetland system (Figure 2). Initially, linkage of the pond with the upland stream contributes to elevated water levels during the spring flood (Figure 5). Once snowmelt waters are drained from both the lowland and upland, the pond looses its connectivity with the stream and its water level drops to its seasonal level (see Figure 5). However, meltwater inputs from a late-lying snowbed (c.a. 180 m away) continues to provide additional meltwater as the season progresses ensuring steady water levels in both the pond and saturated conditions for the adjoining catchment. Examination of the water budget demonstrates that storage remains positive despite high surface outflow during the snowmelt season, deep thaw and evaporation losses during the post-snowmelt season.

The timing and magnitude of rain events coupled with the degree of connectivity of a pond to its landscape is another important consideration in terms of recharge. A late season rain event (10.4 mm) in 2006 elevated water levels higher than estimated, suggesting that additional water inputs came from the surrounding landscape (i.e. stream, late-lying snowbed and saturated catchment) (Figure 5).

Other wetland researchers (e.g. Soranno *et al.* 1999 and Van Hove *et al.* 2006) have also remarked on the importance of linkages with the landscape to buffer the losses of water due to climatic influences. Ponds which are isolated, having limited connection to their surrounding basin (snowbeds, streams, saturated ground) are generally more dependent on meteorological conditions (snowfall, summer rains) for their survival. Seasons with little snow and rain result in these ponds drying out quickly (Woo and Guan 2006). Large rainfall events occurring at critical periods may recharge the ponds if storage deficits can be satisfied. Without adequate inputs, these ponds can be viewed as intermittent and in time may cease to exist. Multiple water linkages appear to be one of the best strategies for arctic ponds to survive changing climatic conditions. In this study, the overlapping contributions of streamwater and late-lying snowmelt water inputs allows this particular pond to maintain a positive water storage despite variable climatic conditions.

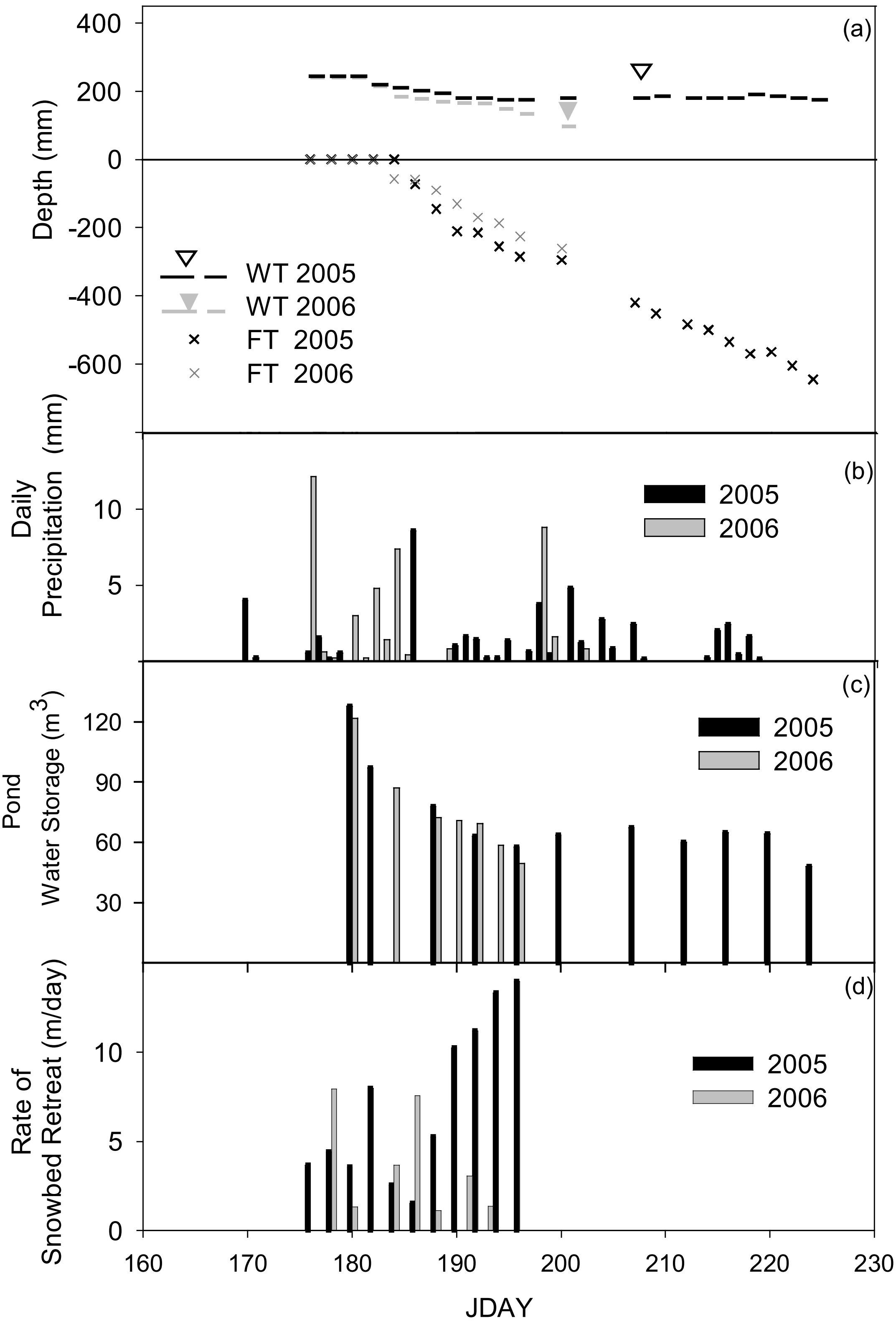

Figure 4. Seasonal regime of ground thaw (mm) and water table response (mm) at the Snowbank-fed pond (a); daily total precipitation amounts (mm) (b); daily pond storage change (m^3) (c), and late-lying snowbed retreat (m/d) in 2005 and 2006 (d). Note data collected at Creswell Bay was not complete in 2006 (only from June 1 to July 26).

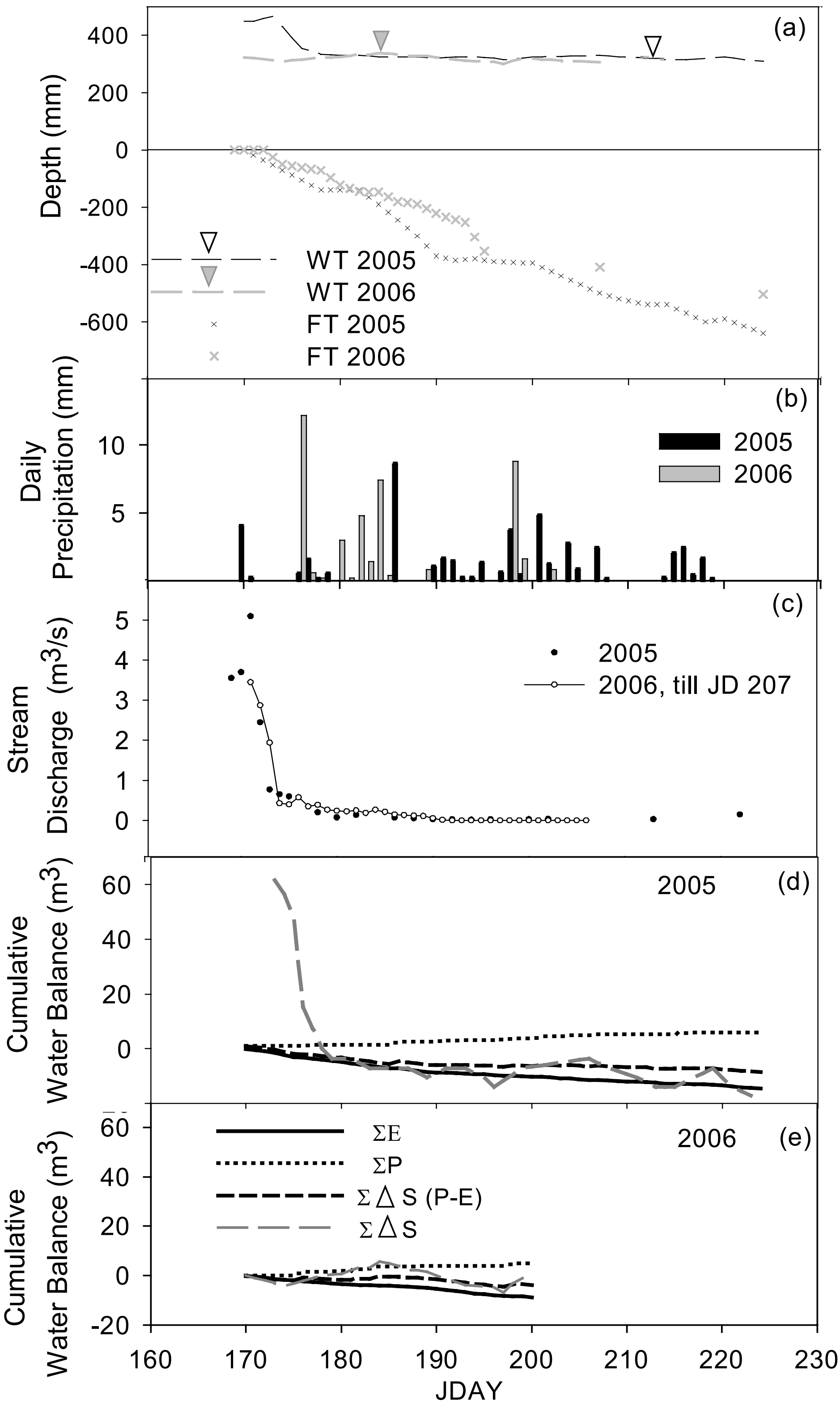

Figure 5. Seasonal regime of ground thaw (mm) and water table response (mm) at the Moraine Medium pond (a); daily total precipitation amounts (mm) (b); stream discharge into the wetland in 2005 and 2006 (c); cumulative water balance components (m^3) in 2005 (d) and 2006 (e). Note data collected at Creswell Bay was not complete in 2006 (only from June 1 to July 26).

4.2.3 Dual role: Coastal zone - frost crack pond

The coastal zone is characterized by coarse sandy soils which thaw rapidly after snowmelt and frost cracks which dissect the area. These cracks run from the slopes that border this wetland zone and are orientated parallel and perpendicular to the wetland. They are in response to isostatic rebound and to the maximum ground temperature gradient arising from the contrast between land and sea (Lachenbruch 1962). These frost cracks appear to play a dual role. At the time of snowmelt and large rainfall events they are conduits for water draining from slopes and are effective in funneling this water further out into the coastal zone. However, their major role in the post-snowmelt period is to serve as 'sinks' and enhance pond drainage and desiccation, especially for small and medium-sized ponds. For instance, Figure 6 shows the water table and frost table pattern for a medium-sized pond in both 2005 and 2006. The strong link of the pond to the frost crack when water tables are compared (R^2 = 0.76, $p< 0.05$) results in seepage of subsurface water from the pond to the crack and subsequent water losses.

The presence of near-by frost cracks is just one more feature compounding to water losses from these coastal-type ponds. For instance, these ponds show little relief and cannot capture as much snow as other sites (155 mm in 2005 vs. 125 mm in 2006). Shallow (mean depth = 0.22 m) and warm water (6.71 ^{o}C) triggered by a dark blue-green substrate which can absorb much radiation enhances evaporation losses (about 2.5 mm/day) (Oke 1987). The sandy texture also enhances much groundwater flow through deep thaw (0.89 m) and high hydraulic conductivity (e.g. K = 2.6 m/d).

The role of frost cracks in pond hydrology was recently described by Woo and Guan (2006). At their study site a frost crack was formed due to thermokarst processes after an exceptionally warm summer with little rain. They concluded that a warmer climate increases the probability for thermokarst occurring along pond rims helping to create natural channels for pond drainage. This response is a slightly different situation than in our study but does help to provide additional evidence of the numerous roles played by frost cracks in high arctic wetland environments.

5. CONCLUSIONS

There are many factors which determine a pond's ability to sustain itself in polar desert environments. Some of these are position in the landscape and size with large ponds, generally receiving water from larger catchment areas. Topography and soil texture are also critical. Depression-type ponds can capture and hold onto more snow than broad, shallow ponds which tend to be windswept. Ponds with sandy soil will have deeper and earlier thaws than silty soils with high ice contents. Here, we consider a few selected ponds in the context of hillslope linkages (i.e. late-lying snowbed, stream and frost cracks). Our study has shown that connectivity to a water source is important in sustaining ponds during variable climatic conditions (2005 vs. 2006) and can help buffer ponds against seasonal water losses (runoff and evaporation). Multiple water linkages provide the best strategy for ponds to sustain themselves over the long-term. Streamwater together with meltwater from late-lying snowbeds provide overlapping sources of water which sustain pond water levels throughout the summer season. A pond dependent on only one water source (e.g. late-lying snowbed) could be vulnerable in the future if this supply disappears in response to a warmer climate (Woo and Young 2006). Ponds not well connected to a reliable hydrological system are the most vulnerable to climatic shifts and are prone to desiccation (e.g. small and medium Coastal ponds). Here, landscape features such as frost cracks also serve as 'sinks' rather than water 'sources', helping to deprive ponds of even more water.

ACKNOWLEDGEMENT

The authors would like to acknowledge NSERC funding to both K. Young and A. Abnizova along with financial assistance from NSTP and York University. Thanks to PCSP for excellent logistical support and to Markus Anastasiades and Ettore Colacchio who served as field assistants in 2005 and 2006 respectively.

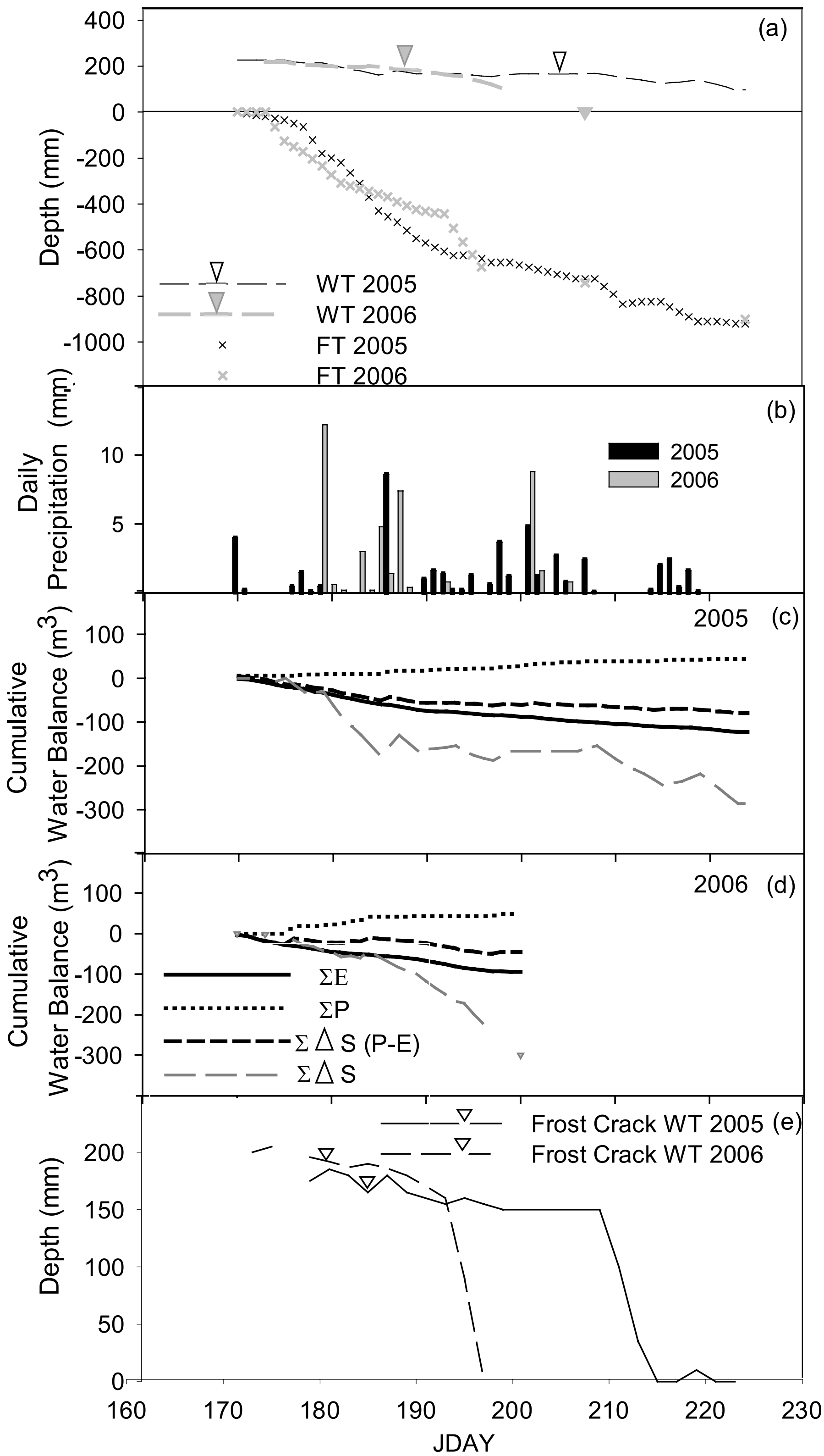

Figure 6. Seasonal regime of ground thaw and water table response at the Coastal Medium pond (a); daily total precipitation amounts (b); cumulative water balance components (m^3) in 2005 (c) and 2006 (d), and seasonal regime of water table at the nearby frost crack 2005 and 2006 (e). Note data collected at Creswell Bay was not complete in 2006 (only from June 1 to July 26).

REFERENCES

Bridgham, S.D., Johnston, C.A., Pastor, J., and Updegraff, K. (1995) Potential feedbacks of northern wetlands on climate change. *BioScience* **45**, 262-274.

Brown, L. and Young, K.L. (2006) Assessment of three mapping techniques to delineate lakes and ponds in a Canadian High Arctic wetland complex. *Arctic* **59**, 283-293.

Dunne, T. and Leopold, L.B. (1978) Water in Environmental Planning. W.H. Freeman and Company, New York.

Fitzgerald, D. and Riordan, B. (2003) Permafrost and ponds. *Agroborealis* **35** (1), 30-35.

Heron, R., and Woo, M.K. (1978) Snowmelt computations for a high arctic site. *Proceedings of 35th Eastern Snow Conference*, Hanover. pp. 162-172.

Hinzman, L. D., Bettez, N. D., Bolton, W. R., Chapin, F. S., Dyurgerov, M. B., Fastie, C. L., Griffith, B., Hollister, R. D., Hope, A., Huntington, Henry P.; Jensen, Anne M.; Jia, Gensuou J.; Jorgenson, Torre; Kane, Douglas L.; Klein, D. R., Kofinas, G., Lynch, A. H., Lloyd, A. H., McGuire, A. D., Nelson, F. E., Oechel, W. C., Osterkamp, T. E., Racine, C. H., Romanovsky, V. E., Stone, R. S., Stow, D. A., Sturm, M., Tweedie, C. E., Vourlitis, G. L., Walker, M. D., Walker, D. A., Webber, P. J., Welker, J. M., Winker, K. S., Yoshikawa, K. (2005) Evidence and implications of recent climate change in northern Alaska and other arctic regions. *Clim. Change* **72**, 251-298.

Lachenbruch, A.H. (1962) Mechanics of Thermal Contraction Cracks and Ice-Wedge Polygons. *Permafrost. Geol. Soc. Am. Sped. Pap.* **70**, 69 pp.

Luthin, J.N. (1966) Drainage Engineering. Wiley, London.

Oke, T.R. (1987) *Boundary Layer Climates. 2nd Edition.* University Press Cambridge, Routledge, Great Britain.

Prowse, T.D., Wrona, F.J., Reist, J.D., Gibson, J.J., Hobbie, J.E., Lévesque, L.M.J. andVincent, W.F. (2006) Climate change effects on hydroecology of arctic freshwater ecosystems. *Ambio*. **35**, 347-358.

Rosenberry, D.O., Stannard, D.I., Winter, T.C., and Martinez, M.L. (2004) Comparison of 13 equations for determining evapotranspiration from a prairie wetland, Cottonwood Lake area, North Dakota, USA. *Wetlands* **24,** 483-497.

Rouse, W., Douglas, M., Hecky, R., Hershey, A., Kling, G., Lesack, L., Marsh, P.,McDonald, M., Nicholson, B., Roulet, N. and Smol, J. (1997) Effects of climate change on the freshwaters of arctic and subarctic North America. *Hydrol. Process.* **11**, 873-902.

Smith, L.C., Sheng, Y., MacDonald, G. M., and Hinzman, L. D. (2005) Disappearing Arctic Lakes. *Science* **308** (5727), 1429.

Soranno, P.A., Webster, K.E., Riera, J.L., Kratz, T.K., Baron, J.S., Bukaveckas, P., Kling, G. W., White, D., Caine, N., Lathrop, R.C., and Leavitt, P.R. (1999) Spatial variation among lakes within landscapes: Ecological organization along lake chains. *Ecosystems***2**, 395-410.

Van Hove, P., Belzile, C., Gibson, J.A.E. and Vincent, W. F.(2006) Coupled landscape–lake evolution in High Arctic Canada. *Can. J. Earth Sci.* **43**, 533–546.

Woo, M. K., Heron, R. and Steer, P. (1981) Catchment hydrology of a High Arctic lake. *Cold Reg. Sci. Technol.* **5**, 29–41.

Woo, M.K. (1997) A guide for ground based measurement of the arctic snow cover. Canadian Snow Data CD, Meteorological Service of Canada, Downsview, Ontario.

Woo M.K. and Young, K.L. (2003) Hydrogeomorphology of patchy wetlands in the high Arctic, polar desert environment. *Wetlands* **23**, 291-309.

Woo, M.K. and Guan, X.J. (2006) Hydrological connectivity and seasonal storage change of tundra ponds in a polar oasis environment, Canadian High Arctic. *Permafrost and Perigl. Process.* **17**, 309-323.

Woo, M.K. and Young, K.L. (2006) High Arctic wetlands: Their occurrence, hydrological characteristics and sustainability. *J. Hydrol.* **320**(3-4), 432-450.

Young, K.L. and Lewkowicz, A.G. (1990) Surface energy balance of a perennial snowbank, Melville Island, Northwest Territories, Canada. *Arct Alp Res.* **22**, 290–301.

Young, K.L. and Woo, M.K.. (2003) Thermo-hydrological responses to an exceptionally warm, dry summer in a High Arctic environment. *Nord. Hydrol.* **34**, 51-70.

Young, K.L. and Woo, M.K. (2004) Queen Elizabeth Islands: problems associated with water balance research, northern research basins water balance. *Inter. Assoc. Hydrol. Sci.* **290**, 237-248.

Climate change impacts on hydrological processes in the Nordic region 2071-2100

Stein Beldring[1]*, Johan Andreasson[2], Sten Bergström[2], L. Phil Graham[2], Jóna Finndís Jonsdottir[3], Lars A. Roald1, Svetlana Rogozova[4], Jörgen Rosberg[2], Merja Suomalainen[5], Bertel Vehviläinen[5], Noora Veijalainen[5]

[1] Norwegian Water Resources and Energy Directorate, PO Box 5091 Majorstua, 0301 Oslo, NORWAY
[2] Swedish Meteorological and Hydrological Institute, 601 76 Norrkoping, SWEDEN
[3] Hydrological Service, National Energy Authority, Grensasvegur 9,108 Reykjavik, ICELAND
[4] Latvian Environment, Geology and Meteorology Agency, Maskavas Street 165, Riga, LV-1019, LATVIA
[5] Finnish Environment Institute, PO Box 140, 00251 Helsinki, FINLAND
**Corresponding author, e-mail: stein.beldring@nve.no*

ABSTRACT
Climate change impact simulations for hydrological processes in the Nordic region for the period 2071-2100 have been estimated using results from global climate models from the Hadley Centre and the Max-Planck Institute, and dynamical downscaling using the Rossby Centre RCAO and RegClim HIRHAM regional climate models. These climate scenarios were used for driving the HBV and WaSim-ETH hydrological models. Present conditions were determined from control runs using observed meteorological data and climate model results for 1961-1990. Maps presenting the spatial distribution of hydrological state variables and fluxes are presented. A moderate increase in annual runoff is expected in most parts of the Nordic region, with a decline in some parts for some scenarios. The changes depend on the spatial distribution of the atmospheric pressure fields as modelled by the two global climate models. Significant changes in the seasonal distribution of runoff are expected. Increase everywhere in the winter, increase in mountainous basins and inland basins in the spring and a decline in coastal and southern basins in the spring. Decrease will occur everywhere in the summer, while autumn runoff will increase everywhere except in southern parts. The occurrence of large snowmelt floods is likely to become more seldom due to earlier snowmelt and reduced snow storage. The combined effect of increase in rainfall intensities, number of rainfall events and total rainfall volume will most likely provide conditions that may be expected to yield larger rain floods.

KEYWORDS
Climate change, water resources, hydrological model

1. INTRODUCTION

Production of electricity in the Nordic countries is dependent on runoff, and possible changes in hydropower production capacity are therefore of large economical importance. Assessment of the future hydrological regime is a production chain where changes in external forcing caused by greenhouse gas emissions are introduced into general circulation models and regional climate models. The climate model results are used for driving hydrological models which determine time series or statistics of hydrological state variables and fluxes for present and future climate conditions. Maps presenting spatial distributions of these statistics, e.g. annual or seasonal mean values and extremes are a useful way of communicating the results from modelling hydrological impacts of climate change. The results presented in this study have been produced by the Hydropower, Hydrological Models group of the Nordic research project Climate and Energy (CE). This project has the objective of a comprehensive assessment of the impacts of climate change on renewable energy sources in the Nordic countries, the Baltic States and Northwest Russia. The CE project is funded by the Nordic Energy Research, the Nordic energy sector and national institutions of the participating countries.

Within the CE project a set of maps of water resources under present and future conditions based on climate scenarios and hydrological modelling techniques have been produced. This may serve as a foundation for assessments of the future production potential of hydropower in the Nordic area. The maps are based on four regional climate scenarios, resulting from two general circulation models, each forced with two greenhouse gas emission scenarios. Climate change scenarios differ substantially due to uncertainties with regard to the climate forcing caused by greenhouse gas emissions, uncertainties caused by imperfect representation of processes in the atmospheric models, and uncertainties with regard to initial conditions. Hydrological climate change maps which are based on ensembles of climate change simulations from model runs using different approaches to predict the future represent one way of quantifying this uncertainty.

2. CLIMATE SCENARIOS

Results from the Max Planck Institute atmosphere-ocean general circulation model ECHAM4/OPYC3 (Roeckner *et al.*, 1999), and from the general circulation model HadAM3H developed from the atmospheric component of the Hadley Centre atmosphere-ocean general circulation model HadCM3 (Gordon *et al.*, 2000) have been used for assessment of climate change impacts on water resources in the Nordic countries. Observed fields of sea-surface temperature and sea-ice dataset were used as lower boundary conditions in the control simulation with HadAM3H. In the climate change experiments, the sea-surface temperature anomaly described by HaDCM3 was added to the observed data to be used as the lower boundary forcing. Assumptions about future greenhouse gas emissions were based on the Intergovernmental Panel on Climate Change (IPCC) Special Report on Emission Scenarios (SRES) A2 and B2 scenarios (Nakicenovic *et al.*, 2000). The general circulation model simulations were used as boundary conditions for dynamical downscaling with two regional climate models. For Finland, Latvia, Norway and Sweden the Rossby Centre Regional Atmosphere-Ocean (RCAO) model (Doscher *et al.*, 2002) was run with boundary conditions supplied by the ECHAM4/OPYC3 and HadAM3H models for both A2 and B2 emission scenarios, resulting in four different hydrological climate change impact simulatios for each country. Regional climate model results for Iceland were supplied by the HIRHAM model (Bjørge *et al.*, 2000) with boundary conditions from the HadAM3H model. Mean values of HIRHAM results from the A2 and B2 scenarios were used as input to hydrological modelling in Iceland. HIRHAM results were provided by the Regional Climate Development Under Global Warming (RegClim) project (http://regclim.met.no).

The hydrological simulations used the time slice approach whereby model simulations representing a slice of time in present climate (control) and in a future climate (scenarios) were performed. The time slice for the control climate was 1961-1990 and for the future climate 2071-2100. The hydrological impact studies were done with off-line simulations with the hydrological models. Observed meteorological data were used as a control climate in all countries, with the exception of Iceland where observed data were replaced by results from the MM5 atmospheric model at spatial resolution 8 by 8 km^2 (Grell *et al.*, 1994). Changes in meteorological variables between the control and the scenario simulations from the regional climate models were transferred to a database of meteorological data. This can be referred to as the delta change approach, e.g. Hay *et al.* (2000) and is a common method of transferring the signal of climate change from climate models to hydrological models. Monthly relative precipitation changes and absolute temperature changes predicted by the regional climate models were used to modify the daily meteorological data driving the hydrological models for the baseline period 1961-1990. The same monthly precipitation changes were used for all years of the impact simulations and for extreme values as well as for average conditions. The number of precipitation days was not changed in the scenario climate. Temperature changes were applied differently. Constant monthly temperature changes for all temperature intervals were applied for the impact simulations in Iceland, Latvia and Norway, while the Finnish and Swedish simulations used a temperature dependent function to take into account that temperature changes in the climate scenarios are most pronounced at low temperatures.

3. HYDROLOGICAL SIMULATIONS

Hydrological simulations were performed on a daily time step with the conceptual HBV model (c.f. Lindstrom *et al.*, 1997) for all countries except for Iceland, where the WaSiM-ETH model (Schulla and Jasper, 2001) was used. The HBV model is a conceptual, semi-distributed precipitation-runoff model originally developed for operational streamflow forecasting. The model includes routines for snow accumulation and melt, soil moisture accounting, groundwater response and river routing. It exists in different versions in each of the Nordic countries. Due to the geological conditions prevailing in Iceland the hydrological model structure must be able to describe groundwater flow in aquifers with large vertical extent. WaSiM-ETH was chosen because it allows the user to choose modules with different levels of complexity for simulation of subsurface processes. The hydrological models were calibrated to catchments representing different runoff regimes and land surface characteristics in each country. Landscape elements which could be expected to have similar hydrological behaviour were parameterised in the same way, and calibrated parameter sets were transferred to ungauged catchments based on a classification of land surface properties. Temperature and precipitation data from the meteorological stations of the different countries were interpolated to the computational elements of the hydrological models.

The hydrological simulations for Finland were done with a spatially distributed HBV model comprising of several small lumped models (Vehviläinen and Huttunen, 2002). The model consist of a rainfall-runoff model and river and lake models. The watersheds in the model have been divided into sub-catchments of approximately 100 km^2. Each of the sub-catchments has its own set of parameters and simulated storages and is divided into 1 km^2 grid cells.

Present conditions in Iceland were evaluated from a control run using the grid based hydrological model WaSiM-ETH (Schulla and Jasper, 2001). The hydrological model was calibrated against runoff data from 70 watersheds covering 1/3 of the country. Then, model parameters were evaluated for ungauged watersheds by comparing model parameters from nearby watersheds with similar characteristics based on a recent classification of watersheds. The hydrological model was applied at a 1 by 1 km^2 grid.

The HBV-96 model (Lindstrom *et al.*, 1997) was used for climate change impacts simulations for three basins representative for different hydrological regimes in Latvia: Irbe basin (1920 km^2) is located in western part of Latvia and discharges to the Baltic sea; Gauja basin (8510 km^2) covers north-eastern part of Latvia and discharges to the Gulf of Riga; Aiviekste basin (8660 km^2) covers eastern part of Latvia and discharges to the Daugava river.

A spatially distributed version of the HBV model (Beldring *et al.*, 2003) was used for hydrological climate change impact simulations in Norway. The model performs water balance calculations for 1 by 1 km^2 square grid cell landscape elements characterized by their elevation and land use. A regionally applicable set of model parameters was determined by calibrating the model with the restriction that the same parameter values are used for all computational elements of the model that fall into the same class for land surface properties.

The HBV-96 model (Lindstrom *et al.*, 1997) was used for interpretation of the impacts of climate change on water resources in Sweden. The model, referred to as HBV-Sweden, was originally set up to calculate runoff and associated transport of nitrogen to the sea (Brandt and Ejhed, 2002). The model simulates hydrological processes in Sweden with more than 1000 sub-basins, which gives an average spatial resolution of approximately 450 km^2.

4. RESULTS AND DISCUSSION

The hydrological simulations have generated a large amount of time series on hydrological variables and fluxes for the land surface computational elements used by the hydrological models. Annual and seasonal mean values and annual extremes of several characteristics are presented in Figures 1, 2, 3 and 4. Evaporation was determined as the sum of all latent heat fluxes from the land surface to the atmosphere; evaporation of intercepted water, transpiration, soil evaporation and open water evaporation. Mean annual maximum snow water equivalent and mean annual minimum soil moisture are the mean values of annual maxima or minima for all years in the control or scenario periods. The entire set of results were presented by Beldring *et al.* (2006).

Maps of projected runoff changes presented in Figures 1 and 2 show that annual runoff will generally increase for the Nordic region, except for southern parts of Sweden. Latvia and some regions in southern Norway will also experience reduced annual runoff for some scenarios. Seasonal runoff change results for the HadAM3H/B2 scenario are presented in Figure 3. There will be an increase in runoff everywhere in the winter, increase in mountainous basins and inland basins in the spring, and a decline in coastal and southern basins in the spring. Decrease will occur almost everywhere in the summer with the possibility for more severe droughts. The exceptions are parts of Finland and some coastal regions in Norway. Autumn runoff will generally increase in northern and high elevation parts of the Nordic region, while a decrease is expected in southern parts. Although there are differences between the climate scenarios used in this study, the projected climate change impacts on runoff conditions in the Nordic region are relatively consistent.

In addition to the runoff maps, there are maps presenting present and future conditions and changes from the present to the future for annual maximum snow water equivalent, number of days per year with snow covered ground, and annual minimum soil moisture. Finally, maps showing evaporation changes from the present to the future have been produced. The changes in these variables for the HadAm3H/B2 scenario are presented in Figure 4.

Runoff changes in the Nordic countries are strongly linked to changes in snow regime. Snow cover will be more unstable and all scenarios indicate increase in winter and autumn runoff in areas where the snow cover has a major impact on runoff in the control climate. These results are caused by the combined effects of higher temperature and more precipitation in the winter in the scenario climate. Reduced snow cover leads to smaller snow melt floods, while increased precipitation where a larger proportion falls as rain will increase rain floods, and possibly also combined snow melt and rain floods.

The projected changes in runoff differ between the two general circulation models HadAM3H and ECHAM4/OPYC3 due to different modes of natural climate variability represented by the two models. These two general circulation models result in different dominating atmospheric circulation patterns, with increasing dominance from the west in ECHAM4/OPYC3 scenarios and a more easterly pattern in the HadAM3H scenarios. This results in different distributions of precipitation, runoff and other hydrological variables (Tveito and Roald, 2005).

Furthermore, the two IPCC SRES scenarios A2 and B2 result in different projections of future radiative forcing and temperature changes, with A2 yielding the largest increase in greenhouse gas concentrations and temperature. These differences influence the hydrological cycle, leading to different changes in hydrological state variables and fluxes.

The model simulations have not considered land use changes caused by climate change or human transformation of the land surface, However, this should be taken into account, as it is likely that changes in land-cover may interact with climate, leading to different projections of future hydrological conditions. Neither were water balance simulations for future climate conditions in glacier covered areas entirely realistic since the areal extent of glaciers were assumed to be constant. There was one exception, however, a dynamical glacier model was used for modelling changes in the extent of Icelandic glaciers before the hydrological model simulations were performed (Johannesson *et al.,* 2006).

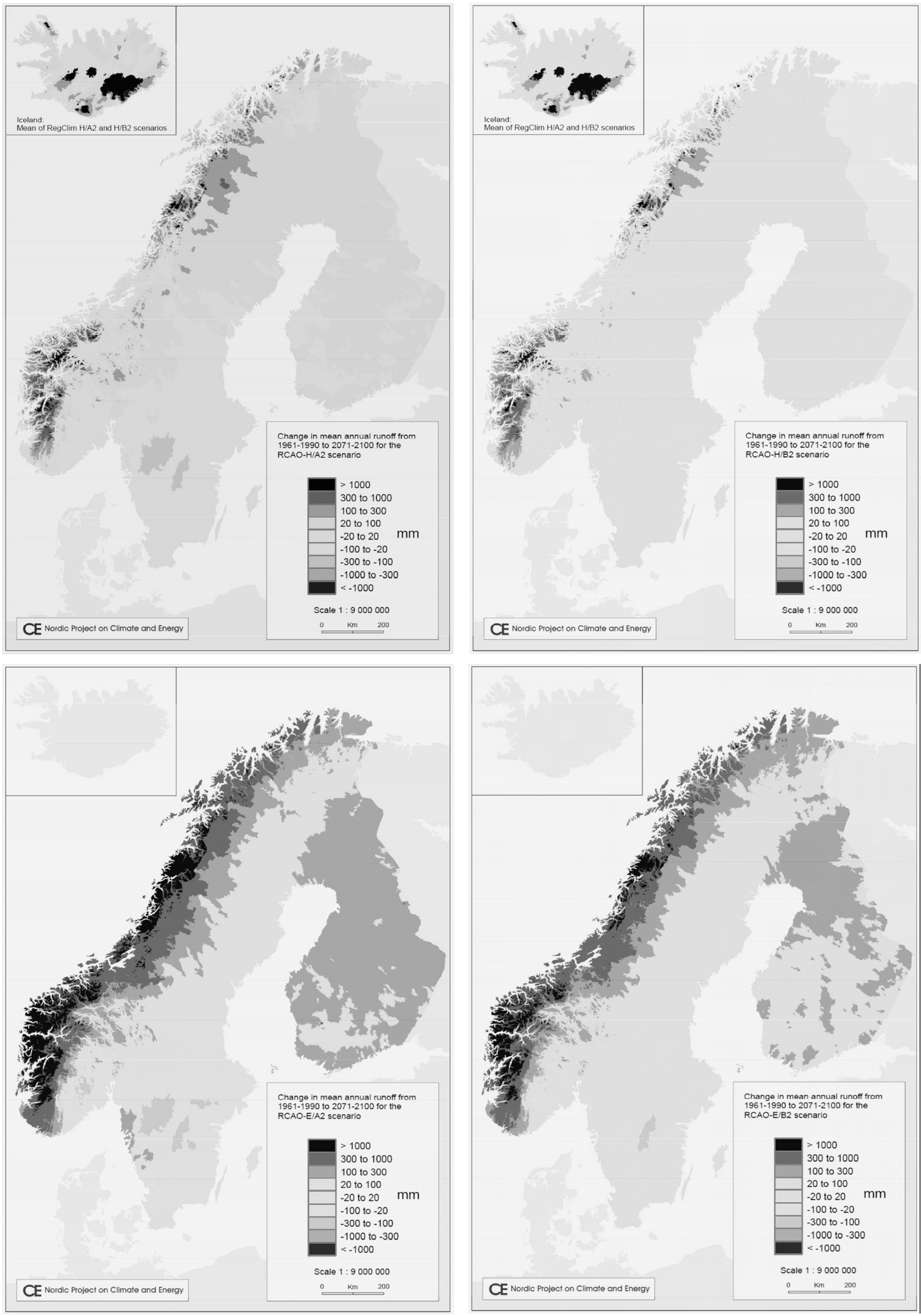

Figure 1. Change in mean annual runoff (mm) for Finland, Iceland, Norway and Sweden from 1961-1990 to 2071-2100. Top left: HadAM3H/A2 scenario. Top right: HadAM3H/B2 scenario. Bottom left: ECHAM4/OPYC3/A2 scenario. Bottom right: ECHAM4/OPYC3/B2 scenario.

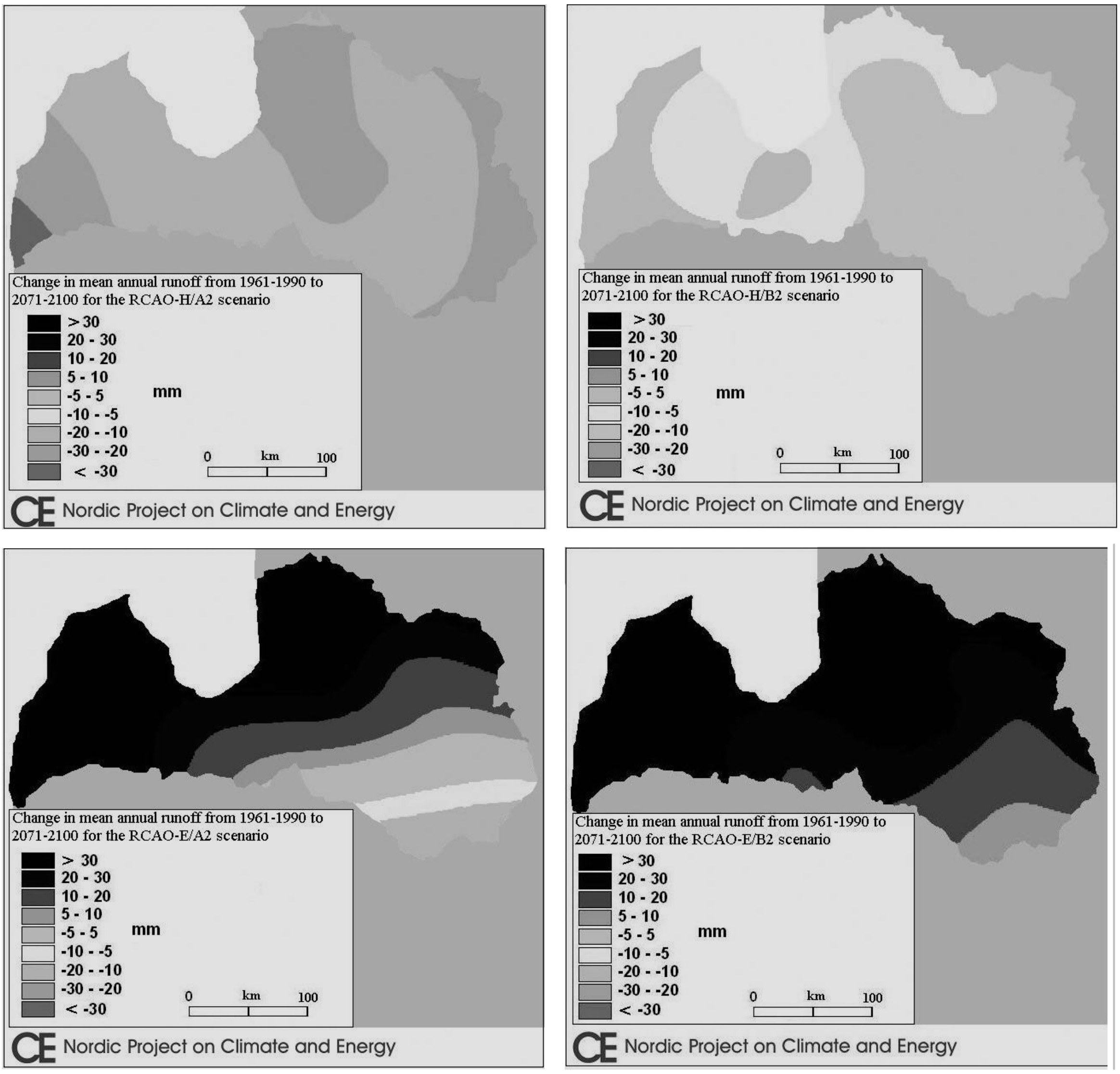

Figure 2. Change in mean annual runoff (mm) for Latvia from 1961-1990 to 2071-2100. Top left: HadAM3H/A2 scenario. Top right: HadAM3H/B2 scenario. Bottom left: ECHAM4/OPYC3/A2 scenario. Bottom right: ECHAM4/OPYC3/B2 scenario.

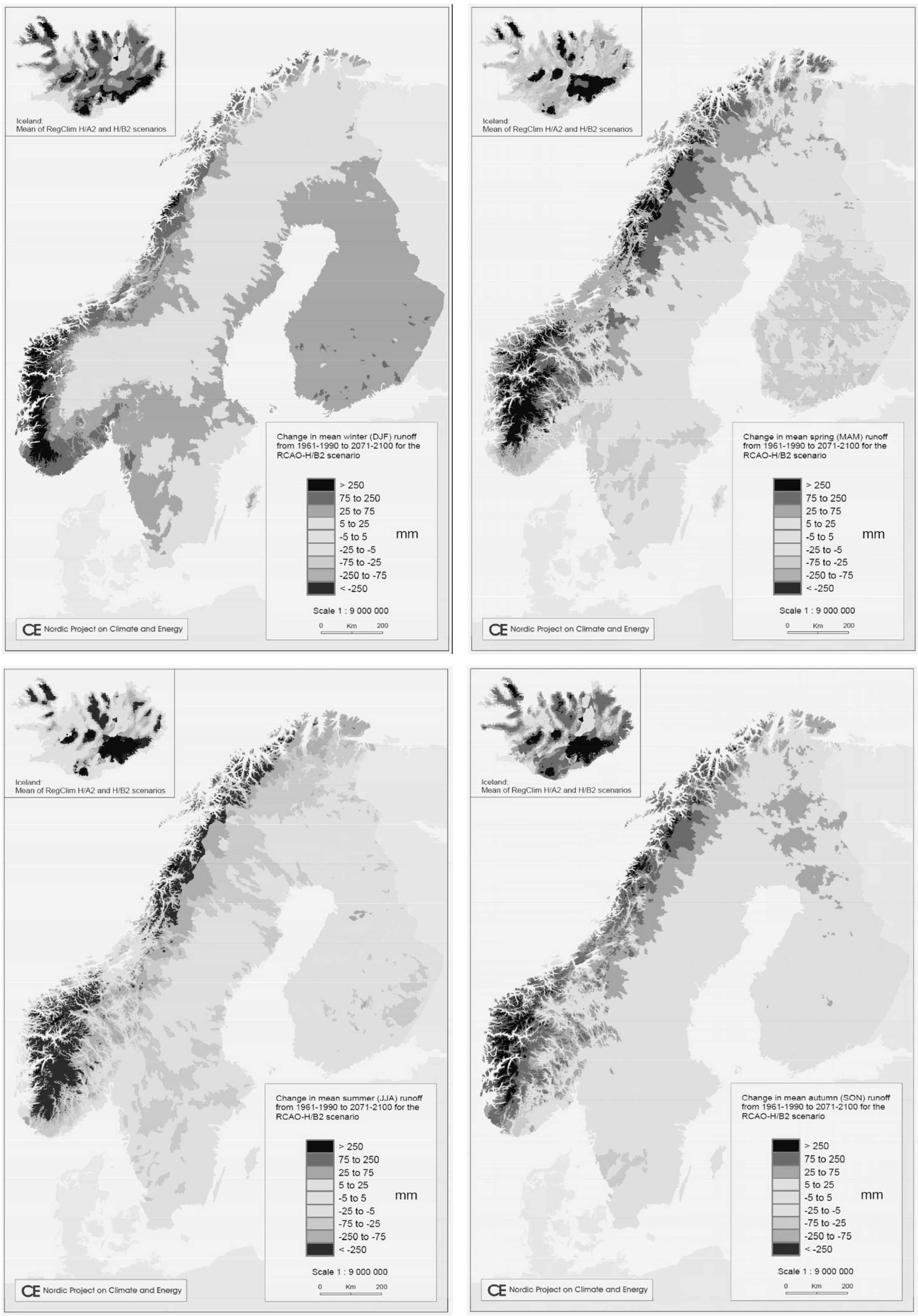

Figure 3. Change in seasonal runoff (mm) for Finland, Iceland, Norway and Sweden from 1961-1990 to 2071-2100 for HadAM3H/B2 scenario. Top left: Winter (Dec., Jan., Feb.). Top right: Spring (Mar., Apr., May). Bottom left: Summer (Jun., Jul., Aug.). Bottom right: Autumn (Sep., Oct., Nov.).

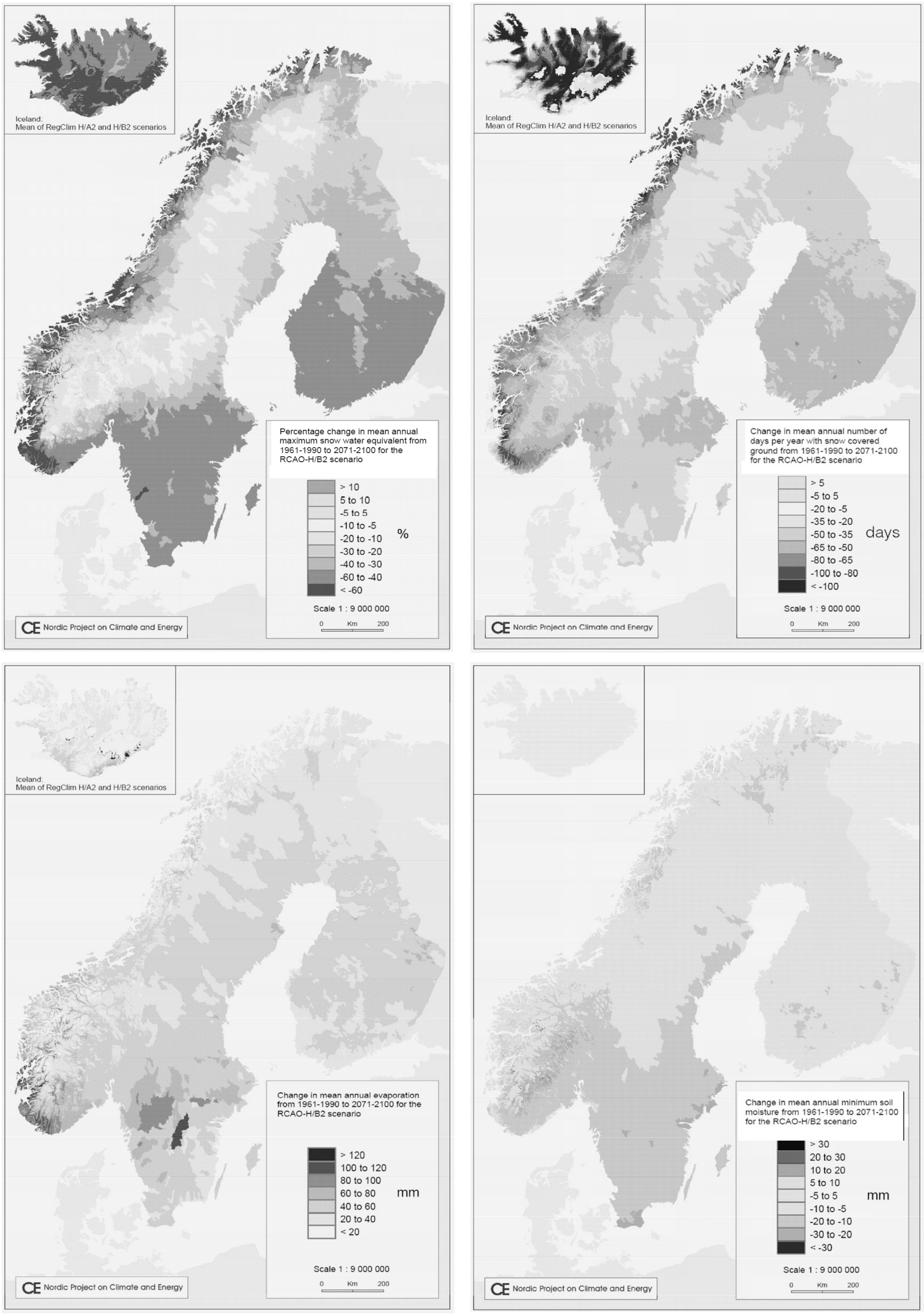

Figure 4. Changes in hydrological characteristics for Finland, Iceland, Norway and Sweden from 1961-1990 to 2071-2100 for HadAM3H/B2 scenario. Top left: Percentage change in mean annual maximum snow water equivalent. Top right: Change in mean annual no. of days per year with snow covered ground. Bottom left: Change in mean annual evaporation (mm). Bottom right: Change in mean annual minimum soil moisture (mm).

Although model structure, process parameterisation, input data and spatial resolution vary between the hydrological models applied in the different countries, the maps present a relatively consistent view of hydrological conditions in the Nordic region. Nevertheless, there are gradients in the values presented by the maps across the borders between Finland, Norway and Sweden. These gradients are too a large extent caused by differences in model structure, model calibration, spatial discretisation and interpolation of precipitation and temperature data to the computational elements of the hydrological models.

5. CONCLUSIONS

Projections of climate change impacts on water resources in the Nordic countries have been quantified using combinations of two greenhouse gas emission scenarios, two general circulation model, two regional climate models and two hydrological models. Overall the maps show an increase in the available water resources, but in some areas dryer conditions are indicated. The latter may be due to decreased precipitation or an increase in evaporation that overrides the increase in precipitation. A closer look at the seasonal maps shows that water shortage may become a problem in some locations for the summer season. The use of several global climate scenarios gives an indication of the involved uncertainties. The hydrological climate change scenarios vary due to different dominance of atmospheric circulation patterns in the general circulation models and different external forcing caused by greenhouse gas emissions.

The results from the CE project show that the impacts of global warming on the hydropower sector can be quite strong. It will shorten the Nordic winter and make it less stable. This leads to more river flow the year around, a profitable situation for the industry. There is also potential for increased production as the highest modelled increase in river flow is simulated in areas with extensive development of hydropower, i.e. the Scandinavian mountains.

Hydrological processes influence the natural environment at a range of spatial and temporal scales through their impacts on biological activity and water chemistry. Furthermore, water is a primary weathering agent for rocks and soils, breaking them down, dissolving them, and transporting the resulting sediments and dissolved solids to the sea. Freshwater discharge and energy fluxes to the ocean, latent and sensible heat fluxes, glacier mass balance, snow cover and permafrost conditions influence the global climate through feedback effects involving atmospheric and ocean circulations. The water resources maps presented in this study are therefore useful for climate change impact studies in natural and social sciences where land surface hydrological conditions exert a major control on the phenomena under consideration.

ACKNOWLEDGEMENT

This study has received financial support from Nordic Energy Research and from numerous national projects. Finland: Ministry of Agriculture and Forestry; Iceland: the National Energy Fund, the Ministry of Industry and the National Power Company; Norway: Norwegian Electricity Industry Association and Research Council of Norway; Sweden: Elforsk, Svenska Kraftnat and Lansforsakringsbolagens Forskningsfond.

REFERENCES

Beldring, S., Engeland, K., Roald, L.A., Sælthun, N.R. and Voksø, A. (2003) Estimation of parameters in a distributed precipitation-runoff model for Norway. *Hydrology and Earth System Sciences* **7**, 304-316.

Beldring, S., Andreasson, J., Bergström, S., Graham, L.P., Jonsdottir, J.F., Rogozova, S., Rosberg, J., Suomalainen, M., Tonning, T., Vehviläinen, B. and Veijalainen, N. (2006) *Mapping water resources in the Nordic region under a changing climate.* CE Report No. 3, CE, Reykjavik, Iceland, 125 pp. ISBN 9979-68-190-X.

Bjørge, D., Haugen, J. E. and Nordeng, T. E. (2000) *Future climate in Norway. Dynamical downscaling experiments within the RegClim project.* Research Report no. 103, Norwegian Meteorological Institute, Oslo, Norway.

Brandt, M. and Ejhed, H. (2002) *TRK Transport - Retention - Kallfordelning. Belastning på havet. ("TRK Transport - Retention - Source Apportionment. Load on the sea", in Swedish).* Naturvardsverket Rapport 5247, Stockholm.

Doscher, R., Willen, U., Jones, C., Rutgersson, A., Meier, H.E.M., Hansson, U. and Graham, L.P. (2002) The development of the regional coupled ocean-atmosphere model RCAO. *Boreal Environ. Res.* **7**, 183-192.

Gordon, C., Cooper, C., Senior, C.A., Banks, H., Gregory, J.M., Johns,T.C., Mitchell, J.B.F. and Wood, R.A. (2000) The simulation of SST, sea ice extents and ocean heat transport in a version of the Hadley Centre coupled model without flux adjustments, *Clim. Dyn.* **16**, 147-168.

Grell, G. A., Dudhia, J. and Stauffer, D. R. (1994) *A description of the fifth-generation Penn State-NCAR Mesoscale Model (MM5).* NCAR Tech. Note NCAR/TN-398+STR, National Center for Atmospheric Research, Boulder, Colorado, 122 pp.

Hay, L.E., Wilby, R.L. and Leavesley, G.H. (2000) A comparison of delta change and downscaled GCM scenarios for three mountainous basins in the United States. *Journal of the American Water Resources Association* **36**, 387-397.

Johannesson, T., Aðalgeirsdóttir, G., Ahlstrom, A., Andreassen, L.M., Bjornsson, H., de Woul, M., Elvehoy, H., Flowers, G.E., Guðmundsson, S., Hock, R., Holmlund, P., Palsson, F., Radic, V., Sigurðsson, O. and Thorsteinsson, T. 2006. The impact of climate change on glaciers and glacial runoff in the Nordic countries. *European Conference on Impacts of Climate Change on Renewable Energy Sources*, Reykjavik, Iceland, June 5-9, 31-34.

Lindstrom, G., Johansson, B., Persson, M., Gardelin, M. and Bergström, S. (1997) Development and test of the distributed HBV-96 model. *Journal of Hydrology* **201**, 272-288.

Nakicenovic, N., Alcamo, J., Davis, G., de Vries, B., Fenhann, J., Gaffin, S., Gregory, K., Grübler, A., Jung, T.Y., Kram, T., La Rovere, E.L., Michaelis, L., Mori, S., Morita, T., Pepper, W., Pitcher, H., Price, L., Riahi, K., Roehrl, A., Rogner, H.-H., Sankovski, A., Schlesinger, M., Shukla, P., Smith, S., Swart, R., van Rooijen, S., Victor, N. and Dadi, Z. 2000. *IPCC Special Report on Emission Scenarios*. Cambridge Univ. Press, 599 pp.

Roeckner E, Bengtsson L., Feichter J, Lelieveld J. and Rodhe H. 1999. Transient climate change simulations with a coupled atmosphere-ocean GCM including the tropospheric sulphur cycle. *J. Clim.* **12**, 3004-3032.

Schulla, J. and Jasper, K. (2001) *Model description WaSiM-ETH*. (PDF available at http://www.iac.ethz.ch/staff/verbunt/Down/WaSiM.pdf, 6 February 2007)

Tveito, O.E. and Roald, L.A. (2005) *Relations between long-term variations in seasonal runoff and large scale atmospheric circulation patterns*. Norwegian Meteorological Institute, met.no report no. 7/2005 Climate, 43 pp.

Vehviläinen, B. and Huttunen, M. (2002) *The Finnish watershed simulation and forecasting system (WSFS).* XXI Conference of Danube Countries on the Hydrological Forecasting and Hydrological Bases of Water Management, Romania, September 2-6.

Measuring snow water equivalent for hydrological applications: part 1, accuracy of observations

Sveta Berezovskaya*, Douglas L. Kane

Water and Environmental Research Center, University of Alaska Fairbanks, PO Box 5860, Fairbanks, Alaska 99775, USA
**Corresponding author, e-mail:* ffslb2@uaf.edu

ABSTRACT
An experiment in northern Alaska has been carried out to evaluate the accuracy of snow water equivalent (SWE) estimations in tundra snowpack. In northern basins, water constrained in the snowpack contributes significantly to both the seasonal and annual water balance. It is critical to realize and address the problems of measuring and processing observational snow data so that this data can be used properly to advance understanding of changes in hydrological systems. A combination of well-developed depth hoar at the base of tundra snowpack and extensive surficial organic soils in permafrost regions can significantly affect snow water equivalent and snow depth sampling accuracy. Experiment in Alaska's Arctic suggest that end-of-winter SWE can be overestimated from 4 to 20% depending on the sampling techniques applied. This error results from the fact that the depth of tundra snowpack is often overestimated. As observers probe the snow depth, it is difficult to recognize the snow-ground interface, and organic material is often incorporated into the snowpack depth estimate. This causes the average snow depth to be overestimated by 11 to 31%.

KEYWORDS
Arctic, Alaska, snow water equivalent, snow depth, tundra snowpack

1. INTRODUCTION

One of the themes highlighted for the 16th International Northern Research Basins Symposium is better understanding of time-space changes in hydrological systems. Our study approaches this task in terms of data quality and accuracy issues. In high latitude watersheds, end-of-winter snow water equivalent (SWE) is a key input for snowmelt runoff analysis and prediction. Even though researchers have made great advances in developing modeling tools to describe snow evolution processes (Liston and Elder, 2006; Liston *et al*., 2007), we still face the challenge of reproducing spatial and temporal snow cover variability accurately, due to the complex interactions involved and limited observational data available for the remote arctic regions. The few snow data available are often marred by problems of measuring and processing. If we can successfully address these limitations, snow data can be used properly to advance our understanding of changes in hydrological systems.

This study is aimed at evaluating estimates of basin average end-of-winter SWE measured in tundra snowpack. Our data comes from Alaska's Arctic, north of the Brooks Range. This area is characterized by *tundra snow*, which differs from lower latitude snowpack in that it is colder, on average shallower, and host to steeper temperature gradients (Benson and Sturm, 1993). Certain properties of tundra snowpack affect SWE sampling accuracy. First, it consists of hard, high-density, wind-packed layers that can be difficult to penetrate with snow sampling instruments. Second, a coarse, lower density depth hoar layer prevails at the base of the snowpack (Sturm and Benson, 2004). Depth hoar crystals can easily fall out of the SWE sampler, so observers have to take care to ensure that the whole snow column is captured.

The snow-ground interface is usually a subtle boundary of large depth hoar crystals and soft organic material. The presence of the organic layer over impermeably frozen mineral soil is typical for Alaska's Arctic. On permafrost sites, lower annual soil temperatures cause reduced rates of plant debris decomposition. As a result a thick, dense ground cover (moss, lichens, vascular plant roots and litter) effectively insulates the mineral soil, lowering soil temperatures and furthering development of organic material referred to as the "*organic layer*". The depth of this organic layer is about 10 - 20 cm, but in some places depth can reach 50 cm (Slaughter and Kane, 1979). By winter's end, the organic layer is very desiccated. The steep temperature gradient within the snowpack, accompanied by a steep vapor pressure gradient, leads to a vertical flux of water vapor, up to 0.025 g cm^{-2} day^{-1} (Slaughter and Benson, 1986). The vertical gradient can cause up to 50% of the water initially available in the organic layer to migrate into the snowpack over the course of the winter.

As far as snowpack measurements go, a snow depth probe can easily penetrate this fluffy, relatively dry organic mat, so it is often inadvertently incorporated into the measured snow depth. This brief paper addresses how the organic layer affects snow depth measurements and snow water equivalent estimates of tundra snowpack. The discussion below covers SWE sampling techniques, results of a snow depth accuracy experiment, and the effect of snow depth overestimation on SWE.

2. SWE SAMPLING TECHNIQUE

The standard method of obtaining SWE is by gravimetric measurement using a sample core. This method serves as the basis for snow surveys in many countries and allows researchers to determine the depth, average density and water equivalent of snowpack. A snow survey usually includes both gravimetric SWE sampling and snow depth measurements collected over a large area; this technique is often referred to as "double sampling". Snowpack is extremely heterogeneous in Alaska (Sturm and Benson, 2003). Double sampling yields an areal SWE estimate with a lower variance than is possible by collecting snow cores only. Rovansek *et al*. (1993) showed that double sampling provides improved SWE estimates and recommended sampling 12 to 15 snow depths for each snow core. However, this optimal ratio of snow depths to water equivalent appeared to vary greatly (from 1 to 23), depending on weather and snow conditions. Currently, we use an optimal ratio of 10; that is, five snow cores are accompanied by 50 depths, taken every 1 meter along a randomly chosen L-shaped transect.

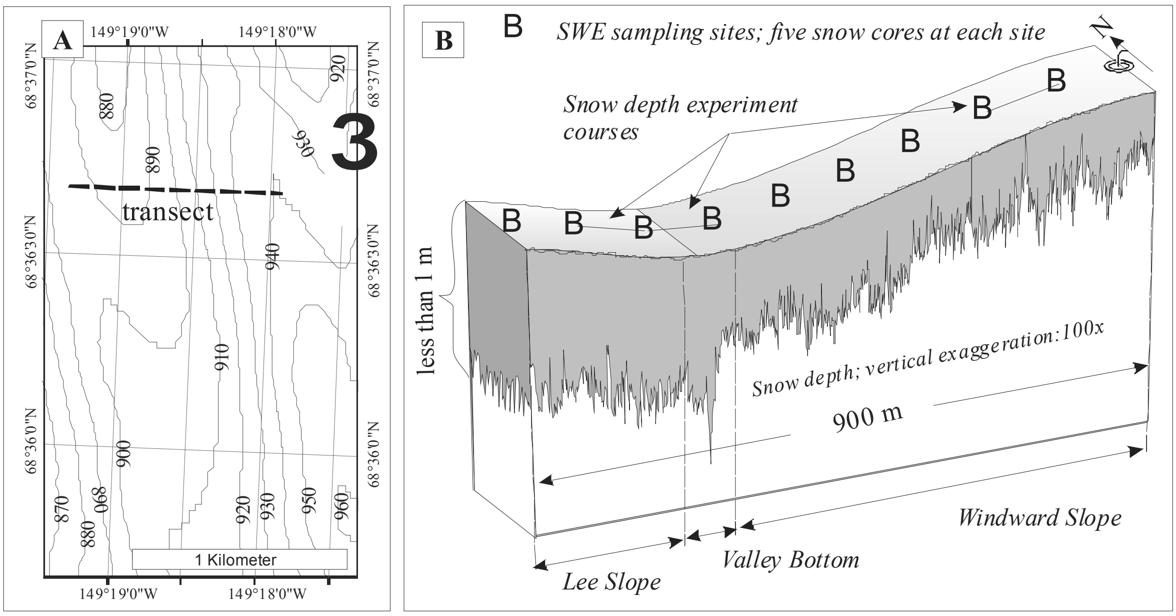

Fig. 1. The Imnavait Creek basin at the Kuparuk River headwaters (A). The Imnavait Creek basin "east to west" transect (B).

Snow cores are sampled using fiberglass tube ("Adirondak") with an inside area of 35.7 cm^2, equipped with metal teeth on the lower end to cut through dense layers. The advantage of the Adirondak for shallow snowpack is that it has a larger diameter than many other types of snow tubes and thus provides a larger sample. To obtain a snow core, the Adirondak tube is pushed vertically through the snow; at this point the

snow depth is recorded. The tube is then driven further into the organic layer and tipped sideways, retaining the vegetation plug that ensures the complete snow column was sampled. The vegetation plug is then removed and the snow is collected to be weighing later, in the laboratory. This procedure allows estimating both snow density and snow water equivalent.
To obtain areal average snow depth, an additional fifty depth measurements are collected using a T-shaped graduated rod (T-probe). The probe is simply pushed through the snow to the snow-ground interface, often including some organic material into the estimated snow depth. To quantify this effect on a basin's average snow depth, we conducted a snow depth experiment (see section 6) in the Imnavait Creek basin.

3. IMNAVAIT CREEK BASIN DESCRIPTION

The study domain covered 2.2 km^2 of Imnavait Creek, a sub-domain of Alaska's Arctic, located in the northern foothills of the Brooks Range at 68.613°N, 149.32°W (Figure 1A). The topography of Imnavait Creek is characterized by gently rolling hills best described by wavelengths of 1 km and amplitudes of 25-75 m. The hills are elongated on south- and north-trending ridges. The west-facing slope is much gentler and longer than the east-facing slope; it constitutes 78% of the basin area.
The Imnavait Creek watershed falls within a large region of sedge tussocks and mosses that cover much of northern Alaska. Occasional groupings of willows, approximately 40 cm high, occur in hillside water tracts and in the valley bottom. The surface organic soils vary from live organic material at the surface to partially decomposed organic matter between 10 and 20 cm in depth. Silt, overlying a glacial till, makes up the mineral soil (Kane *et al*, 1989). Overall, the topography and vegetation of Imnavait Creek are representative of the foothills area north of the Brooks Range.

4. DATA

Snow depths were collected every meter across the Imnavait basin transect (Figure 1A). In 2006, 900 snow depths were taken using the standard snow sampling technique, and 300 snow depths were measured within the snow depth experiment (see section 6). In addition, 50 snow water equivalent samples were taken along the same transect. It should be noted that research teams in this area measure 900 snow depths and 50 SWE every year at the peak of snow accumulation, usually at the end of April. Most of the data in this study are from 2006, unless another year is specified.

5. SNOW DEPTH EXPERIMENT

This simple snow depth experiment included sampling by two methods. First, snow depths were taken every meter along a 900 m transect of the Imnavait Creek basin by experienced observer. Further, we refer to these snow depth as *"standard"*.
Second, measurements were taken at the top and bottom of the snowpack, through the three 100 m courses in the valley bottom, and on the windward and lee slopes (Figure 1B). The probe was pushed though the snow until it hit impermeable ground. The first record was taken at the top of the snowpack. Afterwards, the snow was shoveled to create access to the snow-ground interface, and the second record was taken at the bottom of the snowpack (Figure 2). As snowpack forms, snow grains fill in the upper vegetation; the boundary is fuzzy and determining the bottom of the snowpack is quite a subjective process. For this study, the "bottom" was assumed to be when, to visual observation, the interface appeared to be more than 80% vegetation by volume. This sampling method, even though fairly labor intensive, yields measurements that more closely reflect real snowpack depth. Further, the difference between the top and bottom records is referred to as *"true"* snow depth, as this number represent our most accurate efforts.
Results showed that the average depth of organics is 10 cm on leeward and windward slopes, ranging from 0 to 24 cm. Average organic layer depth for the valley bottom course is slightly less (8 cm) due to the presence of ice in the channel (Table 1). True snow depths were compared against the standard snow

depths. Figure 3 suggests that standard snow depth is generally overestimated in the Imnavait Creek area. For 2006, the average difference between standard and true depths is 9 cm for the slopes and 5 cm for the valley bottom. Given the relatively shallow snowpack, overestimation is about 11-31% of snow depth (Table 1).

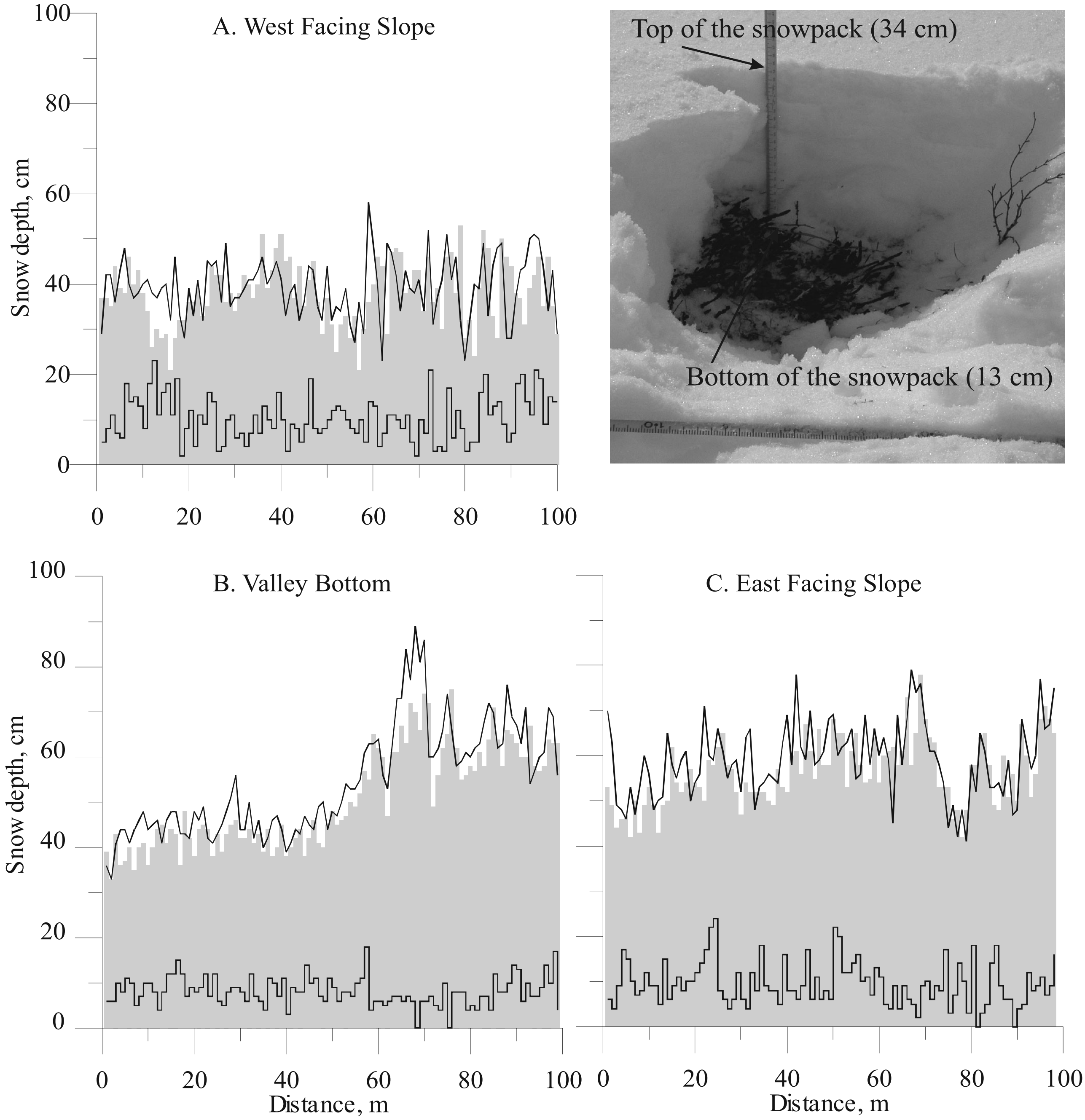

Fig. 2. Snow depth experiment. Top black line shows observations taken at the top of snowpack from impermeable frozen ground; black step line shows observations taken at the bottom of the snowpack (i.e. 0 is ice on the river channel). Grey filled area represents standard snow depth measurements.

Table 1 - Impact of organic layer on snow depth measurements, based on 100 points sampled at each location.

Snow depth, cm	Valley Bottom	Lee Slope	Windward Slope
Standard snow depth	51	57	38
Top*	54	58	39
Bottom*	8	10	10
True snow depth	46	48	29
Difference	5	9	9
Difference, %	11	16	31

* Rod is pushed all the way to the impermeable ground. First record is taken at the top of the snowpack. Afterwards, hole is shoveled to take a record at the bottom of the snowpack. The difference between two is assumed to be a "true" snow depth.

6. EFFECT SNOW DEPTH OVERESTIMATION ON SWE ESTIMATES

Snow water equivalent is defined as

$$SWE = (SD * \rho_s) / \rho_w \tag{1}$$

where ρ_s is snow density, ρ_w is water density and SD is snow depth. Alternatively, snow water equivalent can also be formulated without snow depth. Density is defined as the ratio of mass per unit volume. Since the mass of the sample is the same whether it is snow or water, the relationship can be expressed using respective densities and volumes.

$$\rho_s * A * SD = M = \rho_w * A * SWE \tag{2}$$

where A is the inside area of the probe and M is the sample mass (water or snow). Snow water equivalent can also be defined as

$$SWE = M / (\rho_w * A) \tag{3}$$

In the following discussion, SWE estimated from Eq. 1 is referred as "*standard" SWE* and SWE estimated from Eq. 3 is called "*core" SWE*. Core SWE is estimated without using any snow depth information.

To mitigate any individual snow depth measurement errors, the basin water equivalent was estimated from fifty core SWE samples. Ten SWE sites (5 samples at each site) are equally distributed along the Imnavait transect at 100 meter interval (Figure 2). Since these sites are regularly distributed across the basin, capturing all terrain and vegetation classes, we assume that 50 SWE samples provide a reasonable basin average.

Table 2 - Basin average SWE, estimated from the standard sampling technique (standard), average transect snow depth and basin average density (transect) and fifty snow cores without snow depth measurements (snow cores).

Year	Snow cores	Standard	%	Transect	%
2001*	119	126	6	129	9
2005	119	124	5	123	4
2006	80	95	19	90	12
2007	100	120	20	112	12

* Forty snow cores were sampled in 2001, four at each site.

Core SWE often underestimates the water amount contained in the snowpack (M.Sturm, personal communication). In attempting to quantify underestimation in shallow tundra snowpack conditions, Woo *et al.* (1997) showed that a larger tube diameter increases the accuracy of density determination; he also showed that the Canadian sampler (similar to the Adirondak in diameter) captures snow density within 5% of snow pit estimates. In May 2007, we compared Adirondak densities versus stratigraphic method densities and observed similar results, i.e. sometimes Adirondak underestimated snow densities. For further analysis, we assume that in average Adirondak accuracy varies from 0 to 5 %.
Results show that the standard procedure (five snow densities together with fifty snow depth measurements) yields an estimated 95 mm of SWE in the Imnavait basin. Often many (on the order of 1000) snow depths are sampled along the traverse at 1 m intervals, and then snow density is used to estimate areal SWE (Eq. 1). The transect average snow depth, together with the average density based on the snow cores, yields 90 mm SWE. An average of 50 snow cores suggests that there is 80 mm SWE in the basin. Table 2 shows that in 2001, 2005 and 2006, standard and transect double sampling techniques provide larger amounts of water in the snowpack compared to the core SWEs. Given that snow depth is overestimated, the standard double sampling technique can overestimate SWE up to 20%. SWE estimated by the transect technique is 4 - 12% higher than snow coring.

7. DISCUSSION

As shown above, using average snow depth, acquired with standard snow depth probes, to calculate SWE can cause overestimation of tundra snowpack water content. The difficulty in these interpretations is that actual, accurate SWE is unknown.
Any type of correction to existing snow depth records is difficult to effect, because the error varies strongly from observer to observer, as well as depending on the snow and soil conditions at each site. Avoiding snow depth overestimation will require either adjusting instrumentation or modifying sampling technique. For reliable snow depth observations, instrumentation should reach the ground, but does not penetrate further into the organic material.
Given the extreme snow cover heterogeneity, particularly in the Arctic tundra, we still believe that the double sampling technique gives a reasonable estimate of *spatial snow variability* at each site (Kane and Berezovskaya, 2007). This information can be used to locate a representative place to sample snow cores and to estimate snow water equivalent from snow cores only. For example, at each site an observer would still take 50 depth measurements, then use these to locate an average spot for snow core sampling.

8. CONCLUSIONS

This study suggests that snow water equivalent from any type of double sampling technique tends to overestimate SWE. The experiment in the Imnavait Creek area shows that the depth of tundra snowpack is typically overestimated, because low density organic material (overlaying impermeably frozen ground) may not always be distinguished by the probing observer. Error is larger for the sedge tussocks areas on the windward slopes with shallow snow cover and decreases toward the valley bottom due to the snow-river ice interface at the bottom of the snowpack. In April 2006, the average snow depth based on 100 points courses was overestimated from 11 to 31%. Whereas snow depths show a systematic overestimation error, estimations by snow core tend to be close to, or to underestimate, SWE. The difference between snow core and double sampling SWEs varies from 4 to 20%. The reality is that the true SWE values lie somewhere in between.

ACKNOWLEDGMENTS

UAF/WERC faculty, staff and students collect snow data each year; we greatly appreciate their contribution. Field work by Molly Chambers and Ken Irving contributed a great deal. The authors also greatly appreciate valuable suggestions made by Matthew Sturm. This work is supported through the National Science Foundation, Office of Polar Programs, grant no. OPP-0335941.

REFERENCES

Benson, C.S., W. Harrison, J. Gosink, L. Mayo and D. Trabant (1986) The role of glacierized basins in Alaskan Hydrology, in Kane, D.L., ed., *Symposium: Cold Regions Hydrology: American Water Resources Assoc.*, 471-483

Benson, C. S. (1982) Reassessment of winter precipitation on Alaska's Arctic Slope and measurements on the flux of wind blown snow. *Geophysical Institute, University of Alaska Report UAG R-288*, September 1982, pp.26

Benson, C. S. and M. Sturm (1993) Structure and wind transport of seasonal snow on the Arctic Slope of Alaska. *Annals of Glaciol.,* **18**, 261-267

Kane, D.L. and S. Berezovskaya (2007) Strategies for measuring snow water equivalent for hydrological applications: part 2, spatial distribution. *16th Northern Research Basin Symp* this volume, Petrazovodsk, Russia, Aug 27 – Sep 2.

Kane, D.L., Hinzman, C. S. Benson and K. R. Everett (1989) Hydrology of Imnavait Creek, an arctic watershed. *Holarctic Ecology* **12**, 262-269

Kane, D.L., L.D. Hinzman, C.S. Benson and G.E. Liston (1991) Snow hydrology of a headwater arctic basin 1. Physical measurements and process studies. *Water Resources Research*, **27**(6), 1099-1109

Kane, D.L., J.N. Luthin and G.S. Taylor (1978) Heat and mass transfer in cold regions soils. *IWR-65, Institute of Water Resources*, UAF

Liston, G. E. and K. Elder (2006) A distributed snow-evolution modeling system (SnowModel). *J. Hydrometeorology*, **7**, 1259-1276

Liston G.E., R. B. Haehnel, M. Sturm, C. A. Hiemstra, S. Berezovskaya and R. D. Tabler (2007) Simulating Complex Snow Distributions in Windy Environments using SnowTran-3D, *J. Glaciology*, **53**(181), 241-256

Rovansek, R.J., D.L. Kane and L.D. Hinzman (1993) Improving estimates of snowpack water equivalent using double sampling. *Proceedings of the 61st Western Snow Conference*, 157-163

Sturm, M. and C. S. Benson (2004) Scales of Spatial Heterogeneity for Perennial and Seasonal Snow Layers. *Annals of Glaciol.* **38**, 253–260

Woo, M-K (1997) A guide for ground based measurement of the arctic snow cover. *Canadian Snow Data CD*, Meteorological Service of Canada, Downsview, Ontario, p.30

Effect of climate and morphometry on thermal regime of lakes

Tatiana Efremova*, Nikolai Palshin

Northern Water Problems Research Institute, A. Nevskogo, 50, Petrozavodsk,
Rep. of Karelia, 185030, RUSSIA
**Corresponding author, e-mail: efremova@nwpi.krc.karelia.ru*

ABSTRACT

Generalized from long-term (1945-1989) observational data on water temperature at stations of the Hydrometeorological Service network that describe reservoirs of different types in northwestern Russia, empirical relationships of the thermal regime on various geographical factors are established (lake morphometry, geographical latitude and altitude above sea level, residence time). We have demonstrated that for stable thermal stratification to emerge, a lake must have a certain combination of geometric parameters. Regional boundaries between epi-, meta- and hypothermal types of lakes have been quantified depending on the area and maximal depth of the lakes. Analysis of the results has shown that the temperature in the upper 5 m layer of water mainly depends on the latitude, whereas at a depth of more than 10 m it is more significantly affected by the lake morphometry, inflow and outflow of rivers. Modeled curves describing average annual daily surface temperature values for lakes of different size and depth were received with use of the 6-parameter regression function. All parameters are dimensional and have a clear physical interpretation. This feature favorably distinguishes the function from previously published regression models.

KEYWORDS

Vertical thermal structure, regression model, stratification, epilimnion depth, “biological summer”, geographical factors

1. INTRODUCTION

The water temperature is one of the main factors that govern the rate of biological processes in reservoirs. The relationships between fetch and depth at which a lake would be stratified have earlier been quantified by Lathrop & Lillie (1980), Patalas (1984), Gorham & Boyce (1989). Birge and colleagues made the first description of the water temperature in a lake by means of the continuous function (Birge et al., 1927). Strashkraba (Strashkraba and Gnauk, 1989) has used a harmonic function for the description of the annual cycle of surface temperature and bottom layer in ice-free lakes and rivers in accordance to geographical zoning. The functional description of the average daily cycle of water surface temperature was carried out for Great American Lakes (Lesht and Brandner, 1992) and lakes in Europe (Efremova and Petrov, 1992; Naumenko et al., 2000). The purpose of this investigation was to quantify the effect of climate and morphometry on the thermal regime of lakes.

2. MATERIALS AND METHODS

Analysis of the average annual vertical temperature distribution was based on data received in fifty eight lakes located in North-Western Russia, 55-70°N, (1958-1989), and in eight Finnish lakes (1961-1975) (Kuusisto, 1981). Seasonal variability of average annual water surface temperature was studied using data on 52 lakes of North-Western Russia collected during a period of 1945-1980 at stations of the Russian Hydrometeorological Service network, and data on two Finnish lakes summarized by the Finnish Hydrometeorological Service network (1961-1991) (Figure 1).

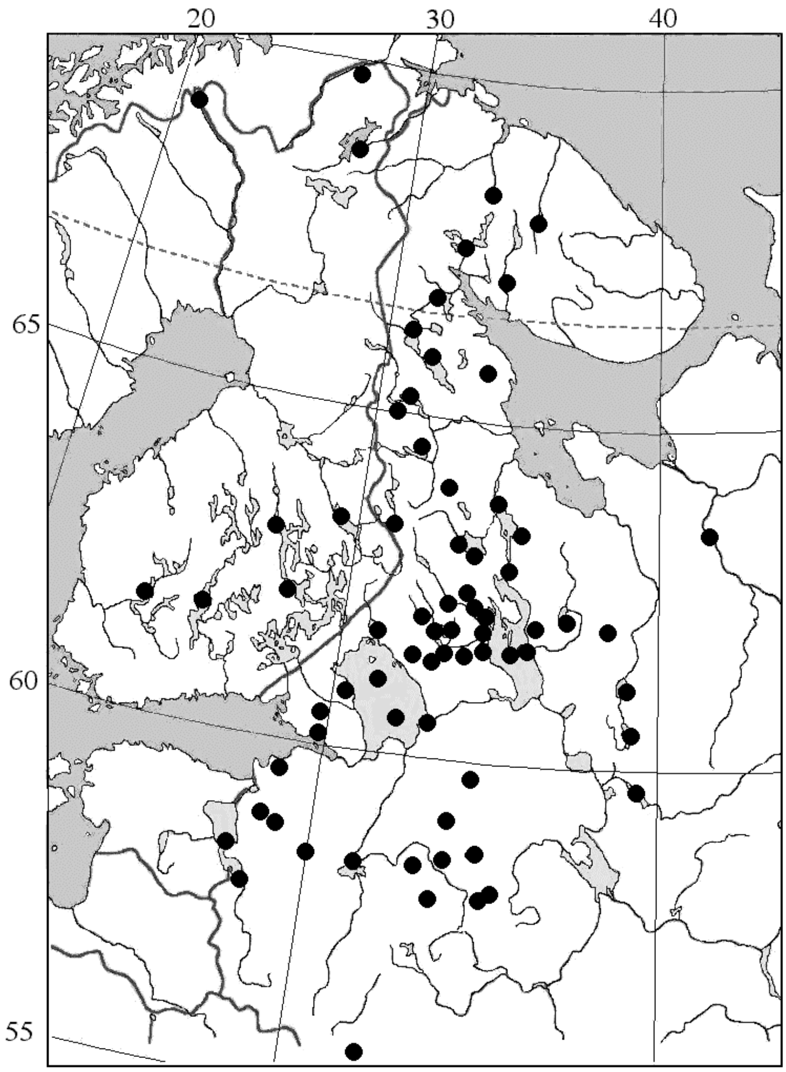

Figure 1. Map of study area and the investigated lakes.

Morphometric features of lakes vary in a wide range: from the largest lakes of Europe – Ladoga and Onego – to the small lakes with area less than 1 km^2. The range of some characteristics of the lakes studied is shown in Table 1. Preliminary statistical analysis shows that there is no correlation between geometric sizes of lakes and latitude, altitude, residence time (R< 0.25). Correlations between the area size and average or maximum depth of research lakes are not high (R < 0.5).

Table 1 Characteristics of the lakes studied

Parameter	Range
Latitude, deg.	55º37` - 69º46` N
Longitude, deg.	20º30` - 41º32` E
Altitude, m asl	4.5 - 463
Area, km^2	0.65 - 17,872
Mean depth, m	1.6 - 46.9
Max depth, m	5 - 230
Volume, km^3	0.002 - 837.9
Residence time, year	0.01-16.7

Registrations of water temperature in these lakes have a different length from 10 to 35 years. This causes some heterogeneity of data, however, general trends of dependency of water temperature from zonal climatic effects and morphometric characteristic are retained. The data were statistically treated using the Newton nonlinear estimation method and multiple regression analysis. We made up the equation and selected the main geographical factors (latitude, altitude, area of lakes, average of the lake depth, depth at the sampling point, inflow and outflow of rivers), exerting influence on water temperature in the lakes. Verification of the stochastic models has been performed with observational data which were excluded from the process of definition of regression relationships.

3. RESULTS

3.1. Types of thermal structure in lakes

The relationship between the stratification type and maximum depth (H_{max}, m) and the area (S, km^2) of the lakes was determined. Location of the lakes in different climatic areas (55-70ºN) causes certain difficulties with their clustering. Therefore, boundaries between hypo-, epi- and metathermal types of lakes (Figure 2) were drawn by the dimensionless temperature Θ,

$$\Theta = \frac{\overline{T}_H - T_{md}}{\overline{T}_0 - T_{md}},$$

where $\overline{T}_0$ and $\overline{T}_H$ are average annual temperatures of the surface and near-bottom layers in late July – early August; T_{md} – temperature of max density.

Empirical formulae for (h_1, h_2) boundaries between different types of lakes have been obtained,

$$h_1 = 6{,}43 + 3{,}51 \lg S \qquad \text{when } \Theta = 0{,}7; \qquad (1)$$

$$h_2 = 17{,}78 + 8{,}55 \lg S \qquad \text{when } \Theta = 0{,}3, \qquad (2)$$

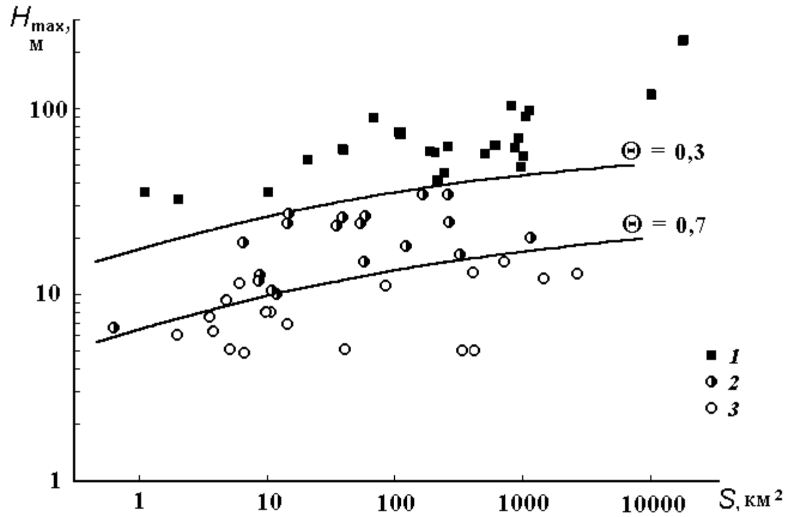

Figure 2. Relationship between stratification of lakes and their area and max depth. *1-3* are hypo-, meta- and epithermal lakes, respectively.

Deeper lakes (hypothermal, $\Theta < 0.3$) are typical representatives of the dimictic lake class with three vertical strata: epi-, meta- and hypolimnion. The water mass in shallow lakes (epithermal, $\Theta > 0.7$) shows transient thermal stratification in summer and occasionally gets overturned down to the bottom due to the wind action or because of water cooling. Medium-depth lakes (metathermal, $0.3 \le \Theta \le 0.7$) normally have two strata that are the upper quasihomogeneous and the lower stratified.

Contrary to the three-class grouping suggested above, Lathrop & Lillie, Gorham & Boyce have grouped the lakes into two classes: stratified and unstratified, wherefore the differentiation limits are different (Table 2). Patalas has clustered the lakes into three classes relying on the depth of epilimnion in relatively deep-water lakes (h_e/H_{max} ~1.0 – homothermal lakes; 0.5 < h_e/H_{max} < 0.9 – lakes with two strata – epilimnion and thermocline; h_e/H_{max} < 0.5 – a three-layer system with epilimnion, thermocline and hypolimnion). For lakes of northwestern Russia, the ratio of epilimnion depth to h_1 and h_2 calculated by formulae (1) and (2) are 0.8-0.9 and 0.3-0.4.

Table 2 Epilimnion depth (h_e), thermocline depth (h_t) and depth needed for stratification to emerge (h_s, h_1, h_2)

L, km	h_e, m		h_t, m		h_s, m		h_1, m	h_2, m
	Patalas	Formula (3)	Araj	Gorham, Boyce	Lathrop, Lillie	Gorham, Boyce	Formula (1)	Formula (2)
1	4.6	4.8	6.2	6.4	7.3	10.8	6.4	17.8
2	6.1	7.1	7.7	8.4	10.3	15.2	8.5	22.9
3	7.2	8.4	8.7	10.4	12.6	18.6	9.8	25.9
4	8.1	9.3	9.5	12.4	14.5	21.5	10.7	28.1
5	8.9	10.0	10.1	14.4	16.3	24.0	11.3	29.7
6	9.6	10.6	10.7				11.9	31.1
7	10.2	11.1	11.2				12.4	32.2
8	10.8	11.5	11.7				12.8	33.2
9	11.3	11.9	12.1				13.1	34.1
10	11.8	12.2	12.5				13.5	34.9

Using data collected by Patalas (1984) from lakes situated in different climatic zones (170 lakes of North America, Poland and Japan) a new formula (3) has been suggested for calculating the epilimnion depth (h_e), which takes not only the fetch (L), but also the geographic latitude (φ) into account.

$$h_e = 4{,}83 + 0{,}119\,\varphi \lg L \quad (r = 0{,}88;\ \text{rms} \pm 1{,}56). \qquad (3)$$

Corrections to h_e from φ proved to be not very high but significant. The prevalent wind mixing mechanisms are different in lakes of different geometric sizes. To estimate how this factor related to the fetch tells on the epilimnion depth we divided the sample into three groups (for small lakes L < 5.5 km, for small and medium-size lakes L < 15 km, for all 170 lakes, including largest ones with $L \leq 33$ km) and found empirical relationship for them.

Close values of regression coefficients and absolute terms in the formulae evidence the stability of the relationships. Estimates of h_e by the above formulae within the L ranges under consideration show a <0.2 m divergence of the calculated values. Thus, the common formula can be employed to calculate h_e for both small and large lakes with areas up to 1000 km^2 situated between 45º and 66º N.

3.2 Vertical thermal structure

The vertical thermal structure of lakes was evaluated on data of measured water temperature on standard horizons 0.1, 2, 5, 10, 15, 20, 25, 30, 40 m. For the analysis we choose the period with the direct thermal stratification under the maximum heat content in lakes (20 July –10 August). We found that an average annual water temperature on different depths in lakes can be represented by following regression equation:

$$T(z) = a_0 + a_1(72 - \varphi) + a_2 Z + a_3 \lg S + a_4 \left(\lg \overline{H}\right)^2 + a_5 h + a_6 \lg K + a_7 E\,, \qquad (4)$$

where φ is latitude of a sampling station (deg); Z altitude (m); S area of lake (km^2); $\overline{H}$ its mean depth (m); h the depth at the point of measurement (m); K residence time (year); $E = S/\overline{H}$ is an openness factor. Parameters $a_0 - a_7$ for different depths are shown in the Table 3, the coefficients of multiple-regression correlations and standard deviations are also computed.

Table 3 Coefficients of multiple-regression correlations *(R)*, standard deviations of water temperature (ε) and parameters $a_0 - a_7$ for different depths (z) equation (4).

z, m	R	ε	Parameters							
			a_0	a_1	a_2	a_3	a_4	a_5	a_6	a_7
0	0,94	0,78	14,16	0,564	-0,0048	-0,12	-0,31	-0,004	0,095	-0,0058
2	0,93	0,78	13,52	0,554	-0,0048	-0,04	-0,31	-0,004	0,103	-0,0059
5	0,86	1,09	11,69	0,553	-0,0033	0,52	-0,66	-0,012	0,364	-0,0054
10	0,83	1,36	8,22	0,391	0,0025	2,14	-1,25	-0,035	1,663	-0,0049
15	0,86	1,09	5,70	0,227	0,0085	2,45	-1,45	-0,029	2,253	-0,0039
20	0,89	0,86	4,94	0,214	0,0097	2,25	-1,50	-0,020	2,141	-0,0049
25	0,92	0,70	2,78	0,261	0,0112	2,00	-1,39	-0,006	1,992	-0,0058
30	0,95	0,63	2,22	0,282	0,0115	1,72	-1,32	-0,000	1,934	-0,0059
40	0,97	0,53	1,73	0,280	0,0115	1,52	-1,11	-0,001	1,754	-0,0058

Change of parameters $a_0 - a_7$ with depth proves a successfully selected regression model. Their vertical distribution shows that zonal effects mostly influence the water temperature in upper layer of lakes. Correlation coefficients (r) between the water temperature on depths 0-5 m and latitude are 0.77 - 0.84. Notice that with increasing depth dependency of water temperature on φ drops down, but it increases on morphometric effects and water flowage. Increase of lake areas leads to the slight reduction of water temperature on depths 0 - 2 m (parameter a_3) and to essential rise of temperature at depths of 10 m and more in hypolimnion. If a mean depth in lakes increases, the water temperature on standard horizons (parameter a_4) decreases. Depth at the point of measurement (a_5) was used for taking into account heterogeneity of the average field of temperature in large deep lakes. For through-flow lakes, small increase of water temperature in the upper layer (0 – 2m) and considerable increase in the thermocline and hypolimnion is typical (parameter a_6). Vertically averaged profiles of the temperature distribution in some lakes, measured and calculated with use of the Eq. (4), are shown in Figure 3.

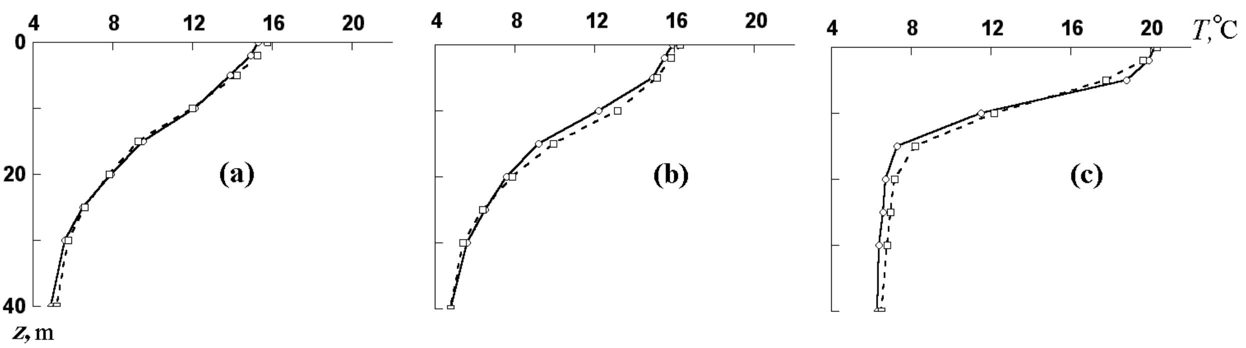

Figure 3. Comparison of the computed (dotted curve) and observed (solid curve) average temperature profiles for a) – Topozero, b) – Onego c) – Valdaiskoye lakes

Obviously, a simple regression model can not take into account all effects related to the seasonal development of the thermal structure in lakes. The main advantage of this model is it’s ability to reconstruct a vertical distribution of the water temperature in lakes that is very important in certain application.

3.3. Annual cycle of the surface temperature in lakes

On the first stage, our purpose was to fit a specific function for each lake to describe the climatology of the surface temperature cycle with use of data observed. Function, which we use, is written as follows:

$$T(t,z) = b_0 + b_1\left\{1 - \frac{1-\exp\left[(t-b_2)b_3\right]}{1+\exp\left[(t-b_2)b_3\right]}\right\}\cdot\left\{1 + \frac{1-\exp\left[(t-b_4)b_5\right]}{1+\exp\left[(t-b_4)b_5\right]}\right\}, \quad (5)$$

where *T(d)* is surface temperature (˚C); d time counted from 1st January (days); $b_0 - b_5$ are empirical parameters.

In our model, we consider the open-water period as time from ice melting in spring till ice formation in late autumn. To find parameters of the model for each lake that results in the lowest mean-squared error between the function and observed data, we used the Newton method. In Eq. (5) two parameters (b_0 and b_1) are related to the min and max function, two non-dimensional parameters (b_3 and b_5) are related to the shape of distribution (asymmetry and kurtosis), and two parameters are related to the dates of maximum growth in spring (b_4) and decrease in autumn (b_2) of surface water temperatures.

On the following stage, we investigated dependencies of model parameters simultaneously from zonal climatic effects, geometrical sizes of lakes, and water exchange. To solve this problem, we used values b_i for all lakes to get a simple expression, common for all parameters, with limited numbers of predictors. We found that the best regression equation is as follows,

$$b_i = a_0 + a_1(72-\varphi) + a_2 Z + a_3 \lg S + a_4(\lg \overline{H})^2 + a_5 \lg K + a_6 P, \quad (6)$$

where $P = \overline{H}/H_{max}$ is a capacity factor. Parameters $a_0 - a_6$ for calculating different model parameters b_i are shown in Table 4, where also multiple-correlation coefficients are placed.

We have established that latitude, area of lakes, and their mean depth mostly influence model parameters b_i and the average annual cycle of water surface temperature. Influence of altitude on the water surface temperature for the given sample of lakes is small, as all lakes are situated within a range 0-200 m. Notice that all model parameters b_i are connected to each other and changing one of them leads to the change of others. The minimal temperatures (parameter b_0) depends on the area of lakes mainly, and maximum temperatures (parameter b_1) from latitude. At the same time, velocity of temperature reduction during the autumn period (parameter b_3) is dependent mainly from the depth of lakes.

Table 4 Parameters a_0 - a_6 for Eq. 6 and multiple-correlation coefficients.

b_i	R	Parameters (Eq. 6)						
		a_0	a_1	a_2	a_3	a_4	a_5	a_6
b_0	0,958	-4,5963	-0,0311	-0,00144	0,984	-0,507	-0,242	-1,17
b_1	0,986	5,3717	0,134	-0,00149	-0,347	0,647	0,129	0,112
b_2	0,838	271,68	0,842	-0,0287	-3,863	0,138	-1,130	-5,09
b_3	0,941	-0,0429	0,00071	-0,00002	-0,00191	0,00922	0,00119	-0,0007
b_4	0,953	148,54	-1,718	-0,0000	2,662	11,02	1,607	-1,282
b_5	0,865	-0,0588	0,00139	-0,00003	-0,0026	0,00683	-0,00008	-0,0128

Curves for average daily surface temperatures (bold lines) resulting from the best fits to Eq. (5) along with 10-day-average observed data for these two lakes and parameters $b_0 - b_5$ calculated with Eq. (6) are shown in Fig. 4 (solid lines). Evidently, coincidence of calculated and observed profiles is remarkably good. Typical differences between observed and simulated water temperatures are about 0.27˚C. Such accuracy makes the equation (1) very useful for modelling a "typical" annual cycle.

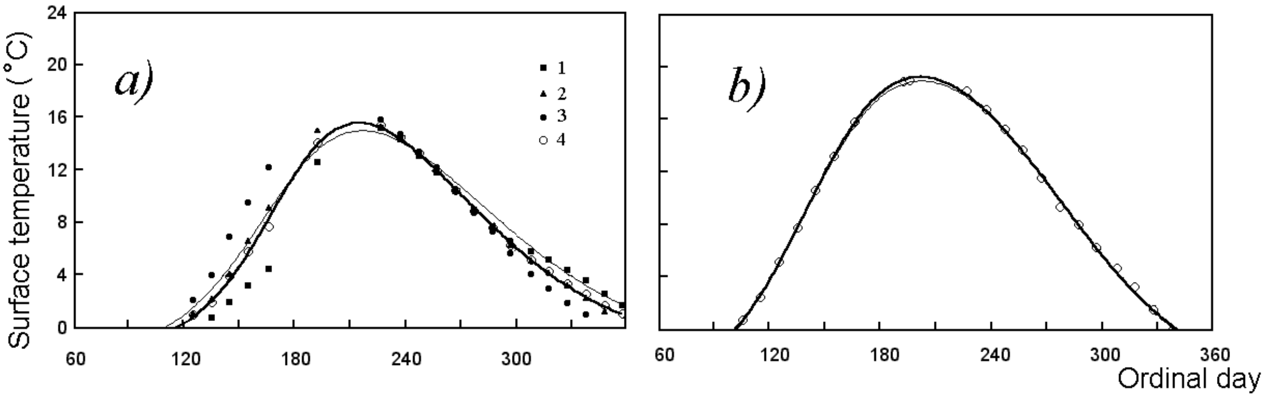

Figure 4. Model curves with best fits to equation 5 (bold lines) and calculation of parameters b_i on Eq. 6 (thin lines) for a) – lake Ladoga, b) – lake Glubokoye. Average 10 days surface temperature (1 – deep-water region, 2 – intermediate region, 3 – littoral region, 4 – all lake).

Figure 5 shows discrepancies between observed values of water temperature and those calculated with use of Eq. 5. The correlation coefficient is rather high (0.99), and a rms value is 0.70˚C. Such accuracy of our method makes it useful for modeling a typical annual temperature cycle for lakes where measurement data is short or completely absent. The method allows defining a surface water temperature for any date, using a limited number of initial parameters. It is effective compared with use of complicated numerical models that need long-term series of meteorological data (air temperature, humidity, wind velocity, cloudiness, solar radiation, etc.).

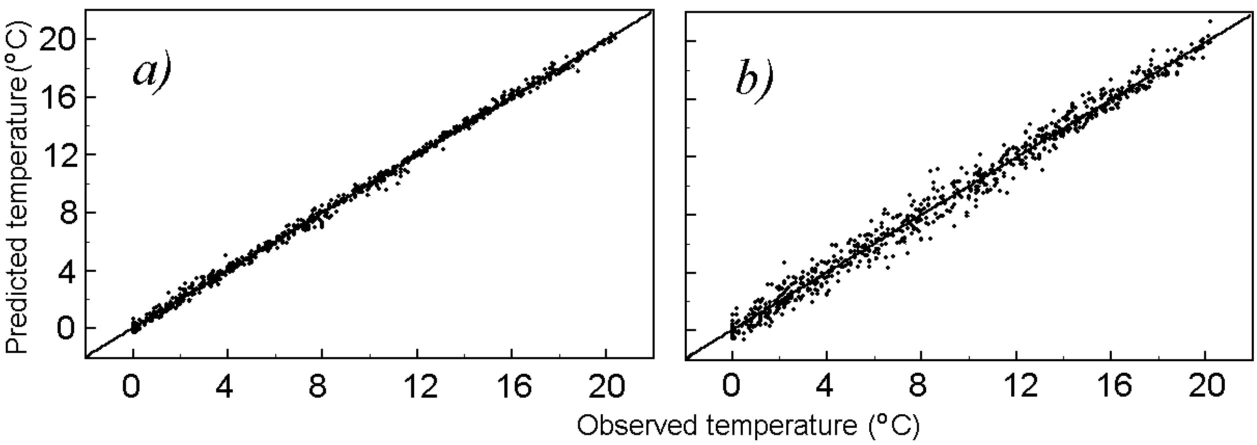

Figure 5. Scattering graph average surface temperature in 47 lakes a) – calculated values with best to Eq. 5 and b) – at calculation parameters b_i on Eq. 6.

3.4. «Biological summer»

The "biological summer" is defined here as a period when the temperature of the upper-layer water in lakes is above 10ºC. Relationships between characteristics of the "biological summer" and various geographic factors were estimated using annual 10-day averaged daily data on the water surface temperature in the lakes. The first step was to smooth them and calculate the daily temperature in accordance with the approximating function (5).

Step-wise regression analysis was performed to find out the weightiest predictors of the "biological summer" characteristics among geographical factors:

$$t_1 = -35 + 2{,}75\ \varphi + 11{,}2\ \lg \overline{H} + 1{,}3\ \lg S + 0{,}014\ Z, \quad (\text{rms} = \pm 3{,}4;\ \ \text{R} = 0{,}96) \tag{7}$$

$$t_2 = 395 - 2{,}15\ \varphi + 9{,}1\ \lg \overline{H} - 0{,}039\ Z - 0{,}89\ \lg S, \quad (\text{rms} = \pm 2{,}6;\ \ \text{R} = 0{,}95) \tag{8}$$

$$t_2 - t_1 = 432 - 4{,}95\ \varphi - 0{,}05\ Z - 2{,}2\ \lg S, \quad (\text{rms} = \pm 4{,}3;\ \ \text{R} = 0{,}97) \tag{9}$$

$$\int_{t_1}^{t_2} T(t,0)dt = 8485 - 103\ \varphi - 57\ \lg S - 1{,}1\ Z - 120\ \lg \overline{H}, \quad (\text{rms} = \pm 97;\ \ \text{R} = 0{,}97) \tag{10}$$

where t_1, t_2, $t_2 - t_1$ are the dates when the water temperature rises above/falls beyond 10ºC in spring, autumn and duration of the "biological summer", respectively; $\int_{t_1}^{t_2} T(t,0)dt$ – total degree days with water temperature above 10ºC; R and rms are shown in brackets.

In equations (7-10), predictors are given in the order of decreasing weight. The factor most strongly influencing all characteristics of the "biological summer" is the geographic latitude, which is directly related to the solar radiation flux onto the water surface. According to determination coefficients (R^2), the proportion of variance of various parameters of the "biological summer" explained by the geographic latitude only is 0.65 to 0.84. For medium-sized lakes of Northwest Russia, the date at which the water temperature transgresses 10ºC grows by 2.8 days with each degree of latitude growth in spring, and decreases by 2.1 day in autumn. Total degree days throughout the "biological summer" fall by 103ºC with each latitudinal degree.

3.5. Response of the vertical thermal structure on climate variations

In stochastic models the water temperature is mainly related to the air temperature (Rogers, 1987; Blumberg, Di Toro, 1990; McCormic, 1990; Robertson, Ragotzkie, 1990). Dependence of the hypolimnetic temperature on the monthly-average wind velocity becomes apparent only in spring, and on the maximal daily wind velocity during the period of summer stratification. The air temperature is a key weather parameter, and its monthly average values are well simulated by the global climate change models compared to other meteorological parameters. Relation between the air temperature and that of water at different depths (0, 5, 10, 15, 20, and 25 m) was studied by the example of the Petrozavodsk Bay, Lake Onego.

The following freely available observational data collected by the Russian (USSR) Hydrometeorological Service were taken into analysis: the air temperature from the Petrozavodsk station and long-term water temperature measured along the raid vertical in the central part of the Petrozavodsk Bay (1958–1989). Exponentional smoothing of data on air and water temperatures was performed with Eq. 5. Determined empirical relationships allow calculating the water temperature in the Petrozavodsk Bay provided data on the air temperature annual course is available. This is essential in estimating seasonal variations of the vertical thermal structure of the bay under different scenarios of the regional climate change or in recovering missing data. The developed model was approved against data on the seasonal variations of the vertical bay thermal structure in 2004-2006.

The observational data analysis reveals that deviations of the monthly average air temperature of 3-5°C during the period of the maximal heating lead to analogous changes of the water temperature in the upper 5-m layer. Within the thermocline, dependence of the water temperature on the air temperature basically decreases. At the 10-m depth these changes comprise of 1-2°C, and at 15-m depth and deeper are close to zero. In the bottom (20-25 m) layer weak reverse dependence (changes in fractions of °C) can be noticed. In the thermocline and hypolimnion, relation between dates and rates of changes of the air and water temperatures during spring warming and autumnal cooling can be traced. This is in a good accordance with results of studies performed in the Great American Lakes: Ontario, Erie, and Michigan (Rogers, 1987; Blumberg, Di Toro, 1990; McCormic, 1990).

4. CONCLUSIONS

Based on the analysis of long-term data obtained in different-type reservoirs of North-Western Russia and Finland, the stochastic models to simulate the thermal structure of poorly studied or newly constructed water reservoirs are developed. They allow efficiently calculate the annual course of the surface water temperature and the vertical thermal structure during maximal warming for any lake on the basis of existing geographical information (latitude, altitude above sea level, object geometry, residence time). By virtue of their simplicity, the models can be used as a tool not only for hydrophysists but for a wider circle of experts (chemists, biologists, ecologists) in solving basic and applied problems.

REFERENCES

Birge E. A., Juday C., March M.W. (1927) The temperature of the bottom deposits of Lake Mendota. - A chapter in the heat exchange of the lake. *Trans. Wisc. Acad*. **23**, 187-232.

Blumberg A. F., Di Toro D.M. (1990) Effect of Climate Warming on Dissolved Oxygen Concentrations in Lake Erie. *Transact. Amer. Fisher. Soc*. **119(2)**, 210-223.

Gorham E., Boyce F. M. (1989) Influence of lake surface area and depth upon thermal stratification and the depth of the summer thermocline. *J. Gr. Lakes Res*. **15**(2), 233-245.

Efremova T. V., Palshin N. I. (2003) Formation of Vertical Thermal Structure in Lakes in Northwestern Russia and Finland. *Water Resources*. **30**(6), 640-649.

Efremova T.V., Petrov M.P. (1992) Modelling of deep-water termic regime of Povenetsky bay. - *Povenetsky bay of Onego lake*. Petrozavodsk, pp. 12-18. (Russian)

Kuusisto E. (1981*) Suomenvesistojen lampotilat kaudella 1961-1975.* Vesihallitus - National Board of Waters, Finland. Helsinki, 40 p.

Lathrop R. C., Lillie R. A. (1980) Thermal stratification of Wisconsin lakes. *J. Wisc. Acad. Sci*. 68, 90-96.

Lesht B. M., Brandner D.J. (1992) Functional representation of Great Lakes Surface temperatures. *J. Great Lakes Res.*. **18** (1), 98-107.

McCormic M. J. (1990) Potential Changes in Thermal Structure and Cycle of Lake Michigan Due to Global Warming. *Transact. Amer. Fisher. Soc*., **119**(2), 183-194.

Naumenko M. A., Karetnikov S. G. (2002) Morphometry and specific Ladoga lake hydrology regim. *Ladoga lake: past, present, future.* Sankt-Petersburg, pp. 16-49. (Russian)

Palshin N. I., Efremova T. V., (2005) Stochastic model of surface temperature annual cycle in lakes. *J. Hydrology and meteorology*. №3. 85-94.

Patalas K. (1984) Mid-summer mixing depths of lakes of different latitudes. *Int. Ver. Theor. Angew. Limnol. Verh* .**22,** 97-102.

Robertson D. M., Ragotzkie R. A. (1990) Changes in the thermal structure of moderate to large sizes lakes in response to changes in air temperature. *Aquatic Sciences*. **52**(4), 360-380.

Rogers G.K. (1987) Time and onset of full thermal stratification in Lake Ontario in relation to lake temperatures in winter. *Canadian Journal of Fisheries and Aquatic Sciences*, **44**(12), 2025-2229.

Strashkraba M., Gnauk A. (1989) *Freshwater ecosystems. Modelling and simulation*. M., Mir, 376 p. (In Russian)

TIME-SPACE CHANGES OF CLIMATE AND WATER SYSTEMS OF KARELIA

Nikolay N. Filatov[1*], Larisa E. Nazarova[1], Yuri A. Salo[1], Arkady Yu. Terzhevik[1]
Leonid A. Rukhovets[2], Gennady P. Astrakhantsev[2]

[1]- Northern Water Problems Institute, Karelia, Russia
[2] - St. Petersburg Institute of Economy and Mathematics, Russian Academy of Science
[*]Corresponding author, e-mail: nfilatov@nwpi.krc.karelia.ru

ABSTRACT
The main aim of the present study is to estimate the regional climate change and response of water ecosystems of largest lakes of Europe and the White Sea. This study includes analysis of long-term data from multi-year records of basic climatic parameters (air temperature, precipitation, evapotranspiration, index of continentality, river runoff, etc.). Variability of the hydrological regime of individual rivers and lakes, as well as the study area at large related to the regional climate change is presented and discussed. As the result of statistical analysis of the climate, water balance and water level for the largest lakes of Europe (Ladoga and Onego) and the White Sea over the period 1880-2004, their noticeable changes were detected. It was found that time series of annual air temperature, precipitation and evapotranspiration over a 120-year period contain significant positive linear trends, and river runoff contains a negative trend for the given period. Considerable climate changes in the region in those years are manifest also in a shorter period of snow cover in the catchments and a longer ice-free period on the lakes. Potential changes (spatial and temporal) in the regional climate and hydrologic regime for the period 2010-2050 were estimated using the results of numerical experiments with the ECHAM4/OPYC3 model and for two IPCC scenarios of the global climate change.

KEYWORDS
Climate change; time series; river watershed; total inflow; ice-free period.

2. DATA AND METHODS

The source material was series of mean monthly and annual air temperature and precipitation values from 26 weather stations (WS) in Republic of Karelia and 12 WS in the Murmansk Region from 1999-2004, as well as annual discharge series from six largest river watersheds of Karelia (rivers Kovda, Kem, Nizhniy Vyg, Suna, Shuja and Vodla). The longest time series were available for weather stations in Petrozavodsk (since 1880), Padany (since 1890), Valaam (since 1874).

To estimate regional climate variability, 1880-2004 time series of data on air temperature, precipitation, total evaporation (evapotranspiration), potential evaporation, streamflow were statistically analyzed, and long-term instrumentally measured data were compared with calculations based on mathematical models. Potential changes in principal climatic characteristics and water balance elements (WBE) for the study area were estimated using the results of calculations based on ocean-atmosphere models. To this end, we employed the previously tested model ECHAM4/OPYC3 (Filatov et al., 2002; Climate of Karelia…, 2004; Filatov et al., 2005) designed for scenario calculations of potential climate change in the quite extensive area comprising Karelia, Arkhangelsk, Murmansk and Leningrad Regions, which contain the catchments and basins of the largest water objects studied: White Sea, Lakes Ladoga and Onego.

3. RESULTS

Analysis of principal tendencies in long-term climatic and hydrological time series from 1880 to 2004 revealed positive linear trends in annual air temperatures, precipitation, total evaporation in Karelia and the

Kola Peninsula (Climate of Karelia…, 2004; Salo Y., 2003). Total streamflow in the region shows a minor negative trend due to a faster increase in total evaporation within the study area compared to precipitation. In the second half of the 20th century, linear trends of annual air temperature were positive, equaling an average of 0.10 °C/50 yrs. in the Kola Peninsula and 0.60 °C/50 yrs. in Karelia.

Analyzing seasonal air temperatures based on data from the weather stations situated in the north of European Russia, we revealed a spatial and temporal differentiation of temperature change tendencies by seasons. Only the spring air temperature shows a positive trend (up to +3.5°C/100 yrs.) throughout the study area. In all other seasons, areas with positive trends are mostly situated in the southern part of the region, close to Europe's largest lakes – Ladoga and Onego.

Figure 1 shows how the climatic norm of annual air temperature was changing with time in Karelia at large. Mean temperature values over 30 years (climatic norm) refer to the middle of the period. Noteworthy is the quite smooth time series of mean multiannual temperatures during the 19th century, and a significant rise of the norm as the industrial period began. Among-year changes of mean annual air temperatures have reflected the warming of the 1930s, followed by a cooling event of 1960-1970, which was, in turn, superseded by a still continuing rise in air temperature in the late 1980s. Note also that the variance of surface air temperature fluctuations increased with time, indicating the climate in the region was growing somewhat less stable. Coefficients of the linear trend of among-year air temperature variations accurately reflect the prevalent directivity of the change. The most severe cooling events of the study period took place in the second half of the 18th and in the mid-20th century. The linear trend coefficient had only positive or zero values from the 1870s to the 1940s. In the 1980s, the sign of the linear trend coefficient changed from negative to positive, and the air temperature has been rising consistently since then.

Analysis of empirical and calculated data has demonstrated that according to IPCC scenarios, not only annual values of climatic and hydrological characteristics but also their distribution among seasons and within a year will change under new climatic conditions. The greatest warming in Karelia is likely to happen in autumn and winter months, whereas the rise in air temperature during spring and summer months will not be so significant.

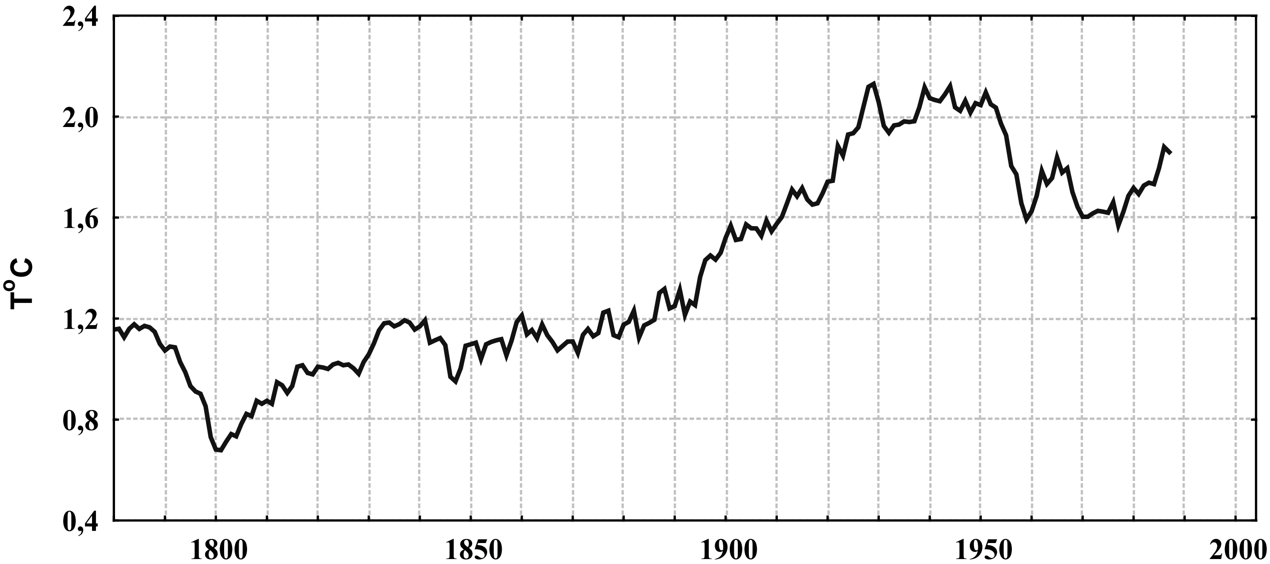

Figure 1. Dynamic of climatic norm of annual air temperature for territory of Karelia region in 1752 -2000. (30-years moving average values).

According to studies of the past two decades (Koronkevich et al., 2003; Shiklomanov et al., 2004), streamflow is increasing in Russia at large, but decreasing somewhat in Karelia (Figure 2), which tells on the water balance of the waterbodies and, hence, on their ecosystems. Where climate changes have been

studied quite thoroughly by now, knowledge about the response of aquatic ecosystems to the changes is still insufficient. In our study, we relied both on data from long-term observations over climate and aquatic ecosystems, and on modeling the change of ecosystems of Karelia's largest waterbodies – White Sea, Lakes Ladoga and Onego (Kondratyev et al., 2002; Climate of Karelia…, 2004; Meleshko et al., 2004).
The change of the thermal regime in the study area is manifest in an increase in the duration of the ice-free period on Lake Onego. The ice-free period in the Petrozavodsk Bay of Lake Onego has grown longer due to an 8-day shift of the spring ice break dates. Analysis of changes in precipitation volumes in the study area over the second half of the 20th century has demonstrated that although linear trends of total monthly precipitation have different directions during a year, total annual precipitation in the Lake Onego catchment has increased over the study period (45 mm/50 yrs. on average). An upward tendency in precipitation volumes is observed at all stations from October to June. From July to September, directions of the trends vary.
Correlations between streamflow and climatic characteristics were determined to assess the effect of climate change on streamflow from Lake Onego catchment. The dependence of temporary storage of water in a basin on mean annual air temperature over the catchment and total annual precipitation was found. Figure 2 shows the values of total influx to Lake Onego observed in 1950-2000 and results of total influx calculations based on the proposed formulae.

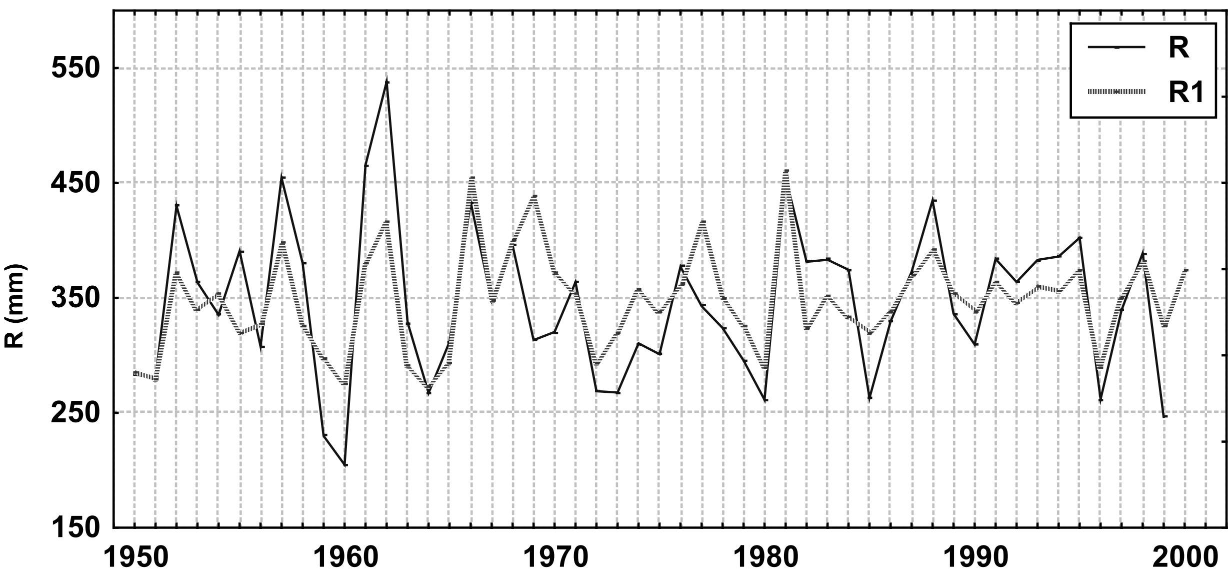

Figure 2. The values of total inflow to Lake Onego observed in 1950-2000 (R) and results of total influx calculations (R1).

It follows from the graphs that the calculated results agree quite well with the measured values. According to the hypothetical scenarios of climate change, a rise or fall in air temperature by 1-2 ^{o}C and a simultaneous in total annual precipitation by 10 and 20% compared to modern values would result in a change in streamflow to Lake Onego as drawn in Figure 3. If the air temperature increases by 1^{o}C, streamflow to the lake may remain unmodified given that total annual precipitation increases by about 3%; a warming of 2 ^{o}C would be compensated by a precipitation rise on 6 %.
Analysis of the data has demonstrated that annual air temperature and total annual precipitation have increased in Lake Onego catchment over the second half of the 20th century, but no change in total streamflow to the lake has so far followed. The detected patterns of change of the main characteristics of the regional climate and the consequences of potential change in the hydrological regime in Lake Onego catchment can be taken into account when planning sustainable water management and conservation of this waterbody, which offers unique possibilities for drinking water supply, transport, energy production and recreation.

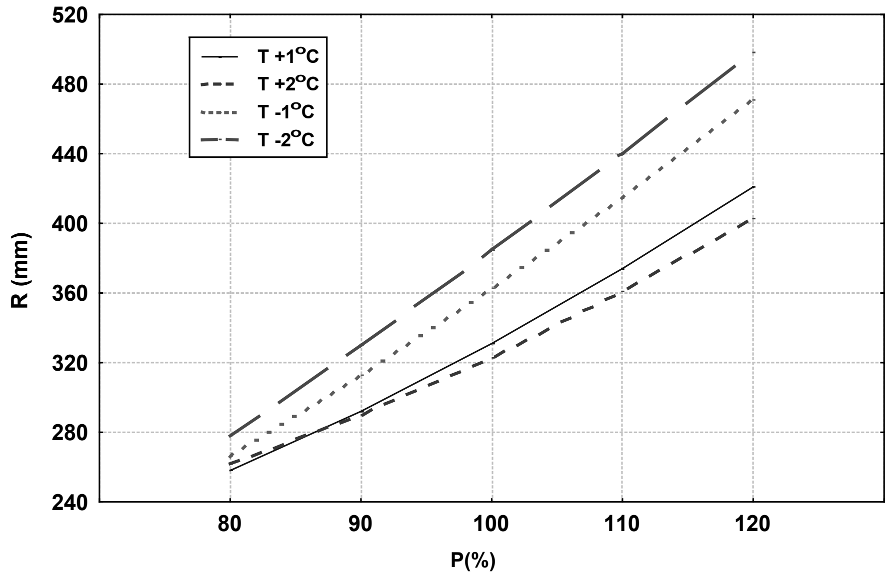

Figure 3. Dynamic of inflow to Lake Onego by different temperature and precipitation change scenarios. (100% - mean annual precipitation at present time).

The coupled thermohydrodynamic and ecosystem models have been applied to study the contemporary situation on water ecosystem of Lake Onego, to understand the main mechanisms of the ecosystem transformation and to learn what may happen in future. Some attention has also been paid to the present state of socio-economic development in the basin and its effect on the water quality of the lakes. The recommendations towards the sustainable development of the region are worked out, and the complex of measures required for rational use of its resources is formulated.

In addition to climatic circulation, the authors have constructed scenarios of Lake Onego circulations which may arise as global warming changes the climate in the lake catchment. The ecological model taking current status and condition into account was applied to these circulation scenarios to predict functioning of the Onego Lake ecosystem in relation to climate change. The main conclusion drawn from the calculations is that climate changes cause no significant changes in the functioning of the lake ecosystem.

The White Sea attracts continuously increasing attention of both researchers and users. This is due to a new stage of developing the resources of the White Sea itself and its catchment area (diamond and gold mining, fish catch, the growing of maricultures, transport of natural gas from the Stockmann gas deposit of the Barents Sea to Western Europe, and consequently, a major change in the entire infrastructure entailing creation of new enterprises). The above-mentioned problems, together with quite a few traditional ones (such as the use of marine bioresources, wood cutting in the catchment area, the impacts of pulp-and-paper industry and wastes discharge of cities and towns located on the sea-shores and in the catchment areas) will require working out scientifically substantiated recommendations for rational use and protection of marine resources.

In spite of the previous efforts, we still lack a systematic knowledge of intrinsic mechanisms of functioning of the White Sea ecosystem and its responsiveness to external forcing. The required sets of coupled thermohydrodynamic and ecosystem models have not been developed. The inherent processes of transport and transformation of the aquatic environment constituents, as well as the regularities in water exchange have not been adequately studied thus far. The same is true for studying the impacts of climate change and anthropogenic forcing upon the marine ecosystem.

Therefore, along with an integrated system approach to the investigation of the whole marine ecosystem, a comprehensive study is required of numerous bays and estuaries of the White Sea because they play a very essential role in the formation of the marine ecosystem, as well as in its functioning. It should be emphasized that only a truly comprehensive research, encompassing multifaceted studies addressing the pool formation of organic matter, production-destruction processes, all forms of nutrients, phytoplankton, etc., can be really effective.

A thorough study of responsiveness of the White Sea ecosystem to anthropogenic impacts is also required. The White Sea is of great scientific significance within the frames of the programme of studying the Arctic seas because it is a rather small semi-closed waterbody, for which it may be much simpler (in comparison with other Arctic seas) to

- estimate the balance of matter and energy;
- investigate energy fluxes and matter flows at the main interfaces;
- work out (obtain) a set of models for diagnostics of the current status and prediction of future variations of the Arctic seas ecosystem;
- assess the ecosystem changes caused by natural and anthropogenic factors.

As a result, some scenarios have been formulated for the estimation of possible changes in the White Sea (WS) ecosystem in response to external impact variations, and certain recommendations have been elaborated for rational utilization of the resources of both the White Sea and its catchment. Development of recommendations concerning optimization of environmental management will make it possible to increase the efficiency of measures aimed at the improvement of the aquatic environment quality and diminish the risks from extraordinary man-induced ecological situations. It will be a significant step towards the revival of the region.

Several numerical models have been developed and exploited to this end, including the ones accounting for the atmosphere-ocean interactions. The employed climate change and marine ecosystem dynamics models have revealed that in the event of both possible climate warming in the region (the scenarios suggested by IPCC) and socio-economic changes in the strand area (several scenarios have been assumed) would not bring about any serious/far-reaching consequences. The pollution level and present status of water quality in the White Sea remain mostly fairly stable. Although, in estuaries of the Severnaya Dvina, Onega and Mezen' Rivers a substantial anthropogenic forcing is going on, this process has not yet resulted in major man-driven alterations to the aquatic ecosystem. In spite of a semi-Arctic geographical location, relatively cold water with enhanced salinity, high dynamic activity (strong tide-ebb currents), the White Sea is characterized by a number of specific hydrophysical features, low level of eutrophication and pollution, high rates of water exchange with the Barents Sea, and some others. The unique data assembled in the course of this study, and their multifaceted analyses constituted a solid base for pursuing a sustainable management of marine resources.

Utilization of these tools will make it possible to achieve science-based decisions aimed at pursuing efficient use and preservation of marine living resources. Because the White Sea models were constructed only for the lowest links of the ecosystem they cannot reflect complex processes of the interactions between plankton, benthos, fishes and seals. Consequently the fulfilled investigation should be considered as the necessary step for the construction of a more complex and complete model of the White Sea ecosystem. On the basis of the investigations it can be stated that:

In the given period of time the White Sea ecosystem state is stable. Average annual temperature will rise on average by 2°C in 50 years as the result of which fluvial run-off to the White Sea waters diminishes by 10-15%. In scenario models increase or decrease of inorganic nutrients by 20% in the river load into the White Sea did not show any notable effect on the phytoplankton succession. Decrease of freshwater input by 20% and increase of air temperature by 2°C resulted in a decrease of the thickness of the ice cover by 0.1 m, a decrease of the mean salinity by about 0.4‰, and intensify the formation of thermocline. That prevents the vertical mixing and leads to a decrease of inorganic nutrients in the surface layer suppressing autumn bloom of the phytoplankton. On the basis of our expert estimation behavior of phyto- zooplankton abundance is likely to correspond to the results obtained by the modeling experiments according to the following reasons:

A water contamination decrease leads to the optimal conditions for zooplankton and phytoplankton communities where human and other unfavorable impacts are minimal.

REFERENCES

Climate of Karelia: variability and influence on water objects and watersheds. Ed. N. Filatov. 2004. Petrozavodsk. 223 p. [in Russian].

Filatov N., Nazarova L., Salo Yu. 2002. Possible climate and water balance changes in Karelia (Russia) during the first half of the XXI century // Large Rivers. V.13. № 3-4. Arch. Hydrobiol. Suppl. 141/3-4. Pp.341-352.

Filatov N., Pozdnyakov D., Johannessen O., et al. 2005. White Sea: Its Marine environment and Ecosystem dynamics influenced by global change. London. Springer-Praxis. 472 p.

Kondratyev, S., Efimova, L., Markova, L. 2002. Estimation of changes of hydrological regime in catchment and inflow in lake depending on climate changees // Ladoga Lake – the past, present, future. Ed. Rumyantsev, V., Drabkova, V. St. Petersburg: Наука. Pp.283-291. [in Russian].

Koronkevich, N., Zaitseva, I. 2003. Modern state of water resources of // Using and protection of natural resourses of Russia. № 9-10. Pp. 83-89. [in Russian].

Meleshko, V., Golitsyn, G., Govorkova, V., Demchenko, P., Eliseev, A., Kattsov, V., Malevsky-Malevich, S., Mokhov, I., Nadezdina, E., Semenov, V., Sporyshev, P., Khon, V. 2004. Possible anthropogenic climate changes in Russia during XXI century: estimation of statistical ensemble of climatic models // Meteorology and hydrology, № 4. Pp. 38-49. [in Russian].

Rukhovets, L., Astrahantsev , G., Menshutkin, V. 2003. Development of Lake Ladoga Ecosystem Models: Modelling of the Phytoplankton Succession in the Eutrophication Process. I. Ecol. Modeling. V. 165. № 1. Pp. 49-77.

Salo, Yu. 2003. Patterns in multi-year variations of water balance elements in Karelia. Doctoral Thesis: Russian State Hydrometeorological University, St.-Petersburg, Russia. 24 p. [in Russian].

Shiklomanov, I., Georgievsky, V. 2004. Variability of river runoff in Russia under global warming // Water balance, resourses of surface waters. Abstracts of . VI All Russian hydrological congress. St. Petersburg: Hydrometeoizdat. P.200. [in Russian].

INCREASING WINTER BASEFLOW CONDITIONS APPARENT IN PERMAFROST REGIONS OF NORTHWEST CANADA

J Richard Janowicz,

Water Resources, Department of Environment, Box 2703, Whitehorse, YT,CANADA
e-mail: richard.janowicz@gov.yk.ca

ABSTRACT
Yukon air temperature trends have been observed to change over the last several decades. Summer and winter air temperatures have increased in most regions except southeastern Yukon. The greatest changes have occurred in western, mountainous regions where both summer and winter temperatures have increased significantly. Hydrologic response was generally found to be characterized with higher year round flows. Mountainous streams were found to have the timing of the freshet advanced, with a progressive decrease in this peak flows moving from south to north.
An assessment of winter low flow conditions was carried out to determine if recent changes were apparent in response to the observed temperature changes. Winter low flows are represented by the mean 7 day low flow. Winter low flows have experienced apparent changes over the last three decades. The greatest changes in winter streamflow appear to be occurring within the continuous permafrost zone, where flows from the majority of sampled streams have increased. Winter low flows trends in streams within the discontinuous permafrost zone generally exhibit positive trends, but are more variable. Winter streamflow trends within the sporadic permafrost zone are not consistent. Increasing winter streamflow trends have occurred from some mountainous regions of alpine permafrost. Other streams exhibit no discernable change, while one stream exhibits a negative change.

KEYWORDS
Continuous, discontinuous, sporadic permafrost, 7-day low flow, trend analysis, Mann-Kendall

1. INTRODUCTION
Yukon temperature and precipitation trends have been observed to change over the last several decades (Janowicz 2001). Summer and winter temperatures have increased in most regions except southeastern Yukon. Summer precipitation has been observed to increase in all regions, while winter precipitation has decreased in all regions with the exception of western Yukon. The greatest changes occurred in western, mountainous regions where both summer and winter temperatures and winter precipitation increased significantly. These observed trends support projections developed by a Canadian Climate Centre GCM (GCMII) (Taylor 1997), which is based on a 100 percent increase of CO_2 in the atmosphere.
While there have been numerous studies carried out in western Canada on the impact of climate change on hydrologic response (Kite, 1993; Burn, 1994; Loukas and Quick, 1996; 1999; Leith and Whitfield, 1998; Whitfield and Taylor, 1998), there has been only limited work to date on the impact of climate change on Yukon hydrology. Janowicz and Ford (1994) used the CCC GCM temperature and precipitation projections, and a correlation approach to assess the impacts of climate change on the water supply to the upper Yukon River. More recently Whitfield and Cannon (2000) and Whitfield (2001) assessed climatic and hydrologic variations between two decades (1976-1985; 1986-1995) for stations in British Columbia and Yukon. They found temperatures to be consistently higher, summer precipitation to be lower and winter precipitation to be higher in the second decade. Hydrologic response was generally found to be characterised with higher year round flows. Mountainous streams were found to have the timing of the freshet advanced, followed by lower summer and fall discharge. Janowicz (2001) carried out an analysis of streamflow to assess the response of the observed temperature and precipitation changes on peak flows, which normally occur as a result of spring

snowmelt. The assessment revealed that there has been a dramatic change in mean annual flood (MAF) in some regions of Yukon over the last 20 years, with a progressive decrease in the parameter moving from south to north. The greatest increases in MAF were observed to occur within the sporadic permafrost zone, from predominantly glacierized systems in western Yukon. Smaller increases were noted in southeastern Yukon. These increases correspond to the observed increase in both summer temperatures and winter and summer precipitation. Peak flows from central and eastern Yukon, within the discontinuous permafrost zone, exhibit very little change. Within the continuous permafrost zone, peak flows were observed to decrease progressively moving northward to the Arctic coast.
This paper summarizes the results of a study carried out to assess trends of minimum winter low flows in northwestern Canada over the last few decades.

2. SETTING AND METHODOLOGY

The analyses was carried out using data from Yukon Territory and the western Northwest Territory west of the 125th parallel of longitude, an area covering approximately 920,000 km^2. This region consists of three permafrost zones: continuous, discontinuous and sporadic (figure 1). Data from all active and recently discontinued (< 5 years) stations, on unregulated streams, with at least 25 years of record were used in the analyses. Because of numerous station discontinuations in the mid-1990s, only 21 stations were available for analyses. These were equally distributed between the three permafrost classes. The 7-day average minimum annual low flow, which normally occurs in late winter or early spring, was assessed in the present study. The 7-day average low flow parameter is a commonly used minimum flow measure which reduces the variability over a single value.

2.1. Trend Analysis

The Mann-Kendall trend test was used to assess trends in the 7-day minimum annual low flow parameter. The Mann-Kendall test is a non-parametric test used for the assessment of trends in time series. It is a simple, robust tool which can readily handle missing values. The standard normal variate value (Z) is calculated which is associated with a specific level of significance. The significance level provides an indication of the strength of the trend. A significance level of 0.001 indicates a very strong trend, 0.01 indicates a strong trend, 0.05 indicates a moderate trend, and 0.1 indicates a weak trend. A level of significance of less than 0.1 indicates there is no discernable trend.

3. RESULTS AND DISCUSSION

Table 1 provides a summary of the trend analyses. The greatest positive trends in winter low flows appear to have occurred in the continuous permafrost zone. It is not possible to statistically validate all trends, since some of the study streams have had predominately “zero” winter flows in past decades, with increasing occurrences of measurable winter low flows in recent years. As with many statistical techniques, the Mann-Kendall tests are not able to handle “zero” flows. Winter baseflows are generally directly related to drainage area. In cold regions the relationship is more pronounced, with smaller drainages having less groundwater inputs to baseflow; therefore, smaller winter flows. In regions of continuous permafrost many streams have “zero” flows. Figure 2 provides an illustration of the positive winter low flow trend for the Arctic Red River (10LA002), with a drainage area of 18,600 km^2. Figure 3 provides an illustration of low flow trends for a smaller stream, Rengleng River (10LC003) with a drainage area of 1310 km^2. Winter low flows in past decades have been nonexistent, while measurable flow during recent winter periods has been observed. The winter flow regime for Caribou Creek (10ND002), with a drainage area of 68.3 km^2, has remained unchanged, with “zero” flows throughout the entire 29 year monitoring period.

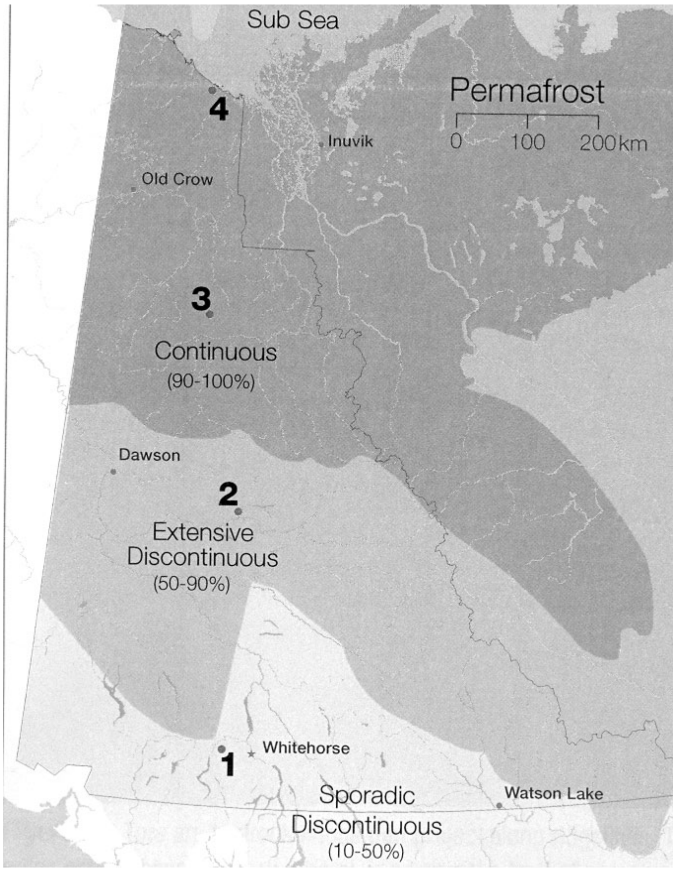

Figure 1. Study Area and Permafrost Zones

Table 1. Mann-Kendall Trend Statistics

Permafrost Class	Station #	Drainage Area (km^2)	Record Period	n	Z Statistic	Significance Level
Continuous	09FC001	13900	1977-05	27	0.83	< 0.1
	09FD002	59800	1962-05	40	1.81	0.1
	10LA002	18600	1969-06	37	4.89	0.001
	10LC003	1310	1973-05	32		
	10LC007	625	1975-06	31		
	10MC002	70600	1975-06	31	3.65	0.001
	10ND002	68.3	1977-06	29		
Discontinuous	09BA001	7250	1961-05	44	1.42	< 0.1
	09BC001	49000	1953-05	52	2.12	0.1
	09BC004	22100	1973-05	33	2.43	0.1
	09DD003	51000	1964-05	42	1.23	< 0.1
	09EA003	7800	1966-05	40	3.44	0.001
	10EA003	8560	1961-06	39	0.94	< 0.1
	10EB001	14600	1964-06	42	2.3	0.1
Sporadic	08AA003	8500	1953-05	53	2.95	0.01
	08AA009	194	1981-05	25	0.82	< 0.1
	08AB001	16200	1975-05	31	0.29	< 0.1
	09AA012	875	1958-05	44	-0.67	< 0.1
	09AC001	6930	1949-05	56	1.49	< 0.1
	09CB001	6240	1975-05	30	2.43	0.5
	10AA001	33400	1961-05	45	0.73	< 0.1

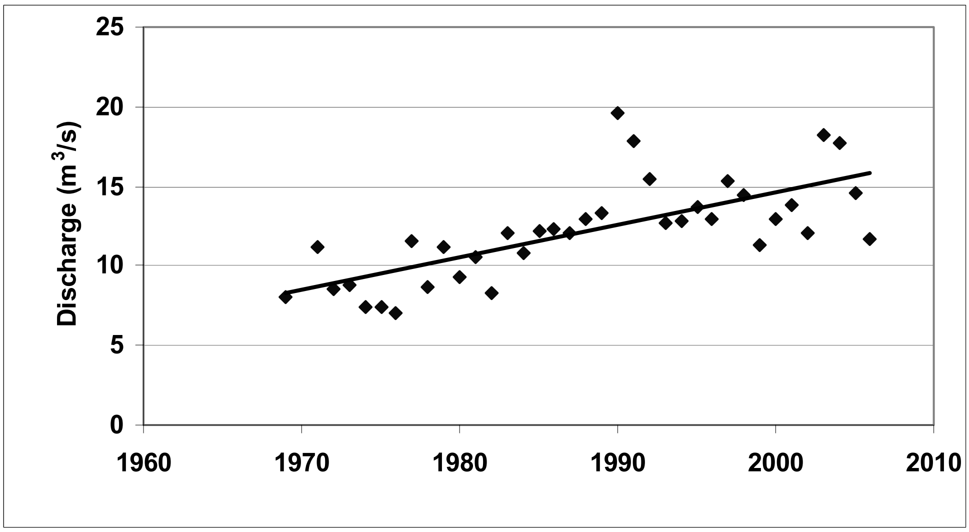

Figure 1. 7-Day Average Minimum Low Flow - Arctic Red River near Mouth

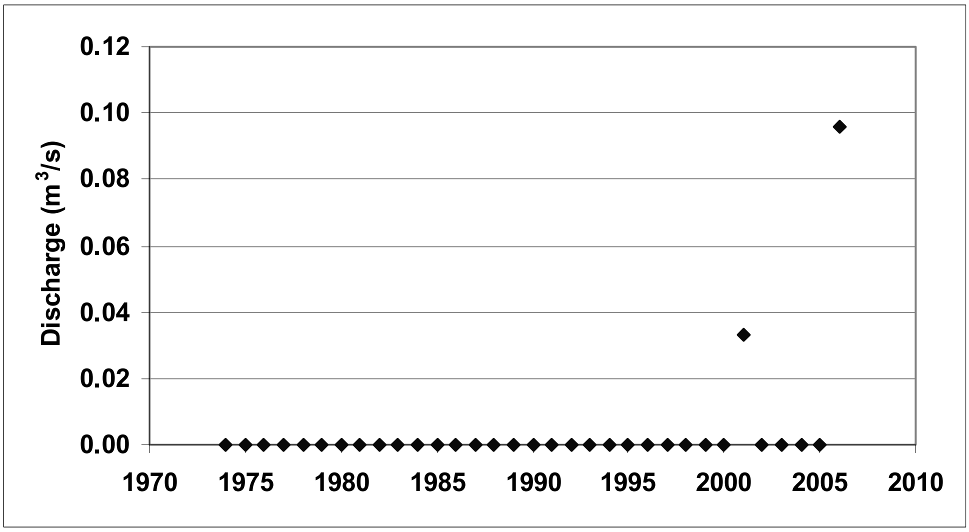

Figure 2. 7-Day Average Minimum Low Flow – Rengleng River at Dempster Highway

Trends of winter low flow regimes, with increasing flows are generally exhibited by streams within the discontinuous permafrost zone. Four of the seven assessed streams have statistically significant positive winter low flow trends. Figure 4 illustrates the increasing trend for Klondike River (09FA003). Even the smallest streams within the discontinuous permafrost zone normally have winter flows, so drainage area is not as strong a factor in influencing winter streamflow, as in the continuous permafrost zone.

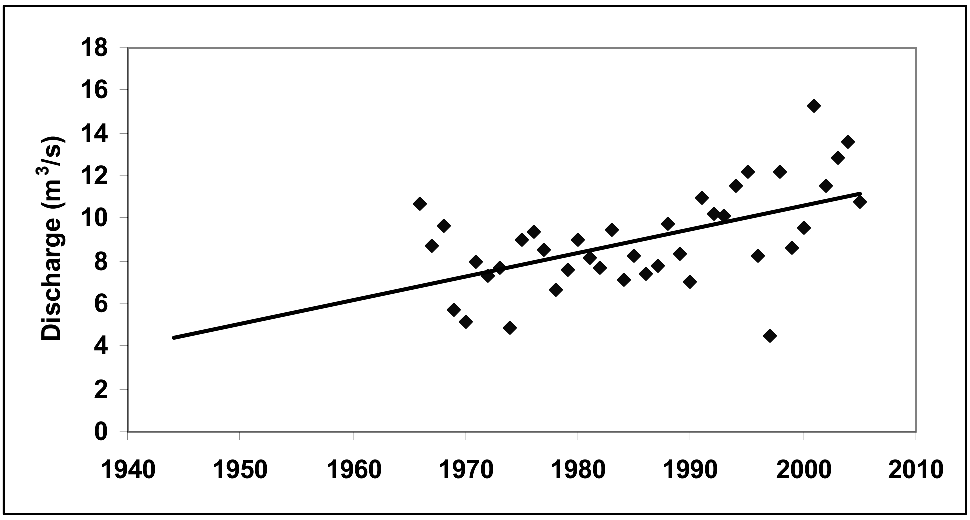

Figure 3. 7-Day Average Minimum Low Flow - Klondike River above Bonanza Creek

Trends of increasing winter low flows are not generally strong within the sporadic permafrost zone. Two of the seven represented streams have statistically significant positive trends. Both of these streams are transitional with the discontinuous permafrost zone, and one of these drains a mountainous region with significant alpine permafrost. Other streams exhibit no discernable change, while one stream exhibits a negative change.

4. CONCLUSIONS

An assessment of winter low flow conditions was carried out to determine if recent changes were apparent in response to the observed temperature changes. Winter low flows are represented by the mean 7 day low flow. The Mann-Kendall test was used to statistically validate observed trends. Winter low flows have experienced apparent changes over the last three decades. The greatest changes in winter low flows appear to be occurring within the continuous permafrost zone, where flows from the majority of sampled streams have increased. Winter low flows trends in streams within the discontinuous permafrost zone generally exhibit positive trends, but are more variable. Winter streamflow trends within the sporadic permafrost zone are not consistent. Increasing winter streamflow trends have occurred from some mountainous regions of alpine permafrost. Other streams exhibit no discernable change, while one stream exhibits a negative change.

REFERENCES

Burn, D.H. (1994) Hydrologic effects of climate change in west-central Canada. Journal of Hydrology, 160, 53-70.

Janowicz, J.R. and Ford, G. (1994). Impact of climate change on water supply in the upper Yukon River. Proceedings of the 62nd Annual Western Snow Conference, Sante Fe, New Mexico, April 18 – 21, 1994.

Janowicz, J.R. (2001) Impact of recent climatic variability on peak streamflow in northwestern Canada with implications for the design of the proposed Alaska Highway gas pipeline. Proceedings of the 13th Northern Research Basins International Symposium & Workshop, Saariselka, Finland and Murmansk, Russia, August 19-24, 2001, 161-169.

Kite, G.W. (1993) Application of a land class hydrological model to climate change. Water Resources Research, **29**(7), 2377-2384.

Leith, R.M. and Whitfield, P.H. (1998) Evidence of climate change effects on the hydrology of streams in south-central B.C. Canadian Water Resources Journal, **23**, 219-230.

Loukas, A. and Quick, M.C. (1996) Effect of climate change on hydrologic regime of two climatically different watersheds. Journal of Hydrological Engineering, **1**(2), 77-87.

Loukas, A. and Quick, M.C. (1999) The effect of climate change on floods in British Columbia. Nordic Hydrology, **30**, 231-256.

Taylor, B. (1997). Climate change scenarios for British Columbia and Yukon. In Responding to global climate change in British Columbia and Yukon, Canada Country Study: Climate Impacts and Adaptation, Volume 1. Edited by E. Taylor and B. Taylor, Environment Canada.

Whitfield, P.H. (2001) Linked hydrologic and climate variations in British Columbia and Yukon. Environmental Monitoring and Assessment, **67**, 217-238.

Whitfield, P.H. and Cannon, A.J. (2000) Recent climate moderated shifts in Yukon hydrology. Proceedings AWRA Conference Water Resources in Extreme Environments, Anchorage, Alaska, May 1-3, 2000. Edited by D.L. Kane. Whitfield, P.H. and E. Taylor. 1998. Apparent recent changes in hydrology and climate of coastal British Columbia. In: Mountains to Sea: Human Interaction with the Hydrologic Cycle. Proceedings of the 51st Annual Canadian Water Resource Conference, Edited by Y. Alila, 22-29.

STRATIGIES FOR MEASURING SNOW WATER EQUIVALENT FOR HYDROLOGICAL APPLICATIONS: PART 2, SPATIAL DISTRIBUTION AT THE WATERSHED SCALE

Douglas L. Kane[1*], Svetlana Berezovskaya[1]

[1] *Water and Environmental Research Center, University of Alaska Fairbanks, Fairbanks, AK 99775,*
**Corresponding author, e-mail: ffdlk@uaf.edu*

ABSTRACT
One of the challenges for hydrologists is to make predictions of the runoff response of Arctic watersheds. This is especially true for snowmelt when data is sparse and of poor quality, solid precipitation is redistributed by wind events and sublimation can deplete the snowpack. At the small watershed scale we can saturate the catchment with measurements to get a good approximation of the snowpack. However, for larger basins this is not logistically possible. In this paper we talk about our present snow water equivalent (SWE) measurement strategy for a group of nested watersheds on the North Slope of Alaska in which we try to capture the spatial variability. We present some concentrated field measurement techniques to evaluate our normal sampling protocol. These results show that our techniques work for capturing SWE variability from scales ranging from 100 m to 10,000 m and possibly more. We cannot capture SWE differences for scales less than a few meters such as an incised stream. We need to couple our field measurement program with a blowing snow model and compare results for large watersheds (>10,000 km^2).

KEYWORDS
Snow distribution, watershed scale, Arctic, Alaska, snow depth, SWE

1. INTRODUCTION

Snow water equivalent (SWE) on the ground at a point cannot be accurately estimated by the amounts of solid precipitation that falls because of large biases in gauged precipitation (Goodison *et al.*1998; Yang *et al.* 2000) and the horizontal wind-blown fluxes and vertical sublimation. Regardless, hydrologists interested in the snowmelt runoff response of a watershed need to know the spatial SWE distribution just prior to melt. Accepting that there is natural spatial variability of solid precipitation amounts due to topographic factors at scales of 10s to 100s of km, redistribution of the snowpack by wind events during or following deposition at various scales surrounding the 1 km distance ensure that the Arctic snowpack at the watershed scale will be very heterogeneous by winter's end. Complicating this further, during the winter months prior to ablation, sublimation is ongoing and primarily controlled by the amount of energy available.

Hydrologically, we are challenged to capture the heterogeneous distribution of this snowpack for use in, for example, hydrologic models for water balance determinations (Bowling *et al.* 2003; Kane and Yang 2004; Lilly *et al.* 1998) and prediction of snowmelt runoff (Zhang *et al*. 2000). We presently have a routine for taking field measurements of both snow depth and snow water equivalent (SWE) at the watershed scale from 2 to over 8,000 km^2 (Figure 1). We address in this paper the question, does this technique adequately capture the snow distribution over these watersheds that range in drainage area by circa five orders of magnitude? There are several logistical obstacles that limit the approaches we can take to quantify snow depth and SWE: first, most of the area is very remote and only accessible by helicopter, second, some of the area is quite mountainous and not even accessible by helicopter and finally, as usual man-power and financial resources are limited.

2. SETTING

The North Slope of Alaska is an extensive area that transitions from the continental divide in the Brooks Range to the Arctic Ocean. There are three distinct topographic regions on the North Slope: mountainous, foothills and coastal plain (Kane et al., 2000). The entire region is underlain with permafrost that reaches a maximum thickness of greater than 600 m. Except for a few isolated riparian areas in the foothills, the area is treeless. Shrubs (0.4 to 1.0 m) are common throughout the watersheds with higher density in foothills; shrubs are increasing in density. The active layer is typically about 50 cm (varies considerable due to vegetation, soils, aspect, slope, etc.) with extensive surficial organic soils overlying mineral soils. Lakes can be found throughout the region, but are found in much greater numbers on the coastal plain. All of the streams are predominantly north draining with some streams having extensive aufeis. Winters start in mid-September with breakup occurring from early May to early June. It can snow on any day of the year with usually three or four snow events during the summer.

3. METHODOLOGY

Through intensive field measurement campaigns we attempted to quantify the snow depth and SWE distribution (Figure 2) at the watershed scale at winter's end. Basically we take 50 snow depth measurements in an L-shaped pattern, along with five SWE measurements at numerous sites in a watershed. The distribution with elevation of snow survey sites in the Kuparuk River basin is shown in Figure 3. In general, the lone criterion for site selection was that the measurement area (generally 25 to 50 m) is representative of a much larger surrounding area (same slope, aspect, vegetation, etc.). This technique however fails to capture snow variability that may exist at smaller scales such as a small-incised drainage.

One feature of our field sampling effort is that the density of the stations decreases significantly as the watershed size increases. The densities are 0.22, 7.1, 23.6 and 106 km^2/site for Imnavait Creek (2.2 km^2), Upper Kuparuk River (142 km^2), Putuligayuk River (471 km^2) and Kuparuk River (8,140 km^2) respectively. The measurements in Imnavait Creek differ from the other watersheds; originally when this was the only watershed being studied, we did a 1000 m transect across the catchment from ridge to ridge, with five SWE measurements every 100 m. It is not realistic to do such transects on larger watersheds.

The rationale for taking five SWE measurements where we get the density and 50 snow depth measurements is that the depth (Figure 4) varies much more than the density (Figure 5). What this means is that in a given amount of time, snow depth measurements will yield more information to quantify the snowpack than will density measurements that yield the SWE. Snowpack densities can vary from 150 to 350 kg/m^3, but typically there are in the range of 200 to 300 kg/m^3 (Figure 5). Snow depth can vary from snow free to over 2 m in localized areas of drifting. From the five density measurements we get an average density that we use with the average of the 50 depths to get an average SWE.

We have compared snow density estimates obtained from the Adirondack tube that we use versus snow pits and Mt. Rose snow sampler used by federal agencies; the results are quite comparable. However, there is a certain amount of error introduced in the depth measurements. In the area of study, surface organic soils prevail. When inserting the probe into the snowpack, it is difficult to ascertain the interface between the bottom of the snowpack where large crystals of depth hoar are found and the surface of the organic soils
(Berezovskaya and Kane, 2007). By taking depth measurements in the usual way with a probe at a 1 m interval, we then excavated a trench along the transect where measurements were made and the true depth could be observed. Results show that we over estimate the snow depth on an average of 8 cm (or in a typical year ~20%). It should be noted that the error associated with snow depth measurement with the probe is greater than the tube. Also a certain human element is linked with the depth measurements in that no two people will do it with the same vigor.

Two other efforts to evaluate how well we are capturing SWE and snow depth variability are *"starburst sampling"*, i.e. detailed sampling in a starburst pattern (Figure 6), and *"scaling sampling",* i.e. snow depth sampling along transects of varying lengths from 1 m to 100,000 m (Figure 7). With the starburst sampling, we can get a very good idea of the snow depth statistics in a circle with a diameter of 100 m. Then subsets of the larger population can be compared with various less intense sampling schemes. For example, from this pattern, we can get eight possible L-shaped sampling schemes with 25 snow depths on each leg or eight L-shaped sampling schemes with 50 depth measurements on each leg.

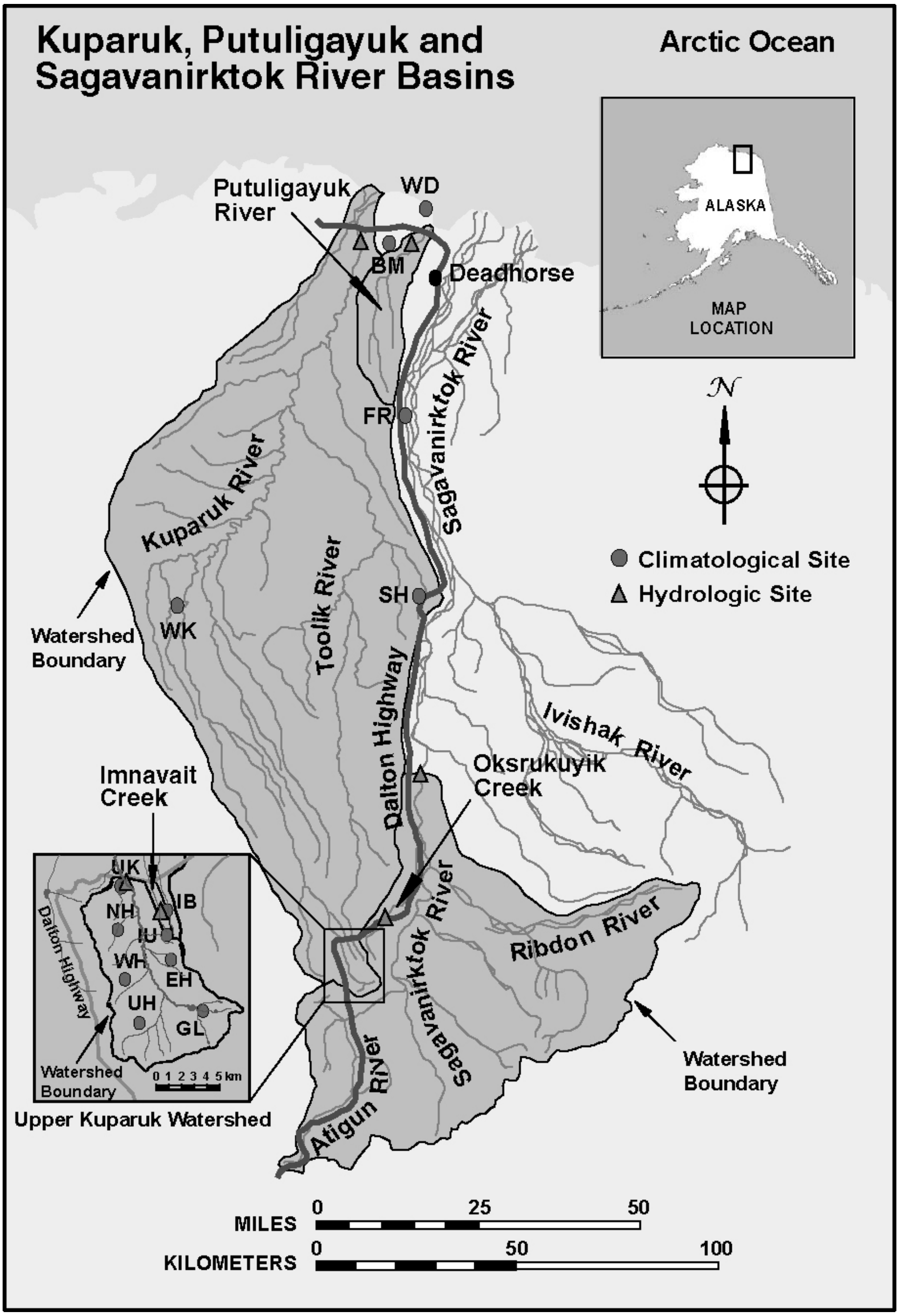

Figure 1. Location map of Kuparuk, Putuligayuk, Upper Kuparuk (insert) and Imnavait (insert) watersheds on the North Slope of Alaska.

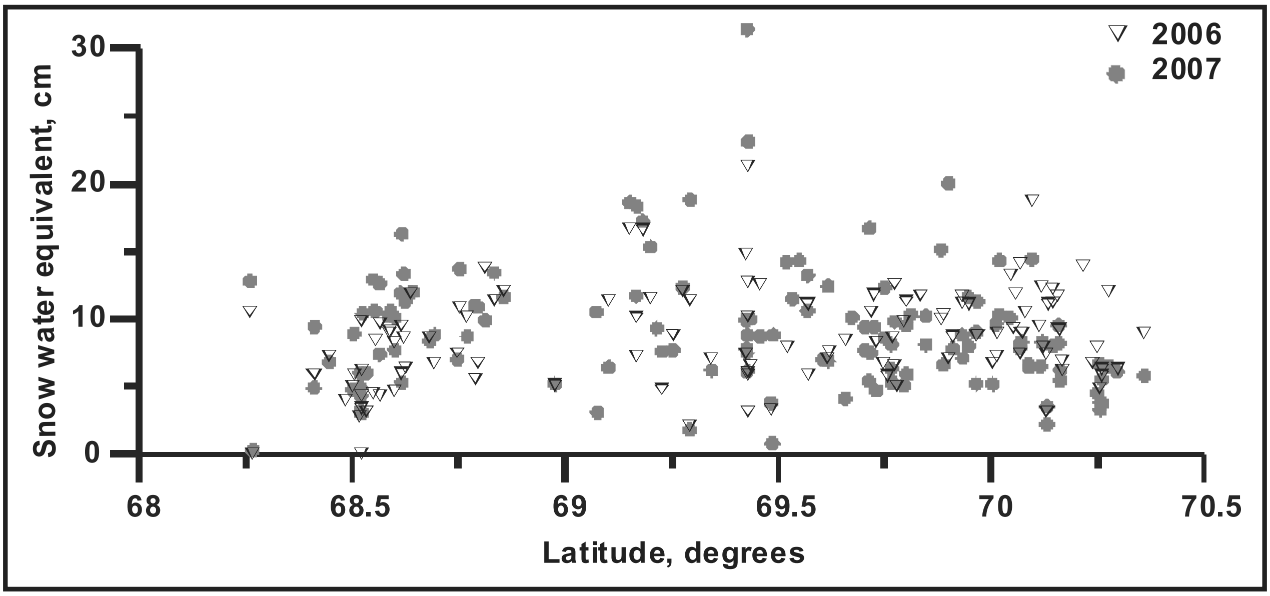

Figure 2. Variation of SWE (cm) with latitude over two winters in the central Arctic of Alaska.

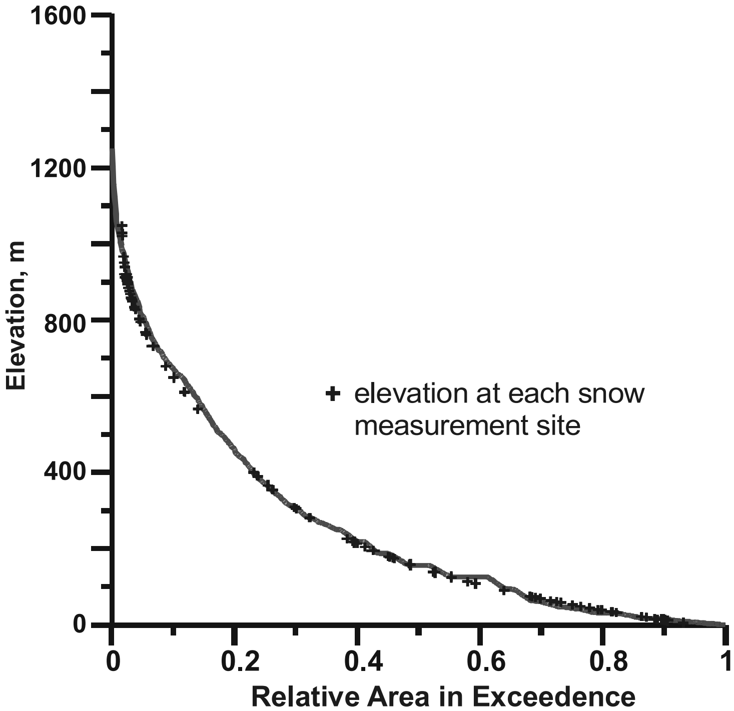

Figure 3. Each symbol on the hypsometric curve for the Kuparuk River basin represents a snow survey site.

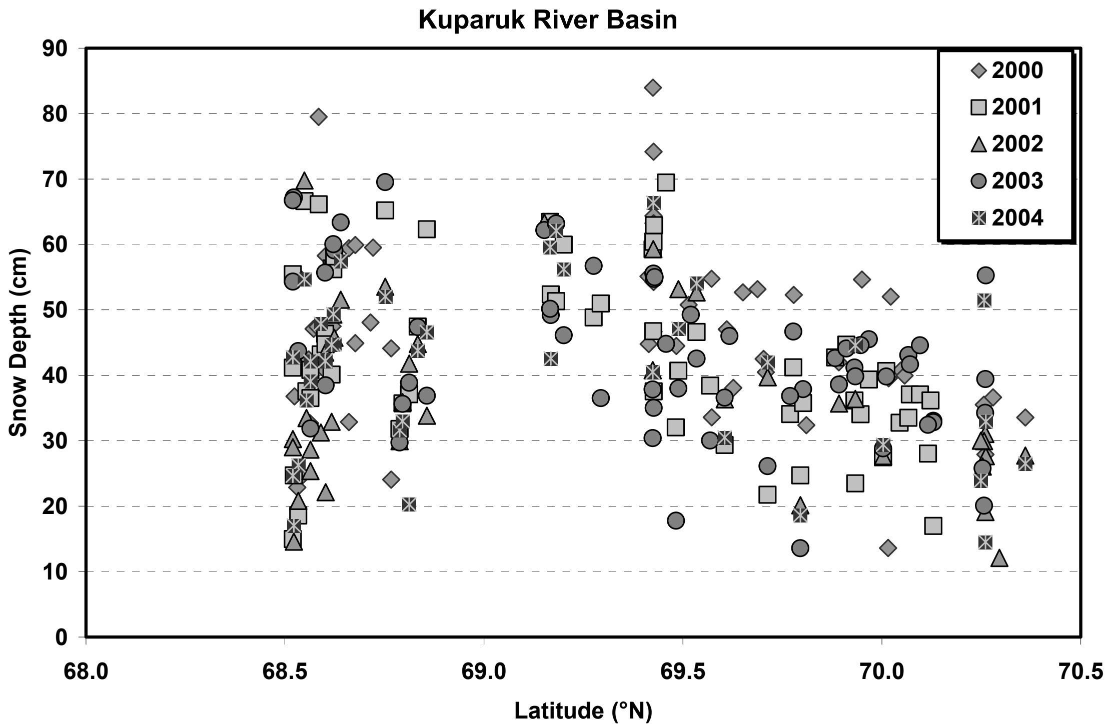

Figure 4. Average snow depth at a site (n = 50) as a function of latitude; individual snow depths can vary by greater than an order of magnitude.

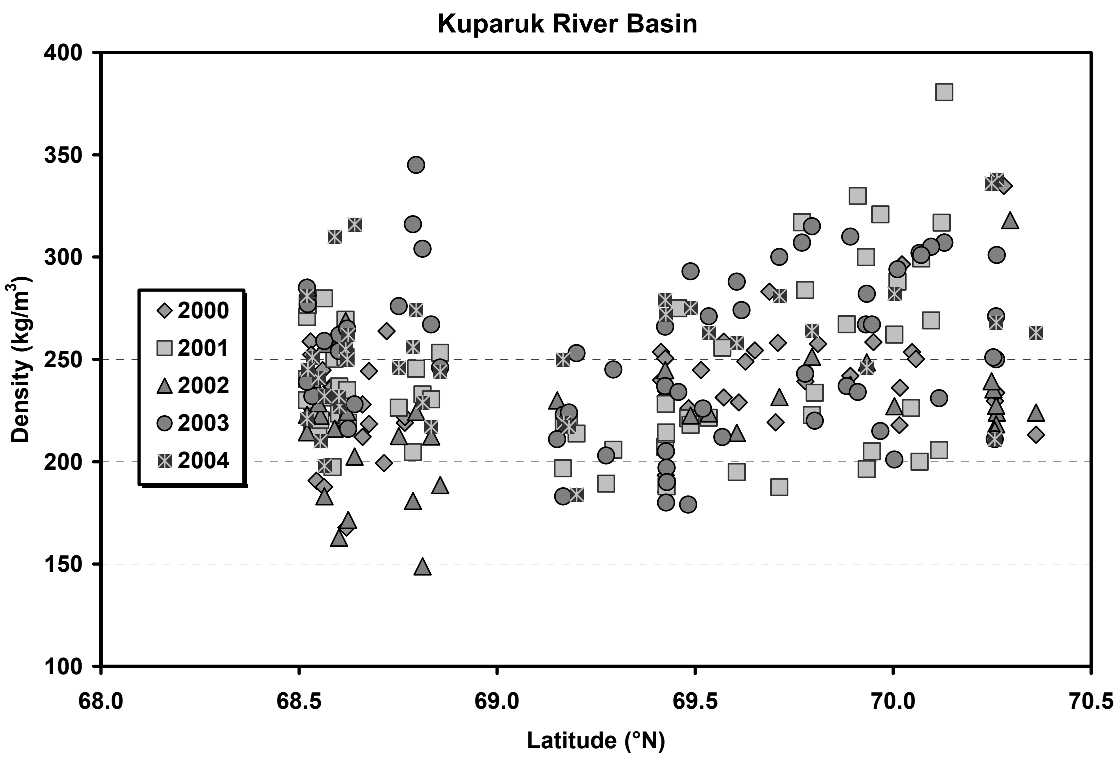

Figure 5. Average snow density (n = 5) as a function of latitude; most densities fall in the range of 250 □50 kg/m^3.

The rationale behind doing the transect studies is to see how much variability there is along transects of varying lengths. Are we amiss at believing that our L-shaped surveys (25 m by 25 m) are representative of much larger areas? Each transect length was divided into 100 equal lengths and the snow depth was then measured at that spacing along a straight line. The only exception is the 100 km long transect (100,000 m) where measurements were made along ten 10 km legs that were parallel. Otherwise the people collecting the data on snow machines would have ended up 100 km from the starting point.

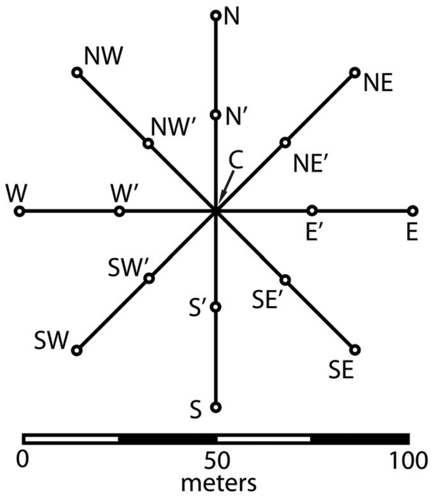

Figure 6. Starburst sampling diagram for snow depth measurements (n = 404) at an intensive site. Various sampling configurations (n = 50 or 100) can be compared statistically with those of all points.

4. RESULTS

4.1 Starburst sampling

The starburst pattern is used to evaluate how well our L-shaped pattern of snow depth measurement at each site captures the statistical average. Snow depths along four transects (N/S, E/W, NE/SW and SE/NW) 100 m long are measured at 1 m intervals (n = 404); in Table 2, three of the possible measurement possibilities are compared (L-shaped 50 measurements, L-shaped 100 measurements and a straight line 100 measurements). The mean of the entire snow depth population is 49.8 cm. The subsets can be identified using Figure 4; for example, the first one reads N' to C (center) to E'. For L-shaped subset (n = 50), the mean varied from 44.1 to 50.3. This can be compared to L-shaped pattern (n = 100) where the mean varies from 48 to 51.9 cm. For the four straight transects (n = 100), the mean varied from 48.8 to 51.1. The standard deviations varied from a low of 6.3 to 10.4 cm. Generally, the 50 measurements scheme gives a fairly representative estimate of the areal mean, capturing 89 to 101% of our best estimate (404 points). The mean of 100 L-shaped measurements varies from 96 to 104 % of entire starburst mean and captures 98 to 101 % of areal snow depth for the straight line (n = 100). Five other starburst-sampling efforts have been carried out with similar results.

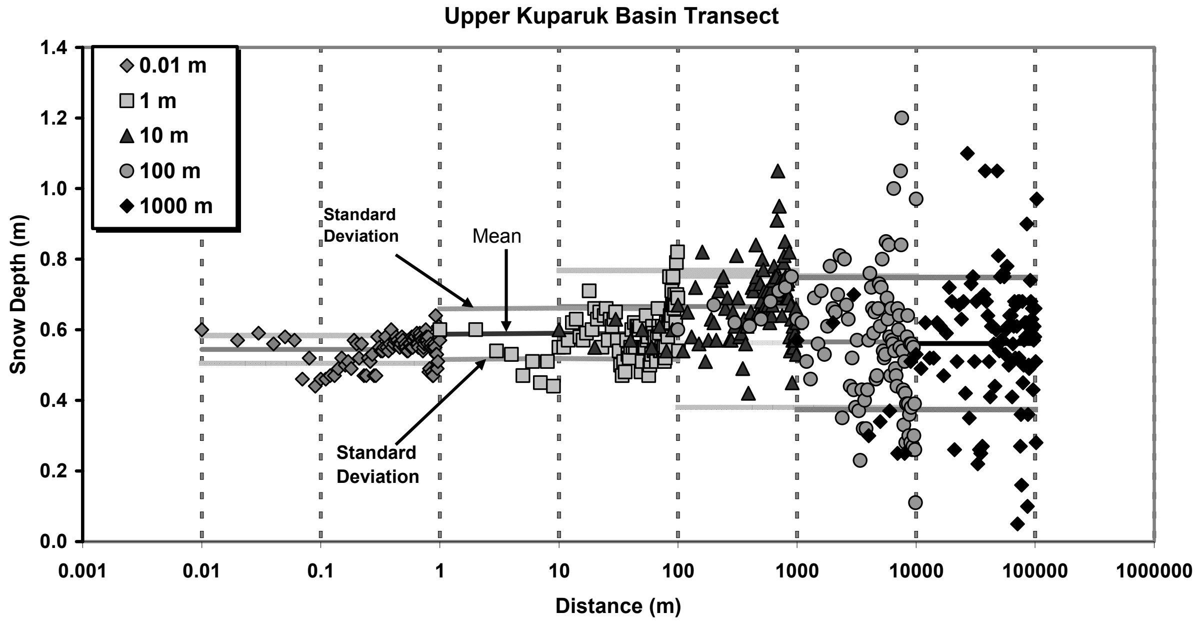

Figure 7. Variation of snow depths (n = 100) along transects of different length.

4.2 Scaling sampling

Scaling sampling allows us to analyze snow depth mean and variance from 100 points over different areal extents (from 1 m to 100 km) and different sampling intervals (from 1 cm to 1 km) thus bridging the gap between our sampling sites to the larger watershed scale. The transect data (Figure 5) shows that although the average depth (n = 100) is quite similar (Table 1) in April 2001 in the Upper Kuparuk drainage, the variability (standard deviation and range) increases with areal data extent. The fact that the 1 m transect mean agrees with the mean of the longer transects is probably a lucky coincidence in that the observer picked an average point. The average depth ranged from 0.54 m (1 m transect) to 0.67 m (10, 000 m). The standard deviation increased from 0.04 (1 m transect) to 0.19 cm (100,000 m transect), as would be expected. The data in the last column represents data collected in Imnavait Creek where 706 snow depth measurements were made along a 1000 km transect every 1.5 m.

4.3 Watershed scale

Our ultimate goal is to quantify the spatial distribution of the SWE at all watershed scales. Some of our past results for predicting the snowmelt runoff response and water balance of Arctic catchments have been less than stellar, especially for large watersheds like the Kuparuk River basin. Water balance determinations for Imnavait Creek, Upper Kuparuk River and the Putuligayuk River have been reasonable and believable for a variety of reasons from the small size of Imnavait catchment to the low-gradient Putuligayuk watershed. Higher than expected runoff ratios for the Kuparuk River (Lilly *et al*. 1998) for some years could only be due to overestimating the distributed SWE or underestimating the runoff.

Since we made those determinations of the runoff ratio, we have increased the density of our distributed SWE measurements for the whole of the Kuparuk River and adjacent watersheds (Table 3). Still, the complexity of SWE pattern requires an extremely large number of sampling points to represent spatial variability unless we have some process understanding that can define pattern features. Our plan is to apply snow transport model for the entire Kuparuk River using annual snow survey data for model calibration (Liston and Elder, 2006). Model performance can be successful with reliable atmospheric forcing, particularly wind and snowfall data, as well as high-resolution terrain and vegetation coverage.

Table 1. Statistics for the measured snow depth (n = 100) along transects of various lengths from 1 m to 100,000 m. The last column with the asterisk represents 706 depth measurements made over 1000 m.

Measurement Spacing (m)	0.01	1.0	10	100	1000	1.5*
Average (m)	0.54	0.59	0.67	0.57	0.56	0.56
Standard Deviation (m)	0.04	0.07	0.10	0.19	0.19	0.10
Minimum (m)	0.44	0.44	0.42	0.11	0.05	0.27
Maximum (m)	0.64	0.82	1.05	1.20	1.10	0.97

5. CONCLUSIONS

Snow depth and SWE are depleted in areas exposed to the wind and enhanced in leeward, low-lying and shrubby Arctic areas discussed here. There is a slight trend of increasing density with increasing latitude, in some years this is offset by decreasing depth with increasing latitude so the variation in SWE is unchanged. From the data presented here, it appears that our measurement scheme of 50 measurements in an L-shaped pattern gives a fairly good representative estimate of the average over 100 m and in some cases for distances of 10s of kms. It is also clear that for small incised streams (~ 2 to 3 m) and abrupt topographic changes (lake edge) of the same scale that we will not capture that variability. This in unfortunate since the SWE in these environments can exceed that in the open tundra by a substantial amount (a factor of 8 in one case measured in spring 2007). This is important hydrologically because this water is situated either in or closely adjacent to the drainage network.

To accurately predict the distribution of snow on the ground in this treeless, windy environment at winter's end, we need good data on winter solid precipitation (presently lacking), good digital elevation data, and a robust blowing snow model. We presently have good digital elevation data for some areas, but not most. Several blowing snow models exist (Pomeroy *et al*. 1997; Liston and Sturm 2002), but they require reliable forcing and assimilation data for successful performance. We could also use better vegetation data sets as shrubs are very efficient at trapping snow. With a combination of good winter precipitation data, digital elevation data and snow transport model, we will be able to use the data collected in the field and presented here for quantifying snow water equivalent distribution in the Arctic. We still have some challenges ahead of us, but it is crucial that we achieve this goal as the snow accumulation and ablation process is an important hydrologic event in the Arctic each year.

Table 2. A comparison of mean and standard deviation of various transects (n = 50 or 100) to the entire starburst data set (n = 404).

Subset	# of Points	Mean (cm)	Std. Dev. (cm)
Entire Starburst	404	49.8	8.1
L-Shaped Pattern, 25 m by 25 m			
N'2C2E'	50	50.3	10.4
E'2C2S'	50	47.5	8.1
S'2C2W'	50	44.1	6.3
W'2C2N'	50	47.2	8.0
L-Shaped Pattern, 50 m by 50 m			
N2C2E	101	51.9	9.0
E2C2S	101	51.9	9.0
S2C2W	101	48.0	8.0
W2C2N	101	49.9	7.9
Straight Transect, 100 m			
N2C2S	101	48.8	8.5
NE2C2SW	101	51.1	8.9
E2C2W	101	50.1	7.3
SE2C2NW	101	49.0	7.8

Table 3. Watershed average snow water equivalent (cm) on the North Slope of Alaska

	2006	2007	2006	2007
		Kuparuk River	Sagavanirktok River	
Mountains	6.7 (n=7)	6.3 (n=7)	7.3 (n=14)	6.7 (n=17)
Foothills	8.9 (n=39)	11.5 (n=41)	9.6 (n=6)	8.3 (n=13)
Coastal plain	9.5 (n=12)	9.9 (n=22)	9.4 (n=7)	7.5 (n=3)
Basin average	8.4 (n=58)	9.2 (n=70)	8.8 (n=27)	7.5 (n=33)

ACKNOWLEDGEMENTS

This work is funded by the National Science Foundation, Office of Polar Programs, OPP-0335941. We would also like to thank all of our fellow researchers that have helped over the years to collect this data.

REFERENCES

Berezovskaya, S. and D.L. Kane (2007) Measuring snow water equivalent for hydrological applications: part 1, accuracy of observations. *16th Northern Research Basin Symp* this volume, Petrazovodsk, Russia, Aug 27 – Sep 2

Bowling, L. C., D. L. Kane, R. E. Gieck, L. D. Hinzman and D. P. Lettenmaier (2003) The Role of Surface Storage in a Low-Gradient Arctic Watershed. Water Resources Research, 39(4), 1087, doi:10:1029/2002WR001466

Goodison, B. E., P. Y. T. Louie and D. Yang (1998) WMO Solid Precipitation Measurement Intercomparison, Final Report. World Meteorological Organization, WMO/TD 462, Geneva Switzerland, pp.212

Kane, D. L., L .D. Hinzman, J. P. McNamara, Z. Zhang and C. S. Benson (2000) An Overview of Nested Watershed Study in Arctic Alaska. *Nordic Hydrology*, 31(4/5):245-266.

Kane, D. L. and D. Yang (Eds.) (2004) Northern Research Basins Water Balance. IAHS, Publication 290, pp.271

Lilly, E. K., D. L. Kane, L. D. Hinzman and R. E. Gieck (1998) Annual Water Balance for Three Nested Watersheds on the North Slope of Alaska. In: Proceedings, Seventh International Conference on Permafrost, A. G. Lewkowicz and M. Allard (Eds.), Yellowknife, Canada, 669-674

Liston, G. E. and K. Elder (2006) A distributed snow-evolution modeling system (SnowModel). *J. Hydrometeorology*, 7, 1259-1276.

Liston, G. E. and M. Sturm (2002) Winter Precipitation Patterns in Arctic Alaska Determined from Blowing-Snow Model and Snow-Depth Observations. *Journal of Hydrometeorology*, 3:646-659

Pomeroy, J. W., P. Marsh and D. M. Gray (1997) Application of a Distributed Blowing Snow Model to the Arctic. *Hydrological Processes*, 11:1451-1464

Yang, D., D. L. Kane, L. D. Hinzman, B. E. Goodison, J. R. Metcalfe, P. Y. T. Louie, G. H. Leavesley, D. G. Emerson, and C. L. Hanson (2000) An Evaluation of the Wyoming Gauge System for Snowfall Measurement *Water Resources Research*, 36(9):2665-2677

Zhang, Z., D. L. Kane and L. D. Hinzman (2000) Development and Application of a Spatially Distributed Arctic Hydrological and Thermal Process Model (ARHYTHM), *Hydrological Processes*, 14:1017-1044.

Trends and variability in unregulated streamflow in Finland

Johanna Korhonen[1*]

[1] *Finnish Environment Institute, Box 140, 00251 Helsinki, FINLAND*
**Corresponding author, e-mail: Johanna.korhonen@ymparisto.fi*

ABSTRACT
This paper presents long-term discharge trends and variability for thirteen time series including both rivers and lake outlets in Finland. These unregulated discharge time series were studied for the longest available period until year 2004 and for the period 1961-2004. The longest discharge time series date back to the mid-1800s. The aim of this study was to examine observed changes and variability in the Finnish discharge regime until so far. The discharge peak flow usually occur in the south in April and in the north in June. In northern Finland the maximum flow of the year is always due to snow melt, but in the southern Finland summer, autumn and winter high flows are also possible. The Mann-Kendall trend test was applied to study changes in annual, monthly and seasonal mean discharges, maximum and minimum flows and in addition the date of peak flow. The trend analysis showed no changes in mean annual flow in general, but the seasonal distribution of streamflow have been shifted. Winter, spring and minimum discharges have increased at least half of the observation sites. The magnitude of increase in winter and spring discharges was 2…10 % per decade. The spring peak has moved earlier for the third of the studied sites with magnitude of 1…3 days per decade.

KEYWORDS
Discharge, trends, variability, Finland, rivers, lake outlets

1. INTRODUCTION

Water resources are highly dependent of climatic conditions. Run-off regime is affected by both precipitation and temperature changes, as well as changes in radiation balances. Finland belongs to the so called humid zone; the major water bodies do not normally dry out. A typical feature in Finland is the abundance of water bodies, both lakes and rivers. The water situation may, however, greatly differ from year to year. Within a year, there is a considerable difference between the winter, when the precipitation is stored in the snow cover, and the summer, when a major part of the rainwater evaporates. In the long run, slightly more than half of the precipitation evaporates and little bit less than half flows into the seas from Finland. Discharge gauging is the most precise method of all water balance component measurements. Future climate scenarios predict both droughts and floods to be increased due to greenhouse effect, therefore it is interesting to examine observed changes in the Finnish streamflow regime hitherto.

There are several earlier studies concerning long-term changes in Finnish discharge regime. Hyvärinen with his colleagues has carried out most of the discharge analysis done in Finland (Hyvärinen and Vehviläinen 1981, Hyvärinen 1988, Hyvärinen and Leppäjärvi 1989, Hyvärinen 1998, 2003). Kuusisto (1992) has also studied long-term runoff from Finland. Finnish streamflow records have also been included in the Nordic runoff studies conducted by Hisdal *et al.* (1995, 2003, 2004) and Roald (1998). Effects of climate change on water resources in Finland have been presented by e.g. Vehviläinen ja Lohvansuu (1991), Hiltunen (1992, 1994), Vehviläinen and Huttunen (1997) just to mention a few anterior.

2. DATA AND METHODS

The data consist of daily mean discharges for thirteen different gauges from the different parts of the country. Both rivers and lake outlets are included in this investigation. Discharges have been determined from water level records by the rating curve method. Many of the watersheds in Finland are regulated

either for water power production or flood mitigation. All the studied sites are unregulated, but some changes (land uplift, changes in land use, ditch drainage, forestry etc.) in the catchment during the years are unavoidable. because there are so many regulated watersheds, the even distribution of studied discharge sites over the country was not possible. Many of the studied lake outlets are situated in the headwaters, since the lower water bodies are regulated. The longest discharge time series in this study date back to the mid-1800s. The study sites and their locations are presented Figure 1. The observation periods, upper catchments and lake percentages are presented in Table 1.
The data were analysed until the year 2004 for the longest available period, and in addition for the period 1961-2004. Trend analysis was applied to annual mean discharges (calendar year), monthly mean and seasonal mean discharges (winter: Dec-Jan-Feb, spring: Mar-Apr-May, summer Jun-Jul-Aug, and autumn: Sep-Oct-Nov), annual maximum and minimum flows and date of the peak flow (maximum). Trends were tested statistically with the non-parametric Mann-Kendall trend test. The level of 5 % was used for the critical significance. Trend slope of the magnitude was calculated using a non-parametric Sen's slope estimator (Sen 1968).

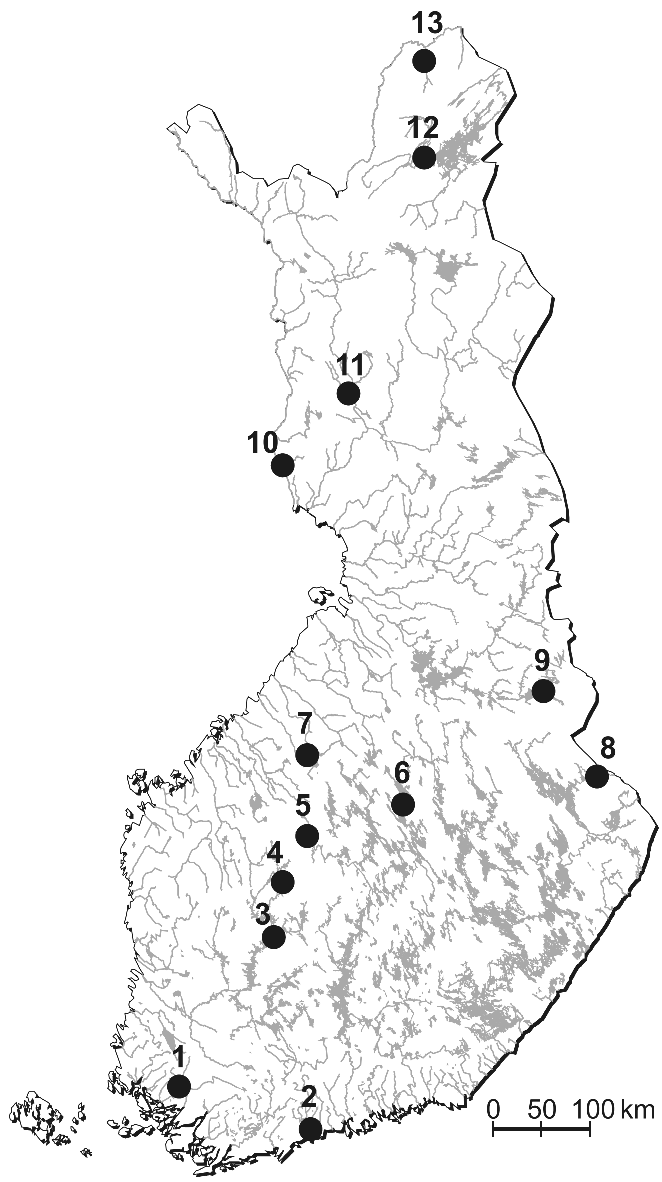

Figure 4. A map of the discharge gauging station locations used in this study.

Table 2. A list of studied rivers and lake outlets including available time period, upper catchment (F) and lake percentage (L) of discharge point.

	Name	Observation period	F (km^2)	L (%)
1.	Aurajoki, Hypöistenkoski (river)	1948-2004	351	0
2.	Vantaanjoki, Oulunkylä (river)	1937-2004	1620	2.8
3.	Muroleenkoski – outlet (lake)	1863-2004	6102	12.2
4.	Kitusjärvi – outlet (lake)	1911-2004	546	9.6
5.	Pääjärvi – outlet (lake)	1911-2004	1214	7.1
6.	Nilakka Äyskoski (lake)	1896-2004	2157	17.9
7.	Lestijärvi - outlet (lake)	1921-2004	363	21.1
8.	Ruunaa – outlet (lake)	1931-2004	6259	13.7
9.	Lentua - outlet (lake)	1911-2004	2045	12.7
10.	Tornionjoki, Karunki (river)	1911-2004	39010	4.7
11.	Ounasjoki, Marraskoski (river)	1919-2004	12303	2.6
12.	Juutuanjoki, Saukkoniva (river)	1921-2004	5160	4.7
13.	Utsjoki , Patoniva (river)	1963-2004	1520	2.6

RESULTS AND DISCUSSION

2.1 Discharge regime and variability

The annual peak flow usually occurs usually in southern coast in April and in northern Lapland in the turn of May and June. In northern Finland maximum flow of the year is always due to snow melt, but in the southern Finland summer, autumn and winter annual maximum flows due to high rainfall are also possible. In the north the minimum flow of the year is recorded in the winter, but in the south both winter and summer flow minima are common. In Figure 2 monthly minimum, mean and maximum discharges for four different discharge gauges are presented. Two of the graphs present the annual discharge regime of river sites and two same for the lake sites.

There is a great variation of discharge from year to year, and especially monthly mean discharges differ greatly between the years. The variation percentage of annual mean discharge varied from 19 to 37%. It was highest in the southern river sites with a small lake percentage and a small area of the catchment. Lowest variations were recorded in northern Finland. The highest variation percentage of the monthly discharges was for February 220% in the river Aurajoki.

The driest years have been at most of the sites 1941 or 1942. The wettest year was not so evident as the drought of 1941-1942, on the contrary it varied between the sites. At many places the year 1981 was a rather wet. The ratio between the wettest and the driest year discharges varied from 3- to 6-folded.

The average ratio between HQ and MQ of each year varied from 2- to 4-fold at lake sites and from 6- to 16-fold at river sites. The ratio is highly dependent on the lake percentage; if the percentage is low, the ratio is high and vice versa.

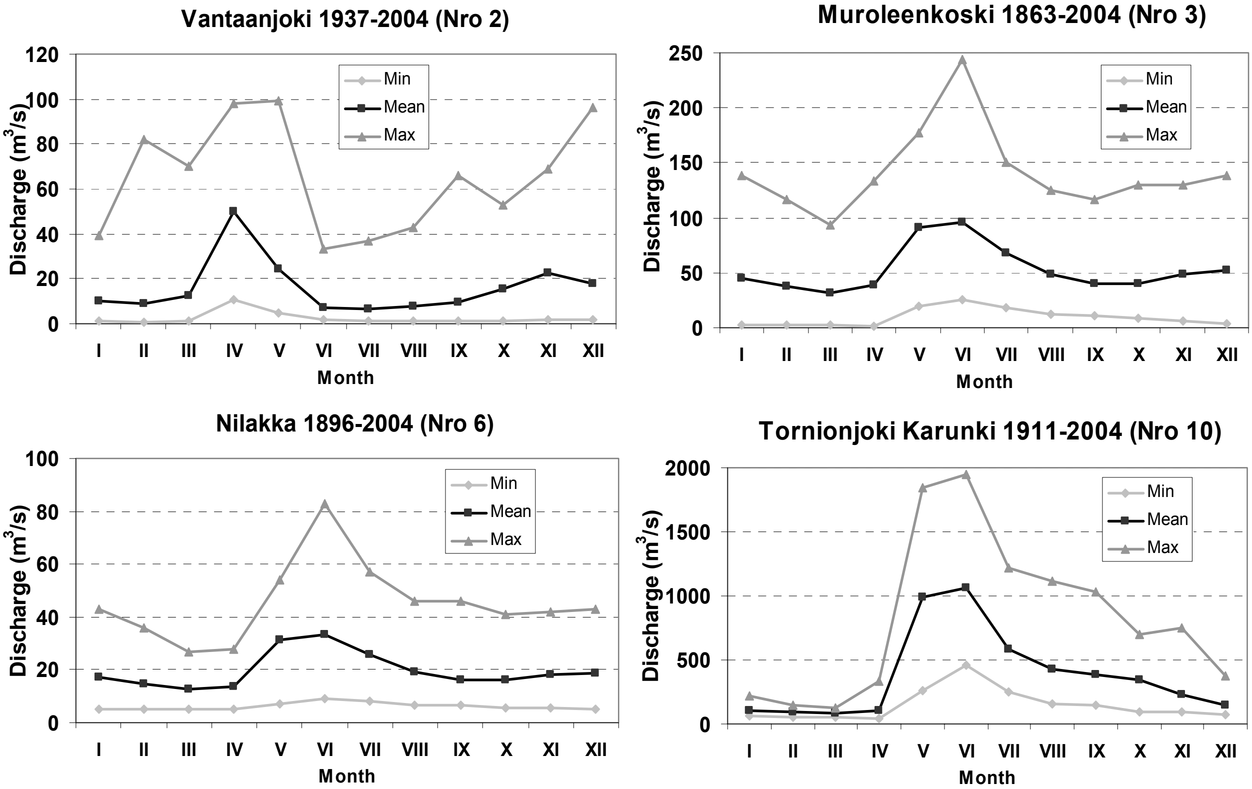

Figure 5. Monthly minimum, mean and maximum discharges for four different discharge gauges.

2.2. Trends

Statistically significant trends in streamflow for the longest possible period until 2004 and for the period 1961-2004 are shown later in Table 2. Eleven of thirteen sites (85 %) had at least some trends detected. There were more statistically significant trends for the whole observation period available than for the period 1961-2004. There were no trends for the annual mean flow in general, only one site (river Tornionjoki) had statistically significant trend for increased discharges. Neither high flows had no long-term changes. The biggest change has happened in the seasonal distribution of flow. The spring peak has moved earlier, statistically significantly at the third of the observation sites. The magnitude of trend for the timing of the peak was 1…3 days per decade. Winter and spring discharges have increased at most sites. 69 % of the time series had significant increase of discharge for spring months an 49 % for winter months. The minimum flow has increased for 46 % of the sites. The magnitudes of discharge increases were typically 2…10 % of the mean flow (of month or season) per decade. The summer flows had increased for only 15 % of the sites. In addition, 1-2 of the time series had negative trends for a few winter, spring or summer mean monthly discharges. Basically, no statistically significant trends in autumn flows were found. Time series of the mean annual discharge and the mean spring (MAM) discharge for different stations are presented in Figures 3 and 4.

Positive trends in winter discharge can be explained by milder winters during the last decades. The increased spring discharge is due to earlier spring peaks; the shift in the peak timing has increased discharges.

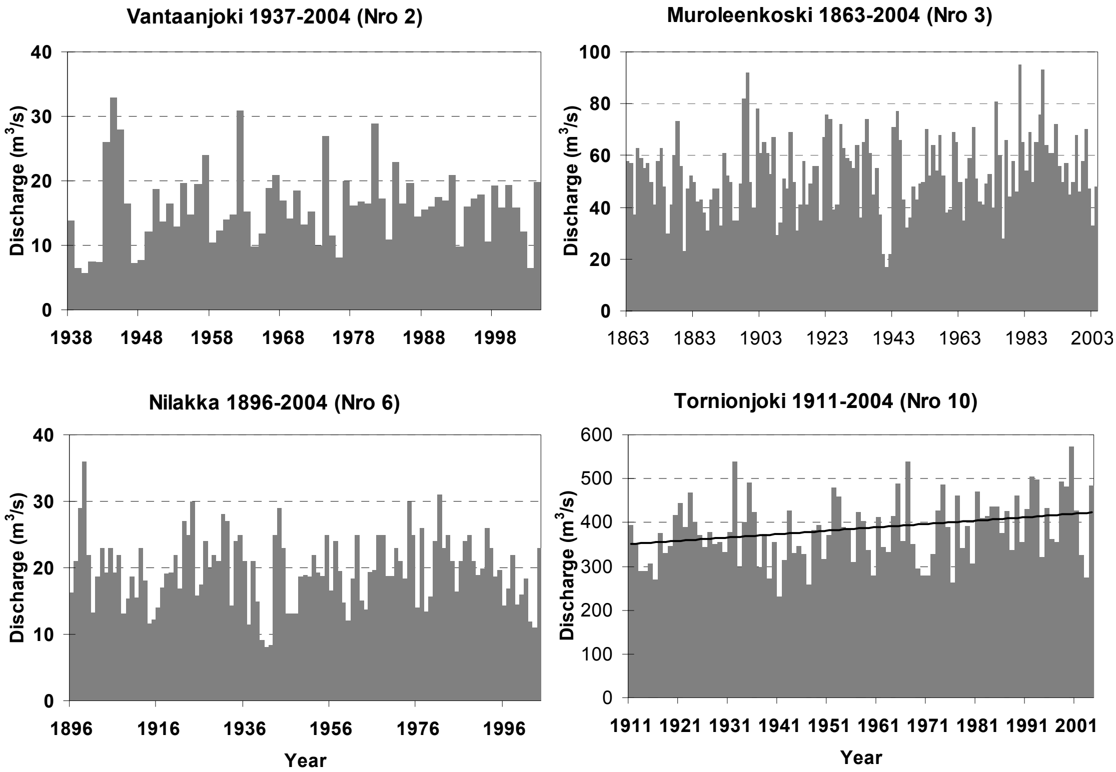

Figure 6. Mean annual (MQ) discharge (m^3/s) for four different discharge gauges.

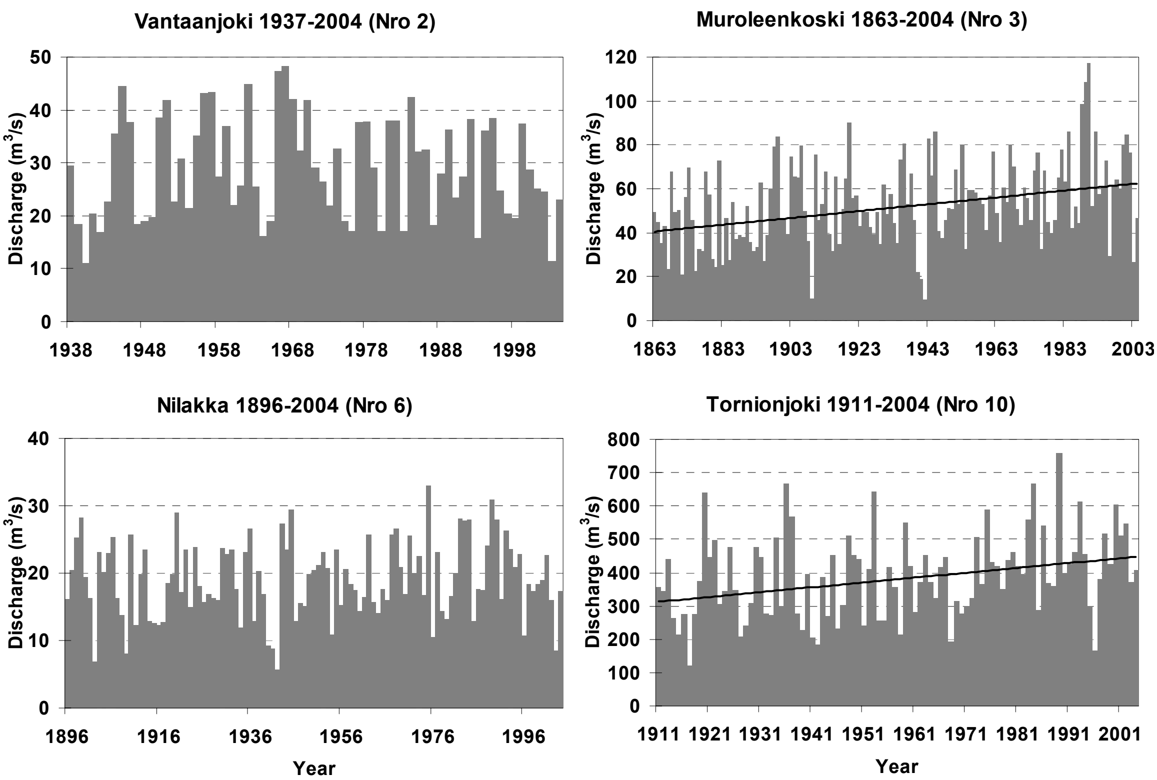

Figure 7. Mean spring (MAM) discharge (m^3/s) for four different discharge gauges.

Table 3. Statistically significant trends for monthly and seasonal mean discharges, maximum and minimum flows and peak flow dates. I-MQ means January mean discharge, II-MQ February mean discharge etc. DFJ-MQ means winter mean discharge, MAM-MQ spring mean discharge etc.

Observation site	Variable and period	+/-	p<	Trend /10 a, %
1 Aurajoki, Hypöistenkoski	II-MQ 1948-2004	+	0,05	0,1 m^3/s (5,0 %)
Period 1948-2004	III-MQ 1948-2004	+	0,01	0,3 m^3/s (9,1 %)
	VI-MQ 1948-2004	+	0,001	0,1 m^3/s (12,5 %)
	VII-MQ 1948-2004	+	0,05	0,05 m^3/s (4,5 %)
	III-MQ 1961-2004	+	0,05	0,5 m^3/s (13,5 %)
	JJA-MQ 1948-2004	+	0,05	0,1 m^3/s (9,1 %)
	DJF-MQ 1961-2004	+	0,05	0,5 m^3/s (18,5 %)
2 Vantaanjoki, Oulunkylä	I-MQ 1937-2004	+	0,05	0,9 m^3/s (8,9 %)
Period 1937-2004	II-MQ 1937-2004	+	0,001	0,8 m^3/s (9,0 %)
	III-MQ 1937-2004	+	0,01	1,0 m^3/s (8,1 %)
	VII-MQ 1937-2004	+	0,001	0,5 m^3/s (7,5 %)
	VIII-MQ 1937-2004	+	0,01	0,5 m^3/s (6,6 %)
	NQ 1937-2004	+	0,001	0,2 m^3/s (10,0 %)
	DJF-MQ 1937-2004	+	0,05	1,0 m^3/s (8,2 %)
	JJA-MQ 1937-2004	+	0,01	0,5 m^3/s (7,0 %)
	HQ (MAM) 1961-2004	-	0,05	12,7 m^3/s (10,8 %)
3 Muroleenkoski	I-MQ 1863-2004	+	0,01	1,5 m^3/s (3,3 %)
Period 1863-2004	II-MQ 1863-2004	+	0,001	1,6 m^3/s (4,3 %)
	III-MQ 1863-2004	+	0,001	1,5 m^3/s (4,8 %)
	IV-MQ 1863-2004	+	0,001	1,9 m^3/s (4,9 %)
	VI-MQ 1863-2004	-	0,05	1,6 m^3/s (1,7 %)
	NQ 1863-2004	+	0,001	0,9 m^3/s (4,3 %)
	HQ-date (spring) 1863-2004	-	0,001	1,0 d
	DFJ-MQ 1863-2004	+	0,01	1,3 m^3/s (2,9 %)
	MAM-MQ 1863-2004	+	0,001	1,6 m^3/s (3,0 %)
4 Kitusjärvi, luusua	No statistically significant trends			
Period 1911-2004				
5 Pääjärvi, luusua	II-MQ 1911-2004	+	0,001	0,3 m^3/s (5,9 %)
Period 1911-2004	III-MQ 1911-2004	+	0,001	0,3 m^3/s (7,3 %)
	IV-MQ 1911-2004	+	0,01	0,5 m^3/s (5,1 %)
	NQ 1911-2004	+	0,001	0,2 m^3/s (28,6 %)
	VII-MQ 1961-2004	+	0,05	0,8 m^3/s (9,1 %)
	MAM-MQ 1911-2004	+	0,05	0,5 m^3/s (3,0 %)
6 Nilakka, Äyskoski	IV-MQ 1896-2004	+	0,05	0,3 m^3/s (2,2 %)
Period 1896-2004				
7 Lestijärvi, luusua	III-MQ 1921-2004	+	0,05	0,05 m^3/s (2,3 %)
Period 1921-2004	IV-MQ 1921-2004	+	0,01	0,09 m^3/s (3,6 %)
	MAM-MQ 1921-2004	+	0,05	0,09 m^3/s (2,8 %)
8 Lieksanjoki, Ruunaa	No statistically significant trends			
Period 1931-2004				
9 Lentua, luusua	II-MQ 1911-2004	+	0,05	0,3 m^3/s (2,2 %)
Period 1911-2004	III-MQ 1911-2004	+	0,05	0,2 m^3/s (1,8 %)
	V-MQ 1911-2004	+	0,05	1,5 m^3/s (2,8 %)
	NQ 1911-2004	+	0,01	0,2 m^3/s (1,5 %)
	MAM-MQ 1911-2004	+	0,05	0,6 m^3/s (2,3 %)
	II-MQ 1961-2004	+	0,01	0,9 m^3/s (6,5 %)
	III-MQ 1961-2004	+	0,001	0,8 m^3/s (6,9 %)
	NQ 1961-2004	+	0,01	0,6 m^3/s (6,1 %)
10 Tornionjoki, Karunki	I-MQ 1911-2004	+	0,001	5,6 m^3/s (5,2 %)
Period 1911-2004	II-MQ 1911-2004	+	0,001	4,7 m^3/s (5,3 %)
	III-MQ 1911-2004	+	0,001	4,3 m^3/s (5,4 %)

	IV-MQ 1911-2004	+	0,01	3,3 m^3/s (3,2 %)
	V-MQ 1911-2004	+	0,01	36,0 m^3/s (3,7 %)
	XI-MQ 1911-2004	+	0,05	9,1 m^3/s (4,0 %)
	XII-MQ 1911-2004	+	0,001	8,2 m^3/s (5,6 %)
	MQ 1911-2004	+	0,01	7,7 m^3/s (2,0 %)
	NQ 1911-2004	+	0,001	3,5 m^3/s (4,7 %)
	DJF-MQ 1912-2004	+	0,001	6,3 m^3/s (5,5 %)
	MAM-MQ 1911-2004	+	0,01	14,5 m^3/s (3,7 %)
	HQ-date (spring) 1911-2004	-	0,01	1,4 d
	V-MQ 1961-2004	+	0,05	73,1 m^3/s (6,9 %)
	HQ-date (spring) 1961-2004	-	0,05	2,9 d
	MAM-MQ 1961-2004	+	0,05	29,6 m3/s (7,0 %)
11 Ounasjoki, Marraskoski Period 1919-2004	III-MQ 1919-2004	+	0,01	0,9 m^3/s (2,7 %)
	NQ 1919-2004	+	0,01	0,7 m^3/s (2,3 %)
	HQ-date (spring) 1961-2004	-	0,05	2,5 d
12 Juutuanjoki, Saukkoniva Period 1921-2004	I-MQ 1921-2004	-	0,05	0,6 m^3/s (2,7 %)
	HQ-date (spring) 1921-2004	-	0,05	1,2 d
	HQ-date (spring) 1961-2004	-	0,01	3,3 d
13 Utsjoki, Patoniva Period 1963-2004	II-MQ 1963-2004	-	0,05	0,3 m^3/s (6,5 %)
	III-MQ 1963-2004	-	0,01	0,3 m^3/s (7,7 %)
	NQ 1963-2004	-	0,001	0,3 m^3/s (9,1 %)

COMPARISON WITH OTHER STUDIES

There are a number of earlier studies concerning long-term changes in runoff in Finland and in the Nordic countries. Anterior studies of long-term changes in runoff or discharge regime have showed a quite similar patterns as this study do. The increase of wintertime discharge in southern and central Finland was presented first by Hyvärinen and Vehviläinen (1980). Later observations and analyses confirmed these findings (Hyvärinen 1988, Hyvärinen ja Leppäjärvi 1989, Hiltunen 1994 and Hyvärinen 1998, 2003). The Nordic studies of trends in runoff regime have revealed considerable differences in different parts of Fennoscandia (Hisdal *et al*. 1995, 2003, 2004 and Roald 1998). Mean annual discharges have been increased especially in some regions in Denmark and Sweden. Positive trends have also been found for Norway and Finland depending on the chosen time period (Hisdal *et al.* 2004). For the period 1941-2002 statistically significant trends are found for Finland probably because the first year of time period (1941) was the driest ever observed at many places in Finland. In Iceland, annual values of discharge do not show clear trends (Jónsdottir 2005). In Karelia, Northwest Russia, the river runoff has decreased during the 20th century (Filatov 2005).

Discharges are naturally highly dependent of precipitation and evaporation. Long-term changes have not been detected for the precipitation time series in Finland (Tuomenvirta 2004), although in the other Nordic countries (Sweden, Norway, Denmark, Iceland) increase have been observed (Hisdal *et al.* 2003, Jónsdottir *et al.* 2005). In Karelia, Northwest Russia precipitation has been increased during the 20th century (Filatov *et al.* 2005). The evaporation time series begin mainly in the late 1950s in Finland, thus such long time series as precipitation and discharge records, are not available for the Class A Pan evaporation. However, for the period 1961-1990 no trends were reported by Järvinen and Kuusisto (1995). Neither precipitation nor evaporation show remarkable long-term trends in Finland. Regardless, the changes in the streamflow have been observed in Finland. However, the annual mean flow in unregulated streams has not changed in Finland in general. The main issue is the change in the seasonal distribution of discharge regime.

CONCLUSIONS

Thirteen Finnish discharge time series of unregulated rivers and lake outlets were examined in this study. The timing of high flow in the rivers varies from April to June from the south to north, respectively. The low flows are recorded in the north in the winter and in the south typically in wintertime or in summertime. Typical variation of annual mean discharge was 20…40 %. It was highest in southern river sites with a small lake percentage and a small area of the catchment. Lowest variations were in northern Finland. The ratio between annual high flow and annual mean flow varied from 2- to 4-fold in lake outlets and from 6- to 16-fold in rivers. Trends of time series were analysed in order to find changes in the historical records. Mean annual, monthly and seasonal discharge trends as well as changes for the extreme values were calculated by the non-parametrical Mann-Kendall trend test. Mean annual flows showed no changes, but the seasonal distribution of flow has changed in most places investigated in this study. The spring peak has moved earlier for the third of the sites. The change has been 1…3 days per decade. Trend analysis showed that the winter, spring and minimum discharges have increased at least half of the observation sites. The magnitude of observed increase in the monthly or seasonal discharge was typically 2…10 % per decade. Positive trends in winter discharge can be explained by milder winters with increased winter precipitation during the last decades. The increased spring discharge is due to earlier spring peaks caused by warming during the spring time; the shift to earlier peak flows has increased discharges. There were no statistically significant changes in autumn streamflow in general.

REFERENCES

Filatov, N., Salo, Y., and Nazarova, L. (2005) Effects of climate change variability on natural water bodies in Northwest Russia. Proc. *15th Northern Research Basins Symposium*, Luleå to Kvikkjokk, Sweden, Aug 29 - Sep 2. pp. 31-40.

Hiltunen, T. (1992) Fluctuations of long discharge time series in Finland. Proc. *Nordisk hydrologisk konferanse 1992*, Alta, Norway, Aug 4-6 1992. NHP-rapport 30. pp. 59-64.

Hiltunen, T. (1994) What do hydrological time series tell about climate change? *Publications of the Water and environment Research Institute* **17**, 37-50.

Hisdal, H., Erup, J., Gudmundsson, K., Hiltunen, T., Jutman, T., Ovesen, N. B., and Roald, L (eds.). (1995) *Historical runoff variations in the Nordic countries.* NHP report No 37.

Hisdal, H., Holmqvist, E., Hyvärinen, V., Jónsson, P., Kuusisto, E., Larsen, S. E., Lindström, G., Ovesen, N. B. and Roald, L. A. (2003) *Long time series, A review of Nordic studies. CWE Long Time Series group.* Report no. 2.

Hisdal, H., Holmqvist, E., Kuusisto, E. and Lindström, G. (2004) Has streamflow changed in the Nordic countries? Proc. *XXIII Nordic hydrological conference, Vol 2,* Tallinn, Estonia, Aug 8-12. NHP Report 48. pp. 633-643.

Hyvärinen, V. (1988) Effects of climatic changes on winter discharge in Finland. Proc. *Nordic Hydrological conference, Vol 1,* Rovaniemi, Finland, Aug 1-3, 1988. NHP-rapport 22. pp. 27-32.

Hyvärinen, V.(1998) Observed trends and fluctuations in hydrological time series in Finland - a review. Proc. *The Second International Conference on Climate and Water, Vol. 3*, Espoo, Finland, Aug 17-20. pp. 1064-1070.

Hyvärinen, V. (2003) Trends and characteristics of hydrological time series in Finland. *Nord. Hydrol.* **34**(1/2), 71-90.

Hyvärinen, V. and Leppäjärvi, R. (1989) Long-term trends of river flow in Finland. Proc. *Conference on climate and water Vol. 1*. Helsinki, Finland. pp. 450-461.

Hyvärinen, V. and Vehviläinen, B. (1981) The effects of climatic fluctuations and man on discharge in Finnish river basins. *Publications of the Water Research Institute* **43**, 15-23.

Jónsdottir, J. F., Jónsson, P. and Uvo, C. B. (2005) Trend analysis of Icelandic discharge, precipitation and temperature series. Proc. *15th Northern Research Basins Symposium*, Luleå to Kvikkjokk, Sweden, Aug 29 - Sep 2. pp. 69-78.

Järvinen, J. and Kuusisto, E. (1995). *Astiahaihdunta Suomessa 1961-1990* (English abstract: Pan evaporation in Finland in 1961-1990), Publications of Water and Environment Administration, serie A 220. pp. 171-178.

Kuusisto, E. (1992) Runoff from Finland in the period of 1931-1990. *Aqua Fennica* **22**(1), 9-22.

Roald, L. A. (1998) Changes in runoff in the Nordic countries, a result of changing circulation pattern? Proc. The second International Conference on Climate and Water. Espoo Finland, Aug 17-20 1998. pp. 1099-1109.

Sen, P. K. (1968) Estimates of the regression coefficient based on Kendall's tau. *Journal of the American Statistical Association* **63**, 1379-1389.

Tuomenvirta, H. (2004) *Reliable estimation of climatic variations in Finland.* Finnish Meteorological Institute Contributions 43. Finnish Meteorological Institute, Helsinki.

Vehviläinen, B. and Lohvansuu, J. (1991) The effects of climate change on discharges and snow in Finland. *Hydrological Sciences Journal* **36**(2), 95-208.

Vehviläinen, B. and Huttunen, M. (1997) Climate change and water resources in Finland. *Boreal Environment Research* **2**(1), 3-18.

Seasonal dynamics of dissolved nitrogen species in two High Arctic rivers, Melville Island, Canada

Melissa Lafrenière

Department of Geography, Queen's University, Kingston, ON, K7L 3N6 CANADA
**Corresponding author, e-mail: melissa.lafreniere@queensu.ca*

ABSTRACT

This study examines the magnitude, seasonal patterns, and characteristics N export from two small watersheds on Melville Island, in the Canadian High Arctic. The dominant N species in both rivers was dissolved organic nitrogen (DON), comprising >80% of the seasonal nitrogen flux from both rivers. The total DON and dissolved inorganic nitrogen (DIN) mass fluxes from the two catchments were similar (242 and 245 kg DON, and 42-45 kg DIN), but there were differences in the patterns and concentrations of the DIN species in the two catchments. The West river had higher initial DON and DIN concentrations that decreased to stable concentrations around 0.150 ppm and 0 ppm by mid July. The East river had variable early season DON and NO_3^-concentrations ranging from 0.138-0.415, and 0-0.125 ppm, respectively. End of season DON and DIN concentrations increased from 0.134 to 0.240, and 0 to 0.085 ppm, respectively. The DOC:DON ratio also decrease from 13 to 6, indicating a change in the composition of dissolved organic matter in this river at the end of season. The total DON fluxes from these two small arctic watersheds are similar to fluxes reported for other catchments in temperate environments.

KEYWORDS

Nitrogen, High Arctic rivers, nutrient fluxes, DON, NO_3^-, NH_4^+.

1. INTRODUCTION

Fluvial input of dissolved organic matter (DOM) represents an important source of carbon and bioavailable nitrogen (N) to freshwater and marine ecosystems (Cole, J. J. and Caraco, N. F. 2001, Cornell, S.*, et al.* 1995, Dittmar, T. 2004, Mayorga, E.*, et al.* 2005, Pace, M. L.*, et al.* 2004). Because N is often the limiting nutrient for phytoplankton growth, the export of nitrogen species (including DON, NO_3^- ad NH_4^++) from the terrestrial catchments plays an important role in aquatic elemental cycles (Dittmar, T. 2004). Two of the primary controls on the export of N from the land surface are the volume and the routing of catchment runoff through shallow soils(Cooper, R.*, et al.* 2007, Hagedorn, F.*, et al.* 2000, Hood, E.*, et al.* 2003a, Perakis, S. 2002, Pinay, G.*, et al.* 2002). Hence, there is a need to understand how the hydrologic components of the climate system influence the interactions between terrestrial nitrogen sources, and the leaching or export of N in stream runoff

Arctic catchments store a significant proportion of the world's soil organic matter (Dittmar, T. and Kattner, G. 2003) and Arctic rivers yield large amounts of terrigenous organic matter relative to other river basins (Hansell, D.*, et al.* 2004). In addition, observations indicate that the central Arctic has experienced substantial warming over the 20th century and models project this warming trend will continue over the next century(ACIA 2005, IPCC 2001, Serreze, M. C.*, et al.* 2000). Observations of recent changes in precipitation and snow cover suggest that precipitation in the Arctic appears to have increased, while snow cover duration and extent have decreased in most areas (ACIA 2005, IPCC 2001, Serreze, M. C.*, et al.* 2000) Through their effect on runoff (timing and quantity), permafrost degradation, and slope stability, these changes in climatic conditions will exert significant influence on nutrient dynamics in terrestrial catchments. There is, therefore, a pressing need to understand the response of terrestrial nutrient dynamics to changing water, permafrost and climate regimes in the High Arctic.

This study examines the magnitude, seasonal patterns, and characteristics N export from two small watersheds on Melville Island, in the Canadian High Arctic. Specifically, the paper discusses the difference in controls on nitrogen concentrations and fluxes from these adjacent watersheds, and evaluates the significance of these fluxes with respect to other temperate environments.

2. METHODS

2.1 Site Description

The research site is Cape Bounty (74°54N, 109°35W), Melville Island, Nunavut (Figure 1). This study reports on the rivers draining the two main watersheds unofficially named West (8.0 km^2) and East (11.6 km^2). The two catchments are topographically similar, consisting of rolling terrain, with elevations ranging from approximately 5 m.a.s.l. to 165 m. a.s.l. Both streams are incised into the surrounding terrain and drain into similar small lakes (Figure 1). The study area is underlain by continuous permafrost that develops an active layer ca. 0.5–1 m deep during the spring and summer. The geology consists of steeply dipping Devonian sedimentary rocks that are covered with glacial and regressive early Holocene marine sediments (Hodgson, D. A.*, et al.* 1984). Vegetation and soil cover is heterogeneous and varies with moisture conditions. The upland regions may be classified as polar desert and generally lack soils and vegetation, while the wetter lowland areas have thin soils and patchy dwarf prostrate shrub tundra vegetation (Walker, D. A.*, et al.* 2005).

2.2 Field methods

Local meteorological conditions during the period of study were captured by two weather stations in the catchment. For the spring and summer of 2006 Westmet (Figure 8) measured temperature at 1.5 m above the ground (0.4°C accuracy) and precipitation (0.2 mm resolution). In addition to temperature and precipitation, Mainmet (Figure 1), monitored solar and net radiation, wind speed and direction, and relative humidity.

Hydrological measurements for both streams were obtained from gauging stations near the lake inlets (Figure 1). Stage was recorded with a logging pressure-transducer and was compensated for atmospheric pressure changes using a second pressure-temperature logger in each river. Discharge was rated at each gauging station using manual area-velocity measurements obtained throughout the seasons with a Swoffer 2100 current velocity meter. Errors on the discharge measurements are estimated to be on the order of 10-15%.

End of winter snowpack depth (snow water equivalent SWE) for 2005 and 2006 was calculated using a terrain classification model to spatially average measurements from 42 transects (McLeod, B.*, et al.* 2005). Each transect was 100m in length, depth measurements were taken every 10m, and density at 0, 30, 50, 70, and 100m. Each transect was marked at each end with a fixed stakes at the time of measurement in 2005. Most of the stakes (38 of 42 transects) were in place upon return in 2006, hence 90% of the measurements were repeated at the same locations each year (±10m). For 2003 and 2004, end of winter SWE were calculated based on a network of only 13 transects (which were part of the 42 transects measured in subsequent years) (Lamoureux, S. F.*, et al.* 2006). Transects were 100m in length, with depth measured every 10m, and one density measurement at the centre of the transect. Mean SWE was calculated for each transect and spatially averaged for each watershed on the basis of terrain type units (channel, slopes, and plateau).

Water samples were collected in amber (HDPE) bottles that were triple rinsed with deionized (DI) water, and then triple rinsed with stream water prior to sampling. The bottles were filled completely to eliminate headspace in the bottle, and transported back to Camp for filtration and processing (Figure 1). All samples were filtered and bottled within 2 hours of collection, stored in snow packed coolers, and refrigerated upon return to the lab at Queen's University. Sample aliquots for dissolved organic carbon (DOC) and total nitrogen (TN) analysis were filtered using pre-combusted glass fiber filters (GF/F) and glass filtration apparatus. The glass filtration apparatus was acid washed and combusted before the field season, then soaked in 30% hydrogen peroxide overnight at the end of each day, and rinsed three times with DI water and sample between each sample. Filtered sample for DOC/TN was collected in 40ml amber glass EPA vials, with Teflon lined septa, and acidified with hydrochloric acid immediately upon return to the lab in Kingston (within 30 days of sampling). Aliquots for dissolved inorganic ion analyses were filtered through 0.45 μm nitrocellulose membrane filters, using a polysulfone filter holder. Ion samples were bottled in plastic scintillation vials.

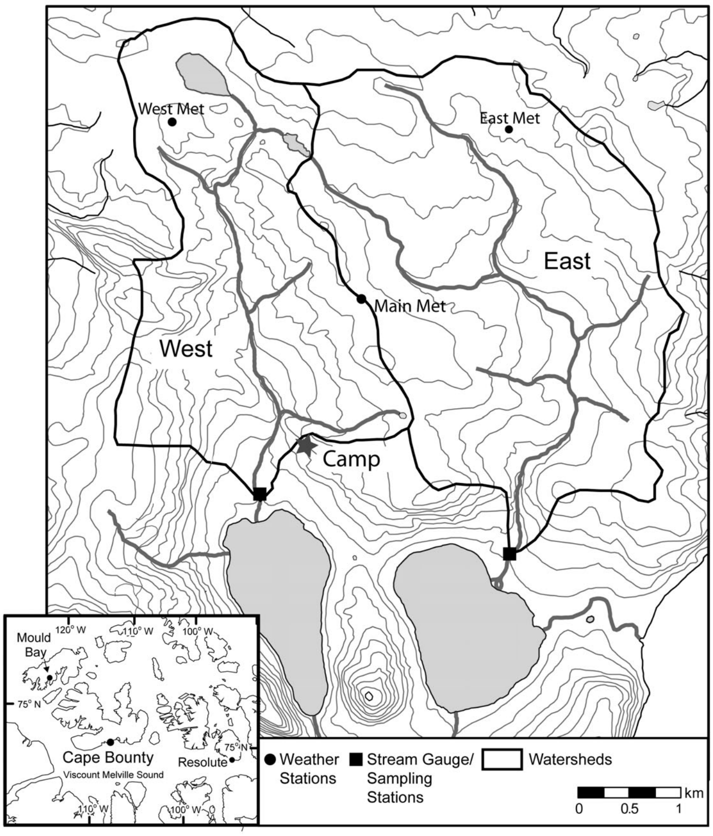

Figure 1. Topographic map of the West and East watersheds at Cape Bounty, illustrating the locations of the weather stations and stream gauging and sampling sites.

2.3 SAMPLE COLLECTION AND ANALYTICAL METHODS

DOC and TN were determined simultaneously by high temperature combustion and NDIR and chemiluminescent detection using a Shimadzu TOC-VPCH/TNM system equipped with high sensitivity catalyst. Error on these analyses were determined to be less than 1% (±0.020 ppm) for DOC and less than 2% (±0.01 ppm) for TN based on duplicate analyses of replicate field samples, and replicate analysis of standards.

Dissolved inorganic anions and cations (including NH^+, NO_3^-, NO_2^-, Na^+, K^+, Mg^{2+}, Ca^{2+}, Cl^-, Br^-, SO_4^{2-}, and PO_4^{3-}) were measured by ion chromatography. The anions and cations were determined simultaneously on separate systems using a Dionex 3000CS system. The anions were separated by gradient elution with 23-40 mM KOH (using an EG II KOH), with a 1.0 ml/min flow rate, and AS18 analytical and guard columns, and self regenerated suppression (ASRS-ULTRA II). Cations were measured isocratically with 23 mM methanesulphonic acid eluent, flowing at 0.5 ml/min with a CS12A analytical and guard columns with self regenerated suppression (CSRS-ULTRA II). Errors on most analytes were less than 1% based on replicate analysis of samples and standards, while errors on NO_3^-, NO_2^-, and NH_4^+ were 1.7% (±0.002 ppm), 20.7% (±0.003 ppm) and 5% (±0.002 ppm), respectively. DIN is reported as the sum of the nitrogen mass from NO_3^-, NO_2^-, and NH_4^+, while DON was determined as the difference between the TN and DIN (propagated error on DON ±0.012 ppm; approximately 5%).

2.4 Mass Flux Calculations

The yields of the DOC and N species were estimated as the product of the measured concentrations and the mean discharge over the period of measurement. In the case where there was only one measurement per day the flux was determined as the concentration times the total mean daily discharge (i.e. mean daily Q in $m^3/s*60$ s/min*60min/hr*24hr/d). Where more than one measurement was available the flux was determined as the product of the concentration and the total discharge accumulated over the time period represented by that sample 12-18hrs, depending on the time of measurement. The overall error on involved in calculating the seasonal mass flux is estimated to be within 15-18%.

3. RESULTS AND DISCUSSION

3.1 Climate and Hydrology

The snow accumulation at the end winter 2006 was the highest observed at this site over the last four years (Table 1). The June air temperatures were near the mean of the past four years, however July 2006 was quite warm relative to the previous three years. The high snowfall yielded the highest discharges recorded over the four years of observation (Table 1).

Table 1: End of winter SWE for West and East catchments and mean June and July air temperatures. Data for 2003, 2004 from Lamoureux *et al.* (2006).

Year	SWE (mm) West	SWE (mm) East	West River Discharge (mm)	June Temp °C	July Temp °C
2003	43	20		-1.0	
2004	82	41	101	-0.1	3.1
2005	70	40	86	2.0	3.1
2006	120	120	171	1.0	6.2

Seasonal discharges in the two streams were similar in 2006 (Figure 2). Both streams began to flow June 18th and peaked June 26th, however the East river had a higher maximum hourly discharge (3.06 m^3/s) than the West River (2.44 m^3/s). The total runoff from the two catchments was 1.40×10^6 m^3, or on a catchment area basis 170 mm from the West, and 120 mm from the East.

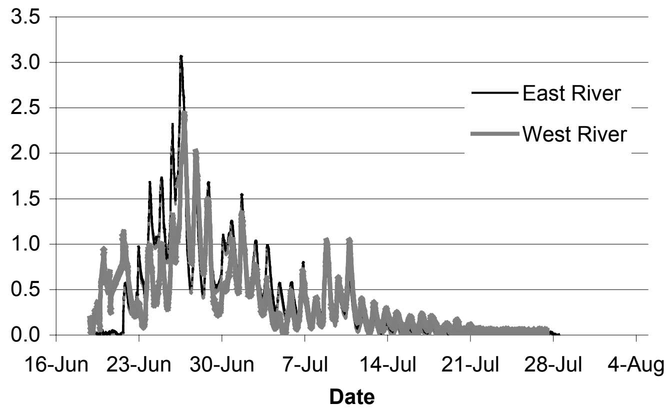

Figure 2. Mean hourly discharge (m^3/s) for West and East rivers 2006.

3.2 N Species concentrations and mass fluxes

The dominant N species in both rivers was DON, which comprised approximately 85% of the seasonal nitrogen mass flux from both rivers (Table 2). The mean DON and DIN concentrations and total mass fluxes for the two catchments were also very similar, but the mean concentrations of the different inorganic N species (especially nitrate (NO_3^-) and ammonium (NH_4^+)) for the two rivers were somewhat different

(Table 2). In both streams nitrite (NO_2^-) was the least abundant of the inorganic N species, but it was slightly more abundant in the East river than in the West. The West river exhibited a slightly higher mean ammonium concentration (0.018 ppm N) than the East (0.011 ppm N), while the East river had much a higher mean concentration of nitrate (0.024 ppm N) than the West (0.011 ppm N, Table 2). Due to the differences in the size of the two catchments, the West catchment is found to export more nitrogen per unit area (30.6 kg DON/km^2 and 5.6 kg DIN/km^2) than the East catchment (21.1 kg DON/km^2 and 3.9 kg DIN/km^2).

Table 2: Arithmetic mean concentrations and seasonal mass flux of nitrogen species and DOC in the West and East rivers.

	DOC ppm	DON ppm	DIN ppm	N-NO_3^- ppm	N-NO_2^- ppm	N-NH_4^+ ppm	DOC: DON	DOC kg	DON kg	DIN kg
West	2.63	0.180	0.031	0.011	0.002	0.018	14.6	3770	245	45
East	2.50	0.200	0.040	0.024	0.006	0.011	12.8	3820	248	42

The West river generally had lower mean DIN and DON concentrations than the East, and ammonium concentrations were often higher than nitrate in the West river (Figure 3). For all the N species, concentrations in the West river were at a maximum at the onset of melt, and decreased exponentially as discharge increased to peak flow (Figure 3). After the peak DON and DOC concentrations continued to decrease slightly, then stabilized or increased slightly towards the end of the season. The DIN concentrations were somewhat different, the DIN concentration was highest in the first sample, the concentration dropped significantly in the second sample, then the DIN concentrations increased with discharge until just before peak (Figure 3a). Figure 4 illustrates that the nitrate concentrations follow a trend that is similar to DOC and DON, and that NH_4^+ is the species driving the increase in DIN with discharge in the early season (Figure 4a). Correlation analysis revealed that in the West river, NO_3^- and NH_4^+ were well correlated with DOC (correlation coefficient r = 0.81 and r = 0.69). However, DON was only weakly correlated with DOC (r = 0.59). In the West river NO_3^- was most strong correlated with DOC (r = 0.81) and K^+ (r = 0.81).

In the East river, concentrations are also at a maximum at the onset of melt, and although the DOC and DON concentrations are variable near the peak in discharge, they remain high on average (Figure 3b). In this stream both DON and DIN concentrations increased gradually after approximately July 14th, while DOC concentrations decline. Figure 4b shows that it is an increase in nitrate concentrations at the end of the season that is driving the increase in DIN. In the East river there is only a weak correlation between DOC and DON (r = 0.44) and little to no correlation between DON and NO_3^- and NH_4^+ (r = 0.22 and r = -0.49, respectively). Here NO_3^- was most strongly correlated with the inorganic ions Cl^- (r = 0.92), Na^+ (r = 0.86) and K^+ (r = 0.83), and showed no correlation with DOC (r = -0.06).

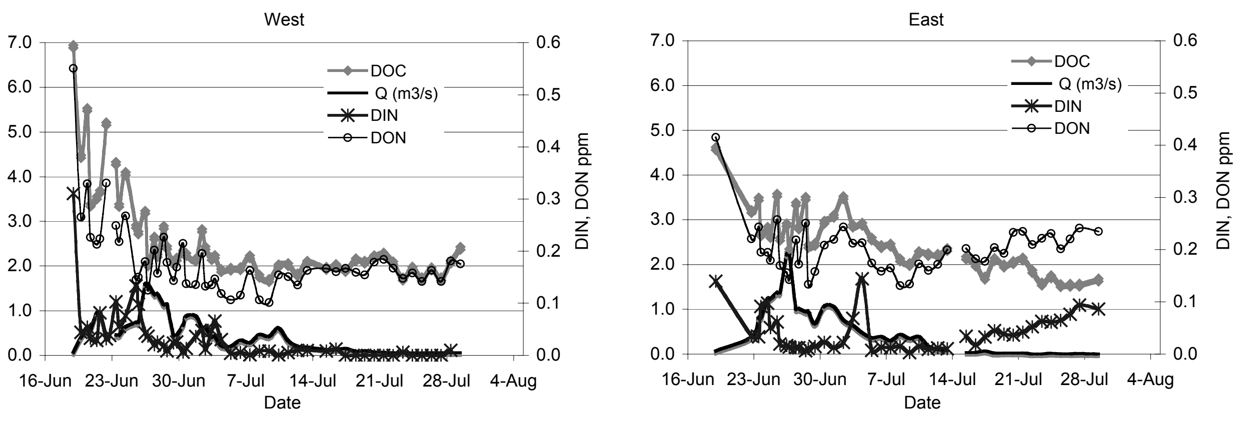

Figure 3. Seasonal variations in concentrations of DOC, DIN and DON plotted with mean daily discharge (m^3/s) for (a) West and (b) East rivers.

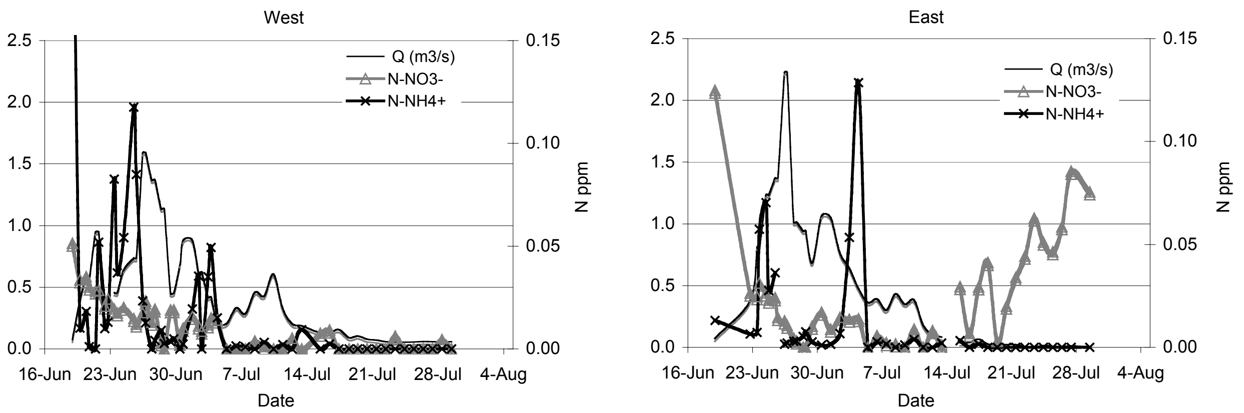

Figure 4. Seasonal variations in concentrations of N from NO_3^- and N form NH_4^+ plotted with mean daily discharge (m^3/s) for (a) West and (b) East rivers.

3.3 Controls on N species and seasonal variations in concentrations

Water flux exerts first order control over the export of solutes from the terrestrial system. However, as nitrogen is a limiting nutrient in most ecosystems, nitrogen losses in stream waters will only occur if the nitrogen cannot be utilized or controlled by the biota in the terrestrial system (Perakis, S. 2002). In principle this means that N can be lost in forms that are unavailable to organisms, such as complex or large organic molecules, or else if there is a spatial or temporal disconnect between the hydrological supply and biological demand of bioavailable forms of N (such as NO_3^- and NH_4^+) (Perakis, S. 2002, Pinay, G.*, et al.* 2002)

The ultimate source of DON is from soluble or leachable soil organic matter, as DON yields in stream water are usually closely related to the composition of soil organic matter and the flow of water through the shallow soil horizons (Cooper, R.*, et al.* 2007, Hood, E.*, et al.* 2003a). The sinks for DON are primarily mineralization reactions (conversion of DON to NH_4^+ by ammonification, and to NO_2^- and NO_3^- via nitrification) and percolation through mineral soils which promotes the retention of DON via sorption reactions and removal by biotic uptake (Hagedorn, F.*, et al.* 2000, Perakis, S. 2002).

The differences in the composition of the N species, and the substantial differences in the relationship between N species and other solutes in the two streams suggest that N losses are controlled by different factors in these two catchments. The West catchment chemistry suggest that most of the N export from this catchment (DON, NH_4^+ and NO_3^-) is related to DOC. Therefore, it appears that the N exports are related to the flushing of the shallow soil horizons, which provide a source of leachable DOM and also NH4+, and NO_3^- that may have built up in soils as a result of mineralization (decomposition) over the course of the previous summer. Note that the DOC and DON concentrations remain stable while the NH_4^+ and NO_3^- concentrations drop to zero for most of the summer (after July 5th). This suggests that although there is still some hydrological connection between the West river and the organic soil horizons in the catchment, either there is limited production of inorganic N (ammonification and nitrification) in these soil horizons, or that any NH_4^+ or NO_3^- that was available at this time (the start of the growing season) was immobilized by catchment biota. The East river displays a very different scenario of control on N export. Here there was only a weak correlation between DOC and DON concentrations, and the dominant inorganic N species (NO_3^-) co-varied with solutes derived from weathering, and atmospheric deposition (e.g K^+, Na^+ and Cl^-). These results suggest that NO_3^- may be largely derived from mineral soil horizons in this catchment. The increase in the DON and NO_3^- concentrations at the end of the summer in the East river, suggest that there was a spatial disconnect between the source of nutrients and areas where there was a biological demand for them (Figure 4). The decrease in the DOC:DON ratio (from ~15-6) and the increase in DON concentrations indicate that there was a change in the dominant source of DOM in the East River over the course of the course of the summer (Figure 5). The higher N content of the DOM likely indicates a more labile DOM, possibly in the form of fulvic acids produced by microbial activity

(McKnight, D. M., *et al.* 1994). Note that in contrast the West river, DOC:DON ratios remain relatively high during recession of flow (Figure 5)

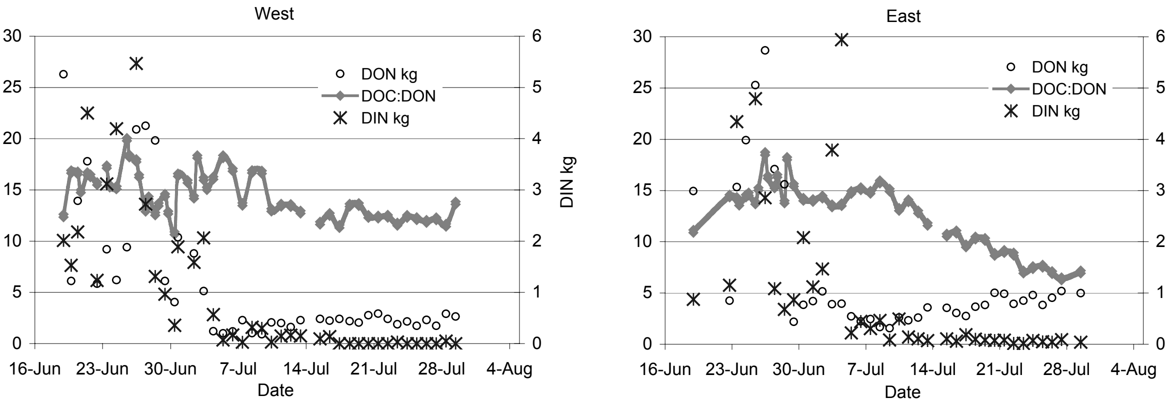

Figure 5. Seasonal DOC:DON ratios, DIN and DON mass fluxes (kg) for (a) West and (b) East rivers.

3.4 N structure and losses relative to other environments

Despite differences in the seasonal patterns of nutrient concentrations in the river, the two catchments have nearly identical seasonal DON, DIN and DOC yields (Table 2). These yields were on the order of 250 kg DON, 45 kg DIN and 3800 kg DOC. When converted to fluxes on a catchment area basis these mass fluxes convert to 475 kg C/km^2, 31 kg N-DON/km^2 and 5.6 kg N-DIN/km^2 for the West and 328 kg C/km^2, 21 kg N-DON/km^2 and 3.9 kg N-DIN/km^2 from the East catchment. The results show that DON is by far the most important vector for N losses from these High Arctic catchments (DON > 80% of total N) (Table 2). The mean concentrations of DON in these High Arctic streams (0.180 to 0.200 ppm), are generally higher than those reported for studies in the Colorado Rocky Mountains (0.023-0.084) and the total DON fluxes from the Cape Bounty catchments (20-30 kg/km^2) are within the range reported for these alpine and subalpine catchments (18-60) (Hood, E., *et al.* 2003b, Williams, M. W., *et al.* 2001) . However, the export of inorganic N from these High Arctic streams is 2 orders of magnitude lower than DIN export in the catchments in the Colorado Front Ranges (Hood, E., *et al.* 2003b, Williams, M. W., *et al.* 2001). The very high DIN exports in these catchments are largely attributed to the high rates of atmospheric N deposition in these mountain ranges. When compared to unpolluted headwater catchments in temperate South American forests, we find that the concentrations of both inorganic and organic N in runoff are higher than in these forested watersheds (Perakis, S. S. and Hedin, L. O. 2002). The mean concentrations for DON, N-NO_3^-, and N-NH_4^+ for the East and West rivers combines are 192 ppb N, 17 ppb, and 15 ppb, respectively. The mean concentrations for the 13 South American study areas were 58.6 ppb DON, 1.9 ppb N-NO_3^-, and 4.9 ppb N-NH_4^+(Perakis, S. S. and Hedin, L. O. 2002). Similar to the Arctic streams where DON accounted for >80% of total N load in streams. DON represented >90% of the total N exported in streams from the unpolluted South American catchments. However, due to the high rates of precipitation (500-6000 mm/yr) in these South American locations, the annual net flux of DON from these areas are estimated for be between 20-350 kg DON/km^2 /yr (Perakis, S. S. and Hedin, L. O. 2002). The author is unaware of any studies of DON and DIN species concentrations and export from Arctic rivers with which to compare these results.

4. CONCLUSIONs

The study finds that although the West and East catchments yield the same seasonal mass of DON and DIN, the controls on DON and DIN in the two watersheds are clearly different. While the West catchment appears to have a consistent source of dissolved organic matter (as indicated by the relatively constant

DOC:DON ratios), there appears to be a gradual change in the composition of the DOM in the East river as flows recede in the summer. The drop in flux of inorganic nitrogen species to near zero values in the West river after the first week in July, suggests efficient retention (biological uptake) of inorganic N in this catchment. In contrast, the rise in the concentrations and fluxes of NO_3^- and DON in the East river over the month of July, suggests biological demand for nitrogen is lower, or spatially disconnected with the N sources in this watershed. Therefore, although the controls on N losses vary across the landscape, the two watersheds likely have similar constraints on the upper limits of total N yields.

DON represents more than 80% of the total mass of N exported from these two arctic catchments, suggesting that DON may be a key source of N for ecosystems downstream. The fact that the mass flux of this DON (and other DIN) species occur long before the beginning of the growing season, suggests that the delivery of these nutrients may be well in advance of the peak of biological demand in aquatic ecosystems downstream. The total mass fluxes of DIN and DON from these small Arctic catchments are not trivial when compared to catchments in more temperate environments. The results of this study seem to suggest that N should not be a limiting factor for aquatic biological productivity, but the timing and composition of the nitrogen being delivered may be the more important constraints on productivity in these ecosystems. There is a need to understand the extent to which the magnitude, composition and timing of the N fluxes from Arctic systems vary with changes in hydrology and climate in order to support the conclusions drawn from this preliminary study.

ACKNOWLEDGEMENTS

The author wishes to thank Polar Continental Shelf Project, Northern Scientific Training Program, ArcticNet, and Queen's University for supporting this work. Valuable field and laboratory assistance was also provided by Brock McLeod, Dana MacDonald, Dave Atkinson, Katherine Middleton, and Hilary Dugan.

REFERENCES

ACIA (2005) Arctic Climate Impact Assessment, Scientific Report, Cambridge University Press, New York.

Cole, J. J. and Caraco, N. F. (2001) Carbon in catchments: connecting terrestrial carbon losses with aquatic metabolism. *Marine and Freshwater Research*. **52**, 101-110.

Cooper, R., Thoss, V. and Watson, H. (2007) Factors influencing the release of dissolved organic carbon and dissolved forms of nitrogen from a small upland headwater during autumn runoff events. *Hydrological Processes*. **21**(5), 622-633.

Cornell, S., Rendell, A. and Jickells, T. (1995) Atmospheric inputs of dissolved organic nitrogen to the oceans. *Nature*. **376**, 243-246.

Dittmar, T. (2004) Evidence for terrigenous dissolved organic nitrogen in the Arctic deep sea. *Limnology and Oceanography*. **49**(1), 148-156.

Dittmar, T. and Kattner, G. (2003) The biogeochemistry of the river and shelf ecosystem of the Arctic Ocean: a review. *Marine Chemistry*. **83**, 103-120.

Hagedorn, F., Schleppi, P., Waldner, P. and Flühler, H. (2000) Export of dissolved organic carbon and nitrogen from Gleysol dominated catchments – the significance of water flow paths. *Biogeochemistry*. **50**(2), 137-161.

Hansell, D., Kadko, D. and Bates, N. R. (2004) Degradation of Terrigenous Dissolved Organic Carbon in the Western Arctic Ocean. *Science*. **304**, 858-861.

Hodgson, D. A., Vincent, J.-S. and Fyles, J. G. (1984) Quaternary geology of central Melville Island, Northwest Territories, Geological Survey of Canada, Ottawa.

Hood, E., McKnight , D. M. and Williams, M. W. (2003a) Sources and chemical character of dissolved organic carbon across an alpine/subalpine ecotone, Green Lakes Valley, Colorado Fron Range, United States. *Water Resources Research*. **39**(7), 1188-1199.

Hood, E., Williams, M. W. and Caine, N. (2003b) Landscape controls on organic and inorganic nitrogen leaching across an alpine/subalpine ecotone, Green Lakes Valley, Colorado Front Range. *Ecosystems*. **6**(1), 35-45.

Lamoureux, S. F., McDonald, D. M., Cockburn, J. M. H., Lafreniere, M. J., Atkinson, D. M. and Treitz, P. (2006) An incidence of multi-year sediment storage on channel snowpack in the Canadian High Arctic. *Arctic*. **59**(4), 381-390.

Mayorga, E., Aufdenkampe, A. K., Masiello, C. A., Krusche, A. V., Hedges, J. I., Quay, P. D., Richey, J. E. and Brown, T. A. (2005) Young organic matter as a source of carbon dioxide outgassing from Amazonian rivers. *Nature*. **436**, 538-541.

McKnight, D. M., Andrews, E. D., Spalding, S. A. and Aiken, G. R. (1994) Aquatic fulvic acids in algal-rich Antarctic ponds. *Limnology and Oceanography*. **39**(8), 1972-1979.

McLeod, B., Lafrenière, M. J. and Lamoureux, S. F. (2005) Quantifying Total Snow Water Equivalence in High Arctic Watersheds *Proceedings and Abstracts 2nd ArcticNet Annual Scientific Meeting*, Banff, Alberta, December 13-16, 2005 (PDF Poster, http://www.arcticnet-ulaval.ca/pdf/ posters_2005/mcleod_et_al.pdf, May 1, 2007)

Pace, M. L., Cole, J. J., Carpenter, S. R., Kitchell, J. F., Hodgson, J. R., Van de Bogert, M. C., Bade, D. L., Kritzberg, E. S. and Bastviken, D. (2004) Whole-lake carbon-13 additions reveal terrestrial support of aquatic food webs. *Nature*. **427**, 240-243.

Perakis, S. (2002) Nutrient limitation, hydrology and watershed nitrogen loss. *Hydrological Processes*. **16**, 3507-3511.

Perakis, S. S. and Hedin, L. O. (2002) Nitrogen loss from unpolluted South American forests mainly via dissolved organic compounds. *Nature*. **415**, 416-421.

Pinay, G., Clément, J. C. and Robert J, N. (2002) Basic Principles and Ecological Consequences of Changing Water Regimes on Nitrogen Cycling in Fluvial Systems. *Environmental Management*. **V30**(4), 481-491.

Serreze, M. C., Walsh, J. E., Chapin III, F. S., Osterkamp, T., Dyurgerov, M., Romanovsky, V., Oechel, W. C., Morison, J., Zhang, T. and Barry, R. G. (2000) Observational Evidence of Recent Change in the Northern High-Latitude Environment. *Climatic Change*. **46**, 159-207.

Walker, D. A., Raynolds, M. K., Daniëls, F. J. A., Einarsson, E., Elvebakk, A., Gould, W. A., Katenin, A. E., Kholod, S. S., Markon, C. J., Melnikov, E. S., Moskalenko, N. G., Talbot, S. S., Yurtsev, B. A. and Team., t. o. m. o. t. C. (2005) The circumpolar Arctic vegetation map. *Journal of Vegetation Science* **16**, 267–282.

Williams, M. W., Hood, E. and Caine, N. (2001) Role of organic nitrogen in the nitrogen cycle of a high-elevation catchment, Colorado Front Range. *Water Resources Research*. **37**(10), 2569-2581.

Influence of the ice - ocean heat flux on the ice thickness evolution in Saroma-ko lagoon, Hokkaido, Japan

Matti Leppäranta[1*], Kunio Shirasawa[2]

[1]Division of Geophysics, Department of Physical Sciences, University of Helsinki, P.O. Box 64 (Gustaf Hällströminkatu 2) FI-00014 Helsinki, Finland;
**Corresponding author, e-mail:* matti.lepparanta@helsinki.fi
[2]Pan-Okhotsk Research Center, Institute of Low Temperature Science, Hokkaido University, Kita-19, Nishi-8, Kita-Ku, Sapporo, Hokkaido 060-0819 Japan; e-mail: kunio@lowtem.hokudai.ac.jp

ABSTRACT
Sea ice grows and decays as forced by the fluxes through the boundaries. In particular, the flux at the lower boundary – the heat flux from the water body into the bottom of the ice sheet – is not very well known quantity. A thermodynamic sea ice model is employed to examine the influence of the oceanic heat flux on the thickness of the ice. Saroma-ko ice station data is used to analyse the physics and calibrate the model. The oceanic heat flux is normally 5–10 W/m^2, and the ice thickness ranges in 30–50 cm; being that thin, the ice has a very active role in the thermodynamics.

KEYWORDS:
Ice - ocean heat flux; Ice thickness; Thermodynamic sea ice model; Measurements; Saroma-ko lagoon

1. INTRODUCTION
Thermodynamic evolution of sea ice thickness is forced by the heat fluxes at its upper and lower boundaries and penetration of solar radiation into the ice sheet. Much research work has been done on the heat fluxes at the upper surface by measurement campaigns and analytical and numerical modelling. The lower boundary, i.e. the heat flux from the liquid water body into the bottom of the ice sheet is less understood. According to measurements this heat flux is of the order of 1–100 W/m^2, which makes a significant contribution to the ice thickness evolution (*e.g.*, Shirasawa *et al.*, 2006). It is also as such important for water body itself being the principal mechanism of heat loss during the ice-covered season.
In numerical models of sea ice thermodynamics the oceanic heat flux has often be used as a tuning factor. Maykut and Untersteiner (1971) employed a constant oceanic heat flux of 2 W/m^2 to obtain the best-fit equilibrium thickness cycle for multiyear ice in the Arctic Ocean in their classical model. Modelling in the Antarctic seas has indicated that there the heat flux can be one order of magnitude larger. In Saroma-ko lagoon, on the northern coast of Hokkaido, Shirasawa *et al*. (2005) obtained the best fit 10-year statistics for the ice and snow thickness using a fixed heat flux of 5 W/m^2.
Ice models usually take a fixed oceanic heat flux and use that as a tuning parameter. It is, however, the next question that what is the influence of the variability of oceanic heat flux on the ice thickness and on the structure of ice as well. This problem is examined here by mathematical modelling using analytical and numerical models (Leppäranta, 1993; Shirasawa *et al*., 2005). This work belongs to the long-term joint research of the authors on ice–ocean thermodynamics (Shirasawa *et al.*, 2006).

2. MATHEMATICAL MODELLING
Simple analytic models provide rather good results for the climatology of sea ice thickness (Leppäranta, 1993). A generalized form including the oceanic heat flux and air – ice interaction reads in differential form

$$\frac{dh}{dt} = a\frac{T_f - T_a}{h + d} - \frac{Q_w}{\rho L} \quad (T_a \leq T_f) \tag{1}$$

where h is ice thickness, t is time, $a = \kappa/(\rho L) \approx 5.5$ cm^2/(ºC·day) is freezing-degree-day coefficient, κ is thermal conductivity of ice, ρ is ice density, L is latent heat of freezing, T_f is the freezing point temperature, T_a is air temperature, $d \approx 10$ cm is effective insulating thickness of the near surface air–snow buffer, and Q_w is oceanic heat flux. The Stefan solution $h^2 = 2aS$, where $S = \int_o^t \max(0, T_f - T_a)ds$, comes from $d = Q_w = 0$ and can be taken as an upper bound for favourable ice growth conditions.

In numerical modelling the temperature profile and resulting heat flow is solved in a dense grid across the ice sheet (Maykut and Untersteiner, 1971; Shirasawa *et al*., 2005). The salinity of the ice is prescribed and together with the temperature determines the brine volume. Comparing with the analytical models, more realistic boundary conditions can be applied and the thermal inertia of the heat flow through the ice can be included. The heat conduction equation is

$$\rho c\frac{\partial T}{\partial t} = \kappa\frac{\partial^2 T}{\partial z^2} - q(z) \tag{2}$$

where c is the specific heat of ice, z is vertical coordinate, and q is the absorption of solar radiation by the ice. The boundaries of the system move according to the heat fluxes resulting in changing of the thickness of the ice, at the bottom $\kappa\partial T/\partial z = \rho L dh/dt + Q_w$ and at the top similarly except that for growth liquid water or slush must be available.

3. RESULTS

Model investigations are made for idealized cases and comparing with observations in the Saroma-ko lagoon located on the northern coast of Hokkaido (Fig. 1). Its surface area is 150 km^2 and its mean depth is 8.7 m. The lagoon is connected to the Sea of Okhotsk via two inlets, and the salinity is about 32 psu. At the beginning of the freeze-up, atmospheric forcing keeps the lagoon open and frazil ice is formed. Ice reaches a maximum thickness of 35–62 cm annually in the southeastern part of the lagoon. There are large spatial variations in ice thickness due to the oceanic heat flux from the inlets.

An example of the data set is shown in Fig. 2. The period of observations of water current, temperature and salinity covered the ice season with freeze-up and breakup dates included.

The deployment of the current meter was made on 6 December 1999 when the lagoon was open and the water temperature was about 3^{o}C. Ice freeze-up started at late January, and the almost entire surface of the lagoon was covered with sea ice. The onset of ice breakup was at early April. The current speed was as high as 10 cm/s before ice freeze-up and reduced to 2-3 cm/s during the ice-covered period. The solid ice cover causes reduction of vertical mixing of the water under the ice, and thus there is not much momentum transfer from the wind to the water body. The main forcing of the circulation comes from the two inlets and some major rivers, and heating of the water body by the heat flux from the bottom sediments and the solar heating becomes active as soon as the snow has melted.

Fig. 3 shows results from measurements of the oceanic heat flux in the Saroma-ko lagoon. The level is at about 10 W/m^2 with fluctuations of 5 W/m^2 around the mean. High frequency variations seem to be quite small.

If the oceanic heat flux is a non-zero constant and air temperature is T_a = constant, the analytic model gives the steady-state solution

$$h + d = \kappa(T_f - T_a)/Q_w \tag{3}$$

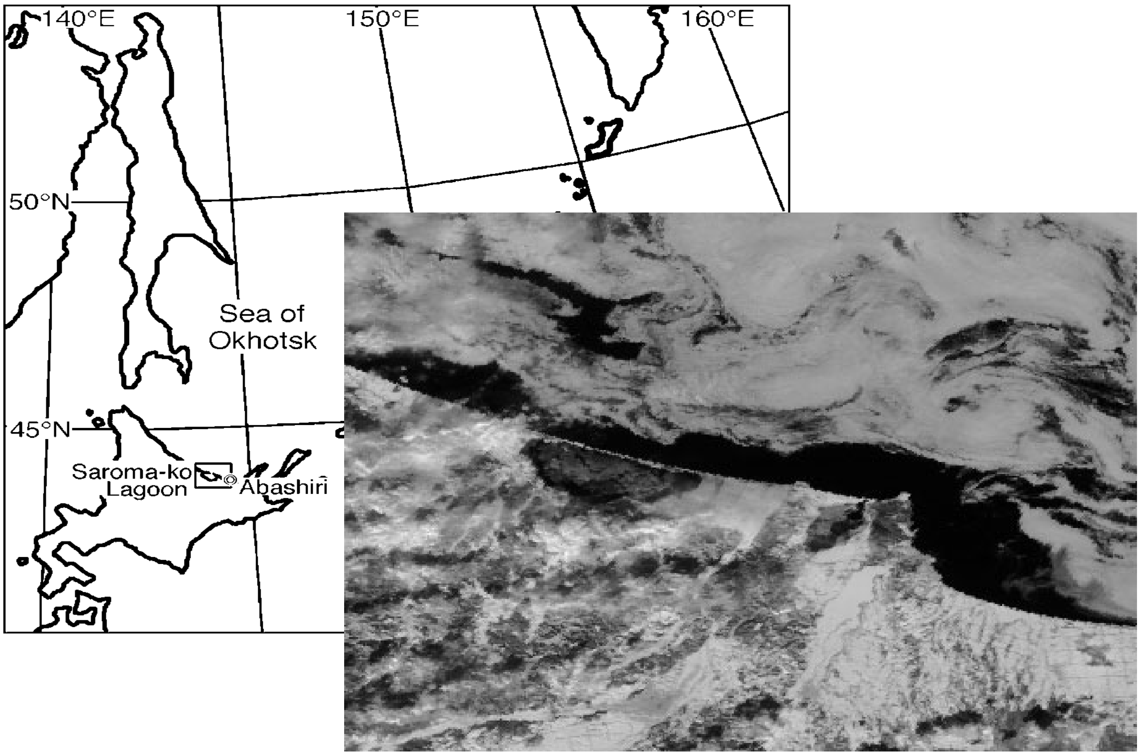

Figure 1. A location map of Saroma-ko lagoon. The picture shows sea ice areas in Saroma-ko lagoon and in the coastal region of the Sea of Okhotsk in white colour.

Since $h \geq 0$ and $d \geq 0$, it is seen that the heat flux of $Q_w = \kappa(T_f - T_a)/d$ is sufficient to prevent ice formation; this works as a simple polynomial equation. If the heat flux is less than that, the steady state ice thickness becomes $h^* = \kappa(T_f - T_a)/Q_w - d$. With T_a = constant, the time evolution is obtained from Eq. (1) as

$$\frac{h}{h^*} + \log\left(1 - \frac{h}{h^*}\right) = -\frac{\kappa(T_f - T_a)}{h^{*2}} t \tag{4}$$

In the beginning ($h \ll h^*$) the ice grows as proportional to the square root of time.

To understand the role of the variable oceanic heat flux, perturbation techniques can be utilized. Writing the ice thickness as $h = h^* + \eta$, and assuming $\eta \ll h^*$, the ice growth equation can be approximated as

$$\frac{d\eta}{dt} = a\frac{T_f - T_a}{h^*}\left(1 - \frac{\eta}{h^*}\right) - \frac{Q_w}{\rho L} \tag{5}$$

For cyclic oceanic forcing $Q_w/\rho L = q_o + q_1 \sin(\omega t)$, the thickness disturbance has a persistent cyclic part

$$\eta = \frac{q_1}{\sqrt{\beta^2 + \omega^2}} \sin(\omega t + \phi) \tag{6}$$

where $\beta = -a(T_f - T_a)/h^{*2}$ is a relaxation constant for ice growth and ϕ is the phase shift. When both relaxation constant and frequency of oceanic heat flux are small, considerable thickness variations result. The amplitude q_1 could be of the order of 1 cm/day, and therefore with $\beta, \omega \ll 1$/day the thickness variations would be 10 cm or more. Consequently, tidal heat transport may show up in the fortnightly cycle but not significantly in diurnal or semidiurnal cycles.

For a numerical modelling effort, a thermodynamic sea ice model (Shirasawa *et al.*, 2005) was used to examine the evolution of ice thickness. As an example, simulations for a 100-day case are shown in Fig. 4. Simulations were performed with zero, nonzero constant, and cyclic oceanic heat flux. The constant was taken as 10 W/m^2 corresponding to a typical level, while in the cyclic case the mean was the same and the amplitude also the same, i.e. the heat flux varied between zero and 20 W/m^2. It is clear that much oceanic heat influences the ice thickness cycle much. In the growth season the differences are small, but when the growth weakens the oceanic heat starts to melt the ice, and the ice break-up comes three weeks earlier. But what is remarkable that the cyclic oceanic heat flux did not much differ from the constant heat flux case as long as the averages are equal. With amplitude of 5 W/m^2 the differences were smaller, and also the higher the frequency was the smaller the difference. The cyclic case of Fig. 4 is therefore exaggerated for illustrative purposes: the amplitude is 10 W/m^2 and the cycle length so 30 days.

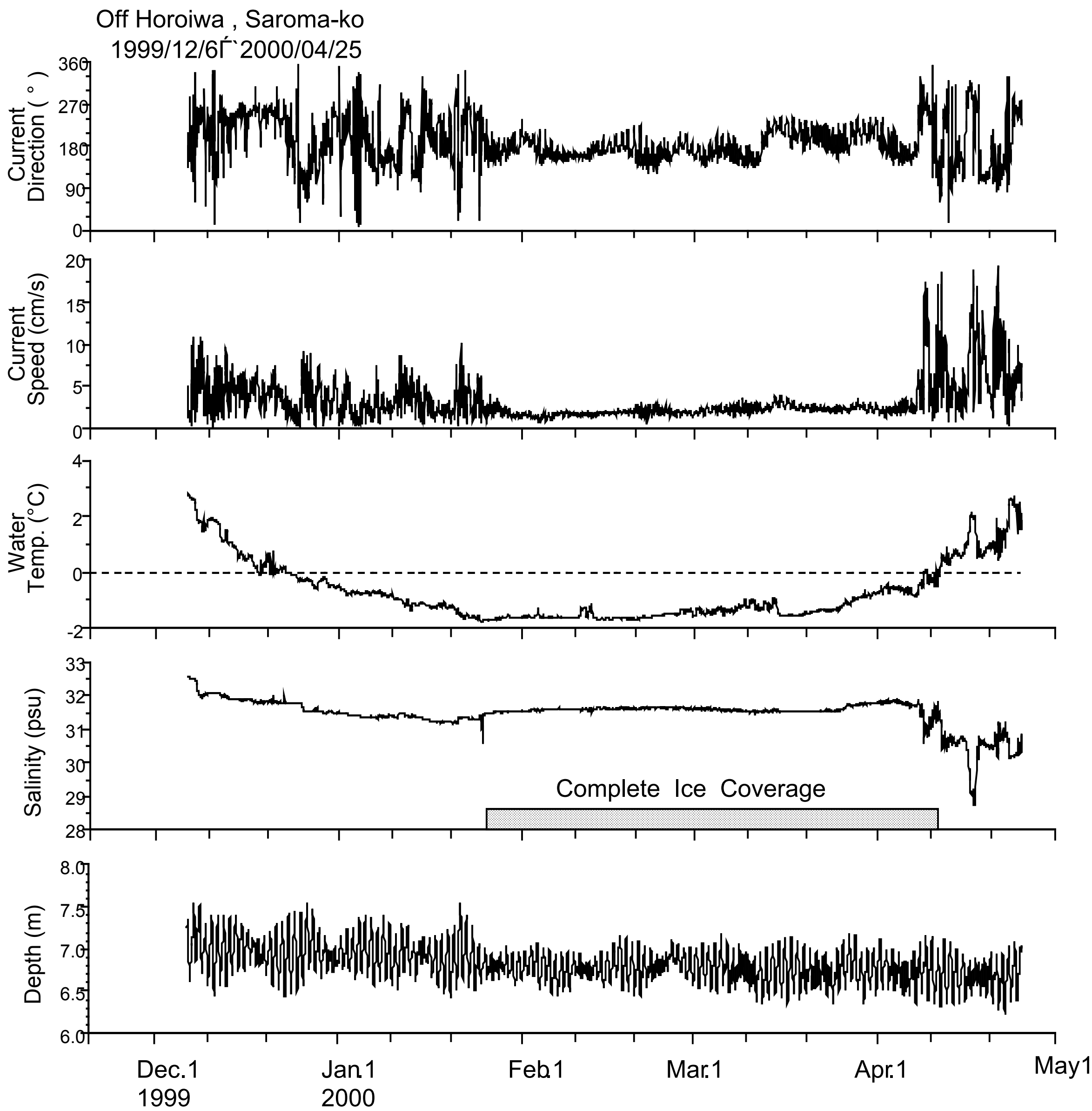

Figure 2. Current speed and direction, temperature, salinity and depth obtained from the mooring station at the central area of Saroma-ko lagoon during the period from 6 December 1999 through 25 April 2000. The complete ice coverage indicates that the almost entire surface of the lagoon is covered with sea ice, except the areas near the inlets. [after *Shirasawa and Leppäranta*, 2003].

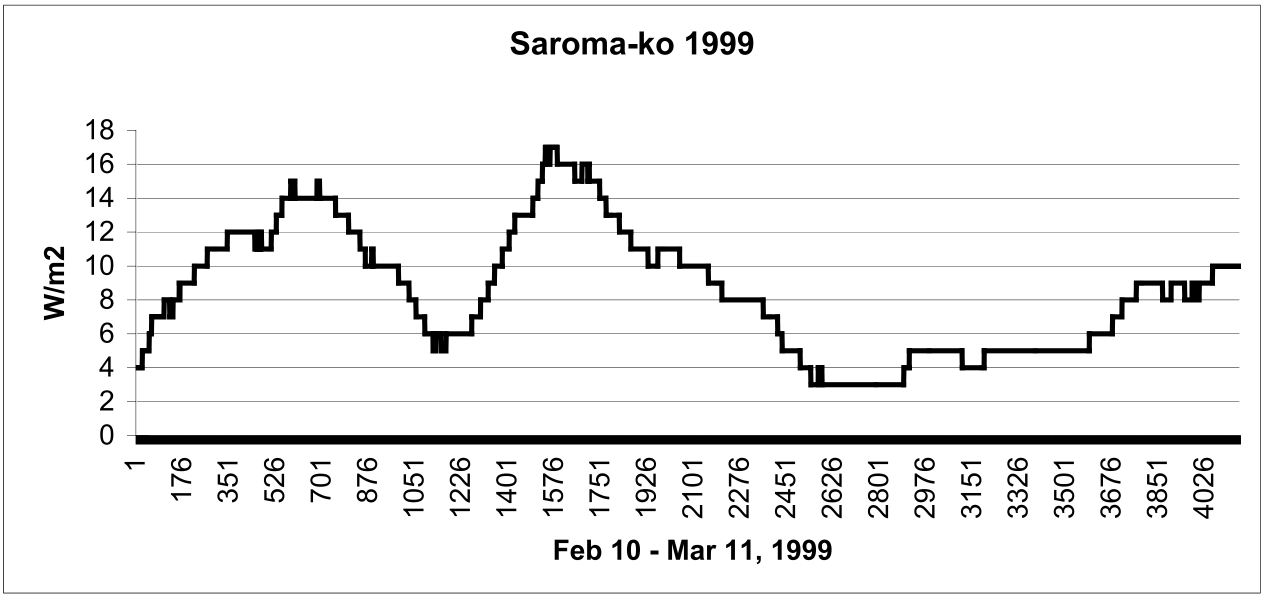

Figure 3. Measurements of the oceanic heat flux in Saroma-ko lagoon during one month based on ice and near surface layer ocean measurements.

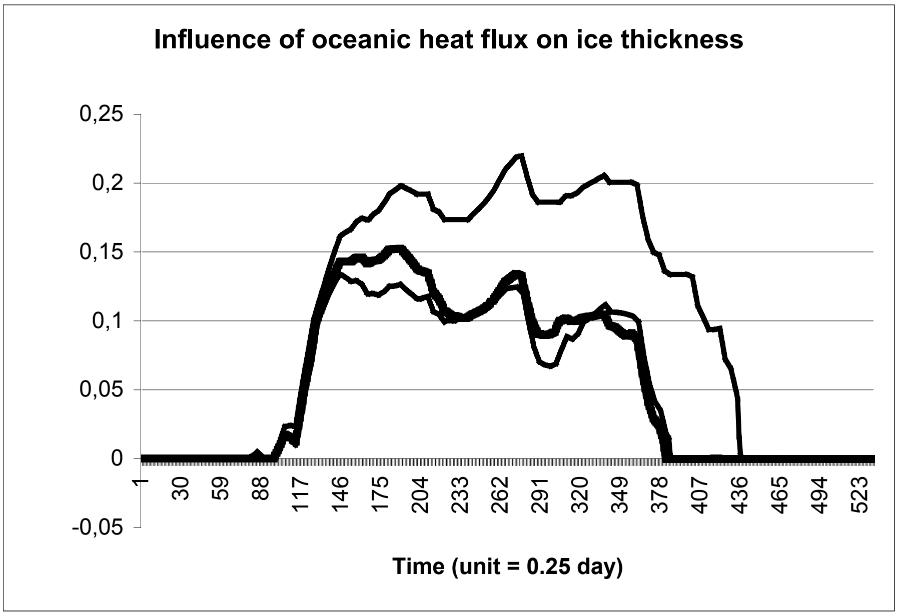

Figure 4. Model simulations for ice thickness (m) in a selected example case: zero heat flux (top thin curve, constant heat flux of 10 W/m^2 (thick curve), and cyclic oceanic heat flux with 10 W/m^2 mean, 10 W/m^2 amplitude and 30-day period (lower thin curve).

4. CONCLUSIONS

The oceanic heat flux from the water body to sea ice has been examined by mathematical modelling. The motivation is that ice grows and decays as forced by the fluxes through the upper and lower boundaries, and in particular the flux at the lower boundary – i.e. the oceanic heat flux – is not very well known quantity. Measurement data of Saroma-ko Lagoon on the northern coast of Hokkaido are also utilised in the analysis.

Analytical models can be used to examine the equilibrium and spin-up of sea ice thickness under fixed external conditions and with perturbation techniques for cyclic oceanic forcing, too. In the cyclic case low frequencies (0.1 cycles per day or less) and low relaxation constants (*i.e.*, fast response times for ice) can lead to remarkable ice thickness cycles. An important feature of the oceanic heat flux is that it influences not only the total ice thickness but also the stratification of the ice sheet, since it melts congelation ice at the bottom and provides thus potential for more snow-ice formation. Modelling work is ongoing in collaboration between the present authors to come up with more extensive conclusions and consider requirements for advanced 1-dimensional ice–ocean thermodynamic modelling.

ACKNOWLEGMENTS

This work belongs to the project "Ice Climatology of the Okhotsk and Baltic Seas" supported by the Japan Society for the Promotion of Science, the Japanese Ministry of Education, Culture, Sports, Science and Technology, and the Academy of Finland.

REFERENCES

Leppäranta, M. (1993) A review of analytical sea ice growth models. *Atmosphere–Ocean* **31**(1), 123–138.

Maykut, G.A. and Untersteiner, N. (1971) Some results from a time-dependent, thermodynamic model of sea ice, *Journal of Geophysical Research,* **76**, 1550–1575.

Shirasawa, K. and Leppäranta, M. (2003) Hydrometeorological and sea ice conditions at Saroma-ko lagoon, Hokkaido, Japan. Proceedings of *the Seminar "Sea Ice Climate and Marine Environments in the Okhotsk and Baltic Seas – The Present Status and Prospects", Seili, Finland, 10-13 September 2001, Report Series in Geophysics, Division of Geophysics, University of Helsinki, No. 46*, pp. 161-168.

Shirasawa, K., Leppäranta, M., Saloranta, T., Kawamura, T., Polomoshnov, A. and Surkov, G. (2005) The thickness of coastal fast ice in the Sea of Okhotsk. *Cold Regions Science and Technology,* **42**, 25–40.

Shirasawa, K., Leppäranta, M., Kawamura, T., Ishikawa, M., and Takatsuka, T. (2006) Measurements and modelling of the water – ice heat flux in natural waters. Proceedings of *The 18th IAHR International Symposium on Ice, Vol. 1,* Sapporo, Japan, 28 Aug. – 1 Sept. 2006, pp. 85–91.

Stefan, J. (1891) Über die Theorie der Eisbildung, insbesondere über Eisbildung im Polarmeere. *Ann. Physik, 3rd Ser.* 42, 269–286.

Using High-Resolution Atmospheric and Snow Modeling Tools to Define Pan-Arctic Spatial and Temporal Snow-Related Variations

Glen E. Liston[1*], Christopher A. Hiemstra[1], Svetlana Berezovskaya[2], Sebastian H. Mernild[3], Matthew Sturm[4]

[1] Cooperative Institute for Research in the Atmosphere, Colorado State University Fort Collins, Colorado 80523-1375, USA
[2] Water and Environmental Research Center, University of Alaska Fairbanks, Alaska 99775-5860, USA
[3] International Arctic Research Center and Water and Environmental Research Center University of Alaska, Fairbanks, Alaska 99775-0292, USA
[4] U.S. Army Cold Regions Research and Engineering Laboratory Ft. Wainwright, Alaska 99703-0170, USA
**Corresponding author, e-mail: liston@cira.colostate.edu*

ABSTRACT

Our long-term goal is to understand the roles of snow in terrestrial Arctic systems. To accomplish this goal we have developed a collection of atmospheric and snow modeling tools used to define spatial and temporal variations in snow depth and properties. This collection of modeling tools includes SnowModel, a spatially-distributed snow-evolution modeling system designed for application in all landscapes, climates, and conditions where snow occurs. SnowModel is designed to run on grid increments of 1- to 200-m and temporal increments of 10-minutes to 1-day. It can be applied using much larger grid increments, if the inherent loss in high-resolution (subgrid) information is acceptable. Simulated processes include: snow accumulation; blowing-snow redistribution and sublimation; interception, unloading, and sublimation within forest canopies; snow-density evolution; and snowpack ripening and melt. Meteorological forcings required by SnowModel are provided by MicroMet, a physically-based, high-resolution (e.g., 1-m to 10-km horizontal grid increment), meteorological distribution model. MicroMet employs relationships between meteorological variables and the surrounding landscape to generate distributions of air temperature, relative humidity, wind speed and direction, incoming shortwave and longwave radiation, surface pressure, and precipitation to drive SnowModel. SnowModel also includes a snow data assimilation sub-model (SnowAssim) that is consistent with optimal interpolation techniques, where differences between observed and modeled snow values constrain modeled outputs. This assimilation approach is unique in that the correction is applied backwards in time to adjust variables prior to the assimilated observations.

There are also features in natural systems not considered in SnowModel. For example, the model assumes that vegetation cover in each model grid cell is uniform. Thus, the model is unable to appropriately simulate features like tree-wells, nor is it able to simulate snow drifts that accumulate behind individual shrubs, such as occurs throughout shrublands of the western United States and Arctic. To expand SnowModel's application, soil moisture, temperature, and runoff-routing sub-models could also be included. This would extend the model's use to a wider range of ecological and hydrologic applications.

In their current form, applying these modeling tools allows us to create distributions of numerous snow-related properties, including snow water equivalent (SWE), snow depth, mixed land-snow albedo (landscape albedo), snowpack layers, type of snow by layer, bulk thermal conductivity, hardness/penetration, mobility/trafficability indices, snow-ground interface temperature, snow-up and snow-melt timing, snow density and grain characteristics, snow characteristics changes in response to changes in atmospheric forcing (climate), snow changes in response to arctic vegetation changes (e.g., increased shrubs), and hydrologic potential (integrated basin peak SWE). Focus regions for our simulations and distributions include arctic Alaska, Greenland, Arctic North America, and the Pan-Arctic. As part of this presentation we will use the above collection of domains and variables to provide examples of our simulated snow-related distributions and variations.

Climate, glacier mass balance, and runoff 1993–2005, and in a long term perspective (106 year), Mittivakkat Glacier catchment, Ammassalik Island, SE Greenland

Sebastian H. Mernild[1*] Bent Hasholt[2] Douglas L. Kane[3] Birger U. Hansen[2]
Bjarne H. Jakobsen[2] Niels T. Knudesn[4]

[1] *International Arctic Research Center and Water and Environmental Research Center, University of Alaska Fairbanks, Fairbanks, Alaska, USA*
[2] *Department of Geography and Geology, University of Copenhagen, Copenhagen, DENMARK*
[3] *Water and Environmental Research Center, University of Alaska Fairbanks, Fairbanks, Alaska, USA*
[4] *Department of Earth Science, University of Aarhus, Aarhus, DENMARK*
**Corresponding author, e-mail: fxsm@uaf.edu*

ABSTRACT
Climate, glacier mass balance, and subsequently river discharge are investigated based on high-resolution time series (1993–2005) from the Low-Arctic Mittivakkat Glacier catchment at the Ammassalik Island (65°N), Southeast Greenland. Meteorological data from the Mittivakkat Glacier catchment (18.4 km^2) together with standard synoptic meteorological data are extrapolated from 1898 to 1993 to estimate variations and trends in air temperature, glacier net mass balance, and catchment runoff. Characteristic variations in meteorological conditions within the catchment, between the coastal (Station Coast) and the glacier area (Station Nunatak) during the investigation period occur: ~15% lower annual solar radiation, four weeks longer snow-free period, and ~50% higher maximum snow depth in the coastal area. Further, decreasing mean annual air temperatures (MAAT) occur in the coastal area (-0.13ºC y^{-1}) during the high-resolution investigation period, indicating an approximately 20-day shorter thawing period, while the higher glacier area undergoes an increasing MAAT (0.09ºC y^{-1}), an approximately 40-day longer thawing period, a 60-day longer snow-free period, and an (linear trend) increasing release of melt water from the exposed glacier surface. The Mittivakkat Glacier net mass balance has been almost continuously negative averaging -0.59±0.51 m w.eq. y^{-1} during the recent continuous observations, corresponding to 0.4% y^{-1} loss of volume. Further, the glacier mass balance observations indicate an increasing negative trend. The total annual runoff from the catchment for the period 1993–2004 ranges between 24.4 and 42.0×10^6 m^3 (1,326–2,282 mm w.eq. y^{-1}), averaging 36.3×10^6 m^3 (1,973±281 mm w.eq. y^{-1}). Changes in air temperature within the last 106 years (1898–2004) show an average increase of 1.3ºC for the catchment: An increase highest for the in winter season of 3.1ºC. The period 1995–2004 was the warmest 10 year period within the approximately last 60 years. The glacier net mass balance from 1898–2004 indicate an average glacier recession of -0.55±0.53 m w.eq. y^{-1}, and a cumulative estimated balance of -56.7 m w.eq.; 89 out of 105 balance years had a negative estimated net mass balance. Average annual runoff (1898–2004) was estimated to 1,957±254 mm w.eq. y^{-1}, with a range between 2,522 and 1,326 mm w.eq. y^{-1}, respectively.

KEYWORDS
Arctic; Ammassalik Island; climate; Greenland; Mittivakkat Glacier; river discharge; glacier mass balance; 106 years perspectives (1898–2004)

1. INTRODUCTION

Over the last 100 years mean global surface air temperature has increased by 0.3 to 0.6°C (e.g., Maxwell, 1997; Kane, 1997). In this period, nine of the ten warmest years measured globally occurred between 1990 and 2001 (WHO, 2001), and it has been suggested that the 1990s were the warmest decade during the past

1,000 years (Crowley, 2000), with the largest air temperature changes in winter time (Box, 2002; Sturm *et al.*, 2005). The Arctic climate is also changing. From the mid-1800s to mid-1900s, the Arctic warmed to the highest temperatures in 400 years (Overpeck *et al.*, 1997). The climate has warmed substantially since the end of the Little Ice Age to present, significantly in the last 30 years (Serreze *et al.*, 2000). The warming has been accompanied by an increase in precipitation in the Arctic of approximately 1% decade^{-1} (ACIA, 2005).

Warming climate will initiate and evolve a cascade of impacts that affect e.g., glaciological and hydrological processes (Hinzman *et al.*, 2005). The Arctic is undergoing a system-wide response to an altered climatic state. New extreme and seasonal surface climatic conditions are being experienced, a range of processes influenced by the threshold and phase change of freezing point are being altered. It appears that first-order impacts to the terrestrial regions of the Arctic expected with a warming climate result from a longer thawing period combined with increased precipitation (e.g., Anisimov and Fitzharris, 2001; Hinzman *et al.*, 2005; Mernild *et al.*, 2007a). The longer snow-free season and greater winter insulation produces secondary impacts that could cause e.g., greater melt of glacier ice and snow, and deeper thaw of the active layer.

The dynamic nature of Greenland is framed by extremes: very cold winter temperatures, highly skewed annual cycle and North–South Greenland trend of solar radiation input, dominance of snow and glacier cover, and relatively low rates of precipitation (expect for the South eastern part of Greenland), all of which results from its elevation, topographic, and geographic position. There are essentially two seasons, one frozen and one thawed, with abrupt transition between them. During the winter or frozen season, which last 6–10 months of the year, unfrozen surface water is rare, and a negative annual radiation balance is established (more solar radiation is lost to space as enters). It is this negative radiation balance that creates the gradient that drive the Greenland and the Arctic climate (Hinzman *et al.*, 2005).

The Arctic hydrological cycle is shifting. The effect of a warmer climate on the hydrological processes in the Arctic are already becoming apparent. Basins with a substantial glacier component consistently display increasing trend in runoff, presumably due to increases in glacier melt. River basins lacking large glaciers tend to show decreasing runoff, probably because evapotranspiration rates have increased faster than increasing precipitation. Information on climate and river discharge in East Greenland was absent before the International Geophysical Year (IGY) 1957–58 (also known as the Third International Polar Year (IPY)). As a contribution, the first simultaneously related measurements of meteorology and terrestrial freshwater runoff was carried out in the Mittivakkat Glacier catchment, Ammassalik Island. In 1972, the Sermilik Research Station, in the Mittivakkat Glacier catchment, was established. Since then, an extensive monitoring program to study the climate-landscape processes and interactions has been on-going. Present, the Mittivakkat Glacier catchment is one of two catchments on the entire east Greenland (along the approximately 3,000 km coast), where permanent automatic meteorological and hydrometric monitoring stations occur. This, due to the rough terrain, harsh climatic conditions, and the remote locations. In the Mittivakkat Glacier catchment studies of simultaneous effects of climate in the form of recorded glacier mass balance changes and measured runoff are carried out so changes in climate can be directly linked to short and long term effects.

The goal of this study is to describe the climate (variations and trends in meteorological conditions) and its effect on the freshwater runoff in the Mittivakkat Glacier catchment with focus on the glacier mass balance during the period (1993–2005) of measurements. Further, we estimate the variations and trends in air temperature, Mittivakkat Glacier net mass balance, and catchment freshwater runoff over a 106 year period from 1898 to 2004, based on nearby standard synoptic meteorological data from the town Tasiilaq (Ammassalik).

2. STUDY AREA

The Mittivakkat Glacier catchment (18.4 km^2) (65°42'N latitude; 37°48W longitude) (Figure 1) is located on the western part of the Ammassalik Island, Southeast Greenland, approximately 15 km northwest of the town of Tasiilaq and 50 km east of the eastern margin of the Greenland Ice Sheet and is separated from the mainland by the 10–15 km wide north-south Sermilik Fiord. The area is considered to be Low Arctic. The catchment is characterized by sporadic permafrost and by a strong alpine relief and ranges in elevation from 0 to 973 m a.s.l., with the highest altitudes in the eastern part of the catchment. The Mittivakkat Glacier catchment is drained by the glacier outlet from the most southwestern part of the Mittivakkat Glacier (31 km^2) through a proglacial valley (Figure 1). The land cover within the catchment (22%; 4.0 km^2) is dominated by bare bedrock in the upper parts, and loose talus and debris-flow deposits in the lower parts of the slopes. Proglacial valley bottoms contain both moranic deposits and fluvial sediments (e.g., Hasholt and Mernild, 2004). The catchment (78%; 14.4 km^2) is covered by parts of the Mittivakkat Glacier complex (a temperate glacier with an average thickness of 115 m), ranging from approximately 160 to 930 m a.s.l. in elevation (Knudsen and Hasholt, 1999). The catchment watershed divide is located partly on the Mittivakkat Glacier: it is a non-stable topographic watershed divide, due to glacier dynamic

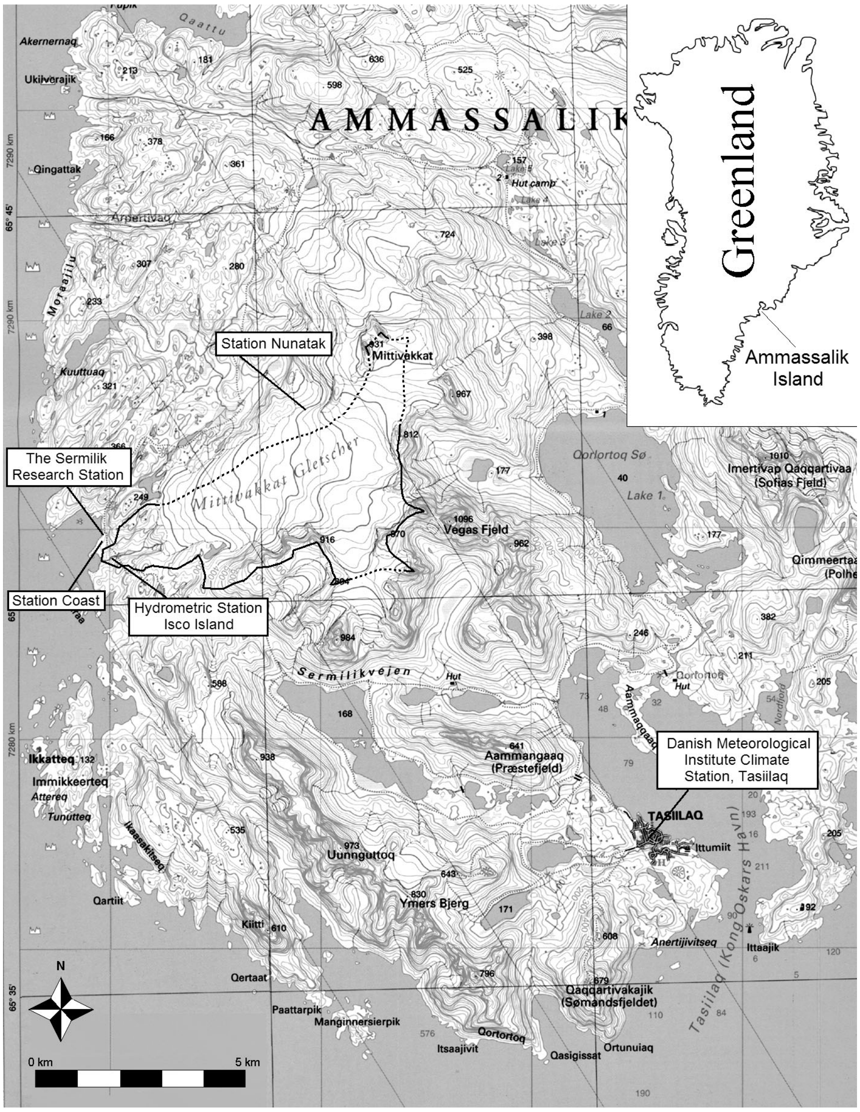

Figure 1: Location map showing the Mittivakkat Glacier catchment (18.4 km^2), Ammassalik Island, including meteorological stations: Station Nunatak (515 m a.s.l.) and Station Coast (25 m a.s.l.), the Danish Meteorological Institute (DMI) climate station in Tasiilaq (Ammassalik), and the hydrometric station at Isco Island. The dashed line indicates the non-stable topographic watershed divide on the Mittivakkat Glacier and the solid-drawn line the topographic watershed divide on bedrock for the Mittivakkat Glacier catchment. The inset figure indicates the general location of the Mittivakkat Glacier catchment within Eastern Greenland (Modified after Greenland Tourism).

and basal sliding (Figure 1). Therefore, a change in catchment size can occur (Mernild *et al.*, 2006c). Avalanches are rare near the glacier. Since 1933 the glacier terminus has retreated about 1.2 km (approximately 16 m y^{-1}), with a decrease in glacier surface elevation up to 100 m (below the 300 m a.s.l. elevation) (e.g., Mernild and Hasholt, 2006).

3. INDICES AND PARAMETRES

The following indices: The accumulated number of Thawing Degree Days (TDD) is the sum of values of positive mean daily air temperatures. TDD is related to release of water from both the snowpack and the exposed glacier ice surfaces after the annual snowcover has ablated. An increase in TDD will cause increased surface melt and catchment runoff.

The elements of the water balance for a drainage basin depend on drainage basin characteristics and processes. Yearly water balance simulation period goes from September through August of the following year; this is mainly due to the annual cycle of the Mittivakkat Glacier net mass balance (Knudsen and Hasholt, 2004; Mernild *et al.,* 2006a). The Mittivakkat Glacier catchment water balance equation (Eq. 1) is:

$$P - ET - R \pm \Delta S = 0 \pm \eta \qquad (1)$$

where P is the precipitation input from snow, rain, and condensation; ET is the evapotranspiration and sublimation; R is total runoff from surface, subsurface, rain, snow, glacier, and nearby catchment contributions; ΔS is change in surface storage (surface depressions, lakes, channels, etc.), subsurface storage, glacier storage and snowpack storage; and η is the balance discrepancy (Error). The total runoff is normally the most reliable component measured in the water balance if the stage-discharge relation is stable and valid. The runoff is an integrated response of the hydrological processes in the catchment and opposite to most other parameters in the water balance, it is not affected by the representativity of the measuring station (Killingtveit *et al.*, 2003).

4. DATA AVAILABILITY AND METHODS

This study is based on meteorological and hydrological data from 1993–2005 measured within the Mittivakkat Glacier catchment and standard synoptic meteorological data from 1898–2005 recorded at the Danish Meteorological Institute (DMI) climate station at Tasiilaq (Figure 1).

A meteorological station, Station Nunatak, has since 1993 continuously every third hour monitored the meteorological conditions on a nunuatak (65°42.3'N; 37°48.7'W, 515 m a.s.l.) situated on the northern side of the Mittivakkat Glacier, close to the equilibrium line altitude (ELA: where annual ablation equals annual accumulation) in order to capture the glacier climate, with sensors registering wind direction (4.0 m above terrain), wind speed and wind gust (2.0 and 4.0 m), air temperature (2.0 and 4.0 m), relatively humidity (4.0 m), incoming and outgoing short-wave radiation and net radiation (4 m) (e.g., Hasholt *et al.*, 2004; Hasholt and Mernild, 2004). Liquid (rain) precipitation was measured 0.45 m above the ground, approximately the height of local roughness (Mernild *et al.*, 2006a). Solid (snow) precipitation was calculated from snow depth sounding observations (Campbell SR50-station) that assumed to have an accuracy of within ± 10–15%.

Later, in 1997 a meteorological station, Station Coast, was established on a rock hill (65°40.8'N; 37°55.0'W, 25 m a.s.l.) in order to record information about the climate in the coastal region, and trends and orographic effects by comparison with the former. Since 1997 the station has continuously every third hour monitored the meteorological conditions in the coastal area. The following sensors were mounted 2 m above terrain: wind direction, wind speed, wind gust, air temperature, relatively humidity, incoming and outgoing short-wave radiation and net radiation. Liquid precipitation was measured 0.45 m above the ground. Solid precipitation was calculated by sounding observations at the hydrometric station Isco Island during winter, and during summer runoff variations were observed. The hydrometric station Isco Island is located close to the coast and approximately 200 m southwest from Station Coast.

After noise was removed from the snow depth data (Campbell SR50), the snow-depth sounding observations were fractionated into liquid (rain) precipitation and solid (snow) precipitation at different air temperatures based on observations from different locations on Svalbard. For air temperatures below -1.5ºC, sounding observations represents solid precipitation in 100% of the events and for temperatures above 3.5ºC precipitation is liquid for 100% of the events, in between (-1.5ºC to 3.5ºC) the fraction of snow and rain is calculated by linear interpolation (Førland and Hanssen-Bauer, 2003). Snow-depth increases at relative humidity <80% and at wind speed >10 m s^{-1} were removed to distinguish between the proportions of real snow accumulation based on precipitation events and blowing snow redistribution. The remaining snow-depth increases were adjusted using a temperature-dependent snow density (Brown *et al.*, 2003), and an hourly snowpack settling rate (Anderson, 1976) for estimating the water equivalent precipitation (mm. w.eq.): snow settles as it accumulates and thus the snow depth on the ground is always less than the initial amount of snowfall. This settling process represents a 10–15% increase in snow precipitation a year (Mernild *et al.*, 2007c). Further, Station Nunatak simulated end-of-winter snow water equivalent (SWE) depth was compared and adjusted against observed Mittivakkat Glacier winter mass balance, showing an average underestimated SWE (snow water equivalent) depth of 29% (1999–2002) (Mernild *et al.*, 2006a) before adjustment due to the exposed station location on the nunatak. During summer the sounder observations in the coastal region was used for river stage variations. All data were logged every third hour. The sensor type, accuracy, and range were described in Hasholt *et al*. (2004). Annual values, for both stations, have been reported in scientific notes since 2002 (Hasholt *et al*., 2004) and until 2004 (Mernild *et al*., 2006b).

The air temperature and TDD from the measured climate stations at the Mittivakkat Glacier catchment have been compared with data from the DMI station in Tasiilaq, in order to generate a time series at the Mittivakkat Glacier catchment covering the last 106 years. Linear regressions of air temperatures between the stations were used on daily basis (Station Coast and Tasiilaq DMI (1997 to 2004): $R^2 = 0.88$; $p<0.01$ (where p is the level of significance), and Station Nunatak and Tasiilaq DMI (1993 to 2004): $R^2 = 0.86$; $p<0.01$)). This allowed us to calculate monthly values for the two stations in the Mittivakkat Glacier catchment for the period 1897–1993. Then we converted this data into cumulative winter TDD (September to May), summer TDD (June to August), and annual TDD values (September to August). When data from the Mittivakkat Glacier catchment are compared to other data series it is clear that the combined meteorological observations and predictions at the catchment are in line with other long records. Further, the summer TDD was related by linear regression to the Mittivakkat Glacier summer mass balance (1995/96 to 2002/03, n = 8) ($R^2 = 0.65$; $p<0.01$), and station DMI winter precipitation (September to May) to the Mittivakkat Glacier winter mass balance (1995/96 to 2002/03) ($R^2 = 0.75$; $p<0.01$), in order to predict the net glacier mass balance for the period 1898/99 to 1994/95. The mass balance measurement on the glacier during 1986/87 showed a net balance of -0.12 m w.eq. y^{-1} (Hasholt, 1988): The estimated value for 1986/87 is -0.15 m w.eq. y^{-1}.

In the Mittivakkat Glacier catchment, the glacier is responsible for up to 90% of the yearly catchment runoff (Mernild, 2006), therefore, the observed net mass balance was related (linear regression) to the annual catchment runoff (September to August) (1995/96 to 2003/04) by linear regression ($R^2 = 0.76$; $p<0.01$) in order to calculate the annual runoff (September to August) from 1898–2004.

Winter and summer mass-balance observations were carried out in late May and early June, and in late August, respectively. During these field campaigns, snow depth, density, and ablation from snow and glacier ice were measured using cross-glacier stake lines spaced approximately 500 m apart: the distance between the stakes in each line were 200–250 m apart (Knudsen and Hasholt, 2004). The assumed accuracy of the observed winter and summer mass balances are each within ±15%; however large errors might occur especially in glacier areas with many crevasses (Knudsen and Hasholt, 2004).

SnowModel is a spatially distributed snowpack evolution modeling system simulating accumulation and loss from snow precipitation, blowing-snow redistribution, sublimation, snow-density evolution, and snowpack ripening and snow and ice melt, and specifically designed to be applicable over the wide range of snow landscapes and climates (Liston and Elder, 2006b). SnowModel includes a micrometeorological model (MicroMet). MicroMet is a quasi-physically-based meteorological distribution model (Liston and Elder, 2006a) designed to produce high-resolution meteorological forcing distributions of meteorological data into the terrestrial landscape. SnowModel simulations have previously been compared against observations in alpine,

Arctic, and Antarctic landscapes (e.g., Greene *et al*., 1999; Liston *et al*., 2000; Hiemstra *et al*., 2002; Liston and Sturm, 2002; Hasholt *et al.* 2003; Bruland *et al.* 2004; Mernild *et al.*, 2006a, 2006c, 2007b). In Eastern Greenland, SnowModel was used and produced maximum discrepancies of 8% in SWE and snow depth, and within ±100 m a.s.l. in spatial snow cover extent (Mernild *et al.*, 2006a, 2006c).
Intra- and inter-annual catchment runoff was simulated through the use of the NAM model (Nedbørs Afstrømnings Model means Rain and Runoff Model in English) (a lumped conceptual Rainfall-Runoff Model) (DHI, 2003a, 2003b; Mernild and Hasholt, 2006). The model describe in a simple quantitative form the behavior of the land phase hydrological cycle by a set linked mathematical statements by simulating hydrological processes as: overland-flow, inter-flow, and base-flow components. This as a function of the moisture content in four different interrelated reservoirs representing: snow storage, surface storage, root zone storage, and groundwater storage. Simulated runoff values for the Mittivakkat Glacier catchment were compared against observed runoff values, with a discrepancy up to 11% in cumulative discharge volume (Mernild and Hasholt, 2006). Observed discharge at the Isco Island hydrometric station was calculated from stage-discharge relationships estimated each year (R^2-values from 0.91 to 0.99) using regression analysis (Figure 1). The discharge cross section has been stable for approximately 30 years, yielding an assumed 10–15% accuracy when a single discharge measurement is made (e.g., Hasholt and Mernild 2004).

5. RESULTS AND DISCUSSION

5.1 Overall climatic conditions

The climate in the Ammassalik area is affected by the East Greenland Polar Sea Current which has both surface temperatures close to 0ºC and drift ice most of the year. Winters are therefore cold with only short periods of above freezing temperatures. Summers are cold with fog at the outer coast, but relatively warm and sunny in the inner parts of the fjords. Winds and precipitation in the area are strongly affected by cyclonic activities around Iceland and along the Greenland east coast: the tracks of low pressure systems typically go from southwest to northeast.

5.2 Meteorological conditions 1993–2005

5.2.1 Solar radiation, albedo, and snow cover

The midnight sun line passes through Tasiilaq, while the polar night line is located about 200 km further north. Surrounding topography, slope/aspect of the terrain, and cloud cover has a great influence on the amount of incident incoming solar radiation. At Station Nunatak the surface is gently sloping from N, NE, and E towards SW and W; significant diurnal variations in solar radiation are measured compared to a horizontal surface. Morning values are lower and afternoon values are higher than average. At Station Coast, the solar measurements are influenced by the mountain to the N and E of the station. In periods with dense cloud cover direct solar radiation is reduced, leaving only diffuse radiation (about 20–30% of potential radiation) to reach the surface. The mean annual solar radiation is respectively 113 W m^{-2} and 95 W m^{-2} for Station Nunatak (1993–2005) and Station Coast (1997–2005), indicating approximately 15% lower annual solar radiation in the coastal area due to the high frequency of dense clouds or thin sea fog (Figure 2). Variations in albedo is also seen in Figure 2, where low values around 15–20% indicate snow-free periods at the stations; a period that occurred approximately 4 weeks earlier in the coastal area compared to the nunatak. However, the maximum average yearly snow depth in the coastal area is 2.2 m, up to ~0.8 m (~50%) higher (1998–2004) than the nunatak. The maximum annual snow depth at Station Nunatak varies between 0.95 m (2002/03) and 1.72 m (2000/01), and at Station Coast between 1.73 m (2002/03) and 2.52 m (1999/00) (Figure 3). During the 6-year period (1998–2004), a continuous winter snow cover each year at Station Nunatak is established between the end of September/beginning of November, and it lasts until the end of June/beginning of July (Figure 4). The number of days with snow cover have decreased by 62 days ($p<0.01$), 43 days in autumn and 19 days in spring: this is from 286 snow cover days (1998/99) to 224 days (2003/04) at Station Nunatak (Figure 4), indicating a longer snow-free season. A reduction probably caused by increased yearly thawing rates (see chapter 5.2.2) and reduced snow precipitation (see chapter 5.2.4).

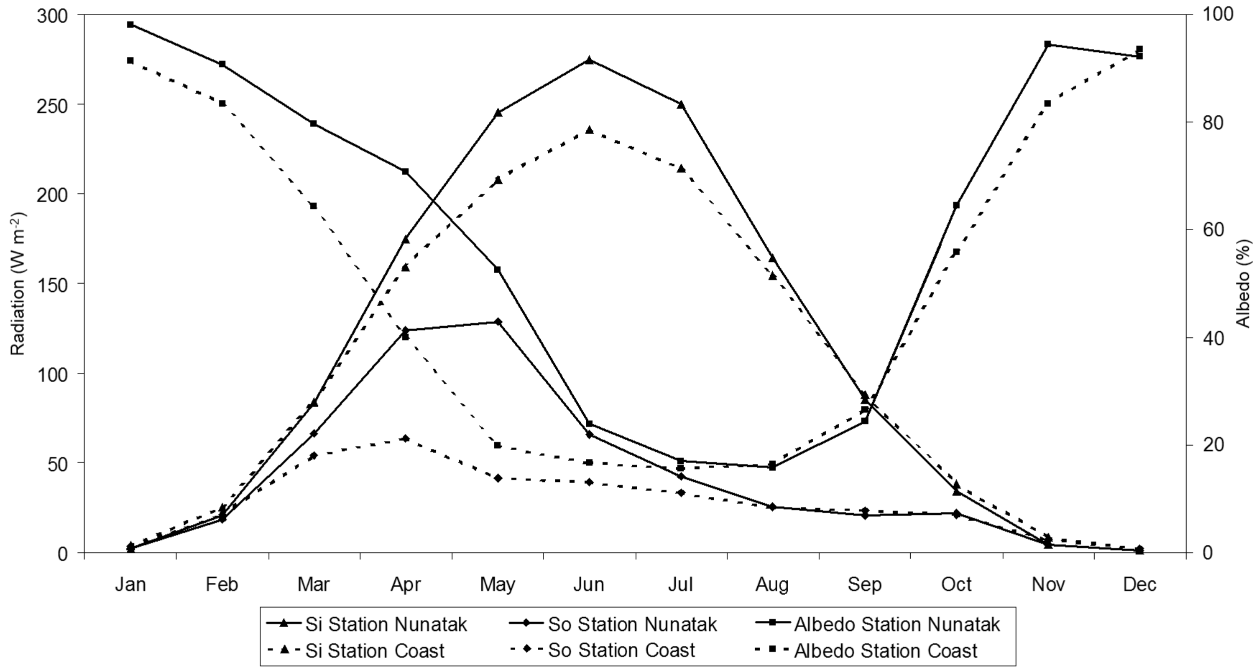

Figure 2: Mean monthly incoming (Si) and outgoing solar radiation (So) and albedo at Station Nunatak (1993–2005) and at Station Coast (1997–2005).

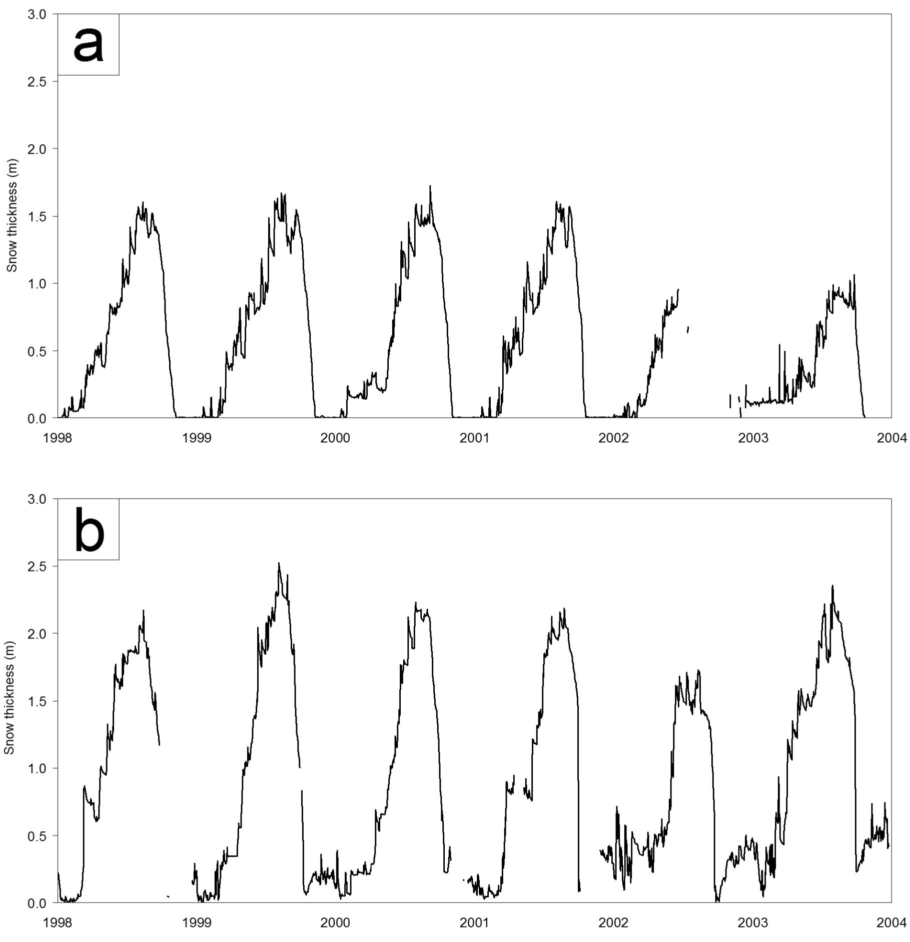

Figure 3: (a) Daily variation in snow depth at Station Nunatak (September 1998 to August 2004); and (b) at Station Coast (September 1998 to August 2004).

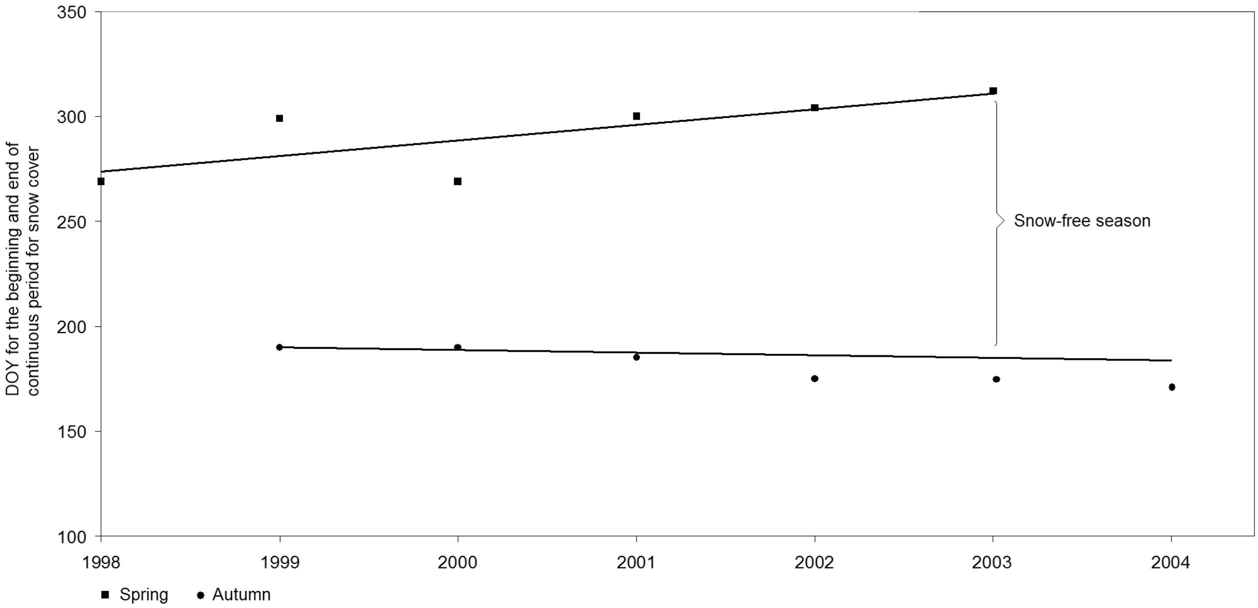

Figure 4: Day of year (DOY) for the beginning and the end of the continuous period for snow cover (1998–2004) at Station Nunatak. The area between the two trend lines indicate the snow-free season.

5.2.2 Air temperature and degree day

The Mittivakkat Glacier catchment mean annual air temperature (MAAT) is -1.7°C (1998–2004) (derived by spatial simulations in MicroMet), -2.4°C (2 m) and -2.2°C (4 m) at Station Nunatak (1994–2004), and -1.1°C (2 m) at Station Coast (1998–2004). The mean air temperature values cover a variation in MAAT from 1998 to 2004, showing increasing MAAT in the upper glacier area (0.06ºC y^{-1}) (Station Nunatak) and decreasing values in the coastal area (-0.13ºC y^{-1}) (Station Coast) (Figure 5a). The difference in MAAT between the stations has decreased from -1.6°C in 1998 to 0°C in 2003 (Figure 5a). This probably emphasizes a shift in continental and maritime conditions. Mean minimum air temperature in February is -9.2°C for Station Nunatak and -7.1°C for Station Coast in contrast to the average warmest month which is July at the nunatak (6.2°C) and August at the coast (4.9°C). A difference in warmest months between the stations, both in value and time, is probably due to e.g., albedo and heat capacity of the water, the Sermilik Fjord, near Station Coast, and the high frequency of dense clouds or thin sea fog. At Station Coast, positive mean monthly air temperatures occur from May to September and at Station Nunatak from June to September, however maximum mean monthly air temperatures is 7.4°C at the nunatak and 6.3°C at the coast (Figures 5b and 5c).

Mean monthly air temperature lapse rates for the Mittivakkat Glacier catchment are shown based on data from the two meteorological stations (Figure 5d). The mean annual air temperature lapse rate was approximately -0.3°C 100 m^{-1} (1997–2004), with an average range between the coldest and warmest mean monthly lapse rate of around 1.0°C 100 m^{-1}. February had the lowest average lapse rate (-0.6°C 100 m^{-1}), while July had the highest (0.4°C 100 m^{-1}) (Figure 5d). The positive average air temperature lapse rates from June to August are highly controlled by the wind regime; during the summer, sea breezes governed by local temperature differences in the heating of sea and land prevail, but they mostly only affecting coastal areas. The same yearly trend is present for periods without the occurrence of dense clouds or thin fog at the coastal (Mernild et al., 2005). The trend in monthly lapse rates is almost similar to other arctic coastal areas e.g., the Zackenberg River catchment (74°N), East Greenland.

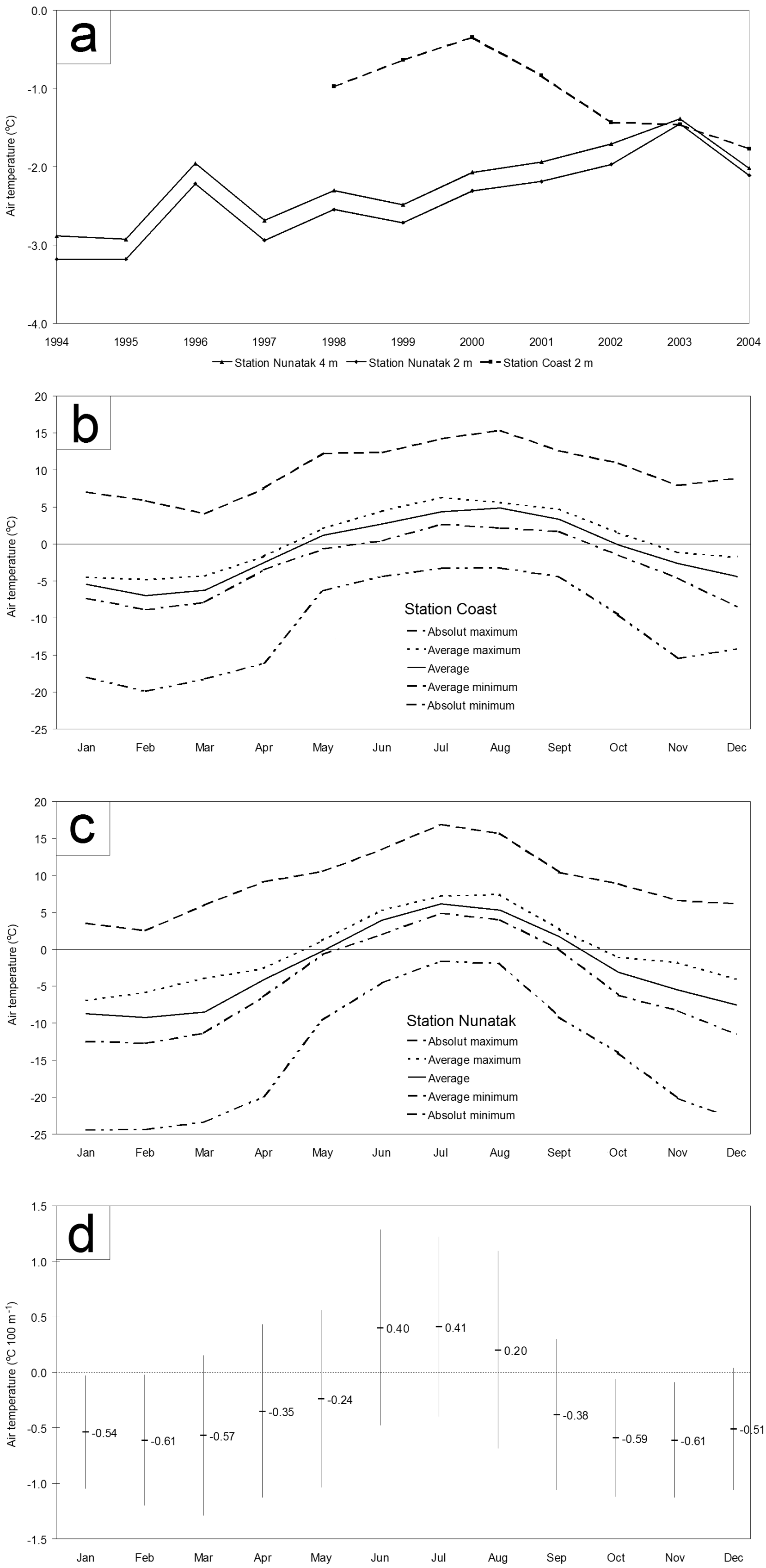

Figure 5: (a) Mean annual air temperature (MAAT) at Station Coast (2 m) (1998–2004) and at Station Nunatak (2 and 4 m) (1994–2004); (b) Station Coast maximum, mean, and minimum monthly mean air temperatures (2 m) for the time period (1998–2004); (c) Station Nunatak maximum, mean, and minimum monthly mean air temperatures (2 m) for the time period (1998–2004); and (d) monthly lapse rates based on air temperature (2 m) from Station Coast and Station Nunatak (1998–2004).

The lower part of the Mittivakkat Glacier catchment; the proglacial valley and the coastal area are highly dominated by the inversion. In summer time (June through August), inversions are present in approximately 85% of the observations (conducted in July 2006), where around 50% of the time inversions occur at 300 m.a.s.l., based on the radio sonde observations. In winter the present of inversion is expected to increase, as the amount of solar radiation and surface temperature decrease and snow and ice cover increase. For Zackenberg, NE Greenland, inversion are present 47–79% of the time in winter and 10–46% in summer/autumn (Mernild *et al.*, 2007c) The same trend is described by Serreze *at al.* (1992) for the Eurasian Arctic, and might also hold true for the Mittivakkat Glacier catchment.
A lateral transect of air temperature variation occurs through the catchment from the coast to the glacier terminus. That indicates a mean higher horizontal air temperature of 2°C and 4°C approximately 1,300 m from the coast (almost half way between the coast and the glacier terminus) compare to the coastal area and the glacier terminus air temperature respectively. This, due to cold sea breezes and katabatic winds (*piteraq*): cold air with a high density which flows towards the Mittivakkat Glacier edge (Mernild *et al.*, 2006b). Horizontal and altitudinal data which are required to account for the spatial variation of numerous variables used in snowmelt, glacier melt, and hydrological modeling at the catchment scale.
For Station Nunatak the trend lines on Figure 6 indicate a longer summer thawing period. In autumn the thawing season was extended by 31 days and in the spring by 10 days; resulting in a net thawing increasing period of 41 days (1993–2004). At Station Coast a decreasing thawing period occurred, with 12 and 6 days shorter autumn and spring thawing period, respectively. At Station Coast the net

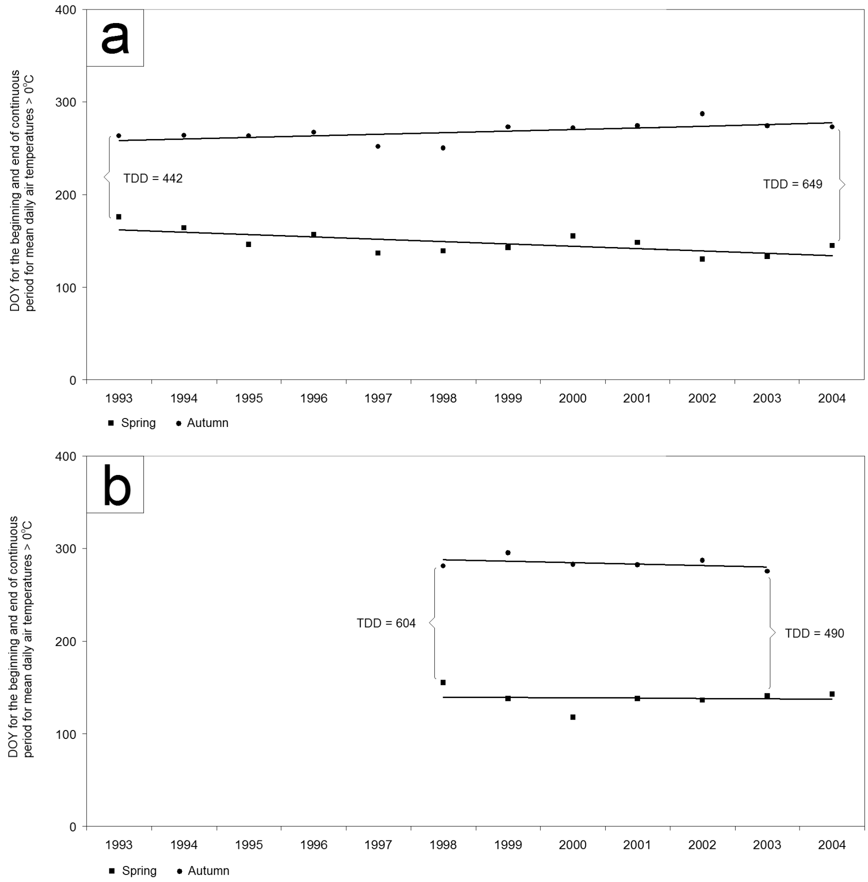

Figure 6: Day of year (DOY) for the beginning and the end of the continuous period for mean daily air temperatures above 0°C for: (a) Station Nunatak (1993–2004); and (b) Station Coast (1998–2004). The trend lines (linear regression) indicates longer thawing season at Station Nunatak, and a shorter thawing season at Station Coast. Furthermore, increasing Thawing Degree Day (TDD: the accumulated number of TDD is the sum of values of positive mean daily air temperatures) occur for Station Nunatak, and decreasing TDD for Station Coast.

thawing period decreased by 18 days (1998–2004). Furthermore, from 1993 to 2004 the yearly TDD increased at Station Nunatak from 442 to 649 (47% increase). No changes in mean TDD day^{-1} on 5.1 from 1993 to 2004 was observed. The opposite occurred for Station Coast, where yearly TDD decreased from 604 (1998) to 490 (2003) (19% decrease). The mean TDD day^{-1} decreased from 4.8 (1998) to 3.7 (2003) (Figure 6).

5.2.3 Wind direction, wind speed, and relatively humidity

Wind directions at both stations are highly dependent on the orographic conditions. At Station Nunatak cold katabatic fall winds, especially from the E, dominate all months around 30% of the time. The presence of the katabatic winds also results in the almost total lack of calms periods. During winter (illustrated by January in Figure 7c) and summer (illustrated by July) the main wind directions are from N to E at Station Nunatak. At Station Coast the wind direction is significantly influenced by the surrounding topography. A valley northeast of the station channels cold katabatic winds, especially in the winter (approximately 50% of the time the wind comes from north (Figure 7c)). Due to this tunneling effect, the gust at Station Coast can be even greater than at Station Nunatak. In the summer the wind system at Station Coast is characterized by sea breezes, mainly coming from S and SW (Figure 7c); This is governed by local temperature differences between the heating of sea and land.

The mean annual wind speed is 3.8 m s^{-1} at 2 m and 4.0 m s^{-1} at 4 m at Station Nunatak (1994–2004), and 4.0 m s^{-1} at 2 m at Station Coast (1998–2004). Wind speed data shows a trend of increasing velocities during the period (Figure 7a). The wind speed is highest in the winter time (Figure 7b), with mean monthly velocities around 6 m s^{-1} and gusts values up to more than 30.0 m s^{-1}. Furthermore, the highest velocities occur from the dominating wind directions. Strong winds (*neqqqjaaq*, similar to a Føhn wind) occur during winter on the Mittivakkat Glacier, mainly coming from the NE and E, and often followed by a *piteraq*. Wind velocities during a *piteraq* can gust to 85 m s^{-1}.

The mean annual relatively humidity is 87% (1998–2004) (derived by spatial simulations in MicroMet), covering a variation showing highest average values at Station Nunatak in winter (83%) due to the relatively lower air temperature, and highest average values at Station Coast in summer (86%) due to the sea breezes (Figure 7c).

5.2.4 Precipitation

The mean annual precipitation at Station Nunatak is 1,784 mm w.eq. y^{-1} (1997–2004), 1,347 mm w.eq. y^{-1} at Station Coast (1997–2004) (Figure 8b), and 1,491 mm w.eq. y^{-1} for the whole of the Mittivakkat Glacier catchment (Figure 8a) (derived by spatial simulations in MicroMet). The total annual solid (snow) precipitation at Station Nunatak is 1,629 mm w.eq. y^{-1} (1999–2004), calculated after applying a wind speed and winter glacier mass balance correction due to the exposed location at the nunatak (e.g., Hasholt and Mernild, 2004; Mernild *et al.*, 2006a), and at Station Coast it is 1,143 mm w.eq. y^{-1}. This indicates a positive orographic effect of 99 mm w.eq. per 100 m for SWE precipitation (Figure 8b) (Mernild *et al.*, 2006a). The 99 mm w.eq. per 100 m precipitation increase between the two meteorological stations is assumed to be closely related to the orographic influence of Ammassalik Island. Comparing the corrected precipitation at the DMI station in Tasiilaq with the adjusted precipitation at Station Nunatak, the orographic precipitation increases 121 mm w.eq. per 100 m (10% per 100 m) during 1997 to 2004. This is almost identical with gradients found and used in mountainous areas of Norway (Young *et al.*, 2006). Previous Ammassalik Island studies (1997/98), Hasholt *et al.* (2003) showed orographic precipitation increases as high as 14% per 100 m. The opposite, a negative orographic effect, occurs for liquid precipitation during summer months indicating an average orographic factor of -7 mm w.eq. per 100 m (1997–2004) (Figure 8c). This is due to the higher frequency of clouds and or thin fog in the coastal area or perhaps because the anticipated liquid precipitation actually falls as snow at higher altitudes (Mernild *et al.*, 2006b).

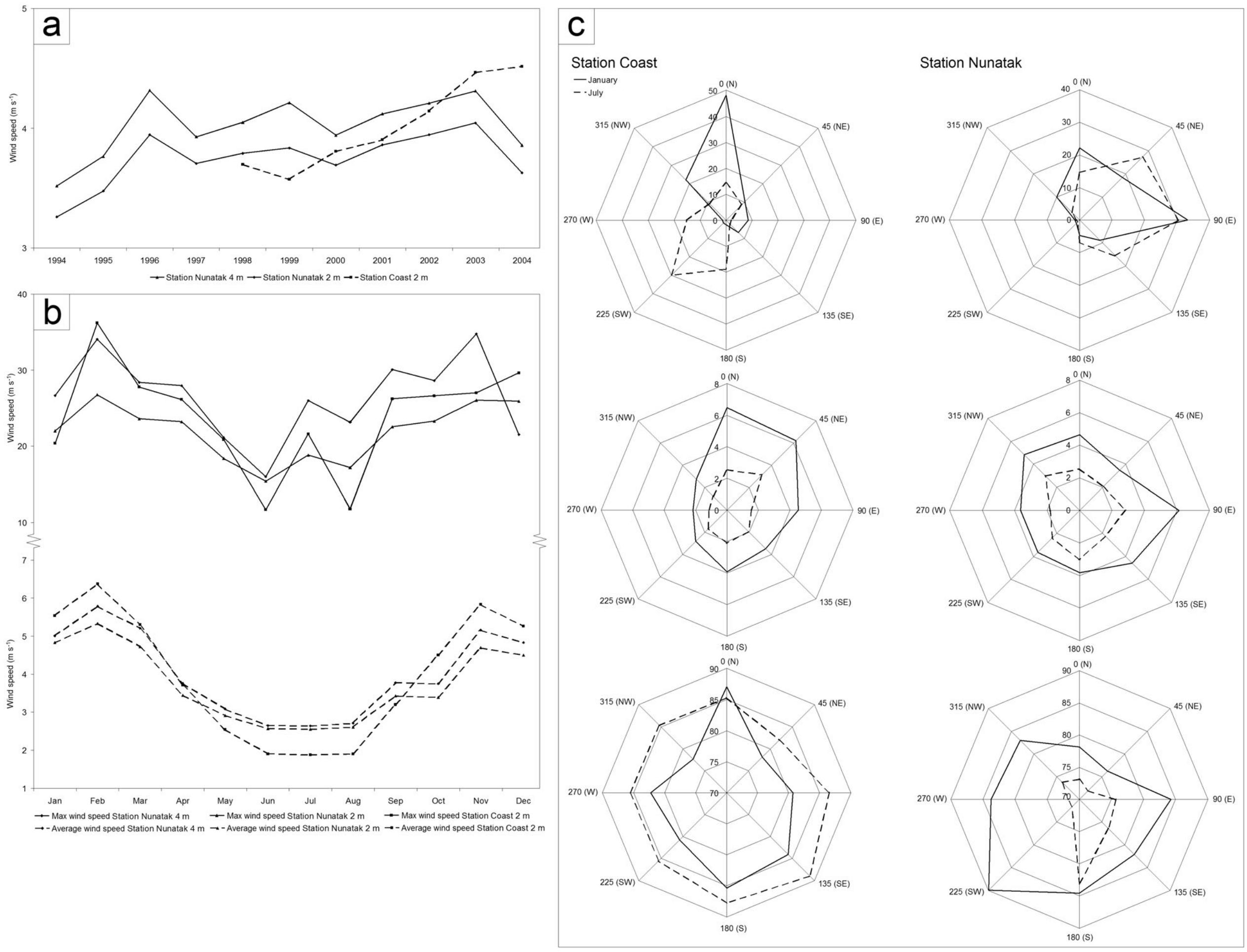

Figure 7: (a) Temporal trends in wind speed as average yearly values (1994–2004) for Station Nunatak (2 m and 4 m above terrain) and Station Coast (2 m); (b) temporal trends in maximum and average wind speed as mean monthly values for Station Nunatak (1993–2005) and Station Coast (1997–2005). Notice the change in scale on the ordinate; and (c) frequency (%) of wind direction, wind speed (m s^{-1}) related to wind direction, and relatively humidity (%) related to wind direction for average January and July for Station Nunatak (1993–2005) and Station Coast (1997–2005).

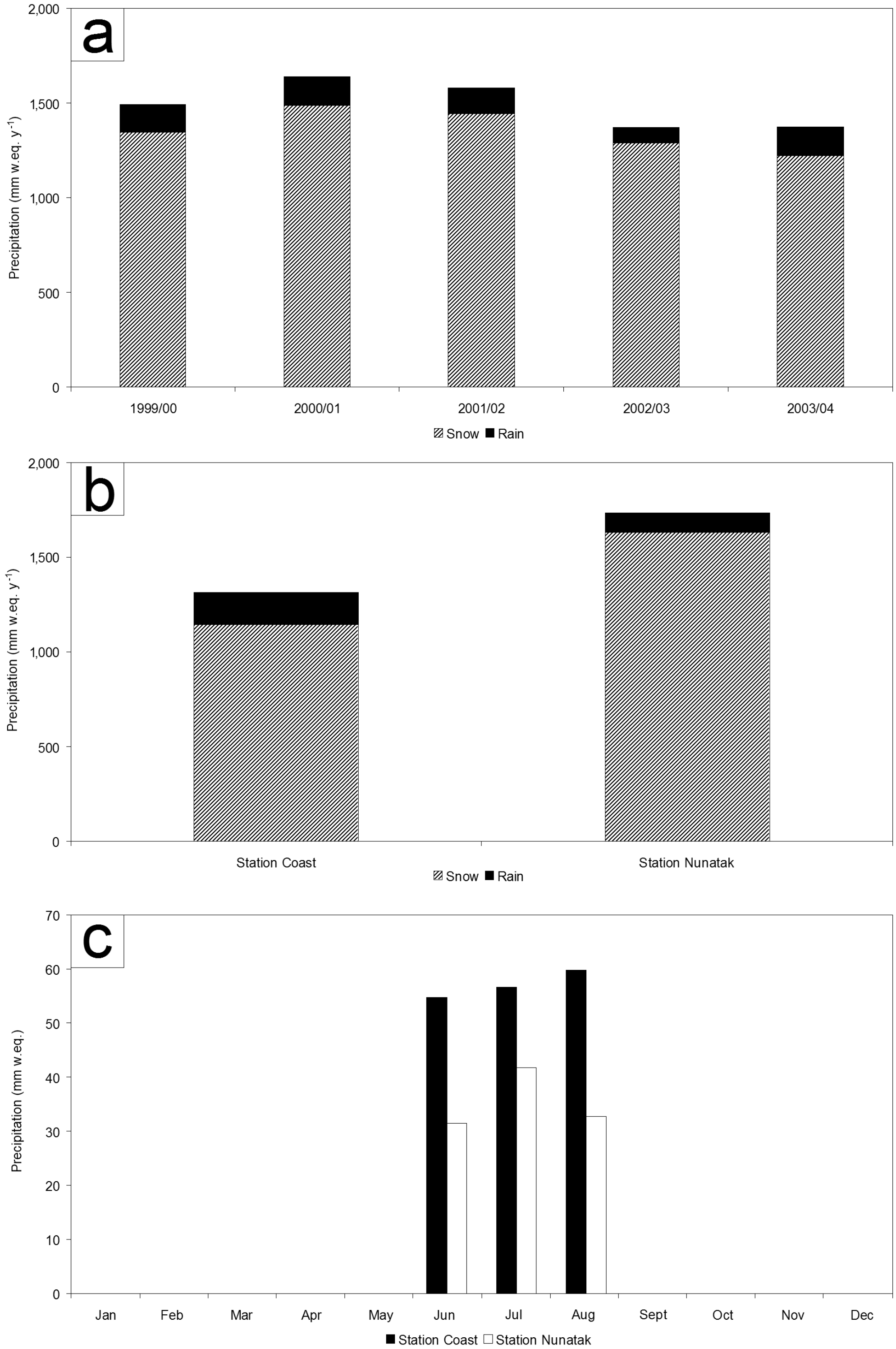

Figure 8: (a) Average annual (September to August) Mittivakkat glacier catchment snow and rain precipitation (1999/2000 to 2003/2004) (derived from Snow and Micrometeorological Model (SnowModel/MicroMet) (Liston and Elder, 2006a; 2006b)); (b) average annual (September to August) snow and rain precipitation at Station Coast (1998/1999 to 2003/2004) and at Station Nunatak (1998/1999 to 2003/2004); and (c) monthly June, July, and August average rain precipitation at Station Coast (1998–2004) and at Station Nunatak (1994–2004).

5.3 Glacier mass balance and runoff conditions 1993–2004

This period of continuous Mittivakkat Glacier mass balance observations since 1995/96 has been one of almost increasing (linear trend) glacier recession (Table 1). Only 1995/96 and 2002/02 had a positive net mass balance of 0.01 m w.eq. y^{-1} and 0.35 m w.eq. y^{-1}, respectively. The average observed winter mass balance (1995 through 2003), summer mass balance (1995 through 2003), and glacier net mass balance (1995 through 2004) are, respectively, 1.27±0.17, -1.80±0.40, and -0.59±0.51 m w.eq. y^{-1}, showing a negative net mass balance (Table 1). Further, an average increasing negative net mass balance occur since the first continuously observations in 1995/96. During the period of observation the Mittiakkat Glacier lost in average 0.59 m w.eq. y^{-1}, corresponding to 8.5×10^6 m^3 y^{-1} based on 78% (14.4 km^2) glacier cover in the catchment, and further corresponding to a 0.4% y^{-1} loss of volume based on 1994 determined glacier volume of $2{,}024\times10^6$ m^3 y^{-1}. This was measured by radio-echo sounding (Knudsen and Hasholt, 1999). The observed net mass balance from 1999 to 2002, based on 100-m-altitudal intervals observations, indicate that the ELA was located around 500–550 m a.s.l., except for 2000/01 where it was above 800 m a.s.l. (Mernild *et al.*, 2006a).

Table 1: Observed winter, summer, and net mass balance for the Mittivakkat Glacier (1995/1996 to 2003/2004) based on data in Knudsen and Hasholt (2004) and Mernild *et al.* (2006). Winter mass balance observations are carried out in late May and early June and summer mass balance observations in late August. (†) Calculated based on observations from 1995/96 to 2002/03. (*) Calculated based on observations from 1995/96 to 2003/04. The Mittivakat Glacier covers approximately 80% of the catchment area (18.4 km^2).

Year	Observed winter mass balance (m w.eq. y^{-1})	Observed summer mass balance (m w.eq. y^{-1})	Observed net mass balance (m w.eq. y^{-1})
1995/1996	1.51	-1.50	0.01
1996/1997	1.41	-1.81	-0.40
1997/1998	1.14	-2.31	-1.17
1998/1999	0.98	-1.75	-0.77
1999/2000	1.23	-2.06	-0.83
2000/2001	1.18	-2.14	-0.96
2001/2002	1.28	-1.78	-0.50
2002/2003	1.40	-1.05	0.35
2003/2004	No data	No data	-1.06
Average and standard deviation	1.27±0.17 (†)	-1.80±0.40 (†)	-0.59±0.51 (*)

At the Mittivakkat Glacier catchment the simulated date of river break-up at the catchment outlet has varied from year to year between 10 May (1998) and 10 June (2003) during the period 1994 and 2004 (Table 2 and Figure 9). The river simulated discharge varies between 1,326 mm w.eq. y^{-1} (corresponding to a runoff of 24.4×10^6 m^3 y^{-1}) for 1999 and 2,282 mm w.eq. y^{-1} (corresponding to a runoff of 42.0×10^6 m^3 y^{-1}) for 2001 (Mernild and Hasholt, 2006). The mean annual simulated river discharge for the period 1994–2004 was 1,973±281 mm w.eq. y^{-1} (corresponding to a runoff of 36.3×10^6 m^3 y^{-1}). High annual runoff peaks occur throughout the runoff season, mainly after periods with high air temperatures and subsequent surface melt (snow and glacier ice melt) and rain events (Figure 9). For example in 2004, where two main runoff peaks: a July 10 peak (11.6 m^3 s^{-1}) caused by a precipitation event, and an August 13 (11.0 m^3 s^{-1}) event due to melt events occurred. Maximum hourly observed river discharge (40.3 m^3 s^{-1}) so far at the catchment outlet was on 4 September 2000 after 36 hours with a mean air temperature of 8.7ºC coupled with 34 mm of precipitation (derived from MicroMet) (a peak discharge not seen clearly on Figure 9, due to the daily time step).

Table 2: Yearly observed and simulated accumulated discharge from the Mittivakkat Glacier catchment, together with maximum observed discharge and simulated date for river break-up (Mernild and Hasholt, 2006). The period goes from September to August followed by the Mittivakkat Glacier mass balance.

	Period with observed discharge	Accumulated observed runoff (mm w.eq.)	Maximum observed discharge ($m^3 s^{-1}$)	Annual accumulated simulated runoff (mm w.eq.)	Simulated date for river break-up (date for river break-up based on photos from the proglacier valley)
1993/1994	30 Jun – 28 Aug	1,307	9.3	2,144	22 May
1994/1995	1 Jul – 31 Aug	1,896	11.7	2,091	27 May
1995/1996	No data	No data	No data	1,864	28 May
1996/1997	No data	No data	No data	2,126	17 May
1997/1998	No data	No data	No data	1,914	10 May
1998/1999	22 Jun – 31 Aug	937	11.7	1,639	23 May
1999/2000	8 Jun – 17 Sept	2,010	6.9	2,145	11 May (13 May)
2000/2001	18 Jun – 15 Sept	1,726	6.1	2,282	23 May (26 May)
2001/2002	10 Jun – 5 Sept	1,871	7.9	1,987	27 May (28 May)
2002/2003	7 Jun – 20 Aug	927	5.7	1,326	8 Jun (10 Jun)
2003/2004	14 Jun – 27 Aug	1,907	10.0	2,190	25 May (26 May)
Average	--------	--------	8.7	1,973	23 May

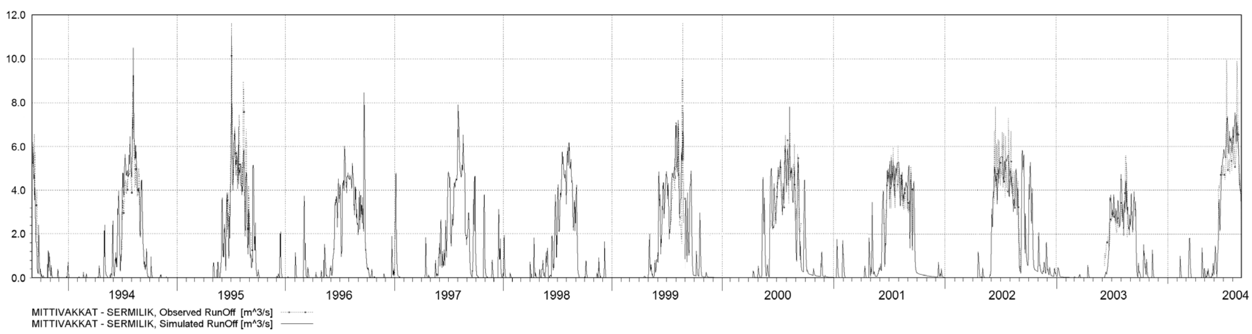

Figure 9: Daily observed and simulated discharge from the Mittivakkat Glacier catchment, Ammassalik Island, from September 1993 to August 2004. However, observed dicharge was missing from 1996, 1997, and 1998. Discharge was simulated by the NAM model; R^2 = 0.77 (Mernild and Hasholt, 2006).

5.4 Air temperature, glacier balance, and runoff in a 106 years perspective

Figure 10 illustrate the mean annual air temperature variation from 1898 to 2004 for the Mittivakkat Glacier catchment (obtained by linear regressions of air temperatures between the Tasiilaq and Sermilik stations). During the 106 year period warming, cooling, and constant air temperatures occurred in different intervals. General periods of warming was observed from 1918 (the end of the Little Ice Age) to 1935 and 1978 to 2004, in accordance with observations from the Arctic in generel by Serreze *et al*. (2000). Air temperature cooling at the Mittivakkat Glacier catchment occurred from 1955 to 1978, and approximately constant temperature conditions from 1898 to 1918 and 1935 to 1955, however the air temperature over the last 106 years has increased statistically significant by 1.3°C. This in contrast to the mean global air temperature increase by 0.3 to 0.6°C (e.g., Maxwell, 1997; Kane, 1997). All four seasons show warming over the period, especially during the winter season with +3.1°C, mainly due to warmer daytime temperatures. It can be concluded that the warmest average 10 year period within the last 106 years was the period from 1936–1946 (-1.8°C), while within

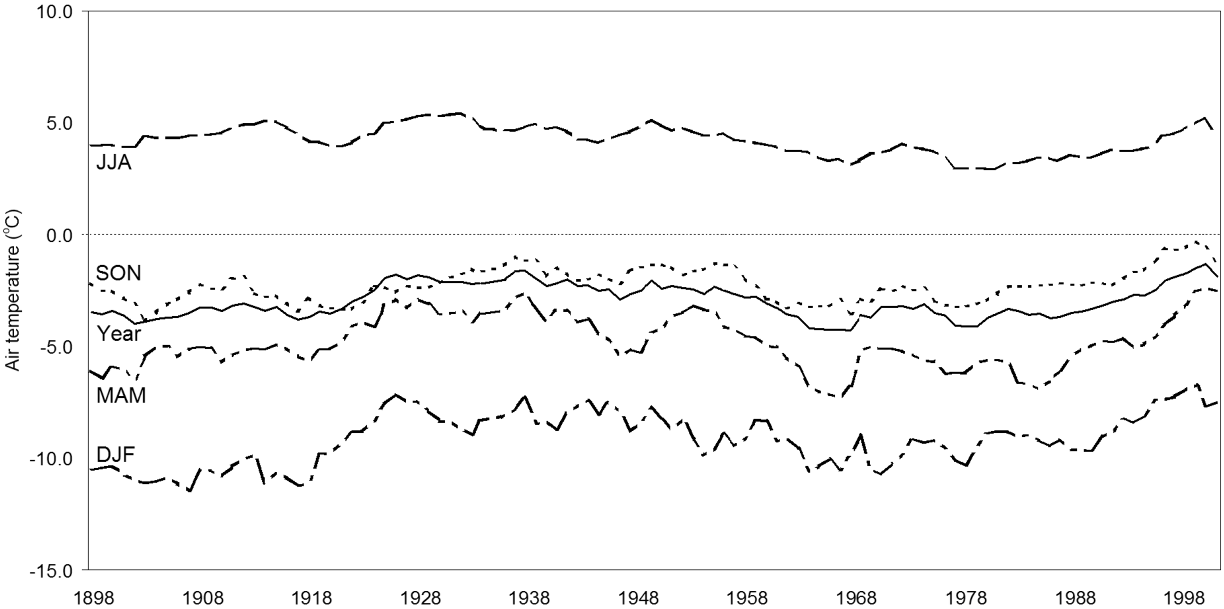

Figure 10: Five-year running mean annual and seasonal air temperature at the Mittivakkat Glacier catchment for the period 1898–2004. The abbreviations are DJM (December, January, and February), MAM (March, April, and May), JJA (June, July, and August), SON (September, October, and November), and Year (January to December). Data (from the DMI station in Tasiilaq) are missing in the period from September 1910 to August 1911 and from January 1971 to December 1972.

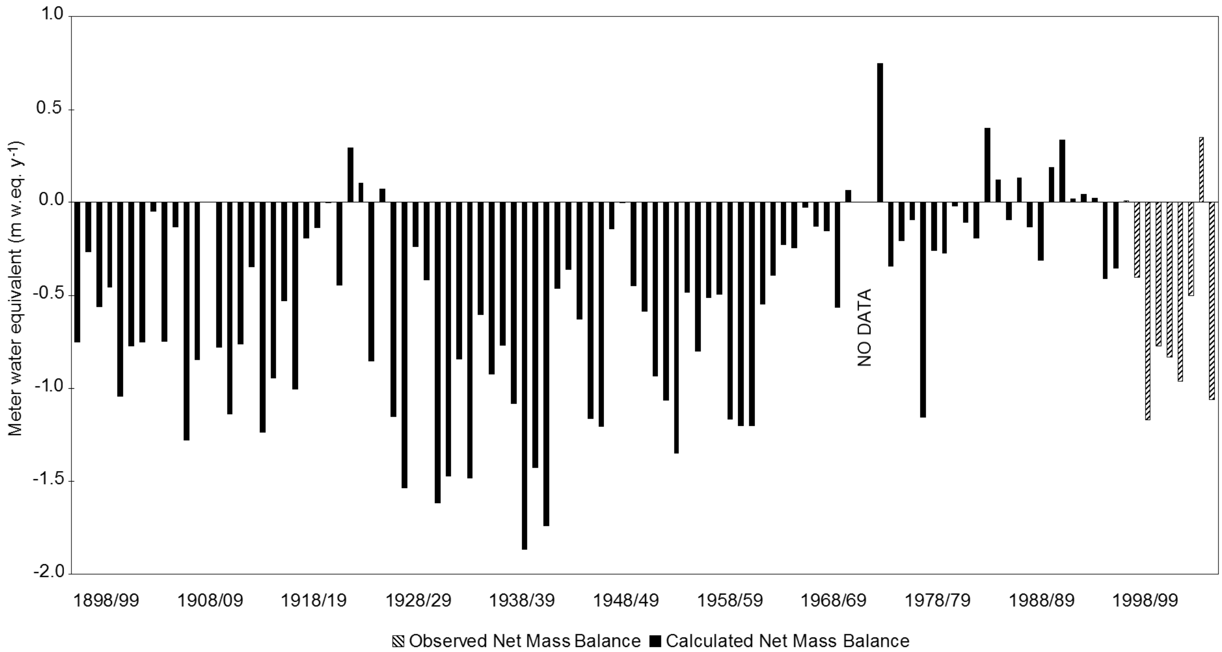

Figure 11: Yearly (September to August) observed (1995/96 to 2003/04) and calculated (1898/99 to 1994/95) glacier net mass balance (change in storage) for the Mittivakkat Glacier. The assumed accuracy of the observed net mass balance are within ±15% (Knudsen and Hasholt, 2004; Mernild *et al.*, 2006).

the last 60 years the warmest 10 year period was the period from 1995–2004 (-2.0°C) for the Mittivakkat Glacier catchment (Figure 10).
A warming climate, as just described, initiates and produce a cascade of impacts that affect glaciological and hydrological processes. Figure 11 shows the estimated Mittivakkat Glacier net mass balance from 1898 to 2004, indicating an average glacier recession of -0.55±0.53 m w.eq. y^{-1}, however maximum and minimum values of 0.75 m w.eq. y^{-1} (1972/73) and -1.87 m w.eq. y^{-1} (1939/40) occur, respectively. During the period, in 89 out of 105 balance years the Mittivakkat Glacier had a negative estimated balance, with a cumulative estimated balance of -56.7 m w.eq. The difference surface elevation based on topographic maps from 1932/33 (Geodædisk Institut 1938) and 1972 (based on aerial photographs) showed that the glacier below the 300 m a.s.l. had melted down as much as 100 m at the 1972 margin. Above 300 m a.s.l. the changes were smaller and at higher levels an increase was observed in places (Knudsen and Hasholt, 2004). Observations from 1933 indicates an almost continuous glacier margin recession on 1.2 km until 2004 (~17 m y^{-1}). The changes in location of the Mittivakkat Glacier margin since 1933 through the proglacier valley are shown on Figure 12. Together with changes in glacier size and shape, changes in internal drainage system and hydraulic response occur, all effecting the hydrological fluxes.
In the Mittivakkat Glacier catchment, the glacier net mass balance and the freshwater runoff is closely related because 78% of the catchment is covered by the Mitivakkat Glacier. Up to 90% of the yearly catchment runoff is explained by the glacier behavior. Average annual runoff was estimated to be 1,957±254 mm w.eq. y^{-1}, with a range between 2,522 mm w.eq. y^{-1} and 1,326 mm w.eq. y^{-1}, respectively (Figure 13).

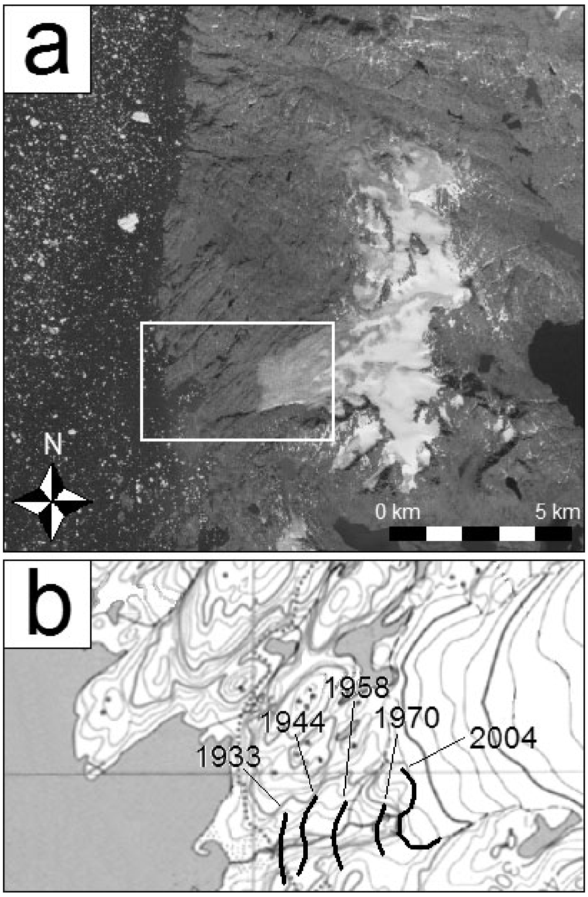

Figure 12: (a) Satellite image of the Mittivakat Glacier, Ammassalik Island August 22 (2004). The topographic map is within the white rectangle (source: www.digitalglobe.com/archive), and; (b) topographic map of the lower Mittivakkat Glacier including the margin and the proglacier valley. Lines indicate the Mittivakkat Glacier margin at different years (source: map modified after Greenland Tourism).

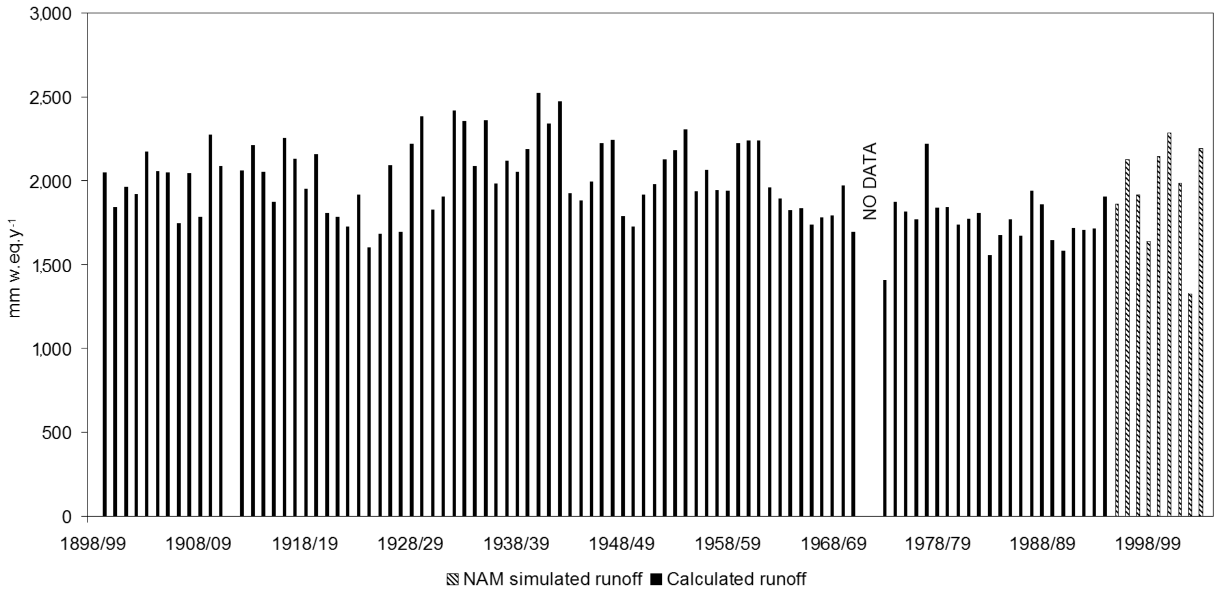

Figure 13: Yearly (September to August) simulated (1995/96 to 2003/04) and calculated (1898/99 to 1994/95) runoff from the Mittivakkat Glacier catchment. Simulated runoff values are based on NAM simulations (DHI, 2003a, 2003b; Mernild and Hasholt, 2006), calibrated and validated against observed runoff values.

6. CONCLUSION

From the above evaluation of twelve years of data (1993–2005) from meteorological stations within the Mittivakkat Glacier catchment on the western part of the Ammassalik Island, Southeast Greenland, we conclude that characteristic trends in meteorological conditions within the catchment have been noted, including increasing air temperature (0.09ºC y^{-1}) in the glacier area (at Station Nunutak) and decreasing values (-0.13ºC y^{-1}) in the coastal area (at Station Coast). Changes in air temperature, impacts both the thawing period and the snow-free period in the lower watershed and glacier net mass balance in the upper watershed. When data from the Mittivakkat Glacier catchment are compared to other data series in the area, it become clear that meteorological observations in the catchment are in line with other long term records, which make it possible to estimate data from the Mittivakkat Glacier catchment back in time to 1898. The 106 year period showed an increasing air temperature, mainly in winter season, but also that the period 1995–2004 was the warmest 10 year period within the approximately last 60 years for the Mittivakkat catchment. Since 1933 the glacier margin had retreated approximately 1.5 km.

ACKNOWLEDGEMENT

This work was supported by grants partly from the Danish National Science Research Council (SNF) (Grant 21-03-0530), the Department of Geography and Geology, University of Copenhagen, the Copenhagen Global Change Initiative (COGCI), University of Copenhagen, and the University of Alaska Presidential IPY Postdoctoral Foundation.

REFERENCES

ACIA, 2005. Arctic Climate Impact Assessment. Cambridge University Press, 1042 pp.

Anderson, E.A. 1976. A point energy balance model of a snow cover. *NOAA Tech. Rep*. NWS 19, 150 pp.

Anisimov, O.A. and Fitzharris, B. 2001. Polar regions (Arctic and Antarctic), in McCarthy, O.F.C.J.., Leary, N.A., Dokken, D.J., and Whits, K.S. (eds.), *Climate Change 2001: Impacts, Adaptation, and Vulnerability.*

Contribution of Working groupe II to the Third Assessment Report of the Intergovernmental Panel on Climate Change, Cambridge University Press, Cambridge, pp. 801–841.

Box, J.E. 2002. Survey of Greenland Instrumental Temperature Records: 1973–2001. International *Journal of Climatology*, 22: 1829–1847.

Brown, R.D., Brasnett, B. and Robinson, D. 2003. Gridded North American monthly snow depth and snow water equivalent for GCM evalutation. *Atmosphere-Ocean*, 41(1): 1–14.

Bruland, O., Liston, G. E., Vonk, J., Sand, K. and Killingtveit, A. (2004). Modelling the snow distribution distribution at two High-Arctic sites at Svalbard, Norway, and at a Sub-Arctic site in Central Norway. *Nordic Hydrology*, 35(3): 191–208.

Cowely, T.J. 2000. Causes of Climate Change over the Past 1,000 Years. *Science*, 289(5777): 270–277.

DHI Water and Environment (2003a). MIKE 11 reference manual. DHI Water and Environmental, pp. 416.

DHI Water and Environment (2003b). MIKE 11 User Guide. DHI Water and Environmental, pp. 422.

Førland, E.J. and Hanssen-Bauer, I. 2003. Climate variations and implications for precipitations types in the Norwegian Arctic. Met. Report, Norwegian Meteorological Institute, Report No. 24/02, 21 pp.

Greene, E. M., Liston, G. E. and Pielke, R. A. (1999): Simulation of above treeline snowdrift formation using a numerical snowtransport model. *Cold Reg. Sci. Technol*., 30: 135–144.

Hasholt, B., Hansen, B.U., Humlum, O. and Mernild, S.H. 2004. Meteorological stations at the Sermilik Station, Southeast Greenland: physical environment and meteorological observations 2002. *Danish Journal of Geography*, 104(2): 47–58.

Hasholt, B., Liston, G.E. and Knudsen, N.T. 2003. Snow distribution modelling in the Ammassalik region, southeast Greenland. *Nordic Hydrology*, 34: 1–16.

Hasholt, B. and Mernild, S.H. 2004. Estimation of water balance in and around the Mittivakkat Glacier basin, Ammassalik Island, outheast Greenland. 290. In Kane, D. L. and Yang, D. (eds.): Northern Research Basins Water Balance, *IAHS Publication*, pp 129–142.

Hiemstra, C. A., Liston, G. E. and Reiners, W. A. (2002): Snow Redistribution by Wind and Interactions with Vegetation at Upper Treeline in the Medicine Bow Mountains, Wyoming. *Arctic, Antarctic, and Alpine Research,* 34: 262–273.

Hinzman, L.D., Bettez, N.D., Bolton, W.B., Chapin, F.S., Dyurgerov, M.B, Fastie, C.L., Griffith, B., Hollister, R.D., Hope, A., Huntington, H.P., Jensen, A.M., Jia, G.J., Joergensen, T., Kane, D.L., Klein, D.R., Kofinas, G., Lynch, A.H., Lloyd, A.H., McGuire, A.D., Nelson, F.E., Oechel, W.C., Osterkamp, T.E., Racine, C.H., Romanovsky, V.E., Stone, R.S., Stow, D.A., Sturm, M., Tweedie, C.E., Vourlitis, G.L., Waker, M.D., Walker, D.A., Webber, P.J., Welker, J.M., Winker, K.S.,and Yoshikawa, K. 2005: Evidence and implications of recent climate change in Northern Alaska and other Arctic regions. *Climatic Change*, 72: 251–298.

Kane, D. 1997. The Impact of Hydrologic Perturbation on Arctic Ecosystems Induced by Climate Change. Global Change and Arctic terrestrial Ecosystems. *Ecological Studies*, 124: 63–81.

Killingtveit, Å., Pettersson, L-E. and Sand K. 2003. Water balance investigations in Svalbard. *Polar Research*, 22: 161–174.

Knudsen, N.T and Hasholt, B. 1999. Radio-echo sounding at the Mittivakkat Gletscher, Southeast Greenland. *Arctic, Antarctic, and Alpine Research*, 31(3): 321–328.

Knudsen, N.T and Hasholt, B. 2004. Mass balance observations at the Mittivakkat Gletscher, Southeast Greenland. *Arctic, Antarctic, and Alpine Research*, 35(4–5): 381–390.

Liston, G.E. and Elder, K. 2006a. A meteorological distribution system for high resolution terrestrial modeling (MicroMet). *Journal of Hydrometeorology*, 7: 217–234.

Liston, G. E. and Elder, K. 2006b. A distributed snow-evolution modeling system (SnowModel). *Journal of Hydrometeorology*, 7: 1259–1276.

Liston, G. E. and Sturm, M. (2002): Winter Precipitation Patterns in Arctic Alaska Determined from a Blowing-Snow Model and Snow-Depth Observations. *Journal of Hydrometeorology*, 3: 646–659.

Liston, G. E., Winther, J.-G., Bruland, O., Elvehøy, H., Sand, K. and Karlöf, L. (2000): Snow and blue-ice distribution patterns on the coastal Antarctic ice sheet. *Antarctic Science* 12(1): 69–79.

Maxwell, B. 1997. Recent Climate Patterns in the Arctic. Global Change and Arctic Terrestrial Ecosystem. *Ecological Studies*,124: 21–47.

Mernild, S.H. 2006: Freshwater Discharge from the coastal area outside the Greenland Ice Sheet, East Greenland, with focus on Mittivakkat, Ammssalik Island (Low Arctic) and Zackenberg (High Arctic). PhD Dissertation, University of Copenhagen, Institute of Geography. 394 pp.

Mernild, S.H. and Hasholt, B. 2006: Climatic control on river discharge simulations from the Mittivakkat Glacier catchment, Ammassalik Island, SE Greenland. *Nordic Hydrology*, 37(4-5): 327–346.

Mernild, S.H., Hasholt, B. and Hansen, B.U. 2005. Meteorological observations 2003 at the Sermilik Station, Ammassalik Island, Greenland. *Danish Journal of Geography*, 105(1): 49–56.

Mernild, S.H., Hasholt, B. and Hansen, B.U. 2006b. Meteorological observations 2004 at the Sermilik Station, Ammassalik Island, Greenland. *Danish Journal of Geography*, 106(1): 131–140.

Mernild, S.H., Hasholt, B. and Liston, G.E. 2006c. Water flow through Mittivakkat Glacier, Ammassalik Island, SE Greenland. *Danish Journal of Geography*, 106(1): 25–43.

Mernild, S.H., Hasholt, B. and Liston, G.E. 2007b. Climatic control on river discharge simulations, Zackenberg River Drainage Basin, NE Greenland. *Hydrological Processes*. Accepted.

Mernild, S.H., Liston, G.E. and Hasholt, B. 2007c. Snow-distribution and Melt Modeling for Glaciers in Zackenberg River Drainage Basin, NE Greenland. *Hydrological Processes*. In Press.

Mernild, S.H., Liston, G.E., Hasholt, B. and Knudsen, N.T 2006a. Snow Distribution and Melt Modeling for Mittivakkat Glacier, Ammassalik Island, Southeast Greenland. *Journal of Hydrometeorology*, 7: 808–824.

Mernild, S. H., Sigsgaard, C., Rasch, M., Hasholt, B., Hansen, B. U., Stjernholm, M. and Petersen, D. 2007. Climate, river discharge and suspended sediment transport in the Zackenberg River Drainage Basin and Young Sound/Tyrolerfjord, Northeast Greenland. In Rysgaard, S. and Glud, R. N. (Eds.), Carbon cycling in Arctic Marine ecosystems: Case study Young Sound *Meddr. om Grønland*, *BioScience* 58: 24–43.

Overpeck, J., Hughen, K., Hardy, D., Bradley, R., Case, R., Douglas, M., Finney, B., Gajewski, K., Jacoby, G., Jennings, A., Lamoureux, S., Lasca, A., MacDonald, G., Moore, J., Retelle, M., Smith, S., Wolfe, A., and Zielinski, G. 1997. Arctic environmental change of the last four centuries. *Science*, 278: 1251–1256.

Serreze, M. C., J. D. Kahl and R. C. Schnell 1992: Low-level Temperature Inversions of the Eurasian Arctic and Comparisons with Soviet Drifting Station Data. *Journal of Climate*, 5: 615–629.

Serreze, M.C., Walsh, J.E.,Chapin, F.S., III Osterkamp, T., Dyurgerov, M., Romanovsky, V., Oechel, W.C., Morrison, J., Zhang, T., and Barry, R.G. 2000. Observational evidence of recent change in the northern high latitude environment. *Clim. Change*, 46: 159–207.

Sturm, M., Schimel, J., Michaelson, G., Welker, J.M., Oberbauer, S.F., Liston, G.E., Fahnestock, J. and Romanovsky, V.E. 2005. Winter Biological Processes Could Help Convert Arctic Tundra to Shrubland. *BioScience*, 55(1): 17–26.

WHO, 2001. WHO Statement on the Status of the Global Climate in 2001. WHO#670. World Meteorological Organization, Geneva, Switzerland, 84 pp.

Young, K.L., Bolton, W.R., Killingtveit, Å. and Yang, D. 2006. Assessment of precipitation and snowcover in northern research basins. *Nordic Hydrology*, 37(4–5): 377–391.

Numerical analysis of migration and accumulation of pollutants near to bottom of water bodies

Vladimir E. Putyrsky

Institute of Water Problems of Russian Academy of Science,
Gubkin, 3, Moscow, RUSSIA
e-mail: putyrsky@aqua.laser.ru

ABSTRACT

Scientific and methodological problems are examined of the pollutant dispersion within inland water bodies and water courses by interaction between the fluxes at the divides of water, atmosphere and near-to-bottom areas (Putyrsky, 1993). With the use of a semi-empirical turbulent diffusion equation, regularities in the pollutant area from technogenic sources were investigated with taken into account the sedimentation processes. Mathematical models have been developed for modeling the processes of accumulation of pollutants in the bottom sediments off-shore and water systems in river valleys. Analyzed were also the data on migration of the carcinogenic components within Lake Valday (North-western Russia). A method has been proposed for the quantitative estimation of a number of hydro-physical factors through an approximation of experimental data by any equations theoretically proved as well as mathematical solutions of the inverse problems.

KEYWORDS

Pollutant dispersion; numerical analysis; water bodies; near-to-bottom areas.

1. INTRODUCTION

Divides of water bodies, particularly the bottom, are reformers, accumulators and sources of substances and energy. In relation to the consequences of technogeneous impact on water bodies, there often appear the cases when the bottom sediments become a dominant factor of pollution, which affect the phone concentration of pollutants. Until the time, a non-significant attention was paid to the studies of the flux properties on the borders with diverse hydro-physical conditions. It is true about the processes at the "water – bottom" divide. However, investigations in the area are greatly upraised at this time, that is caused with certain achievements of modern science, and is related to a need of solving the problem of secondary pollution. The problems of this type appear by accumulation of technogeneous pollutants within bottom sediments.

2. METHODS

Investigations are based on a theoretical description of the space-and-time inhomogeneities in migration and accumulation of suspended particles. Main stages of the work are:

1) analysis of the nature data available,
2) development of a hydrodynamic model for interaction between fluxes within the near-to-bottom zone,
3) realization of the model based on numerical algorithms.

Besides, the methodological problems are discussed of the pollutant dispersion, with an accent on the bottom sediment pollution areas as well as their accumulation within silt. Evaluations were done of advection and diffusion of technogeneous pollutants.

Macro-scale hydro-physical dispersion of pollutants was studied with the use of the following differential equation:

$$\frac{\partial c}{\partial t}+u\frac{\partial c}{\partial x}+v\frac{\partial c}{\partial y}+(w-w_{\Pi})\frac{\partial c}{\partial z}=\frac{\partial}{\partial x}(K_x\frac{\partial c}{\partial x})+\frac{\partial}{\partial y}(K_y\frac{\partial c}{\partial y})+\frac{\partial}{\partial z}(K_z\frac{\partial c}{\partial z})-\frac{c}{\tau}+ \quad (1)$$
$$+Q(t)\ \delta(x-a)\delta(y-b)\delta(z-d),$$

Where c is concentration of the pollutant; w_n its gravitation velocity; τ is the constant of biochemical destruction; δ is the "delta"-function; t is the time elapsed; x, y, z are the co-ordinates with basis at the water surface; u, v, w are the components of the flow velocity by the relative co-ordinate axis; K_x , K_y , K_z are the turbulent diffusion coefficients for longitudinal, transversal and vertical directions; $Q(t)$ is the power of the pollutant source at the point A (a, b, d).

In the most of cases, which arise by pollution of shallow water and off-shores, we neglect the vertical transport of pollutant. Used widely is a consideration about the so-called "solid lid" for the cases when the surface water deformations are small in comparison with deep. Considering also are the deep average changes of the hydrodynamic and hydro-chemical parameters without attention to the "buoyancy", i.e. the averaging procedure is simply:

$$\bar{c}(x,e,t)=\frac{1}{H}\int_0^H c(x,y,z,t)dz \quad (2)$$

where H is the deep of the shallow water body.

The vertical transfer in such "bulk" models is described through the boundary conditions on free water surface and bottom. Turbulent fluxes of the pollution particles are as follows:

$$q_x=-\rho\overline{u'c'},\quad q_y=-\rho\overline{v'c'}, \quad (3)$$

where u′, v′, c′ - the turbulent fluctuations of the liquid velocity and the concentrations of the pollutant across their average values u, v, c; the hyphen above signifies averaging over the ensemble.

Transfer of pollutants across the boundary "water-air" through the molecular film is described by the following equation:

$$q_A=\frac{M_{1d}\beta}{\delta_A}(\kappa_r c_A-c),\ z=0, \quad (4)$$

where q_A is the mass transfer through the film; β is the factor rendering chemical reaction; δ_A the film deep; K_r the pollutant solubility; M_{1d} is the molecular diffusion coefficient within the surface layer above the water. Investigations of the factors are critically important and will be a focus of the future efforts.

The pollution transport to the bottom for the time T is as follows:

$$Q = q_B T,\ \ T = n\,\Delta t \quad (5)$$

And the averaged concentration within the bottom silt is

$$\bar{c}_* = Q/h_*, \quad (6)$$

where h_* is the silt deep.

The pollutant flux within silt is described by the following equation: $q_{B*}=M_{2d}\dfrac{\partial c_*}{\partial z},\ \ H<z<H+h_*$ (7)

where M_{2d} is the coefficient of molecular diffusion. And by integration, we have

$$c_* = A + z\ q_* / M_{2d}\,. \quad (8)$$

3. STUDY RESULTS

Investigating the large-scale hydro-physical dispersion of suspended particles, we have solved the problem of modeling the advection from a source situated in the Vistula lagoon (Putyrsky, Frolov, 2004). Degree of pollution of the shallow lagoon, which is peculiar collector for waste water, is the utmost for the Baltic region. Character of the water exchange between the lagoon and the Baltic See is mainly affected by river runoff, that has been proved by absence of vertical stratification of salinity.

Granulometrical composition of the suspended particles is mainly *alevrolythres*. Particles of the sizes are able to be suspended during a long time and moved within the lagoon water over significant distances. All the above mentioned allows to consider the Vistula lagoon as a quasi-stationary source for pollution of adjacent areas.

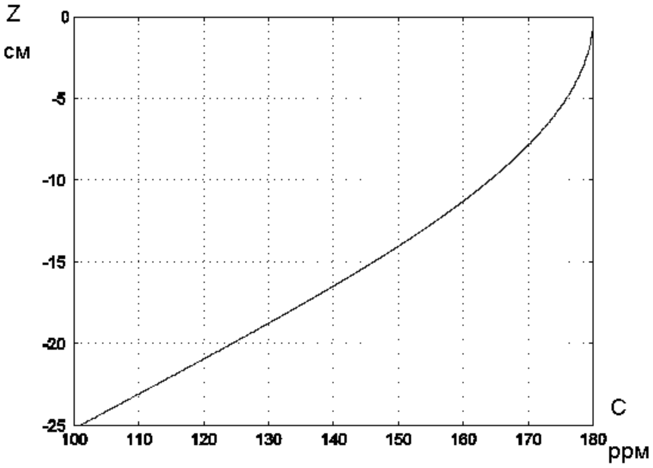

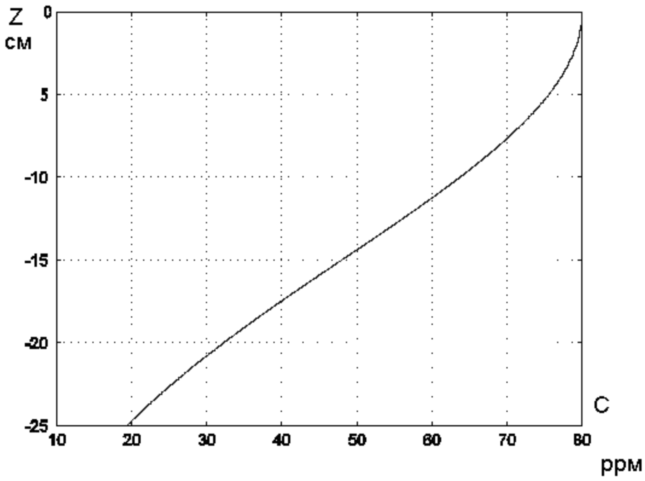

Figure 1. Calculated distribution of concentration (ppm) within the sea bottom Sediments formed by diffusion for different deeps (Z, cm): left – for lead, right – for zinc.

The results obtained have led to a conclusion about a significant influence of the waste water from the Vistula lagoon on the quality of off-shore water of Kaliningrad Region of Russia. Important values of the pollutant fluxes to the bottom are observed over the aquatic area between Baltiysk (Russia) and Liepaya (Latvia). Areas of the bottom technogeneous pollution are formed even by only short-time period which is the synoptic period. The results are given and labeled on the Figure 1.

The best fit for zinc and lead of experimental and computed data has been achieved by the following parameters of the diffusion equation:

tM_{2d} = 270 cm^2 for zinc and tM_{2d} = 110 cm^2 for lead

where tM_{2d} is diffusion coefficient and t is time.

REFERENCES

Putypsky, V.E. (1993) Hydro-physical aspects of interaction between inland waters – NAUKA Publ. House, Moscow, 120 p.

Putyrsky, V.E. and A.P. Frolov (2004) Processes of pollution of the bottom sediments (on an example of the Baltic shore of the Kaliningrad Region). – *Geoecology*, No. 2, pp. 122-129.

Some spatial patterns in the water balance structure for the river basins within European Russia

Yuri A. Salo

Northern Water Problems Institute, 50 A. Nevskogo St., 185030 Petrozavodsk, Republic of Karelia, RUSSIA
e-mail: yuris@nwpi.krc.karelia.ru

ABSTRACT
This paper presents the results of estimation of basic annual and mean annual water balance characteristics (precipitation, evapotranspiration, and runoff) in 182 river basins within European Russia and neighbour countries in the period 1950-1985. The aim of the paper is to assess spatial (first of all, latitudinal) variability in the change of water storage, and both of the runoff and the evapotranspiration coefficients, which characterize the water balance structure as a whole. It was found over an annual time scale that a change of water storage in high latitudes is strongly dependent on annual air temperature and, to a lesser extent, on precipitation. Conversely, the annual amount of precipitation is the main factor controlling the change of water storage in southern, relatively dry regions. It is shown that the change of water storage is more temperature-sensitive in northern river basins than in southern ones. Also, a semi-empirical curve and a simple formula are suggested to estimate typical zonal ("standard") values of the runoff coefficient as a function of the dryness index within the study area over a long-term scale.

KEYWORDS
River basin; European Russia; water balance structure; change in water storage; runoff coefficient; evapotraspiration coefficient.

1. INTRODUCTION

The water balance structure of river basins depends on both zonal and azonal factors. The main zonal factor is the geographic location (or – more specifically – the latitude) of a catchment. In general, the incoming solar radiation, surface albedo, mean annual temperature, potential evaporation, and evapotranspiration decrease with increasing latitude. Conversely, there is a noticeable downward latitudinal trend in mean annual river runoff characteristics from north to south. The effect of azonal features (topography, sea-level elevation, lake coverage, forest coverage of a catchment, etc.) results in essential deviation of major climate and water balance elements from their common tendencies in a given natural zone.

The problem of both zonality and azonality in the context of variability of the water balance structure has been discussed and studied in detail by Bulavko (1971), Kuzin (1973), Babkin and Vuglinsky (1982). Principal spatial patterns in heat and moistening regimes of the territory of Russia as a whole and the factors behind these patterns were described, in particular, by Budyko (1974), and Zhakov (1982).

It has been recently found for several river basins located in the northern taiga zone (Republic of Karelia and the Kola Peninsula, Russia) that annual changes in water storage within a basin depend both on the area-averaged annual air temperature and on the annual amount of precipitation (Salo, 2005). Therefore, in the relatively cold and humid northern regions, the air temperature is the main control of water accumulation within a catchment. It has be noted also that in these conditions, the correlation between the air temperature and the change in water storage has a negative sign, and absolute values of the correlation coefficient reach 0.7 or more.

Thence, one of the goals of the present study is to assess the latitudinal (i.e. zonal) differences in the degree to which air temperature and precipitation affect changes in water storage over an annual time scale within European Russia (ER). Traditionally, the water balance structure over a long-term scale is defined through both the runoff coefficient and the evapotranspiration coefficient, which characterize the relative shares of river runoff and evaporation from the drainage area in the water budget. It was therefore interesting to estimate the runoff coefficient as a function of the Budyko's dryness index within the studied territory, where the dryness index varies from 0.34 in the far north to 2.93 in the south of ER (Budyko, 1974).

2. DATA AND METHODS

Data from instrumental measurements and calculations of basic annual climate and water balance characteristics (air temperature, precipitation, evapotranspiration, and runoff) in 162 river basins evenly distributed over European Russia were used in this study. In addition, twenty basins located in the Baltic states, Belarus and Ukraine were also included in the analysis. All these 182 catchments are situated in various physiographic conditions (Figure 1).

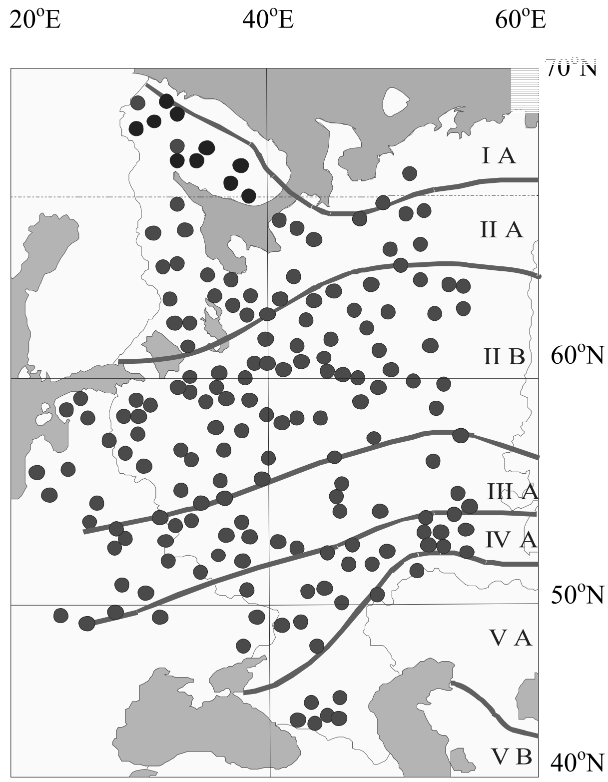

Figure 1. Map of the study area and locations of the investigated catchments.

According to Kaminski's climatic classification (Drozdov *et al.*, 1989), they are as follows: tundra (marked as I A in Figure 1), paludified taiga (II A), central forest zone (II B), forest-steppe zone (III A), chernozem belt (IV A), semi-desert (V A), and desert zone (V B). The studied rivers vary from 1,000 to 20,000 km^2 in drainage area, and from 17 to 533 mm in annual runoff. Mean annual air temperature in the catchments ranges from -2.9 to 11.1°C, and the precipitation norm – from 350 to 854 mm per year. For each of basin, data for the same 36-year period (1950-1986) were taken into consideration.

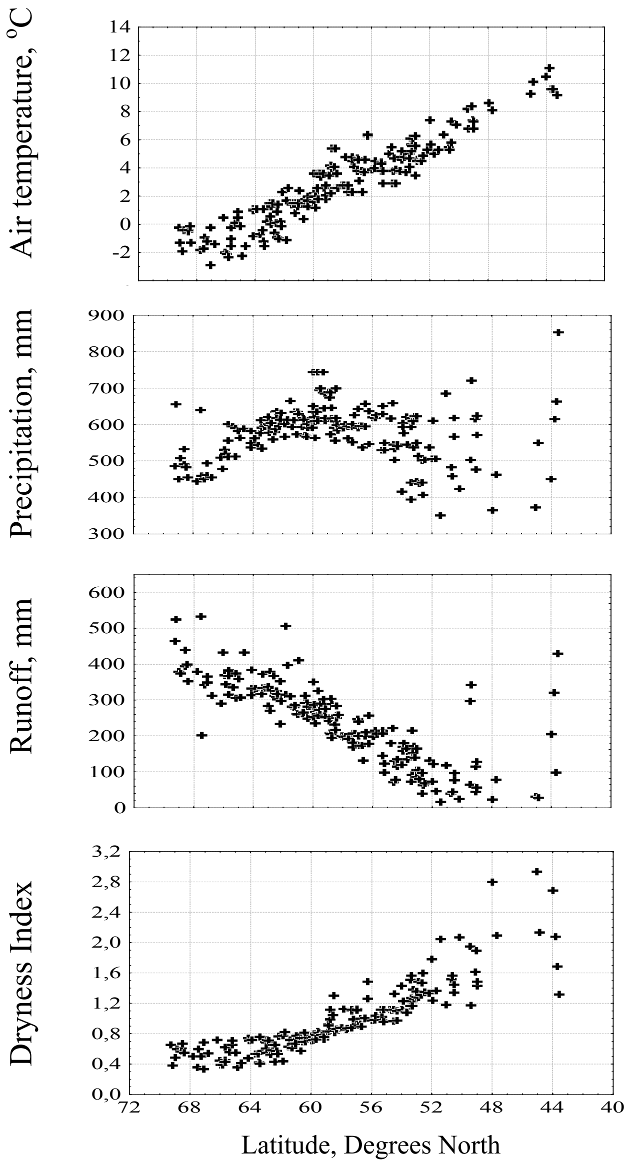

Figure 2. Average annual air temperature, precipitation, total runoff, and dryness index as a function of the latitude of the studied river basins.

As seen from Figure 2, there is a clear tendency in the change of basic climate and water balance elements from zone to zone of the study area, except for mountain and semi-mountain catchments (foothills of the Caucasus far in the south, below 45°N, and the Ural Mountains in the east of ER) due to the strong effect of elevation a.s.l. and to peculiarities in the formation of the hydrological regime in mountainous areas.

In this study, the water balance equation over an annual time scale is drawn as follows:

$$P - E - R \pm W \pm \varepsilon = 0, \tag{1}$$

where P is precipitation; E is evapotranspiration; R is total runoff (sum of surface and subsurface runoff); W is change in both surface and subsurface storage; and ε is the integral component including the balance

discrepancy, error of each water balance element measured or estimated, and error due to unknown elements not included in Equation (1). All values are in mm (10^{-3} m).
The formula after Ol'decop for estimation of evapotranspiration E is used as follows:

$$E=E_o tanh(P/E_o), \qquad (2)$$

where $tanh(P/E_o)$ is the hyperbolic tangent function of the ratio of precipitation to potential evaporation E_o. The latter value has been expressed as an empirical formula $E_o=E_o(T)$, as follows (Salo, 2007):

$$E_o=329 +62T+2.14T^2, \qquad (3)$$

where T is mean area-averaged annual air temperature in a given basin in a given year, ^oC.
The ratio of potential evaporation, E_o to precipitation, P commonly known as the aridity or dryness index (φ) after Budyko (1974). Regions with $\varphi>1$ are broadly classified as dry since the evaporative demand cannot be met by precipitation. Conversely, similarly regions with $\varphi<1$ are classified as wet. The index may also be related to climatic regimes in a broad sense, e.g. arid, semi-arid, sub-humid, and humid regions are defined by the aridity index ranges of $12>\varphi>5$; $12>\varphi>5$; $5>\varphi>2$; $1> \varphi>0.75$; and $\varphi <0.75$, respectively (Arora, 2002).
In our study, the Budyko's formula, $\varphi = E_o/P$, was used as the basic formula to estimate zone-to-zone changes in the water balance structure.

3. WATER BALANCE STRUCTURE FOR CATCHMENTS WITHIN ER

First, the correlation of the change in water storage, W with annual air temperature, T and precipitation, P was estimated for each of the 182 basins for the same period of 1950-1986. Herewith, it was assumed that value ε in Equation 1 is included in W and its contribution to the sum ($W+\varepsilon$) is negligible.
Figure 3 illustrates latitudinal regularity in the coefficient of correlation between W and T (Figure 3a) and between W and P (Figure 3b).
The coefficient of correlation between W and T is negative for all basins tested and r(W, T) reaches up to -0.8 for the catchments located in the tundra and paludified taiga zones. It can be concluded that in high latitudes, annual air temperature exerts a stronger influence on the accumulation/discharge of water in catchments, and accounts for up to 65 per cent of the variability in W, while in southern latitudes – for not more than 10 per cent.
There is no clear regularity in the common latitudinal tendency in the correlation between the change in water storage and annual precipitation (Figure 3b). We can only estimate that the correlation between W and P generally increases from north to south, and that precipitation influences changes in water storage more noticeably in the steppe and semi-desert zones in comparison with the tundra and forest regions.
The relationship between the coefficients of determination $r^2(W, T)$ and $r^2(W, P)$, and the dryness index $\varphi = E_o/P$ has also been studied. As one can see from Figure 3c, the leading climate characteristic influencing W in wet regions ($\varphi<1$) is air temperature. As the dryness index decreases, the influence of T upon W lessens nonlinearly, so that for semi-arid regions ($\varphi>2$) the effect becomes insignificant. Taking a common tendency for an increase in $r^2(W, P)$ with increasing index φ (Figure 3d) into consideration, we can conclude that the effect of precipitation on the change of water storage in wet regions is at least not so strong as in semi-arid and arid regions.
Secondly, water balance structure was studied in relation to the dryness index. Over a mean annual time scale, the water balance equation can be written in a non-dimensional form as follows:

$$K_R + K_E = 1, \qquad (4)$$

where K_R is the runoff coefficient, K_E is the coefficient of evapotranspiration. All values in Equation 4 are calculated as annual means.

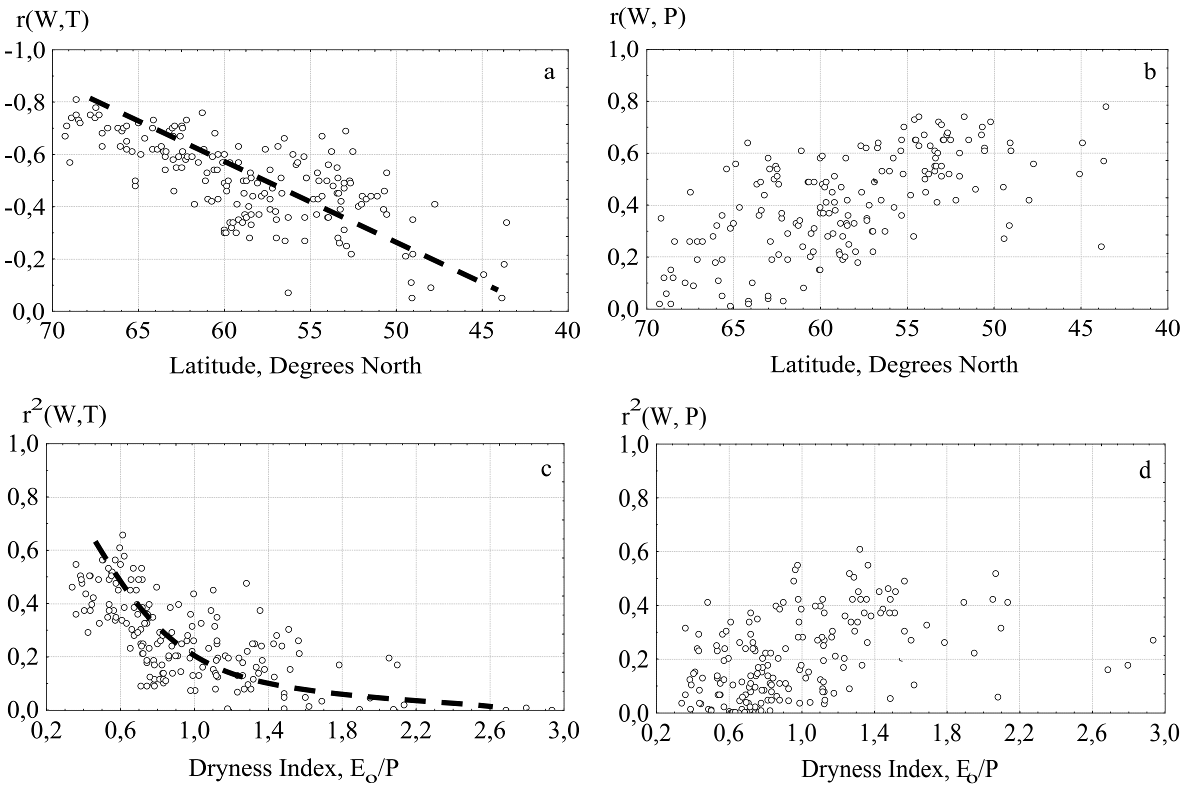

Figure 3. Coefficients of correlation (r) and determination (r^2) of water storage W with annual air temperature and precipitation as functions of the latitude and the dryness index.
and total runoff as a function of latitude of studied river basins.

Two variants of K_R and K_E calculations were carried out. In the first case, initial precipitation, P (corrected only by wetting and evaporation losses) was used to calculate these coefficients as K_R=R/P and K_E = E/P, respectively. In the second case, precipitation was corrected for each of the 182 river basins using the water balance approach and calculation scheme proposed by Salo (2005, 2006). The advantage of this method is that it enables finding mutual conformity between corrected precipitation P_c, runoff R, and evapotranspiration E_c calculated using P_c, in accordance with the trinomial water balance equation:

$$P_c - R - E_c = 1, \tag{5}$$

$$K_R^* = R/P_c, \quad K_E^* = E_c/P_c,$$

$$K_R^* + K_E^* = 1. \tag{6}$$

Thus, in the second case, the coefficients K_R^* and K_E^*, too, were considered in this study.
Figure 4 demonstrates a non-linear decrease of runoff coefficients in relation to reduction of the dryness index in these two cases. One can see from the left-hand graph that for a dryness index of $\varphi<0.8$, there is a noticable rise in K_R values. On the contrary, where corrected precipitation values have been taken into account, there is full functional correspondence between the runoff coefficient and the dryness index. It is important that the curve in Figure 4b agrees well with a theoretical limit $K_R \rightarrow 1$ under $E_o/P \rightarrow 0$.

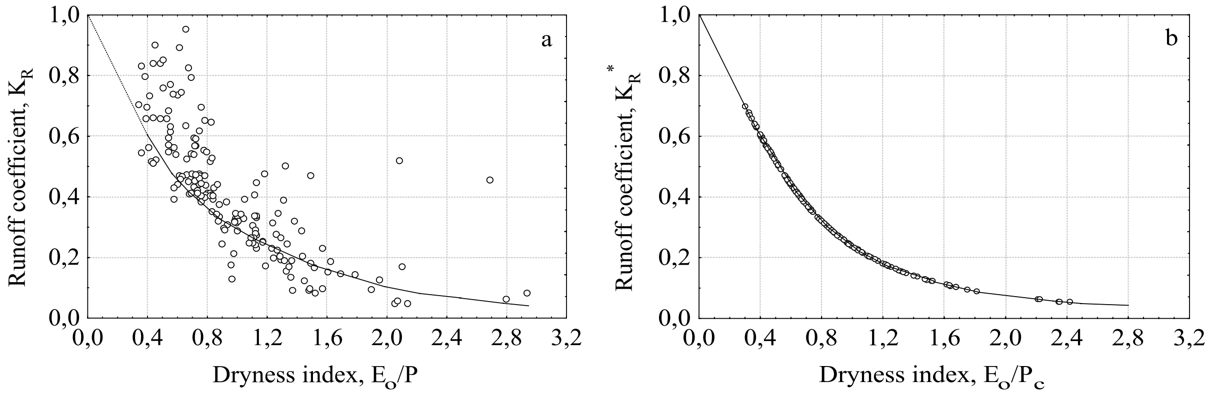

Figure 4. Graphs of the dependence of runoff coefficients $K_R = K_R(E_o/P)$ and $K_R^* = K_R^*(E_o/P_c)$.

Thus, the curve plotted in Figure 4b can be considered to be semi-empirical, suitable for estimating typical (or "standard") values of the runoff coefficient as a function of the dryness index in ER. In the analitical form, the dependence can be presented as follows:

$$K_R = \exp(-1.4 \cdot \varphi), \qquad (7)$$

where $\varphi = E_o/P_c$ is the Budyko's dryness index calculated using corrected precipitation P_c.

By analogy with Figure 4b and taking Equation 6 into account, the semi-empirical curve $K_E^* = K_E^*(E_o/P_c)$ can also be plotted easily.

We can assume that any (whether positive or negative) deviation of actual runoff coefficients from"standard" ones would be due to the effect of local (i.e. azonal) factors, in particular, to the percent cover of lakes and mires in a catchment. This assumption, in turn, requires an additional study.

4. CONCLUSIONS

A key finding of this study is that the difference in the degree of effect of annual air temperature and precipitation on water storage has been detected and estimated. In high latitudes, air temperature is the leading climate parameter controlling accumulation/discharge of water in catchments, whereas annual precipitation plays the second part. Conversely, in the relatively dry arid and semi-arid regions, precipitation affects annual changes in water storage more than air temperature.

Consequently, water storage is more temperature-sensitive in northern river basins than in southern ones. In general, this conclusion agrees well with estimations of catchment's sensitivity to present-day climatic conditions as well as to possible climate change (Vinnikov, 1986; Kovalenko, 1993; Bobylev *et al.*, 2003).

Also, a semi-empirical curve and a simple formula of the relationship between the runoff coefficient and the Budyko's dryness index have been obtained. They provide a possibility to estimate typical zonal values of the runoff coefficient as a function of the dryness index within the study area over a long-term scale.

The results reported above relate to European Russia, which is characterized, in general, as a relatively flat territory. Applicability of the results to mountain and semi-mountain regions is uncertain and requires that the characteristics typical of these regions (sea-level elevation, stream gradient, mean watershed slope, etc.) are included into consideration. Probably, other formulae would be more suitable for calculating potential evaporation and evapotranspiration in mountainous catchments.

REFERENCES

Arora, V.K. (2002) The use of the aridity index to assess climate change effect on annual runoff. *J. Hydrol*. **265** (2002), 164-177.

Babkin, V.I., Vuglinsky, V.S. (1982). *Water balance of river basins.* Hydrometeoizdat, Leningrad (in Russian).

Bobylev, L.P., Kondratyev, K.Ya., Johanessen, O.M. (2003) *Arctic Environment Variability in the Context of Global Change.* Springer. Praxis Publ. Chichester, UK.

Budyko, M.I. (1974). *Climate and Life*. Academic Press, Orlando, FL.

Bulavko, A.G. (1971).*Water balance of river basins*. Hydrometeoizdat, Leningrad (in Russian).

Drozdov, O.A., Vasiliev, V.A., Kobysheva, N.V., Raevsky, A.N., Smekalova, L.K., Shkolny, E.P. (1989) *Climatology*. Hydrometeoizdat, Leningrad (in Russian).

Kovalenko, V. V. (1993) *Modelling of Hydrological Processes.* Hydrometeoizdat, Leningrad (in Russian).

Kuzin, P.S. (1973). The water balance method and its practical applications. *Meteorol. and Hydrol.*, **4**, 99-106 (in Russian).

Salo, Yu. (2005) Effects of climate change variability on natural water bodies in Northwest Russia. Proc. *15th Northern Research Basins Symposium*, Luleå to Kvikkjokk, Sweden, Aug 29 - Sep 2. pp. 31-40.

Salo, Yu. (2006) Method for correction of annual precipitation records using the water balance approach. *Nord. Hydrol.* **37** (4-5), 433-440.

Vinnikov, K.Ya. (1986) Sensitivity of the Climate. Hydrometeoizdat, Leningrad (in Russian).

Zhakov, S.I. (1982) *General Laws of Energy and Moistening Regimes over the USSR Area*. Hydrometeoizdat, Leningrad (in Russian).

Climate effect on the hydrological regime of the kola peninsula rivers

A. V. Semenov[1*], V. N. Ozhigina[1]

[1]*Murmansk Hydrometeorology and Environmental Monitoring Administration*
Murmansk, Russia
**Corresponding author: leader@kolgimet.murman.ru*

ABSTRACT
Results of statistical estimations of the basic climate and hydrological characteristics for typical river basins (Kola, Ponoi, Umba, Lotta) and weather stations (Murmansk, Kanevka, Umba,) within the territory of the Kola Peninsula, Russia, are presented. For these stations during the period 1961-2006 the rate of change of mean annual air temperature is 0.2-0.4˚C in 10 years. The change of mean temperature varies among seasons, being most explicit in winter and spring. Warming intensity is the highest in winter and the lowest in summer. The second position in the intensity of warming belongs to spring. Positive trends are detected also in the annual precipitation, annual runoff and the flood peak dates time series for the same period.

KEYWORDS
Kola Peninsula, air temperature, runoff, peak date, linear trend.

1. INTRODUCTION
Climate of the Kola Peninsula is exposed to the attenuating influence of surrounding seas, especially of the heat carried from Northern Atlantic by warm currents. As a result, the southwestern part of the Barents Sea remains free of ice even in coldest winters, and air temperatures on the coast in January and February are close to those in areas situated 10° further south (Figure 1). The thermal regime on the southern coast of the peninsula is somewhat harsher, since the White Sea freezes over in winter. As one moves inland, the influence of the seas diminishes rapidly (Yelshin, Kouprijanov, 1970).
The aim of the present study is to determine the effect of climate change in the Kola Peninsula on the hydrological regime of its rivers in the period from 1961 to 2006. The paper considers the relationship between shifts in the dates of flood onset and peaks, and changes in mean spring (April-May) air temperature. Also, correlation between change in annual streamflow and changes in total annual precipitation in the same period was analysed.

2. RESULTS
The spring season is defined according to the classification of seasons worked out by Yakovlev (1961) for the Kola Peninsula. In this classification, winter is from November through March, spring – April and May, summer – June through August, autumn – September and October (Yakovlev, 1961).
Correlations of the dates of flood onset and peak with changes in mean air temperature of the spring season were studied for the rivers belonging to different drainage basins: River Kola – Barents Sea basin, Rivers Ponoi and Umba – White Sea basin, and River Lotta, which flows through western parts of the Kola Peninsula and belongs to the Verkhne-Tulomskoye impoundment reservoir drainage basin. Analysis of temporal variability of mean seasonal air temperatures and total annual precipitation was based on data from weather stations of the Murmansk Hydrometeorology and Environmental Monitoring Administration situated in watersheds of the rivers, i.e. the weather stations Murmansk, Kanevka, Umba and Upstream Lotta, respectively.
Linear trend coefficients were computed for the 1961-2006 period to estimate current tendencies in the change of mean annual air temperature. The computation results are shown in table 1.

Table 1. Linear trend values for mean annual and mean seasonal air temperatures (˚C in 10 yrs.) in the period from 1961 to 2006

Station	Linear trend, ˚C in 10 yrs.				
	Mean annual	Winter	Spring	Summer	Autumn
Murmansk	0.3	0.4	0.3	0.2	0.1
Umba	0.3	0.4	0.3	0.2	0.2
Kanevka	0.2	0.2	0.4	0.1	0.1
Upstream Lotta	0.4	0.5	0.3	0.2	0.2

The rate of change of mean annual air temperature is 0.2-0.4˚C in 10 years. The change of mean temperature varies among seasons, being most explicit in winter and spring. Warming intensity is the highest in winter (linear trend coefficient is 0.2-0.5˚C in 10 years) and the lowest in summer (linear trend coefficient is 0.1-0.2˚C in 10 years). The second position in the intensity of warming belongs to spring (linear trend coefficient is 0.3-0.4˚C in 10 years).
Let us consider the effect of change in mean spring air temperature on the dates of flood onset and peak in the rivers selected. We regard the date of maximum water discharge during the flood as the flood peak.

2.1. River Kola, Murmansk Weather Station

The River Kola acts as the predictor in hydrological forecasts for rivers of the Kola Peninsula. The linear air temperature trend over the spring season at the Murmansk weather station is +0.3° in 10 years.
Figure 1 shows the diagram of flood onset and peak dates plotted for the Kola River for years 1961-2006. One can see a tendency towards earlier onset and peak of the flood: a shift of 1.5 days in 10 years for the onset dates, and 3.2 days in 10 years – for the peak dates. The trend contribution (R^2) to total variation of the flood onset dates is 4.3%, of the flood peak dates – 15.9%.

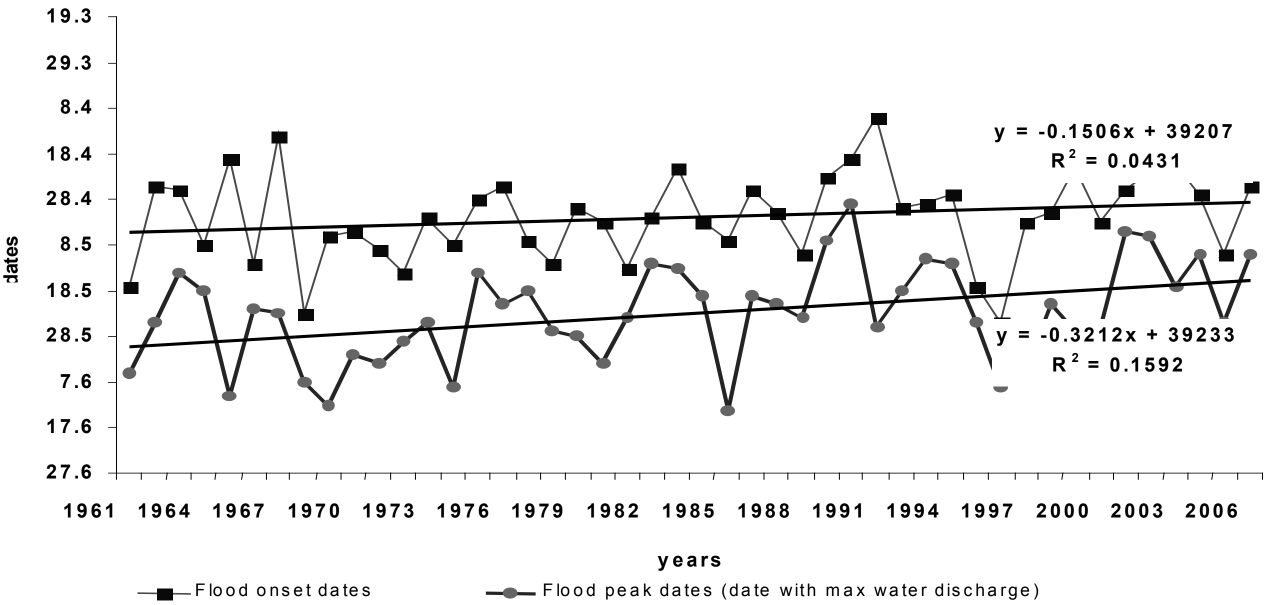

Figure 1. Flood onset and peak dates, River Kola, 1961-2006.

2.2. River Ponoi, Kanevka Weather Station

The River Ponoi is the longest river in the Kola Peninsula (426 km). The river watershed area is 10 200 km^2 (Yelshin & Kouprijanov 1970).

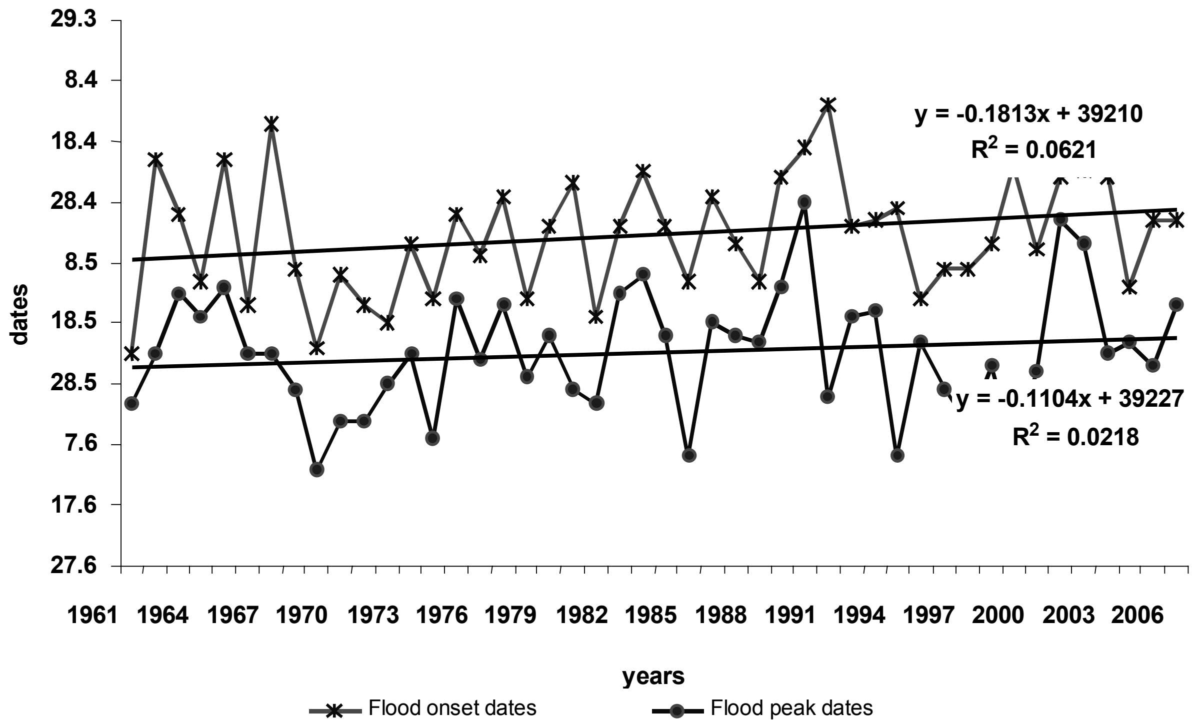

Figure 2. Flood onset and peak dates, River Ponoi – Kanevka station, 1961-2006.

The linear air temperature trend over the spring season at the Kanevka weather station (fig. 2) is +0.4° in 10 years. The shift towards earlier onset of flood is 1.8 days in 10 years, the trend contribution (R^2) to total variation of the flood onset dates is 6.2%. The shift towards earlier flood peak dates is less significant – 1.1 days in 10 years (R^2 = 2.2%).

Similar diagrams were plotted for Rivers Lotta (site – Kallokoski rapid) and Umba (site – Payalka rapid). Results of the calculations are summarized in table 2.

Table 2. Coefficients of the linear trend of air temperature, flood onset and peak dates

River-site, (weather station)	1961-2006 linear trend coefficients for			Reliability of approximation - R^2 (contribution of the trend to total variation, %) for	
	spring air temperature, (ºC in 10 yrs.)	flood onset dates $D_{f.o.}$ (days in 10 yrs.)	flood peak dates $D_{f.p.}$ (days in 10 yrs.)	flood onset dates	flood peak dates
Kola – 1429th km of the Oktyabrskaya railway (Murmansk)	+0.3	-1.5	-3.2	4.3	15.9
Ponoi – vil. Kanevka (Kanevka)	+0.4	-1.8	-1.1	6.2	2.2
Lotta – Kallokoski rapid (Upstream Lotta)	+0.3	-1.7	-2.4	5.9	10.0
Umba – Payalka rapid (Umba)	+0.3	-1.8	-2.2	7.3	12.2

Note: $D_{f.o.}$ – *flood onset dates;*
$D_{f.p.}$ – *flood peak dates (dates of max water discharge).*

Judging by the results of estimating the linear trend of flood onset and peak dates summarized in table 2, the increase in mean spring air temperature by + 0.3 - +0.4º C in 10 years from 1961 to 2006 has told on the timing of flood onset and peak, shifting them towards earlier dates. In the past 46 years, the onset of flood on the rivers has been shifting to earlier dates by an average of 1.5-1.8 days in 10 years, the peak of flood – by 1.1-3.2 days in 10 years. The rate of shift to earlier flood peak dates differs among rivers, the greatest rate observed on River Kola (3.2 days in 10 yrs.), the lowest rate – on River Ponoi (1.1 days in 10 yrs.).

Table 3. Values of the linear trend of total annual precipitation (mm in 10 yrs.) and annual streamflow (km^3 in 10 yrs.) over the 1961-2006 period.

River-post, weather station (WS)	Coefficient of the linear trend of total annual precipitation (mm in 10 yrs.)	Coefficient of the linear trend of annual streamflow (km^3 in 10 yrs.)	Reliability of approximation - R^2 (contribution of the trend to total variation, %)
Kola -1429th km of the Oktyabrskaya railway (Murmansk)	4	0.05	5.7
Ponoi – vil. Kanevka (Kanevka)	-1	0.10	7.8
Lotta – Kallokoski rapid (Upstream Lotta)	3	0.00	0.4
Umba – Payalka rapid (Umba)	5	0.01	0.2

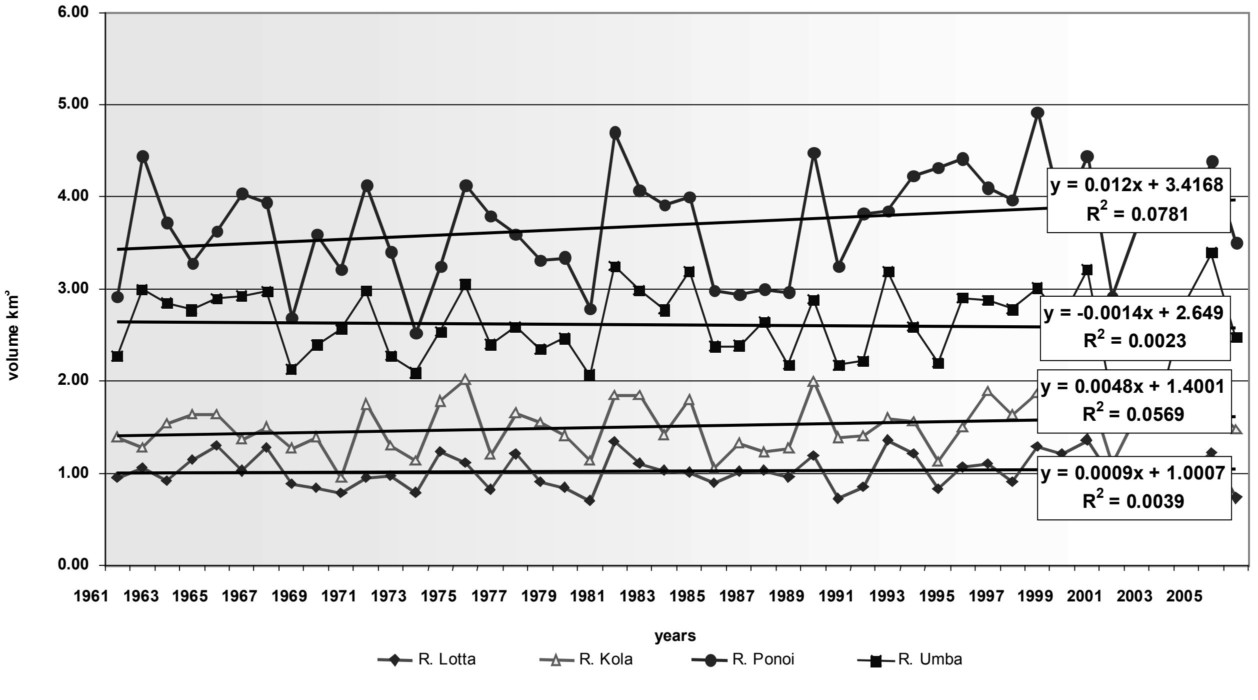

Figure 3. Annual runoff of rivers within the Kola Peninsula

Let us consider the effect of total annual precipitation on annual streamflow.
As seen from table 3, the highest coefficient of the linear trend of total annual precipitation is 5 mm in 10 years (Umba WS), the lowest one is -1 mm in 10 years (Kanevka WS). The linear trend of total annual precipitation is insignificant, and so is the linear trend of annual streamflow, which values vary from 0.0 (River Lotta) to 0.10 (River Ponoi) km^3 in 10 years (Fig. 3). One can conclude from the data in table 3 that precipitation amounts and river water content have changed little over the past 46 years.

REFERENCES

Davydov, A.A. 2001. Changes in the Kola Peninsula air temperature and Barents Sea ice status in the second half of the 20th century. Secular changes in marine ecosystems of the Arctic. Climate, marine Periglacial, bioproductivity. Kola Research Centre of RAS Publishers. Apatity. p. 291-297. [in Russian]

Davydov, A.A., Semyonov, A.V. 2005. Change of the air temperature in the Kola Peninsula and Spitzbergen Archipelago, in the ice status of the Barents Sea in the second half of the 20th century. Proceedings of the International Scientific-Industrial Forum "Great Rivers". Gidrometeoizdat. St. Petersburg. p. 299-300. [in Russian]

Yelshin, Yu.A., Kouprijanov, V.V. 1970. Surface water resources of the USSR, Vol. I. Kola Peninsula. Gidrometeoizdat, Leningrad. p. 26, 44. [in Russian]

Yakovlev, B.A. 1961. Climate of the Murmansk Region. Murmansk Book Publishers. p. 24-27. [in Russian]

Arctic sea ice transformations: present situation and future scenarios

Elena V. Shalina, Leonid P. Bobylev, Svetlana I. Kuzmina

Scientific Foundation "Nansen International Environmental and Remote Sensing Centre" , S.Petersburg
elena.shalina@niersc.spb.ru

ABSTRACT

The sea ice cover, which presently is perennial in the Arctic Ocean and at least seasonal in its marginal seas, is an important component of the global climate system. A consensus in the climate modelling community is that global warming should be amplified in the Arctic due to feedback processes within the atmosphere–ocean–ice climate system. The amplified warming suggests a drastic reduction of the sea ice cover. First changes will be mostly pronounced in the marginal seas of the Eurasian sector. That should increase offshore activities and marine transportation over the Northern Sea Route, inducing on the other side such changes in the navigation conditions as increased storminess and unpredicted moving of ice floes and making offshore activities more dangerous.

The most consistent, quantitative means to monitor the Arctic sea ice cover is from satellite-borne passive microwave sensors. In the presented study merged "inter-calibrated" SMMR-SSM/I time series have been produced and analysed, establishing the trend of the Arctic sea ice cover of about 3% per decade. The reductions have been mostly pronounced in the European sector in winter and the Siberian-Alaskan sector in the summer, with the record of low arctic ice minima in 2002 - 2005. The pronounced summer reductions imply changes in the character of the ice cover – i.e., reduced amount of perennial, multi-year (MY) ice. The negative trend in MY ice area analysis is often cited as evidence of a substantial change in the ice cover. However, capabilities and limitations of passive microwave algorithms to estimate of the relative coverage of FY and MY ice have not been quantitatively established. The uncertainties are greatest in the marginal seas. In this study the QuikSCAT scatterometer data was used as a complimentary source of information that assisted in separating first year and multi year ice, improving algorithm of multi year ice retrieval and describing multi year ice movement in the periods when passive microwave retrievals cannot provide a stable picture. NORSEX calculations and QuikSCAT-based retrievals were validated using available SAR images, ice charts and in situ ice type observations.

A set of model predictions is used to quantify changes in the ice cover through the twenty-first century, with greater reductions expected in summer than winter. In summer, a predominantly sea-ice-free Arctic is predicted for the end of this century.

Keywords: Arctic environment, sea ice, perennial ice, sea ice reduction, passive microwave satellite data, scatterometer data

Processing of Radar Precipitation Data as Applied to Watershed Hydrology

Vladimir A. Shutov

Valday Branch of the State Hydrological Institute, Russia.
e-mail: hydrosphere@mail.ru

ABSTRACT
Problems of calibration of weather radar are addressed. Methods have been developed aimed at how to process the radar-based precipitation data for hydrology applications. Aggregated data (10x10 km) are suggested to be reasonably sufficient for that aim. Basic properties of precipitation fields are examined: (1) spatial coverages and areal reduction factor, (2) conditional frequency distribution function of "at-cell" rain rates by specified spatially averaged rates and, (3) spatial structural function (variogram). Examples of data processing and analysis are given to expound upon the ideas of how to describe precipitation patterns. For flood forecasting, a procedure is proffered to reveal those rain rates exceeding threshold which is correlated with antecedent soil moisture content on a small (2000 km^2) river basin.

KEYWORDS
Radar precipitation estimates; radar calibration; data processing; precipitation statistics;

1. INTRODUCTION
Radar precipitation measurements at Valday, Russia have a long history. They were carried out since 1980s targeted to update the runoff models that time (Becker et al., 1988, Rumjantsev *et al*., 1985) and to develop the methods for flood forecasting. Problems of measurement accuracy were given attention, for that a special dense rain gauge network has been developed in western part of the radar surveillance within drainage basin of the Polomet' river. Presently a new generation radar is being installed.
Engineering hydrology mainly consists of probabilistic computations of flood runoff. Its methods should be improved if the radar-based areal precipitation data would be obtained that is important just for Russia because of low density of observational network. Special problems appear when evaluating the environmental impact of a large linear construction such as main roads and pipelines on flow generation. A convenient way of how to apply both spatial patterns and time series of precipitation to operational hydrology is only being developed (Shutov, 2002, 2004).

2. ON THE METHOD OF CALIBRATING THE RADAR DATA
Calibration of the radar in Valday was conducted with special network within the Polomet' river watershed (Becker et al., 1988). The network consisted of multiple (up to 37) pluviographs arranged in nested groups of gauges to determine both areal precipitation and its auto-correlation function. Hourly (3-hourly) rain rates obtained by pluviographs were interpolated onto grid cells 1 x 1 km each with averaging over 3 x 3 km and 10 x 10 spatial units. As was found, the ratios of G/R vary from 0,5 to 3,8 for 3-hourly rates and be less ranged (0,6 to 2,2) for daily amounts (left Figure 1). Thoroughly implemented calibrations (Michelson *et al*., 2000) result in more scattered values: for instance, G/R = 1 at 100 km off the radar site varying from 0.5 to 2.5 if to limit by standard deviation (±σ), and from 0.2 to 5.0 by ±2σ.

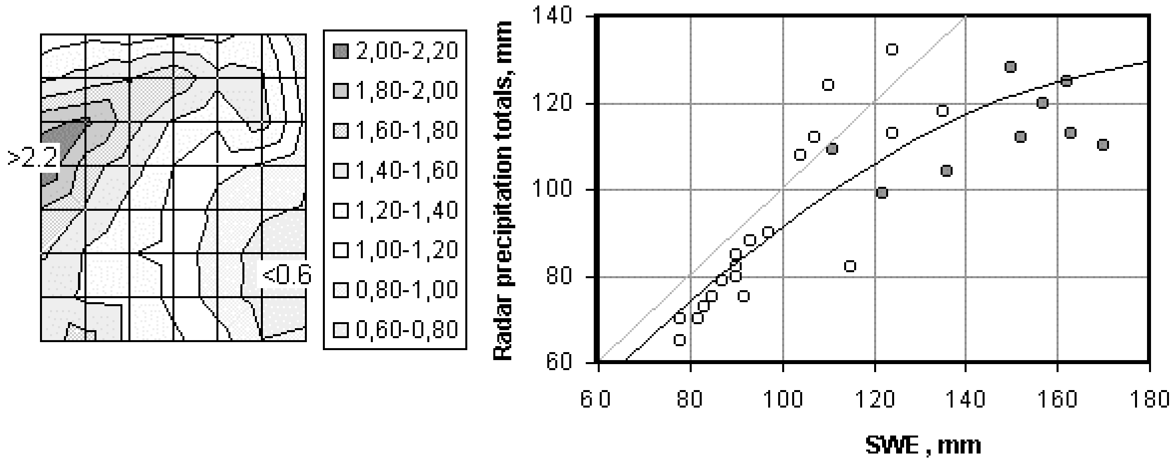

Figure 1. Calibration of the radar located at Valday against land-based observational data sources. Left: A pattern of the *G*/*R* ratios for summer rainfalls (only western part of the radar surveillance); Right: Radar precipitation totals calibrated against snow water equivalent (SWE) by snow surveys for the entire area and for the *Upper Polomet'* river basin (darkened points).

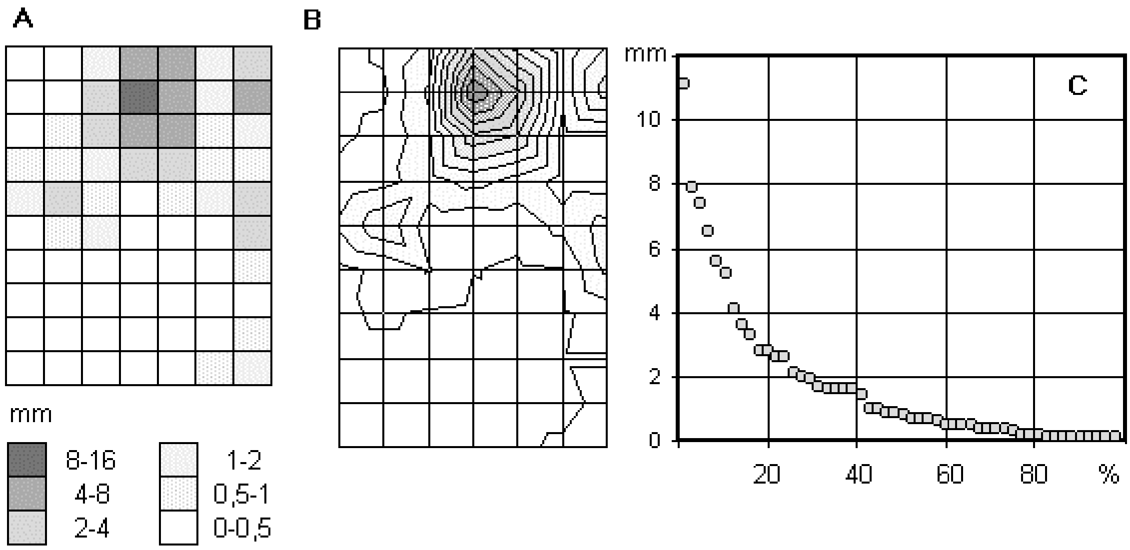

Figure 2. An example of the special radar data processing for a late August day in Valday,
A) Fragment of the traditional radar image: precipitation quantized by dBZ levels (in mm);
B) Contour map depicted a pattern of daily rainfall rates normalized by sigma $(R - R_{av})/\sigma$;
C) Frequency distribution (spatial statistics) of "at-cell" precipitation rates (mm/day).

Of a particular importance is that G/R values are not randomly distributed (Figure 1). Analyzing upon such maps, one can infer about specific inaccuracies which are correlated with local terrain features and, more slightly, depending on what atmospheric processes are going on. Much frequently cases for the area are heavy rainfalls increasing just in front of the wind-exposed slope of the Valday Hills. Here, the rainfall rates can be underestimated (G/R > 1). Another was observed during winter, when underestimated were those snow amounts fallen onto the hills. There are considerable biases (darkened points in Figure 1) between the snow water equivalents (SWE) and the radar precipitation total estimates.

3. SPECIAL DATA PROCESSING

For engineering hydrology applications, we propose (Shutov, 1999, 2000) some additional sub-routines based on matrix algebra (the primary data are acquired as matrices), in particular:

- Accumulation over several time intervals. So, daily totals can be acquired by summing up hourly rain rates, as well as total of daily rates over an examined flood, etc.
- Association, which is to select the maximum rain rate from each couple of cells of associated matrices A and B that is: A U B = max {RA, RB}. This procedure allows to reveal those heavy rains which are able to create extreme floods, a focus of interest for hydrology applications.
- Normalizing the matrix elements by a specified value such as standard deviation σ or a rate of several frequency (quantile) to make the patterns comparable (mid Figure 2).
- Quantization of rainfall rates to reject an appointed threshold value, except for those used by pre-processing from each “at-cell” value. This allows to map those areas where rain rates exceed the threshold which may either be arbitrary or be correlated with antecedent wetness of the basin. The latter approach is to reveal the area of effective (produced runoff) rainfalls.
- Ranging the rates to develop a frequency distribution (right Figure 2). This is the most convenient and widely used in engineering hydrology.

4. PRELIMINARY RESULTS

4.1. Empirical variograms

Areal distribution of rainfall rates is mapped using an interpolation procedure which implies the structural function (variogram) obtained previously. Empirically it is determined as follows:

$$V(L) = [R(x + L) - R(x)]^2 \qquad (1)$$

Where x is horizontal co-ordinate, L is the space between neighboring cells, R are precipitation estimates. The empirical variograms were approximated with the following:

$$V(L) = K \, Ln\,(L) + M \qquad (2)$$

Parameters of were found varied depending on precipitation genetic type and, that is of an essential importance, on the direction (by latitude or by longitude) at which the V(L)-functions are evaluated.

4.2. Statistics of at-cell and spatially averaged values

We have found a simple way to reflect precipitation stochastically which is synthesis of the joint probability density function (PDF) of at-cell Rj and areally averaged Rav rainfall rates. The distribution summarizes multiple individual PDFs obtained using the 5-th procedure (of those mentioned above). It seems that the PDF-values of such a distribution may be proffered as a parameter in computation of rain-induced floods. Such data processing procedure has resulted in statistical estimates (partial PDFs) of rainfall rates at several grid cells by specified areal averages over entire study area.

Slow rainfalls dominate throughout most of the area (sized 80x100 km) by $R_{av} \leq 7$ mm/day, but the secondary peaks appear if there are more heavy rainfalls. They are corresponding with the areas of higher intensity within rainfall fields, which are often called embedded cells.

The frequency diagrams drawn for both areal and at-site values allow to consider precipitation as a space-time stochastic process. The data were used as “at-site”of long-term gauge observations at multiple sites located within the Polomet’ river basin. Frequency curves have been found similar for space and time that is an evidence of ergodicity of rainfall patterns.

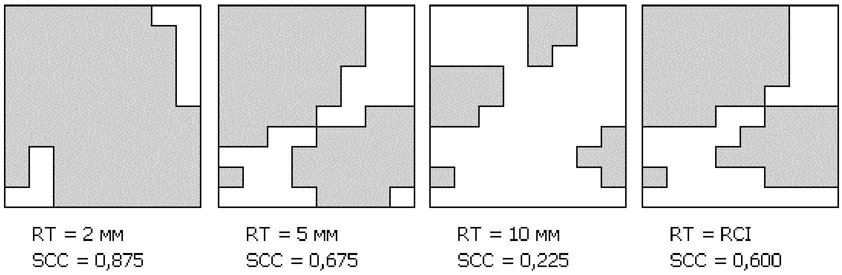

Figure 3. Sketch of radar images showing the spatial reduction of precipitation, decreasing (left to right) the spatial coverage coefficient (SCC).
The threshold values (RT) are conventional or dependent on the runoff intensity (RCI)

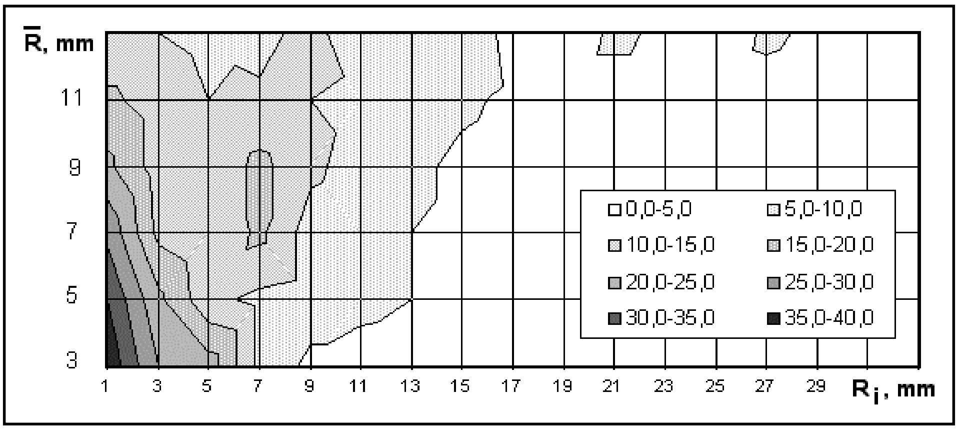

Figure 4. Conditional probability (p,%) of precipitation rates (mm/day) within several cells (Rj) by fixed spatial averages (R) for the Valday radar precipitation polygon.
Note: the diagram as well as the data we obtained at this time are preliminary and have been shown here only for illustration of the method mentioned above.

5. DISCUSSION AND A FUTURE OUTLOOK

Considering that has been mentioned on adjustment technique, for hydrological applications it is rather to use a coarse grid, whereas the finest resolution cannot be practicable (without dense rain gauge network) as resulted in undeterminable errors in both radar and gauge precipitation estimates. Recollect, the spatial units of the order of 100 km^2 quite correspond with the lower limit of the scale which are of a particular interest. Small drainage basins are, indeed, not so runoff productive to draw a great attention for flood warning. Besides, the better timing we took was one day to eliminate errors and catch a real response in runoff. Also, we should examine only that fraction of the radar surveillance for which rain gauge data are available, thereby the radar data may be presumed as sufficiently accurate.

As to spatial coverage, there appears a successive way, which is to determine spatial extent for only rainfalls exceeding a specified intensity. Quite a problem remains: how to predict this threshold depending on wetness if there are no soil moisture data available. We may operate with the water cycle components either observed or calculated. Another way is to replace the actual soil moisture data with an index, for instance, the Antecedent Precipitation Index (Seuna, 1983) defined by past rainfall events.

As was found, convective rainfalls are characterized with asymmetrical variograms, their parameters are different for rectangular directions. This fact can result from an influence of the Valday Hills oriented longitudinally. Diapason (de-correlation distance) is found equal approximately to 50-60 km for both convective and frontal rains that corresponds to the distance for snowfalls. Power function (Equation 2) testifies the self-similarity over various spatial scales that allow for the fractal models.

Existent methods to calculate runoff enable to assess that fraction of the basin area, where the runoff depths can be higher than a specified value. On the other hand, one can evaluate what runoff depth can be expected after rainfall from a selected area. With the use of detailed soil map, one would determine where these areas subjected to flood are located. Further reforms would be with an evaluation of spatially distributed runoff coefficient to replace. It will be realized based upon soil moisture and those basic soil physical properties which are responsible to infiltration.

REFERENCES

Becker, A., N.I. Kapotova, S.A Kondratjev and N.A. Livanova. (1988) A rainfall-runoff simulation model for operational use in radar-based system for flood forecasting. – *Transactions of the State Hydrol. Inst.,* 331 issue, pp. 3-16 (in Russian).

Michelson D.B., T. Andersson, J. Koistinen, C.G. Collier, J. Riedl, J. Szturc, U, Gjertsen, A. Nielsen and S. Overgaard. (2000). *BALTEX Radar Data Products and their Methodologies. – SMHI, Repts Meteorol. and Hydrol*., No. 90. Stockholm, Sweden. 80 pp.

Seuna, P. (1983) Infiltration and its dependence on some physiographic factors. – *Publ. of the Water Research Inst*., Helsinki, No. 50, pp. 29-40.

Shutov, V.A. (1999) Use of radar precipitation data for runoff computations. – In: A. Herrmann (Eds.) Experimental *Hydrology with Reference to Processes in Small Research Basins. Proc. of the Int'l Workshop*, St. Petersburg, Russia, pp. 158-167.

Shutov, V.A. (2000) Processing the radar precipitation data for engineering hydrology – In: D.L. Kane (Ed.) *Water Resources in Extreme Environment*. *Proc. of the AWRA Spring Specialty Conf., Anchorage*, Alaska, USA, 1-3 May 2000, pp. 315-321.

Shutov, V.A. (2002) Conceptual basis of using the radar and hydro-physical data in operational and engineering hydrology. – *Meteorol. and hydrol*., No. 7, pp. 57-70 (in Russian).

Shutov, V.A. (2004) Adaptation of the radar data on atmospheric precipitation to applied hydrology. – *Water resources*, Vol. 31, No. 3, pp. 273-282 (in Russian).

Scale influences on the representation of crucial stores in a heterogeneous northern basin

Christopher Spence[1*] Jason Hosler[1],

[1] *Environment Canada, 11 Innovation Blvd., Saskatoon, Saskatchewan, S7N 3H5, CANADA*
**Corresponding author, e-mail: chris.spence@ec.gc.ca*

ABSTRACT
Hydrological connectivity controls runoff response in those northern landscapes that can be characterized as patchy or heterogeneous. This is problematic for catchment modeling because how to efficiently represent connectivity over space and time in a patchy landscape is not necessarily obvious. The pattern of hydrological elements over which a drainage network passes is considered in an attempt to understand how the landscape heterogeneity should be sampled in order to best represent it for the purposes of runoff modeling. The present study addresses how drainage density and sampling frequency influence the nature of the probability density function of hydrological elements along a drainage network in a typical heterogeneous subarctic Canadian Shield catchment. Upon generating fifty five sequences, the results imply that these two factors do influence sequence representation, and that the typical or representative sequence is one dominated by lakes. The gross variation in this sequence can be characterized into three phases. These phases were a function of the rate of change in drainage density with defined minimum contributing area. Since drainage density can be representative of the moisture state of a catchment, the results imply that parameterization of patchy landscapes for hydrological modelling needs to be dynamic and may need to be a function of the moisture state of the catchment.

KEYWORDS
Storage, Canadian Shield, Modelling, Hydrological elements, Streamflow

1. INTRODUCTION

Recent field studies (Carey and Woo, 2001; Hutchinson and Moore, 2000; Spence and Woo, 2003; Tromp van Meerveld and McDonnell, 2006) have highlighted the importance of basin heterogeneity, geometry, topology and dynamic hydrological connectivity in hillslope and catchment runoff generation. After studying hydrological and energy budget processes in the northern Canadian Shield physiographic region where connectivity has a profound influence on the runoff signal, Spence and Woo (2006) proposed an element threshold concept of runoff generation that perceives heterogeneous catchments as comprised of "hydrological elements". Hydrological elements are areas within a catchment that function hydrologically in a homogenous manner over time at a given scale of interest. Spence and Woo note the importance of the elemental geometry and topology of elements for runoff generation, which may need to be represented in model structures in order to correctly simulate when they contribute to downstream runoff.

The hydrologic response of a watershed to an impulse can be interpreted as a function of the probability density function, *pdf*, of travel times to the outlet along the drainage network. These *pdf's* have been equated to Strahler (1952) stream order (Wang et al., 1981), basin width function (Mesa and Mifflin, 1986), basin magnitude (Boyd, 1978) and basin area function (Robinson et al., 1995). Using a *pdf* of topographic index, Beven (1986) is one of the few works directly relating the landscape to the runoff response. The present study considers the pattern of hydrological elements (Spence and Woo, 2006) over which the drainage network passes in an attempt to understand how the landscape patchiness should be sampled in order to best represent it for the purposes of hydrological modeling.

A literature review by the authors did not reveal any application deriving the probability density functions of the distribution of elements (or similar areal catchment components such as the hydrological response unit of Leavesley and Stannard (1990)) in a watershed. Similar questions about sampling effects on element *pdf's* (Becker and Braun, 1999) would apply to this activity as much as deriving the *pdf* of components of a drainage network. Melville and Martz (2004) and Helmlinger et al. (1993) show that arbitrarily assigned minimum contributing area thresholds do not necessarily change scaling properties. The effect of decreasing sampling on basin and drainage network delineation, and derived topographic variables has been found to be non-linear (Armstrong and Martz, 2003), but the persistence of symmetries is often observed (Marani et al., 1991). The present study addresses the following questions:

1) Does a) drainage density or b) sampling frequency influence the nature of the cumulative density function of hydrological elements along a drainage network?
2) Do changes in these two factors influence the eventual element sequence representation?
3) Is there a typical or representative sequence?

2. RESEARCH BASIN

Baker Creek is a water course characterized by lakes connected by short channels that drains ~150 km^2 into Great Slave Lake in Canada's Northwest Territories (Figure 1). The portion of the watershed that was investigated is upstream of the Baker Creek at the outlet of Lower Martin Lake Water Survey of Canada (WSC) hydrometric gauge (07SB013), draining a ~137 km^2 basin area.

In most years, the largest input of water to the basin is during the spring freshet (Spence, 2006) and the hydrological regime of Baker Creek is described best as subarctic nival (Church, 1974) as this melt dominates the annual hydrograph of Baker Creek. Baker Creek's drainage network is very dynamic with storage thresholds throughout the basin significantly controlling its extent. The extent is generally at its maximum during the spring freshet as snowmelt inputs easily overcome soil storage thresholds kept low by frozen conditions. Relatively high runoff from the uplands brings headwater lake levels above their outlet elevations, permitting flow to proceed to the main channel (Mielko and Woo, 2006). As spring gives way to summer, low intermittent rainfall-runoff from uplands and intermediate wetlands in the basin becomes disconnected from the main channel as evaporative and outflow losses drop levels in intervening lakes below their outlet elevations. By mid summer in a dry year only the three lowest lakes in the system can be hydrologically connected to the outlet of Lower Martin Lake. This equates to only 4% of the basin area (Spence, 2006).

Four land cover types dominate the basin. Exposed Precambrian bedrock is common throughout the basin (27%), particularly in the northeast portion. Open black spruce (*Picea mariana*) forest with an understory containing dwarf willow (*Salix* spp.), Labrador tea, and blueberry (*Vaccinium augustifolium*) occupies 24% of the basin. Bogs, fens and peat plateaus are all present as wetlands occupy 15% of the basin. Hummocky topographic surfaces formed by glacial erosion result in surface water accounting for 21% of the basin area. There are 349 perennial lakes in the basin with a median lake area of 5,400 m^2. The vast majority of lakes are smaller than 0.5 km^2 (97%), yet eight lakes larger than 1 km^2 skew the mean lake area to 88,800 m^2.

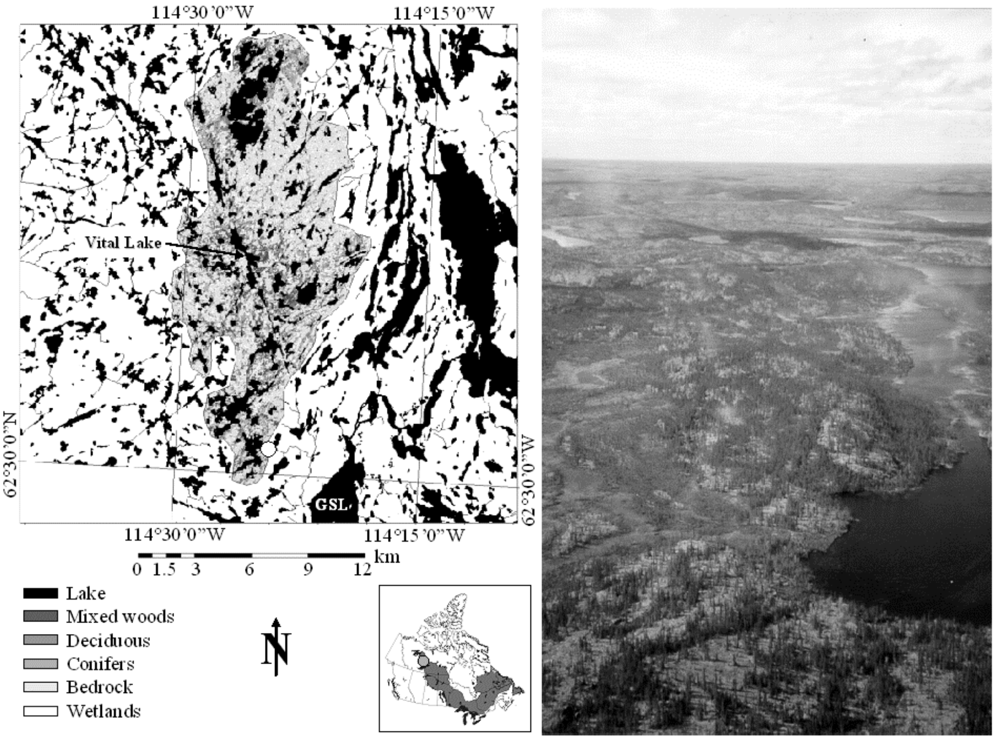

Figure 1: The location of the Baker Creek research catchment illustrating land cover, and notable lakes and a picture of the typical heterogeneous subarctic Canadian Shield landscape. The white circle on the map denotes the location of Water Survey of Canada hydrometric gauge 07SB013 Baker Creek at the outlet of Lower Martin Lake. GSL denotes Great Slave Lake. The shaded area of the reference map refers to the extent of Canadian Shield ecozones.

3. DATA SOURCES AND MANIPULATION

For the purpose of this study, it was assumed that the total range of hydrological elements in the Baker Creek catchment could be captured using land cover variation. This is not necessarily so. For instance, aspect can have an influence on the snowmelt processes that dictate hydrological functioning of exposed bedrock during the spring freshet (Spence and Woo, 2002). However, including aspect in the definition of a Baker Creek basin hydrological element, while more realistic, made the analyses more complicated than was felt necessary. The questions posed by the study could be answered without this added complexity.

Distributed land cover data was derived from Landsat TM satellite imagery. An unsupervised classification with channels 2,3,4,5 and 7 over representative terrain created sixteen classes. Ground truthing from air and ground surveys suggested that amalgamating these sixteen classes into six; coniferous forest, deciduous forest, mixed-wood forest, wetlands, bedrock and lake, would best represent the variation in land cover. Using the classified representative area, a supervised classification was implemented for the remainder of the catchment, resulting in the land cover distribution illustrated in Figure 1. The land cover raster map was imported into ArcInfo 9.0 and converted into a shapefile to permit interaction and analyses with the layers created with the catchment digital elevation model.

A Digital Elevation Model (DEM) of the catchment was obtained by clipping Canadian Digital Elevation Data (CDED) (Natural Resources Canada, 1999). Systemic errors due to the contour map data source and the relatively coarse 25m grid size were removed manually with PCI Geomatics software. Corrections were based on field observations and mapping of the drainage network and catchment boundaries as part of previous studies in the catchment (Spence, 2006).

Drainage networks were derived from the corrected DEM using the Arc Hydro Tools extension software to ArcInfo 9.0 (Maidment, 2002). Flow direction and accumulation were defined with the D-8 method

(Fairchild and Leymarie, 1991). Drainage networks, including stream heads and confluence points representing different wetness conditions were defined with eleven stream definition thresholds, or minimum contributing areas, ranging from 5 ha to 50 km^2. The land cover layer attributes were added to the attribute table of each network's stream head and confluence attribute table, which already included distance from the catchment outlet. This permitted each point to be analysed with respect to its land cover and placement along the drainage network. The outlet was defind as the location of the Water Survey of Canada hydrometric station gauge at the outlet of Lower Martin Lake described above.

Probability and cumulative density functions (*cdf's*) of distances from the outlet for each land cover type were derived for each of the eleven defined drainage networks. Probabilistically derived element sequences were derived by selecting the land cover that had the maximum value of:

$$P(L_i | D_j) \tag{1}$$

where L is land cover of type i and D is a distance j in kilometres from the outlet.

This approach assumes that the most representative land cover at a specific distance from the outlet is the one with the highest probability of occurring at that distance. These distances were defined at five different frequencies (1, 2, 4, 6, and 10 km from the outlet).

The efficiency with which individual hydrological elements will transfer runoff downslope or downstream is a function of not only topology but also the relative size of adjacent elements (Spence and Woo, 2006; Spence, 2006; Woo and Mielko, 2007). If it is assumed that area is a good surrogate for the actual storage capacity of an element, flow will be transmitted through an element i if:

$$R_T = \frac{A_i}{A_{i-1}} < 1 \tag{2}$$

where R_T is the transfer ratio, and A_i is the area of element i and A_{i-1} is the area of the element immediately upslope of A_i. This approach assumes that the storage capacity per unit area between the two elements is identical, so Eq. 2 needs a weighting factor based upon the relative nature of the elements i and $i-1$ such that flow will be transmitted through an element i if:

$$R_T = (\frac{A_i}{A_{i-1}}) \cdot F_{i,i-1} < 1 \tag{3}$$

where $F_{i,i-1}$ is a factor defined as the relative storage capacities of elements i and $i-1$. There is local evidence that exposed bedrock storage capacities can be defined as 16 mm (Spence and Woo, 2002; Landals and Gill, 1972). The average storage capacity of a lake could be resolved as its average depth below its outlet elevation, assumed to be 2000 mm for this study. Soil depths are 2 m on average in the Yellowknife region (Wolfe, 1998). Accounting for an average porosity of 40%, storage capacities per unit area in soil covered elements (i.e., conifers, mixed woods, wetlands and deciduous stands) could be 800 mm. Actual storage capacity values of lakes and soil columns will change with lake level, snow, ice and ground frost conditions. For this exercise, all three values were assumed constant over time and among elements.

$$R_T = (\frac{A_i}{A_{i-1}}) \cdot F_{i,i-1} > 250 \tag{4}$$

is a special case of R_T. In these instances, element i tends to be so large that it contains enough storage to maintain outflow in between runoff events. The transfer of water from element i is controlled by storage within element i rather than the relative volume of runoff from element $i-1$. They tend to be very large lakes relative to the contributions that they receive and tend not to intercept and halt the lateral transfer of runoff (Spence, 2006).

Element area applied in Eqs. 2-4 was estimated as the average patch area of the predominant land cover type patch at each sampling interval identified with Eq 1. Eqs. 2-4 were used to amalgamate the probabilistically derived sequences derived using Eq. 1 into sets of geometrically adjusted sequences that included only those elements that tended to intercept and store streamflow from upstream. Both the geometrically adjusted and probabilistically derived sequences were analyzed to determine if either drainage density or sampling frequency has an influence on the sequence representation. Commonalities were searched for in an effort to resolve the typical or representative sequence of elements in the Baker Creek basin.

4. RESULTS

4.1 Cumulative density functions

The drainage networks defined with the eleven defined minimum contributing areas are illustrated in Figure 2. Minimum contributing areas of 5 ha reflect wet conditions and drainage densities of ~145 km/km^2, typical of those that occur during spring snowmelt. A negative power function related both drainage density and sample size to minimum contributing area (Figure 3). At the largest minimum contributing area of 50 km^2, the drainage density was 0.09 km/km^2. This density has been observed in the Baker Creek catchment at the end of dry summers (Spence, 2006).

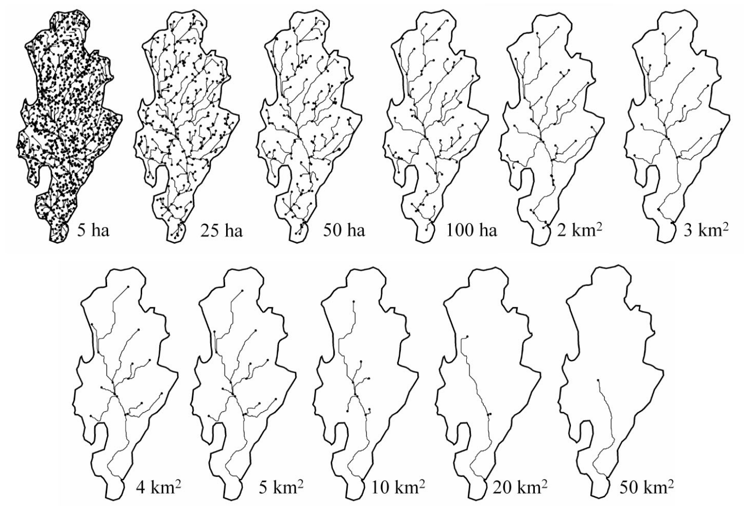

Figure 2: Drainage networks defined with each of the eleven minimum contributing areas, including the locations of land cover sample points.

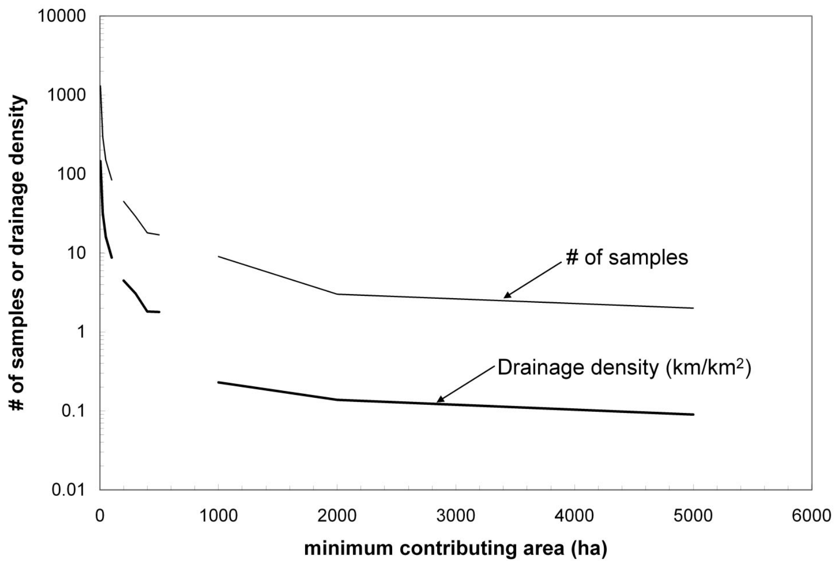

Figure 3: The non linear relationship between minimum contributing area, drainage density and the number of samples of land cover.

The eleven drainage networks each sampled at five frequencies produced 55 sets of cumulative distribution functions (cdf's) of distance from the outlet. All land cover types experienced a similar effect to their cumulative distribution functions when drainage density was changed. In general, the cdf tended to shift up and to the left of the 5 ha curve with decreasing drainage density. For example, beyond a 5 ha minimum contributing area the probability increased that a lake would occur closer to the outlet. This pattern changed to one which saw a higher probability of the lake occurring near the middle of the basin once minimum contributing areas were increased beyond 2 km^2. At the three largest minimum contributing areas (i.e., above 10 km^2) there is significant departure and variability from the rest of the curves (Figure 4). Only subtle changes in the shapes of cdf's derived from dense drainage networks were observed when sampling frequency changed (Figure 5a). The response of less dense networks to changes in sampling frequence was more variable (Figure 5b) and showed little consistent pattern.

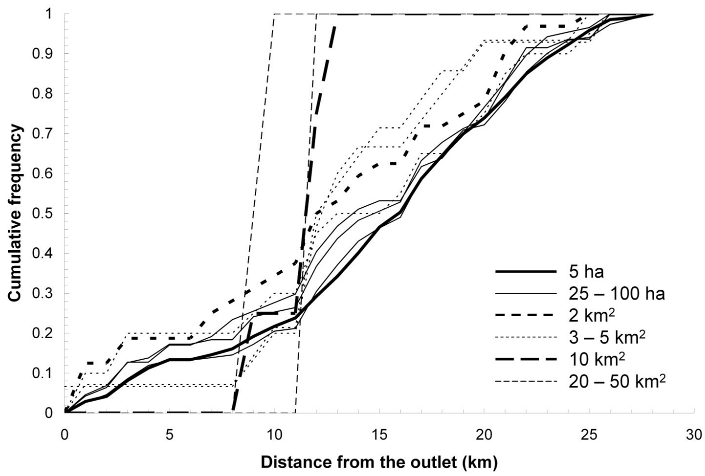

Figure 4: Variation in cumulative distribution functions of the water land cover type with minimum contributing area.

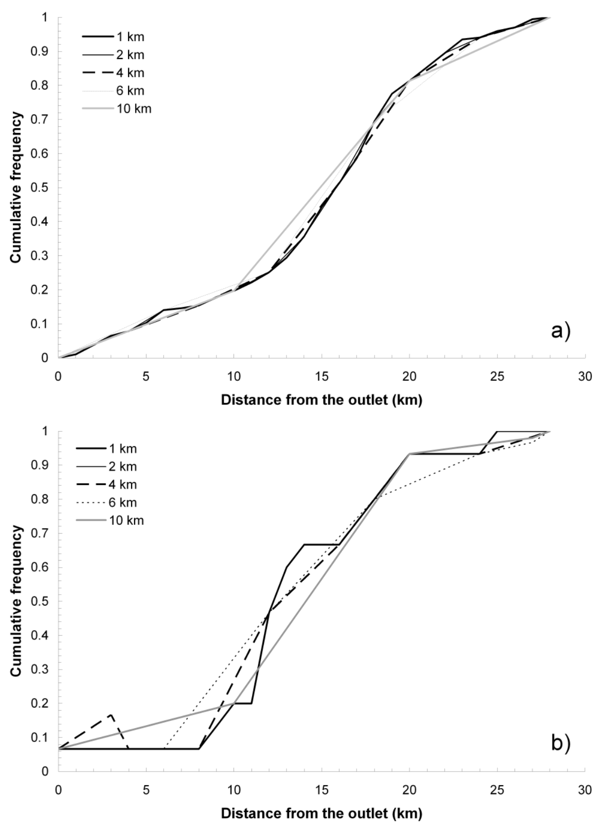

Figure 5: Variation in the cumulative distribution function of the conifers land cover type with sampling frequencies when minimum contributing area is defined as 5 ha (a) and the variation in the cumulative distribution function of the lake cover type with sampling frequency when minimum contributing area is defined as 5 km^2 (b).

4.2 Probabilistically derived sequences

Element sequences derived from the 5 ha minimum contributing area drainage network contained only lakes and conifers (Table 1). As sampling frequency diminished, conifers became even less common and lakes were the only selected elements at the largest sampling intervals when 5 ha was the defined minimum contributing area. There was convergence towards a sequence of three lakes among all the denser networks with decreased sampling (Tables 1-5). Nil samples in the frequent sampling sets began to appear when the minimum contributing area reached 2 km^2. Element variability along the sequence was at its highest among all 55 sets at the frequent sampling intervals (1-2 km) of these intermediately sized drainage networks (2-5 km^2) (Tables 1-5). A third group of sequence sets at minimum contributing areas of 20 and 50 km^2 were characterized by a lack of samples to define a complete sequence at the coarsest sampling interval of 10 km (Tables 1-5).

Table 1: Probability sequences with a sampling frequency of one kilometer. W denotes a lake; C, conifers; B, exposed bedrock, D, deciduous forest; T, wetlands; M, mixed woods. Bolded values denote storing elements identified using Eqs. 2-4.

	Minimum contributing area										
DFO (km)	5 ha	25 ha	50 ha	100 ha	2 km^2	3 km^2	4 km^2	5 km^2	10 km^2	20 km^2	50 km^2
0-0.9	***W***	***W***	***W***	W	W	W	***W***				
1-1.9	C	W/C	W	W							
2-2.9	W	***W***	***W***	W	***W***	***W***					
3-3.9	W	W	W/D	B/T							
4-4.9	***W***	W	W	W							
5-5.9	W	C	C								
6-6.9	***W***	***W/B***	W	***W***	***W***						
7-7.9	***W***	***W/C***	C	***W***	***W/C***						
8-8.9	***W***	***W***	***W***	W	W	W	W	W	***W***	W	
9-9.9	W	W	***W***	W	W	W	W	W	C	***W***	
10-10.9	W	W/C	W/C	W	W						
11-11.9	W	***W***	***W***	***W***	***W***	***W***	W	***W***	W		
12-12.9	***W***	W	W	W	W/C	***W/M***	***W***	***W***	W		W
13-13.9	***C***	***W***	***W***	W	***W***		***W***	***W***	T		
14-14.9	W/C	C	***W***	***C***	*W/D*	D/T	***W/D***	D	***D***		
15-15.9	C	C	C	B/D	C/B/D	W/B	C/D	C/D	***C***		
16-16.9	***C***	W	***W***	W	W	W	***W***	***W***			
17-17.9	W	***W***	W	C	C/T		W	W			
18-18.9	W	***W***	W	W	***W***	***W***		***W***		T	
19-19.9	W	C	W	***W***	W/C	W/B	W/C	W			
20-20.9	***W***	***W***	***W***	***W***	W	W					
21-21.9	W	W	***W***	W	W	W					
22-22.9	W	***W***	W	M/T	M	M			M		
23-23.9	***W***	***W***	***W***	***W***							
24-24.9	W	C	W	C	W	W		W			
25-25.9	***W***	***W***	***W***	***W***	C	W	W				
26-26.9	***C***	***W***	***C***	***C***							
27-27.9	W	W	C								

Table 2: Probability sequences with a sampling frequency of two kilometers.

	Minimum contributing area										
DFO (km)	5 ha	25 ha	50 ha	100 ha	2 km^2	3 km^2	4 km^2	5 km^2	10 km^2	20 km^2	50 km^2
0-2.9	***W***	***W***	***W***	W	W	***W***	***W***				
2-3.9	***W***	***W***	W	W	***W***	***W***					
4-5.9	C	C	***W***	***W***							
6-7.9	***W***	***W***	***W/C***	***W***	***W***			W			
8-9.9	W	W	W	W	W	W	W	W	W/C		
10-11.9	W	***W***	***W***	W	W	***W***	W	***W***	***W***	***W***	
12-13.9	***W***	***W***	***W***	***W***	***W***	***W/M***	***W***	***W***	***W/T***		***W***
14-15.9	C	C	C	C	D	W/C/D/T	D	D	***C/D***		
16-17.9	W	W	W	W	W	W	***W***	W			
18-19.9	W	W	W	***W***	W	W	W/C	W			
20-21.9	W	W	***W***	W	W	W				T	
22-23.9	***W***	***W***	W	***W***	M	M			M		
24-25.9	***W***	***W***	***W***	***W***	W/C	W	W	W			
26-27.9	C	W	C	C							

Table 3: Probability sequences with a sampling frequency of four kilometers.

	Minimum contributing area										
DFO (km)	5 ha	25 ha	50 ha	100 ha	2 km^2	3 km^2	4 km^2	5 km^2	10 km^2	20 km^2	50 km^2
0-3.9	***W***	***W***	***W***	***W***	***W***	***W***	***W***				
4-7.9	C	***W***	***W***	***W***	***W***						
8-11.9	W	***W***	***W***	***W***	W	***W***	***W***	***W***	***W***	***W***	
12-15.9	***W***	***W***	W	W/C	***W***	***W***	***W***	***W***	W/C/D/T		***W***
16-19.9	W	W	W	W	W	W	W	W		T	
20-23.9	***W***	***W***	W	W	***W***	W			M		
24-27.9	W	W	W	W	W/C	W	W	W			

Table 4: Probability sequences with a sampling frequency of six kilometers.

	Minimum contributing area										
DFO (km)	5 ha	25 ha	50 ha	100 ha	2 km^2	3 km^2	4 km^2	5 km^2	10 km^2	20 km^2	50 km^2
0-5.9	***W***	***W***	***W***	***W***	***W***	***W***	***W***				
6-11.9	***W***	***W***	***W***	***W***	W	***W***	***W***	***W***	***W***	***W***	
12-17.9	W	W	W	W	W	W	***W***	***W***	W/C/D/T		***W***
18-23.9	W	W	W	W	***W***	W	W/C	W	M	T	
24-27.9	W	W	W	W	W/C	W	W	W			

Table 5: Probability sequences with a sampling frequency of ten kilometers.

	Minimum contributing area										
DFO (km)	5 ha	25 ha	50 ha	100 ha	2 km^2	3 km^2	4 km^2	5 km^2	10 km^2	20 km^2	50 km^2
0-9.9	***W***	***W***	***W***	***W***	***W***	***W***	W	W	W/C	***W***	
10-19.9	W	W	W	W	***W***	W	W	W	W/C	T	***W***
20-27.9	W	W	W	W	W	W	W	W	M		

4.3 Element area

The densest drainage networks exhibited a bimodal patch area distribution with larger average elements near the outlet and at the top of the catchment (Figure 6). These values are likely skewed by the larger Martin and Duckfish Lakes in these locations. The distribution of patch area becomes unimodal towards the center of the catchment at minimum contributing areas of 10 km^2 and more. This effect, too, is a result of sampling over lakes in the smaller sets.

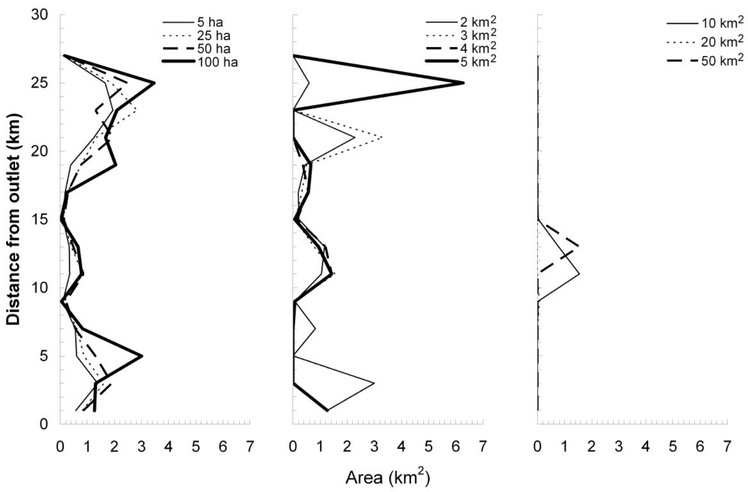

Figure 6: Distribution of average patch area as a function of distance from outlet for various minimum contributing areas, using a sampling frequency of 1 km.

4.4 Geometrically adjusted sequences

Lakes dominated the selections even more once the element sequences were adjusted for geometric effects (Tables 1-5). In the 5 ha drainage network, there were fewer storing elements relative to the total in the probabilistic sequence. This ratio initially increased when 25 ha or 50 ha defined networks were applied, then decreased through networks defined with minimum contributing areas from 100 ha to 4 km^2 and to a stable level in the sparse networks. Some of this effect was due to a reduction in the number of selected elements overall, but not in the middle range of network densities, where no storing elements were selected among the upper reaches of the drainage networks. A series of t-tests revealed that the mean number of storing elements in networks defined with minimum contributing areas of 5 ha – 100 ha, 2 km^2 – 10 km^2, and 20 – 50 km^2 were each significantly different, assuming constant sampling frequency.

5. IS THERE A TYPICAL SEQUENCE?

The different sequences derived from different drainage network densities (Tables 1-5) suggest that the number and location of crucial stores along the drainage sequence of Baker Creek will change with wetness conditions. In an abstract sense, when conditions are very wet the influence of lakes as stores in a catchment is reduced; just as the number of key stores relative to the total number of elements. The number of stores increases when vertical hydrological processes such as evaporation begin to predominate in elements when contributing areas and incoming runoff decrease. When conditions are very dry, fewer elements remain connected to the stream so those elements in the upper reaches become irrelevant to the direct delivery of stream water to the outlet.

The results suggest that this dynamic of changing sequences and storages is non linear. Physically, this is a necessity because the creation and dissolution of stores along a drainage sequence is a threshold process. Upscaling of this threshold process to the catchment scale produces a curve, as different portions of the catchment contribute under different conditions. The dynamics of this curve can be deduced from that expressed in Figure 3. It illustrates how the minimum contributing area influences the resultant drainage density and number of samples. The breaks in the curve coincide with changes in the nature of the defined sequence of elements along the Baker Creek drainage network. There are three distinct phases. When minimum contributing area is small, conditions are wet, and drainage density in the catchment is high, the sequence is controlled by several lakes along the system. When minimum contributing area is of a magnitude of square kilometres, the watershed is in a state of flux as it could be drying or wetting. As the moisture state of the watershed dries, the storing elements located high in the system remain important in the sense that they continue to prevent headwater runoff from proceeding to the active water course, but they are themselves disconnected by degrees of separation. The watercourse becomes concentrated along a main trunk of a less than a dozen lakes, of which only some can act as stores. The number of stores in the watershed decreases to a few key locations.

This result is partially a sampling effect. The larger lakes in the catchment are longer than 1 km and can contain wholly several "headwater" basins when the minimum contributing area is defined as 5 ha. The effect is a sequence where individual lakes are partitioned into more than one reservoir. These reservoirs are merged when the sequence is adjusted for geometry, reducing the number of stores in the new sequence. In this sense the watershed is initially oversampled by a drainage network defined with a minimum contributing area of 5 ha.

It is conjecture, but the nature of the curves illustrated in Figure 3 and density of key storage elements in Tables 1-5 should vary among catchments and especially among landscapes due to the influence of relief and slope length on drainage density (Selby, 1985). They may be indicative of how quickly a given watershed can wet or dry up. The information provided by such curves and tables could suggest how susceptible a watershed is to rapid changes in contributing area. Such information would be of importance to flood forecasters that need to predict the response of disconnected watersheds that are strong threshold systems.

6. CONCLUSIONS

The results show that the drainage density has an influence on the shape of the cumulative distribution function of elements along a stream network. The slope of the cumulative distribution function continually steepens as density decreases. The likelihood that a given element will appear closer to the outlet increases as density decreases. However, at the smallest densities, there is convergence towards the centre of the watershed. This location is a function of the methodology chosen and the scale of this particular catchment. In contrast, changes in sampling frequency produced only subtle changes in the shapes of the cumulative distribution functions.

Lakes dominated all 55 sequence sets. This result, too, was a function of the methodology and landscape. Tributaries of Baker Creek tend to meet at lakes. Using confluences as sample points resulted in an oversampling of lakes at each distance from the outlet, especially in the denser networks. This was exacerbated because many of the confluential lakes are larger than the smallest selected minimum contributing areas, which increased sampling at edges within lakes.

The three typical sequence classifications were a function of sampling and drainage density. Change in the drainage density is indicative of change in basin moisture state. When the catchment is wet, drainage density is high and there are fewer key stores in the sequence than when the drainage is relatively less dense. As drainage density decreases, the irrelevance of storing elements in the upper portions of the watershed to the direct delivery of runoff to the catchment outlet is represented by the lack of sampling. The results imply that parameterization of key storages along disconnected stream networks for runoff modelling needs to be dynamic and may need to be a function of the moisture state of the catchment. Testing of hydrological models with different parameterizations of sequences during different known moisture states may reveal when crucial stores in disconnected stream networks need to be addressed for improved representation of catchment water fluxes.

ACKNOWLEDGEMENT

Thank you to Dr. Alain Pietroniro for providing the land cover dataset, and Jessika Töyra for assistance editing the digital elevation model.

REFERENCES

Armstrong, R.N., Martz, L.W. (2003) Topographic parameterization in continental hydrology: a study in scale. *Hydrological Processes* **17**, 3763-3781.

Becker, A., Braun, P. (1999) Disaggregation, aggregation and spatial scaling in hydrological modeling. *Journal of Hydrology* **217**, 239-252

Beven K. (1986) Runoff production and flood frequency in catchments of order n: An alternative approach. In: Gupta, V.K. et al. (eds), *Scale Problems in Hydrology*. Reidel, pp 107 – 131.

Boyd, M.J. (1978) A storage routing model relating drainage basin hydrology and geomorphology, *Water Resources Research* **14**, 921-928.

Carey, S.K., Woo, M.K. (2001) Slope runoff processes and flow generation in a subarctic, subalpine catchment, *Journal of Hydrology* **253**, 110-129.

Church M. (1974) Hydrology and permafrost with reference to North America. Proc. *Permafrost Hydrology Workshop Seminar 1974*, Ottawa, pp 7 - 20.

Fairchild J., Laymarie P. (1991) Drainage networks from grid digital elevation models, *Water Resources Research* **27**, 29-61.

Helmlinger K.R., Kumar, P., Foufoula-Georgia, E. (1993) On the use of digital elevation model data for Horontian and Fractal Analyses of Channel networks. *Water Resources Research* **29**, 2599-2613.

Hutchinson, D.G., Moore, R.D. (2000) Throughflow variability on a forested hillslope underlain by compacted glacial till, *Hydrological Processes* **14**, 1751-1766.

Landals, A., Gill, D. (1972) Differences in volume of surface runoff during the snowmelt period: Yellowknife, NWT. In: *The Role of Snow and Ice in Hydrology*, IAHS Publication #107, pp 927-942.

Leavesley, G., Stannard, L. (1990) Application of remotely sensed data in a distributed parameter watershed. In: Kite, G. and A. Wankiewicz (eds.), Proc. *Applications of Remote Sensing in Hydrology*, NHRI Symposium #5, Saskatoon, pp 47 – 68.

Maidment, D.R. (2002) *Arc Hydro: GIS for Water Resources*. ESRI Press, Redlands.

Marani, A., Rigon, R., Rinaldo, A. (1991) A note on fractal channel networks, *Water Resources Research* **27**, 3041-3049.

Melville, J.K., Martz, L.W. (2004) A comparison of data sources for manual and automated hydrographical network delineation, *Canadian Water Resources Journal* **29**, 267-282.

Mesa, O.J., Mifflin, E.R. (1986) On the relative role of hillslope and network geometry in hydrologic response. In: Gupta V.K. et al. (eds.), *Scale problems in hydrology*, Reidel, pp 1-17.

Mielko C., Woo, M.K. (2006) Snowmelt runoff processes in a headwater lake and its catchment, subarctic Canadian Shield, *Hydrological Processes* **20**, 987-1000.

Natural Resources Canada (1999) Canadian Digital Elevation Data: Standards and Specifications, 13 pp.

Robinson, J.S., Sivapalan, M., Snell, D.J. (1995) On the relative roles of hillslope processes, channel routing, and network geomorphology in the hydrologic response of natural catchments, *Water Resources Research* **31**, 3089-3101.

Selby, M.J. (1985) *Earth's Changing Surface; An Introduction to Geomorpohology*. Clarendon Press, Oxford, 607 pp.

Spence C., Woo M.K. (2002) Hydrology of subarctic Canadian Shield: bedrock upland, *Journal of Hydrology* **262**, 111-127.

Spence C., Woo M.K.(2003) Hydrology of subarctic Canadian Shield: Soil-filled valleys, *Journal of Hydrology* **279**, 151 - 166.

Spence C., Woo M.K. (2006) Hydrology of subarctic Canadian Shield: Heterogeneous headwater basins, *Journal of Hydrology* **317**, 138-154.

Spence, C. (2006) Hydrological processes and streamflow in a lake dominated water course, *Hydrological Processes* **20**, 3665-3681.

Strahler, A.N. (1952) Dynamic basis of geomorphology, *Bulletin of the Geological Society of America* **63**, 923-938.

Tromp van Meerveld, H.J., McDonnell, J.J. (2006) Threshold relations in subsurface stormflow: 2. The fill and spill hypothesis. *Water Resources Research*, **42**: W02411, doi:10.1029/2004WR003800.

Wang, C.T., Gupta, V.K., Waymire, E.D. (1981) A geomorphologic synthesis of non-leariy in surface runoff, *Water Resources Research* **17**, 545-554.

Wolfe, S.A. (1998) *Living with Frozen Ground: A Field Guide to permafrost in Yellowknife, Northwest Territories*. Geological Survey of Canada Misc. Report 64. 71 pp.

Woo, M.K., Mielko, C. 2007. Flow connectivity of a lake-stream system in a semi-arid, Precambrian Shield environment. Hydrological Processes, (in press).

Moss beneath a leafless larch canopy: influence on water and energy balances in the southern mountainous taiga of eastern Siberia

Kazuyoshi Suzuki,[1] Jumpei Kubota,[2] Hironori Yabuki,[1] Tetsuo Ohata,[1] and Valery Vuglinsky[3]

[1]Institute of Observational Research for Global Change, JAMSTEC, Yokosuka, 237-0061, Japan
[2]Research Institute for Humanity and Nature, Kyoto, Japan
[3]State Hydrological Institute, St. Petersburg, Russian Federation
**Corresponding author, e-mail: skazu@jamstec.go.jp*

ABSTRACT

The southern mountainous taiga of eastern Siberia has a sparse larch canopy and an understory dominated by a thick moss layer. The physiology of moss is very different from that of other plants, as mosses lack roots and vascular systems and take up water directly. During May 2002 we conducted hydrological and meteorological measurements in the taiga of eastern Siberia to investigate the role of understory moss on water and energy balances within a leafless larch forest. We found that below-leafless canopy net all-wave radiation partitions into 39% latent heat flux and 39% sensible heat flux, while the mean daily Bowen ratio is about 1. Ground heat flux on the moss surface is also an important factor, as it comprises 22% of net all-wave radiation. Evaporation from moss beneath the leafless canopy was 24 mm during the 1-month observation period, representing 23% of the water flux into the larch forest. This finding implies that moss intercepted 23% of the water flux into the larch forest. In addition, evaporation from the moss understory during May 2002 comprised 22% of total evapotranspiration previously estimated above the canopy (April to October 2001). We conclude that moss is an important component of the water and energy balance in larch forests in the taiga region.

KEYWORDS

Eastern Siberia, leafless larch canopy, moss, water and energy balance

INTRODUCTION

The physiology of mosses is very different from that of other plants, as mosses lack roots and vascular systems and take up water directly. Mosses dominate the boreal landscape in central Canada (Rapalee *et al.,* 2001), and McFadden *et al*. (1998) noted that shading of the moss layer by the canopy reduces ground heat flux and increases sensible heat flux in shrub tundra in arctic Alaska. These results indicate that the moss layer strongly affects the energy balance and dominant landscape in boreal regions of North America. In a study of the effects of moss on water balance, Price *et al.* (1997) reported that moss intercepts 23% of annual throughfall precipitation input water in a boreal forest in northern Manitoba, Canada.

Although most previous studies of the effects of moss on water balance have been undertaken in North America, where the mosses cover land surfaces, mosses also dominate the understory landscape in southeastern Siberia; however, the effects of moss on water and energy balances in this region are not well understood. In a study of the effect of mosses and lichens on water and energy balances in northern Eurasia, Zhuravin (2004) demonstrated that reindeer moss intercepts 5 mm of precipitation during each rainfall event and estimated annual evaporation from the reindeer moss in the steppe forest of eastern Siberia to comprise 30% of evaporation from permafrost-taiga soils. These results also indicate that the moss layer restricts evaporation from the ground surface and that understory vegetation is an important land cover to consider when describing stream discharge in eastern Siberia.

Kelliher *et al.* (1997) and Ohta *et al*. (2001) found that understory evaporation is especially important in the plain taiga of eastern Siberia in the middle of the Lena Basin, because of the sparse upper canopy in this area. Ohta *et al*. (2001) measured evaporation from a single *Larix cjanderii* over the period mid-April to mid-October 1998 in an area dominated by cowberry understory and found that the measured understory evaporation represented 35% of total evapotranspiration recorded above the larch canopy. For a pine (*Pinus densiflora*) flatwoods forest in north Florida, USA, Powel *et al.* (2005) found that the contributions of the understory sensible and latent heat fluxes to the above open forest fluxes were approximately equal. Thus, if an overstory canopy is sparse, it is also important to consider the water and energy balances below the canopy.

The understory in the upper Lena Basin, southern mountainous taiga region, Siberia, comprises mosses and lichens, while the overstory is a sparse larch canopy. Kubota *et al*. (2004) calculated the water and energy balance in this region for the period April to October 2001. Seasonal variations in evapotranspiration above larch canopies in the plain taiga of the middle Lena Basin and mountainous taiga of the upper Lena Basin have been previously documented by Ohta *et al*. (2001) and Kubota *et al*. (2004), respectively. Seasonal variations in evapotranspiration are significant during the period following snowmelt when the larch canopy is leafless.

The Bowen ratio (ratio of sensible heat flux to latent heat flux) during May in the plain taiga is much higher than that measured in the southern mountainous taiga region at the same time of year, even though the timing of snowmelt is identical at both sites. The difference in Bowen ratios therefore reflects the difference in latent heat flux during the leafless period. This indicates that latent heat flux from understory moss in the southern mountain taiga is large even during the leafless period. The aim of the present study is to examine the effect of understory moss on the water and energy balances beneath a leafless larch canopy in the southern mountainous taiga region, Siberia.

2. Methodology

2. 1 Site Description

The catchment of the Nelka River (Mogot experimental watershed) is located in the southern mountainous region of eastern Siberia (55°N, 124°E), approximately 60 km north of Tynda, Amur region, Russia (Fig. 1). The Nelka River Basin is about 12 km long and 2.5 km wide, with a total area of 30.8 km^2. Slopes within the main valley face northeast and southwest, while elevation within the basin varies from about 550 to 1150 m above sea level. The meteorological observation site used in the present study (tower site in Fig. 1) is located at 608 m elevation, in the lower section of the main valley.

Forest covers more than 90% of the area in the watershed. The larch forest (*Larix cjanderii*) has a plant area index (PAI) of 0.4, as measured from a fisheye photograph during the leafless period and defined as the summation of the area of one side of a tree per unit horizontal area. In 2002, snow melted during early May and larch leaves emerged in early June. Understory vegetation in the study area consists of a 10 to 15 cm thick layer of true mosses (*Aulacomnium turgidum*, *Cetrari cucullate*) and lichens (*Cladina arbuscula*); these mosses and lichens cover the ground over more than 90% of the watershed. The physical properties of the moss and soil at the study site are as follows: moss bulk density, 120 kg m^{-3}; soil particle mass density, 2200–2460 kg m^{-3}; soil bulk density, 280–560 kg m^{-3}; and saturated-soil filtration coefficient, 1.0×10^{-4}–3.0×10^{-4} m s^{-1}. In contrast with the moss and surface soil of arctic tundra in eastern Siberia (Sato, 2004), moss from the present study is denser and thicker. We were unable to locate a water table within the moss or surface soil layer, which is consistent with the findings of Suzuki *et al*. (2006) who demonstrated that most snowmelt water in the region infiltrates into the frozen ground and then refreezes within the organic soil layer. We assumed that following the disappearance of surface snow, the water table was located within the frost table.

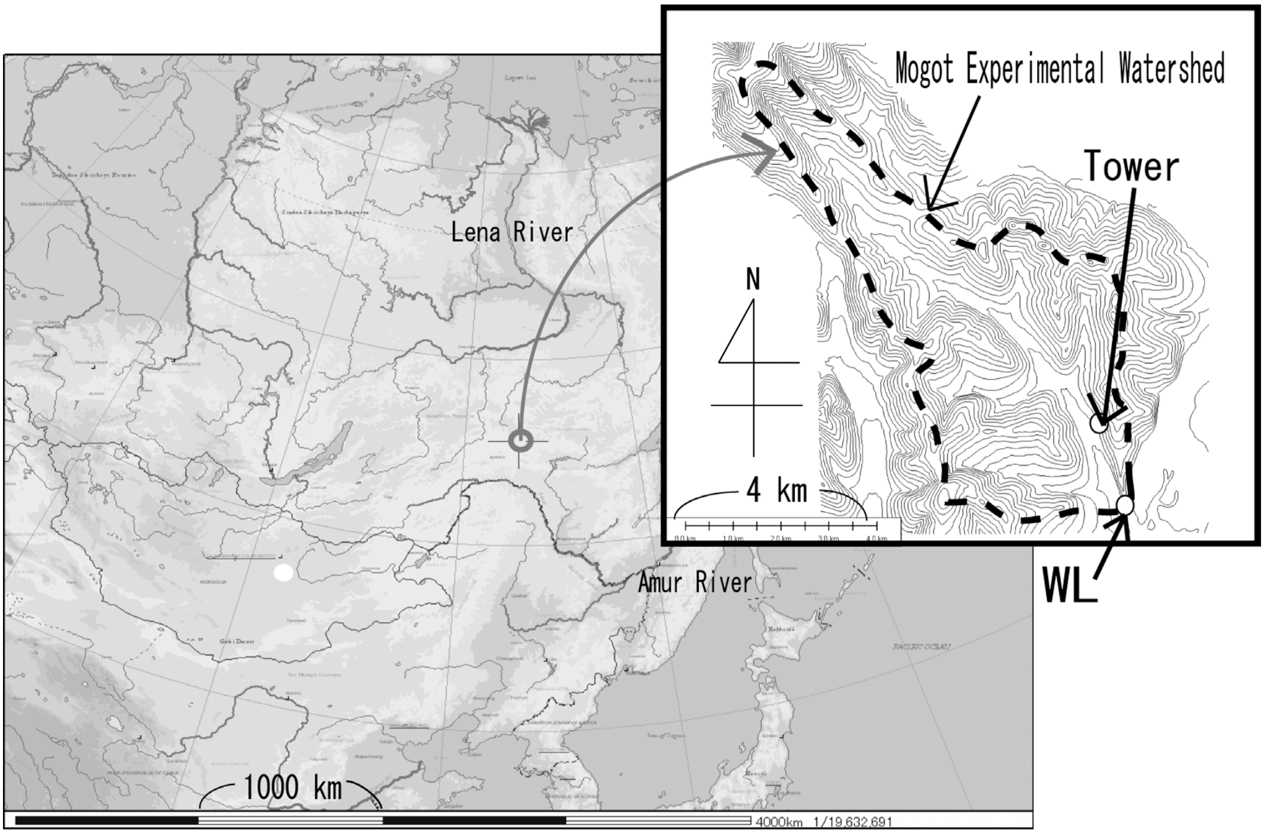

Figure 1 Location of observation site, eastern Siberia. An inset map denotes the catchment of the Nelka River (Mogot experimental watershed), Amur region (WL, water level measurement point; Tower, meteorological observation site).

2.2 Measurements

For most of the observation period (28 April to 31 May 2002 for hydrological measures and 28 April to 30 June 2002 for meteorological measures), the forest was leafless and free from snow cover. We observed hydrological and meteorological elements at sites above and below the larch forest canopy and at the mouth of the Nelka River. Hydrological measurements included precipitation measured with a Tretyakov gauge at 0800 and 2000 h each day, snow water equivalent measured via a snow survey (total snow density at 50 m intervals and snow depth at 10 m intervals) along the main valley near the meteorological station every 10 to 15 days, and river discharge recorded at the mouth of the Nelka River using both automatic water level and direct flow measurements at site WL (see Fig. 1). Meteorological observations included turbulent fluxes, air temperature, relative humidity, wind speed, incident short-wave radiation, reflected short-wave radiation, and net all-wave radiation. Turbulent fluxes above the moss and beneath the larch canopy at the tower site were measured using a three-dimensional ultrasonic anemometer (DA-600, Kaijo, Tokyo, Japan) and an open-path infrared gas analyzer (AH-300, Kaijo). The measurement interval for turbulent fluxes was 10 Hz. Data were collected by a data logger (LG-300, Oriental Electronics Inc., Kyoto, Japan) and written to a hard disk every hour. Measurements of air temperature, relative humidity, wind speed, incident short-wave radiation, reflected short-wave r adiation, and net all-wave radiation were made above the larch canopy at a height of about 10 m and again at a height of 1.85 m above the soil surface.

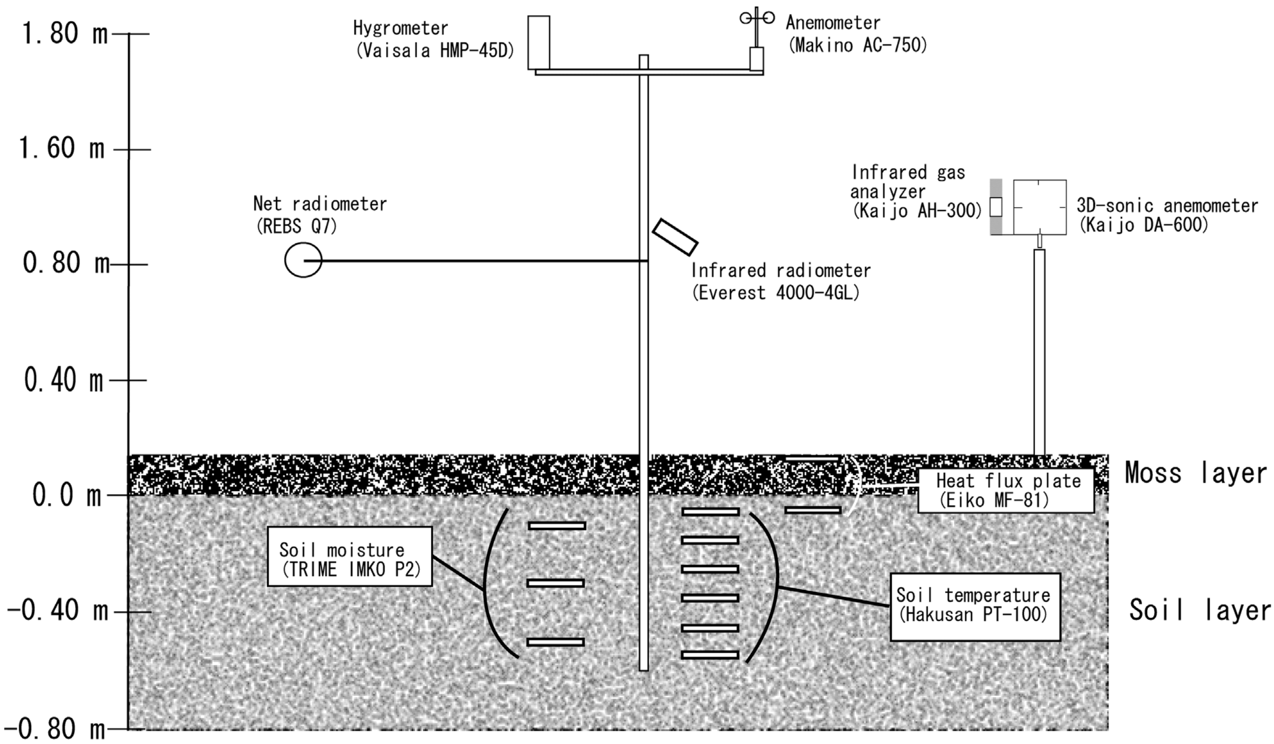

Figure 2. Schematic diagram of the automatic meteorological measurement system used in the present study.

Figure 2 provides a schematic diagram of the meteorological measurement system assembled in the understory. Moss surface temperature was measured using an infrared radiometer (Everest 4000-4GL) at an angle of 45° to the vertical at 0.85 m height above the soil surface. Soil temperature was measured using a thermometer (PT-100, Hakusan, Tokyo, Japan) at depths of 0.05, 0.15, 0.25, 0.35, 0.45, and 0.55 m below the soil surface. The ground heat flux was measured using two heat flux plates (Eiko-81F, Tokyo, Japan) at the moss and soil surface. For measuring ground heat flux at the moss surface, we installed half the heat flux plate into the moss layer at a depth of 1 cm and the other half under a small stone. We recorded air temperature, relative humidity, wind speed, incident and reflected short-wave radiation, net all-wave radiation, air pressure, wind direction, and surface temperature using data loggers (CR-10X, Campbell, Utah, USA and Datamark 3300, Hakusan, Tokyo, Japan) at 10 min intervals.

2.3 Theory

Water balance on the forest floor beneath the larch canopy

The water balance in a leafless forest can be expressed as:

$$\int P(t)dt + dSWE = \int D(t)dt + \int E(t)dt + dS \qquad (1),$$

where P is the throughfall precipitation beneath the canopy (mm h^{-1}), $dSWE$ is the change in snow water equivalent (mm), D is discharge (mm), E is evaporation from the understory (mm h^{-1}), dS is the soil moisture change (mm) during the observation period, dt is the observation period (d), and t is the given day. In this study we ignored the evaporation of water intercepted by the canopy because the canopy was leafless during the observation period and had a PAI of 0.4. Therefore, we assumed that precipitation in this open site was equivalent to throughfall precipitation.

Energy balance on the forest floor beneath the larch canopy

The energy balance on the forest floor beneath the larch canopy can be expressed as:

$$R_N = H + lE + G \qquad (2),$$

where R_N is the net all-wave radiation beneath the canopy (W m^{-2}), H is the sensible heat flux beneath the canopy (W m^{-2}), lE is the latent heat flux beneath the canopy (W m^{-2}), and G is the ground heat flux at the moss layer (W m^{-2}). The sensible (H) and latent (lE) heat fluxes beneath the canopy are described using the eddy covariance method:

$$H = C_P \cdot \rho \cdot \overline{w'T'} \qquad (3)$$

and

$$lE = l \cdot \rho \cdot \overline{w'q'} \qquad (4),$$

where C_P is the specific heat of air (kg kg^{-1}), ρ is the air density (kg m^{-3}), $\overline{w'T'}$ is the covariance in vertical wind speed and air temperature (m s^{-1} K), l is the latent heat of water vaporization (J kg^{-1} K^{-1}), and $\overline{w'q'}$ is the covariance in vertical wind speed and specific humidity (m s^{-1}).

Energy balance closure is an important measure of the quality of turbulent flux data (Baldocchi *et al.*, 1997; Anthoni *et al.*, 2002). Figure 3 shows the relationship between hourly net all-wave radiation and an hourly summation of energy balance components (sensible and latent heat fluxes + ground heat flux) for measurements made during May 2002. The slope of the linear regression for the relationship is 0.93, with an intercept at 5.3 W m^{-2}. The strong correlation (r^2 = 0.95) indicates that the hourly energy balance can be described with reasonable accuracy by summing each individual energy balance made within that hour .

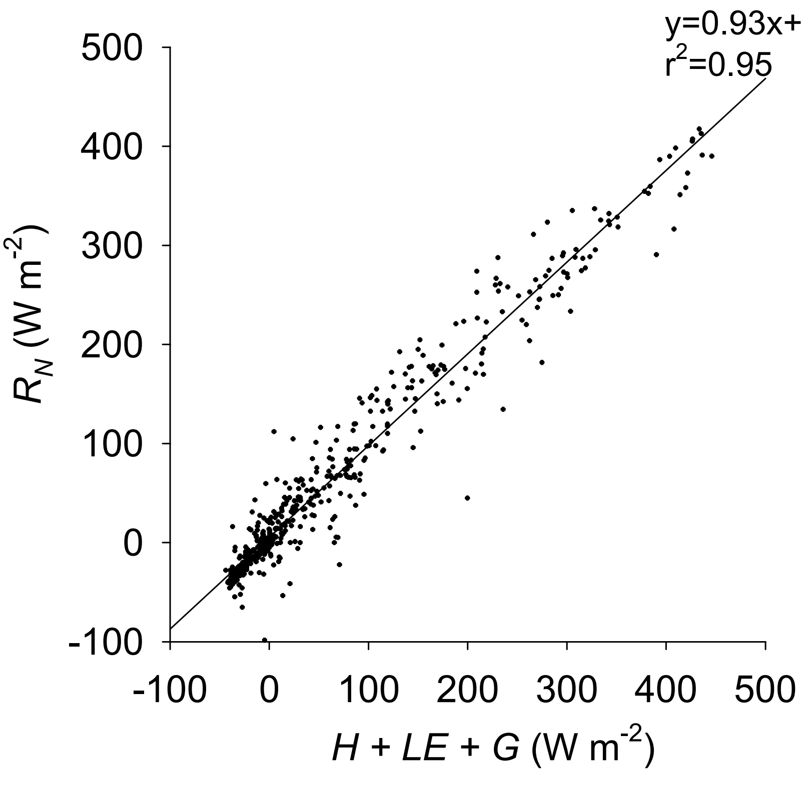

Figure 3. Relationship between hourly net all-wave radiation (R_N) on the moss and hourly summation of energy balance components (sensible [H] and latent [lE] heat fluxes on the moss plus ground heat flux [G]), as recorded during May 2002.

A point measurement of net all-wave radiation and ground heat flux beneath the canopy in this study would not represent the mean values beneath a larch canopy. Figure 4 shows the crown projection diagram with observation sites marked. Canopy coverage is sparse, with marked spatial variation in canopy coverage. Although we do not have the data necessary to verify the degree to which the net all-wave radiation and ground heat flux in the present study is spatially representative, we do refer to these energy balance components in the following discussion.

3. CONCLUSIONS

Net all-wave radiation below a leafless canopy in the southern mountainous taiga of eastern Siberia is partitioned into 39% latent heat flux and 39% sensible heat flux, while the daily Bowen ratio is about 1. Ground heat flux on the moss surface is important, as it comprises 22% of net all-wave radiation. The presence of the moss layer results in decreased soil temperature compared with that of bare soil. A large amount of the ground heat flux is absorbed by the moss layer. The absorbed energy within the moss layer results in increased moss temperature, increased sensible heat flux above the moss, and a low and constant soil heat flux under the moss layer. Finally, understory moss evaporation beneath the leafless canopy was 24 mm during the 1-month observation period, which represents 23% of the water flux into the larch forest. Thus, we assumed that the moss intercepted 23% of the water inflow into the forest floor; this value is comparable with the 22% of total evapotranspiration estimated above the larch canopy from April to October 2001 by Kubota *et al*. (2004).

ACKNOWLEDGMENTS

This project was coordinated by the GEWEX Asian Monsoon Experiment (Prof. Tetsuzo Yasunari, Nagoya University). We thank Dr. Masuyoshi Matsuda of MTS Inc. and the staff of the State Hydrological Institute for their assistance in conducting the intensive fieldwork.

REFERENCES

Anthoni PM, Unsworth MH, Law BE, Irvine J, Baldocchi DD, Van Tuyl S, Moore D. 2002. Seasonal differences in carbon and water vapor exchange in young and old-growth ponderosa pine ecosystems. *Agricultural and Forest Meteorology* **111**: 203-222.

Baldocchi DD, Vogel CA. 1996. Energy and CO_2 flux densities above and below a temperate broad-leaved forest and a boreal pine forest. *Tree Physiology* **16**: 5-16.

Baldocchi DD, Vogel CA, Hall B. 1997. Seasonal variation of carbon dioxide exchange rates above and below a boreal jack pine forest. *Agricultural and Forest Meteorology* **83**: 147-170.

Campbell GS, Norman JM. 1998. *An Introduction to Environmental Biophysics*, 2nd ed. Springer-Verlag: Berlin; 315.

Kelliher FM, Hollinger DY, Schulze ED, Vygodskaya NN, Byers JN, Hunt JE, McSeveny TM, Milukova I, Sogatchev A, Varlargin A, Ziegler W, Arneth A, Bauer G. 1997. Evaporation from an eastern Siberian larch forest. *Agricultural and Forest Meteorology* **85**: 135-147.

Kelliher, F. M., J. Lloyd, A. Arneth, J. N. Byers, T. M. McSeveny, I. Milukova, S. Grigoriev, M. Panfyorov, A. Sogatchev, A. Varlargin, W. Ziegler, G. Bauer, and E. D. Schulze, 1998: Evaporation from a central Siberian pine forest. *Journal of Hydrology*, **205,** 279-296.

Kubota J, Suzuki K, Yamazaki Y, Ohata T, Vuglinsky V. 2004. Water and energy budget in the southern mountainous region of eastern Siberia. In *Proceedings of the 6th International Study Conference on GEWEX in Asia and GAME*, Matsumoto J, Higuchi A, Nakamura K, Yasunari T (eds). GAME Publ. no. 11; CD-ROM.

McFadden JP, Chapin FS, Hollinger DY. 1998. Subgrid-scale variability in the surface energy balance of arctic tundra. *Journal of Geophysical Research-Atmospheres* **103**: 28947-28961.

Ohta T, Hiyama T, Tanaka H, Kuwada T, Maximov TC, Ohata T, Fukushima Y. 2001. Seasonal variation in the energy and water exchanges above and below a larch forest in eastern Siberia. *Hydrological Processes* **15**: 1459-1476.

Powell TL, Starr G, Clark KL, Martin TA, Gholz HL. 2005. Ecosystem and understory water and energy exchange for a mature, naturally regenerated pine flatwoods forest in north Florida. *Canadian Journal of Forest Research-Revue Canadienne De Recherche Forestiere* **35(7)**: 1568-1580.

Price AG, Dunham K, Carleton T, Band L. 1997. Variability of water fluxes through the black spruce (*Picea mariana*) canopy and feather moss (*Pleurozium schreberi*) carpet in the boreal forest of northern Manitoba. *Journal of Hydrology* **196**: 310-323.

Rapalee G, Steyaert LT, Hall FG. 2001. Moss and lichen cover mapping at local and regional scales in the boreal forest ecosystem of central Canada. *Journal of Geophysical Research-Atmospheres* **106**: 33551-33563.

Sato N. 2004. Water transport process of the air-vegetation-soil system in the Arctic tundra. Ph.D. diss., Hokkaido University, Sapporo, Japan.

Suzuki K, Kubota J, Ohata T, Vuglinsky V. 2006. Influence of snow ablation and frozen ground on spring runoff generation in the Mogot Experimental Watershed in the southern mountainous taiga of eastern Siberia. *Nordic Hydrology* **37**, 21-29.

Suzuki, K., Kubota, J., Yabuki, H., Ohata, T, Vuginsky, V. 2007. Moss beneath a leafless larch canopy: influence on water and energy balances in the southern mountainous taiga of eastern Siberia. Hydrological Processes, **21**, In press.

Zhuravin SA. 2004. Features of water balance for small mountainous watersheds in East Siberia: Kolyma Water Balance Station case study. In Northern Research Basins Water Balance (Proceedings of a workshop held at Victoria, Canada, March 2004), Kane D, Yang D (eds), IAHS Publ. no. 290; 28-40.

Analysis of streamflow response to variability of climate in northwestern North America

Ming-ko Woo[1*], Robin Thorne[1],

[1] *School of Geography and Earth Sciences, McMaster University, Hamilton, Ontario L8S4K1, CANADA*
**Corresponding author, e-mail: woo@mcmaster.ca*

ABSTRACT
Variability of climate is expected to affect interannual streamflow fluctuations. Snowmelt discharge is particularly important in northern latitudes and in northwestern North America, the Pacific Decadal Oscillation which is strong in the cold season, may exert influence on interannual variations in spring high flows. However, the rivers of Alaska, Yukon, Northwest Territories, British Columbia and Alberta have variable response to this climate signal. An analysis of the flow of some rivers in this region indicates that rivers draining the Pacific coast may be positively correlated with PDO and some rivers in the interior may correlate negatively. Not all river flows have significant correlation with the PDO, as non-climatic factors such as location, topography and storage can modify the climatic effects. Furthermore, interdecadal fluctuations may be erroneously interpreted as trends. Caution must be exercised when using short records to detect long-term trends in streamflow.

KEYWORDS
Arctic environments; thirtieth anniversary; conference paper; paper template; electronic files

1. INTRODUCTION

Climatic variability has been found to affect variations in surface air temperature and precipitation. Frey and Smith (2003), for example, noted that the Arctic Oscillation is important in driving the observed temperature and precipitation trends in western Siberia. The Pacific Decadal Oscillation (PDO) in North America similarly influences the temperature and precipitation regimes of the region. The Arctic Oscillation and the PDO are expected to have teleconnection with river discharge of the Hudson Bay drainage in Canada (Déry and Wood, 2004) and with the flows of southeastern Alaskan rivers (Neal *et al*. 2004). In the temperate and subarctic latitudes of northwestern North America, variations of streamflow have important implications on the environment, ecology and economic activities, including floods and droughts, aquatic habitats and salmon migration, hydropower generation and irrigation.

The spring season in northern areas is especially important in terms of water supply and hazards as many of their rivers receive large influx of water from snowmelt. The PDO signals are notably stronger in the cold season than in the summer, and would likely induce year to year variations in spring discharge. There has also been a growing interest in streamflow trends (Burn et al., 2004; Peterson et al., 2002; Zhang et al., 2001), largely driven by climate warming concerns, but the short record length of most northern rivers may render it difficult to distinguish long-term trends from medium-term variability. The present study examines the linkage between discharge and the climate variability signal on a regional scale and assesses the role of inter-decadal streamflow variability in flow trend identification.

2. NORtHWESTERN NORTH AMERICA

Northwestern North America encompasses Alaska, Yukon and Northwest Territories, British Columbia and Alberta. Western Cordillera, with chains of lofty mountains, plateaus and valleys, dominate the region. The mountains present a barrier to the eastward passage of the Pacific air and often prevent the outbreak of cold Arctic air to the Pacific coast. East of the Cordillera lie the Interior Plains and the Canadian Shield. Several climates zones exist in the region, including cold temperate, subarctic and arctic climates in maritime and continental settings. Most river flow exhibits a nival regime in which spring melt generates high flows that are orders of magnitude larger than the winter discharge, and the spring freshet is followed by a decline in flow but the recession flow is revived occasionally by summer rainstorms. Rivers along the Pacific coast have a mixed response to rainfall and snowmelt that vary in proportion depending on fluctuations of the freezing altitude (Waylen and Woo 1982).

3. DATA SOURCES AND ANALYSIS

This study uses climate station and hydrometric data for Canada and Alaska. The northern region has a sparse data network. Many stations do not extend back beyond 1960 and the number of stations also declined since the 1990s (Shiklomanov *et al*. 2002). Air temperature and precipitation are provided by Environment Canada and by the Alaskan Climate Center at University of Alaska Fairbanks (http://climate.gi.alaska.edu). Canadian streamflow data are taken from HYDAT and Alaskan data are obtained from http://nwis.waterdata.usgs.gov. We included only those stations with streamflow record that cover 1965-2005 and with less than five years of missing data. PDO indices are obtained from http://jisao.washington.edu/pdo/PDO.latest. This study used the average PDO values of October-March for each year. Streamflow and climate data were correlated with PDO using non-parametric Spearman correlation. Similarly, streamflow series were correlated with time for linear trend analysis. Spatial patterns of the correlation coefficients were then mapped with solid (positive) and dashed (negative correlation) isolines.

4. PDO AND STREAMFLOW CORRELATIONS

Positive or warm PDO corresponds with period of high temperature and low precipitation in the winter. As examples, the weather stations at Fairbanks (64°48’N,147°51’W) and Talkeetna (62°19’N,150°5’W) in Alaska, yield positive correlation between their winter air temperature and PDO, but the winter precipitation of Fairbanks correlates negatively with PDO. This confirms that positive PDO values are associated with warm and dry winters.

Figure 1 maps the spatial pattern of locations where monthly streamflow is correlated with the winter PDO, for the spring season. As the timing of spring runoff differs among different environments in northwestern North America, three separate maps are provided, for the months of April, May and June (Woo and Thorne 2002). One prominent feature is a lack of significant correlation for many parts of the region. Several factors can confound the relationship between streamflow and the climate. Topography can modify the climate variation signals (Moore *et al*. 2003) to complicate the pattern of streamflow response. The presence of lakes upstream of gauging stations (e.g. Camsell River in Northwest Territories at 65°35’N,117°45’W) can buffer the flow response to the climatic variables. Glacierized basins may produce larger melt in the warm PDO years, but enhanced melt may be countered by the low winter precipitation during these years. Fleming *et al*. (2006) noted that hydroclimatic filtering effect of basin glacierization is important in determining local interannual flow fluctuations. These and other non-climatic considerations can effectively negate the influence of climatic factors on the variability of streamflow (Woo *et al*. 2006).

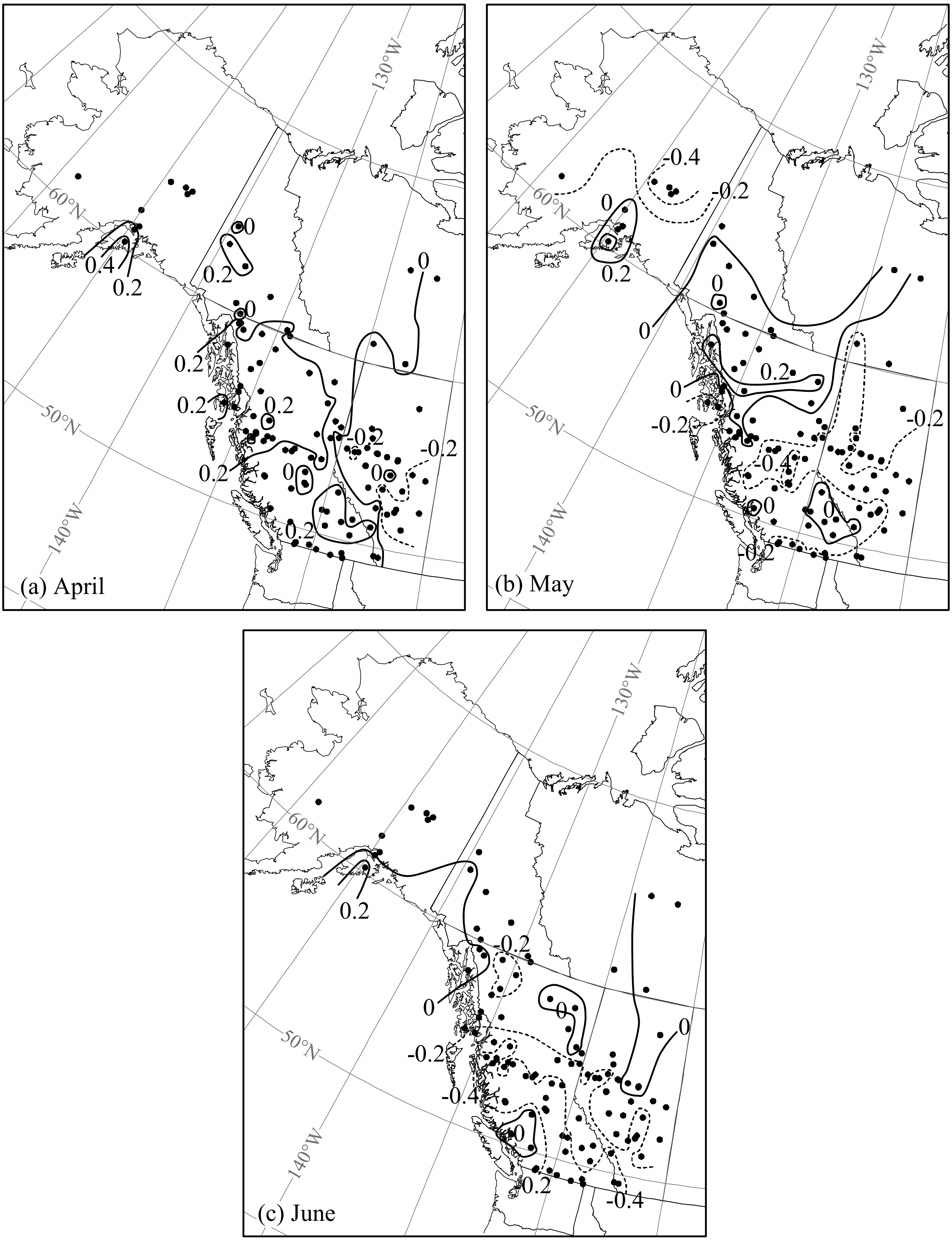

Figure 9 Spatial patterns of correlation (r-values) between mean flows of (a) April, (b) May and (c) June, and Oct-to-Mar PDO. Dots indicate location of stations that provide data for this study. Solid or dashed isolines indicate positive or negative correlation, respectively.

Areas of significant correlation are disbursed in two different zones. Coastal areas usually have winter rain at low altitudes and snow accumulation on high grounds so that both winter and spring high flows are possible. Rivers like the Kenai in Alaska (60°29'N,149°48'W) show positive flow correlation with PDO for the months of January to April. The high correlation for the winter months may be attributed to more frequent occurrence of rainfall than snowfall to generate high winter runoff during warm PDO years. This interpretation is consistent with Neal *et al.*'s (2002) finding that warm-PDO winter flows are typically higher than the cold-PDO winter discharge. Positive correlation for the month of April indicates that warm PDO years bring forth higher discharge possibly due to early melt of snow at high elevations.

Inland areas possess zones with significant negative correlation between PDO and streamflow in the snowmelt season. This arises because warm PDO years accumulate less snow so that the spring-melt discharge is reduced. The timing of spring runoff differs in different parts of the region. Thus, high negative correlation occurs in April and May for the Interior Plains, in May for interior Alaska, and in June for interior British Columbia with high elevation zones. It is noted that the January-March air temperature of Prince George (53°9'N,122°7'W) in interior British Columbia shows a significant positive correlation with winter PDO, but this does not have a positive effect on streamflow. The flow is more responsive to winter precipitation which tends to be low during the warm PDO winters.

5. STREAMFLOW TREND VERSUS VARIABILITY

The conventional approach in trend analysis assumes that changes in streamflow during 1960-99 followed an approximately linear trend. Analysing the time series with this implicit assumption, the Spearman rank correlation suggests that spring flow in many rivers arrives earlier in recent years (e.g. in the Mackenzie Basin, see Woo and Thorne, 2003) due to increased warming in April to advance the timing of snowmelt. The Pacific coastal rivers also show an increase in streamflow. Several mountain rivers in the Cordillera experience a flow reduction that may be attributed to an early rise in the spring high flow, followed by a compensating decline in the recession flow.

While it is convenient to pool the entire length of historical record into a single time series for linear trend analysis, detailed scrutiny of most data series suggests periodic variations that cannot be ignored. It is well established that a major shift in the atmospheric general circulation occurred during the mid-1970s that affected the climate of many regions of the world (e.g. Mantua *et al*., 1997; Trenberth, 1990), including northwestern North America. The regime shift has been attributed to a multidecadal oscillation in the North Pacific climate and is manifested in large scale indices, including the PDO. In view of the distinct climatological shift in the mid 1970s, it is physically sound to divide the 1960-99 streamflow data into two sub-periods (i.e.1960-74 and 1975-99) and examine the flow changes within each period. An example of the spring (April to June) discharge of North Thompson River (51°36'N,119°54'W) in Figure 2 illustrates the break in its time series that may be linked to the shift in the climatic regime.

The spatial pattern of spring flow in 1960-74 shows declining runoff on the leeward side of the Cordillera and little change on the windward side (Fig. 3). The 1975-99 pattern indicates increasing spring runoff on the windward aspect and a moderation of the runoff decline in the interior. A shift in the large-scale circulation regime has induced a strengthening of the onshore winter airflow. This enhanced flow interacts with the formidable topographic barrier of the Cordillera to deposit greater snowfall on the windward side, accompanied by reduced winter precipitation in the leeward areas in the Mackenzie and Yukon river basins. The shift in spring runoff after the 1970s reflects such changes in winter snow accumulation (released by subsequent spring melt) in these respective areas. Given the possible link of streamflow with the regional climate forcing, a shift in streamflow should be viewed as an abrupt jump rather than as part of a linear trend.

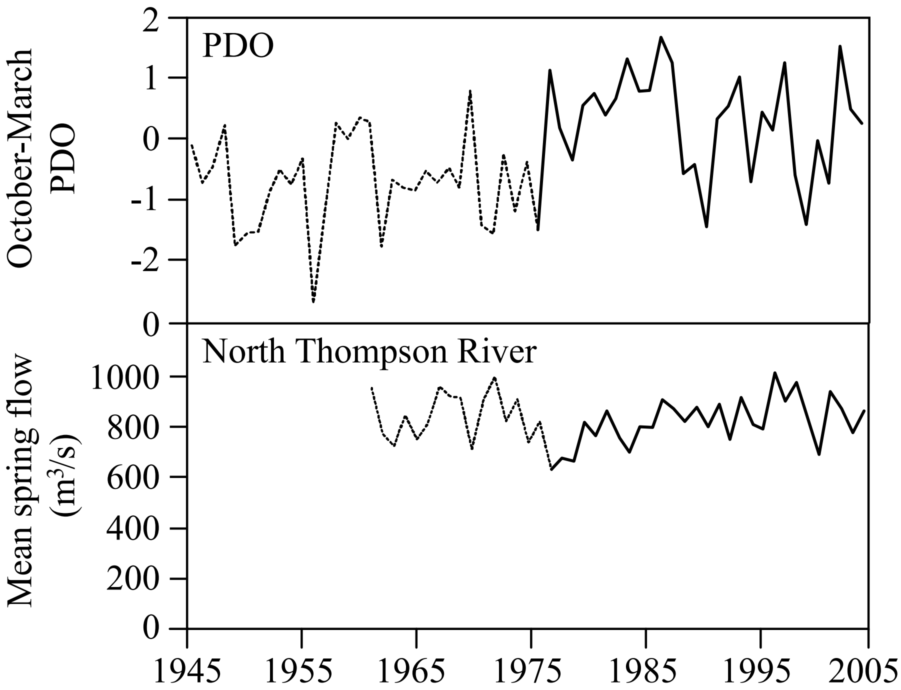

Figure 10 Time series of mean winter PDO (Oct-Mar) and mean spring flow (Apr-June) of North Thompson River, showing a shift in their regimes in the 1970s.

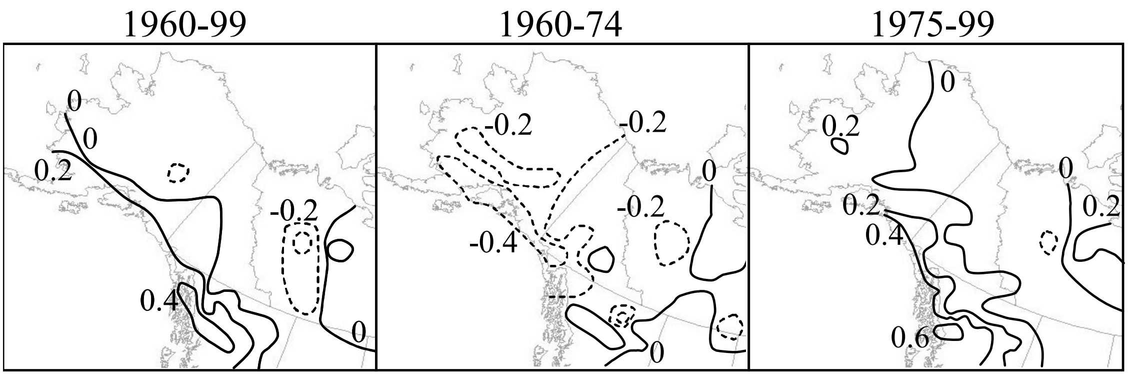

Figure 11 Trends in mean streamflow (discharge correlated against time) for 1960-1999, 1960-79 and 1980-99 periods for the spring season (April to June). Solid or dashed isolines of r-values indicate positive or negative correlation, respectively

6. CONCLUSIONS

Climatic factor is expected to play an important role in causing interannual variations in streamflow. There is evidence that the winter PDO is correlated with the spring discharge in parts of northwestern North America. In the coastal zone, warm winters yield more rain than snow and the flow will increase. In inland areas, warm PDO years with low snow accumulation lead to reduced runoff. However, there are large parts of the region where the interannual variations in streamflow and climate are not significantly correlated. Local streamflow response to the regional climate forcing is complicated by such factors as terrain and basin storage. These considerations complicate the linkage between the variability of regional climate and streamflow in particular locations, particularly for areas with complex and rugged terrain.

In the past decades, there has been a prominent shift in the climatic regime in the North Pacific which affects northwestern North America. Our analysis shows that the change in streamflow within each climatic regime is weak, but the change is large between the two regime periods. A trend emerges if the entire 40-year (1960-99) time series rather than the climatologically driven regime segments are considered. Such a trend is a statistical artifact of combining two sub-populations of streamflow, each responding to a different climatic forcing. This result offers a cautionary note against inadvertent interpretation of short-term regime shift as an indication of long term trend in hydrological data.

ACKNOWLEDGEMENT

This study was funded by the Natural Sciences and Engineering Research Council of Canada through the Mackenzie GEWEX Study.

REFERENCES

Burn, D.H., Cunderlik, J.M. and Pietroniro, A. (2004) Hydrological trends and variability in the Liard River basin. *Hydrological Sciences Journal* **49**, 53-67

Déry, S.J. and Wood, E.F. (2004) Teleconnection between the Arctic Oscillation and Hudson Bay river discharge. *Geophysical Research Letters* **31**, L18205, doi: 10.1029/2004GL020729

Fleming, S.W., Moore, R.D. and Clarke, G.K.C. (2006) Glacier-mediated streamflow teleconnections to the Arctic Oscillation. *International Journal of Climatology* **26**, 619-636

Frey, K.E. and Smith, L.C. (2003) Recent temperature and precipitation increases in West Siberian and their association with the Arctic Oscillation. *Polar Research* **22**, 287-300

Mantua, N.J., Hare, S.R., Zhang, Y., Wallace, J.M. and Francis, R.C. (1997) A pacific interdecadal climate oscillation with impacts on salmon production. *Bulletin of American Meteorological Society* **78**, 1067-1079.

Moore, G.W.K., Alverson, K. and Holdsworth, G. (2003) The impact that elevation has on the ENSO signal in precipitation records from the Gulf of Alaska region. *Climatic Change* **59**: 101-121

Neal, E.G., Walter, M.T. and Coffeen, C. (2002) Linking the pacific decadal oscillation to seasonal stream discharge patterns in Southeast Alaska. *Journal of Hydrology* **263**, 188-197

Peterson, B.J., Holmes, R.M., McClelland, J.W., Vörösmarty, C.J., Lammers, R.B., Shiklomanov, A.I., Shiklomanov, I.A. and Rahmstorf, R. (2002) Increasing River Discharge to the Arctic Ocean. *Science* **298**, 2171-2173

Shiklomanov, A.I., Lammers, R.B. and Vörösmarty, C.J. (2002) Widespread decline in hydrological monitoring threatens pan-Arctic research. *EOS* **83(2)**, 13-17

Trenberth, K.E. (1990) Recent observed interdecadal climate changes in the Northern Hemisphere. *Bulletin of American Meteorological Society* **71**, 988-993

Waylen, P. and Woo, M.K. (1982) Prediction of annual floods generated by mixed processes. *Water Resources Research* **18**, 1283-1286

Woo, M.K. and Thorne, R. (2002) Comment on "Detection of hydrologic trends and variability" by Burn, D.H. and Hag Elnur, M.A., 2002. Journal of Hydrology 255, 107-122. *Journal of Hydrology* **277**, 150-160

Woo, M.K. and Thorne, R. (2003) Streamflow in the Mackenzie Basin, Canada. *Arctic* **56**, 328-340

Woo, M.K., Thorne, R. and Szeto, K.K. (2006) Reinterpretation of streamflow trends based on shifts in large-scale atmospheric circulation. *Hydrological Processes* **20**, 3995-4003

Zhang, X., Harvey, K.D., Hogg, W.D. and Yuzyk, T.R. (2001) Trends in Canadian streamflow. *Water Resources Research* **37**, 987-998

Role of Snow in the Hydrology of a High Arctic Riparian Wetland

Kathy L. Young*

Dept. Geography, York University, Toronto, Ontario, M3J 1P3 CANADA
**Corresponding author, e-mail:klyoung@yorku.ca*

ABSTRACT
Riparian wetlands are unique strips of saturated and vegetated ground forming important links between terrestrial landscapes and aquatic zones. These linear wetlands are common features in High Arctic landscapes yet their hydrology is not well understood. Woo and Young (2003) provide some information on their hydrology through their study on Cornwallis Island-a polar desert environment. They found that water tables in the wetland continually remain high from seasonal snowmelt runoff and extended over-bank flooding from snow-chocked stream channels. Here, I describe the hydrology of a riparian wetland situated within a polar oasis landscape near Eastwind Lake, Ellesmere Island, Nunavut (80°80'N, 85°35'W) during the 2006 field season. Unlike the Woo and Young (2003) study, snow in the channel does not promote a period of extended over-bank flooding but instead serves as a dam blocking most stream water from entering and flooding the wetland. It is only during a warm, sunny period that the snow dam melts and the wetland becomes recharged. Meltwater from late-lying snowbeds located further upstream is essential for maintaining saturated conditions for the duration of the season.

KEYWORDS
Arctic hydrology, channel snow, High Arctic, permafrost, riparian wetland

1. INTRODUCTION

Riparian wetlands are unique strips of saturated and vegetated ground forming important links between terrestrial landscapes and aquatic zones. They serve to both modify and be modified by fluvial and chemical processes and have been well studied in temperate environments (e.g. Cole and Brooks 2000; Toner and Keddy, 1997; Hauer and Smith, 1998; Vidon and Hill 2006). Cole and Brooks (2000) suggest that these wetlands are the wettest when compared to other wetland-types and with some exception show the smallest range in hydrologic behaviour. They indicate that duration of inundation and saturation for most riparian sites is about 81%. Toner and Keddy (1997) suggest that the duration of flooding and the frequency of flooding is important for determining plant type structure. Woody plants succeed herbaceous plant in areas with both infrequent flooding and duration. Vidon and Hill (2006) and others have focused on defining the biogeochemistry of these zones and their ability to deplete nitrogen-rich waters draining from upslope agricultural fields.

These linear wetlands are also common features in high arctic landscapes running along streams and rivers, yet their hydrology is not well understood. Woo and Young (2003) provide some information on their hydrology through their study on Cornwallis Island-a polar desert environment. Here, these researchers found that water tables in the wetland continually remain high from seasonal snowmelt runoff and extended over-bank flooding from snow-choked stream channels. Due to diluted conditions, cation levels remain low, in comparison to groundwater-fed depression-type wetlands. Here, I describe the hydrology of a riparian wetland situated within a polar oasis landscape near Eastwind Lake, Ellesmere Island, Nunavut (80°80'N, 85035'W) during the 2006 field season. Unlike the Woo and Young (2003) study, snow in the channel does not promote a period of extended over-bank flooding but in fact initially serves as a dam, blocking stream water from entering and flooding the wetland prior to its disintegration. This study investigates how the wetland responds to these conditions along with contributions of meltwater from late-lying snowbeds which exist in the stream channel and along steep slopes and valleys. A combination of field data (climate, hydrology) and a snowmelt model (Woo and Young 2004) are employed to explore the dual role of snow (blockage/recharge) in the hydrology of a High Arctic riparian wetland.

2. STUDY AREA

This study took place from early May to early-August 2006 near Eastwind Lake, Ellesmere Island, Nunavut (80°80'N, 85°35'W). The wetland is situated about 20 km inland from Eureka, a government weather station (Figure 1). The wetland site is composed of a broad flood-plain characterized by a main stream channel running through it and a series of water pathways or streamlets. Elevation ranges from 142 m at its inlet to 136 m at its outlet-a gradient of 0.05. The wetland shows a high degree of variability. Some areas are well vegetated and contain much wet meadow-type vegetation (e.g. *Cotton-grass, Moss, Sedges, and Graminoids*), while other zones are void of plant life and are better described as gravely mud-flats. These latter areas are routinely subjected to stream waters which deposit much silt and detritus here, as the current slows through the area. A soil profile dug in the middle of the wetland indicates a thin, organic layer over a saturated, gravely-silty soil grading to clay with depth. Orange iron stains indicative of water-logged conditions occur throughout the soil profile. The area is below the marine-limit, set at 150 m a.s.l. The stream which floods and recharges this wetland originates near the peak (~590 m) of Black Top Ridge, a ridge which runs in a southwest to northeast direction across the Fosheim Peninsula, from Eureka Sound to Greely Fiord. This stream, referred here as Black Top Ridge Creek (BTRC), is just one of many which drain this high ridge and empty into adjacent wetland zones. Snow typically persists on the ridge and in steep gullies much longer than the lowland wetland, owing to the cooler conditions here.

The area can be described as having a polar-oasis type climate (Woo and Young 1997 and Woo and Guan 2006). It typically experiences warmer and drier conditions than elsewhere in the High Arctic, as it is sheltered by near-by mountains from low pressure systems that originate in the Arctic Ocean (Maxwell 1980; Young and Woo 2004a, b and Woo and Guan 2006). Summers are warmer than the coastal Eureka station (see Woo and Guan 2006). In 2006, snow cover was low over the landscape with much of the snow blown into low-lying areas (i.e. stream channels and depressions). However, due to a cool and cloudy spring, snowmelt was delayed until May 24 and persisted 21 days, 11 days longer than in 2005. The 2006 season was also much cooler (~400 thawing degree-days) and wetter than 2005, which was one of the warmest on record for this area (over 500 thawing degree-days at Eureka, see Woo and Guan 2006). Summer rainfall in 2006 amounted to 39 mm up until Aug. 8 (end of fieldwork) and then an additional 30 mm fell between Aug 9-14 at Eureka (Woo and Guan, 2006). Only 27 mm fell in 2005 at the study site, in comparison to 19 mm at the Eureka weather station. Growing conditions were less favourable in 2006 than 2005. In 2006, growing- degree days totalled 138 versus 224 in 2005. This resulted from 17 fewer growing days (>5°C) in 2006 than 2005, when the same time span is considered.

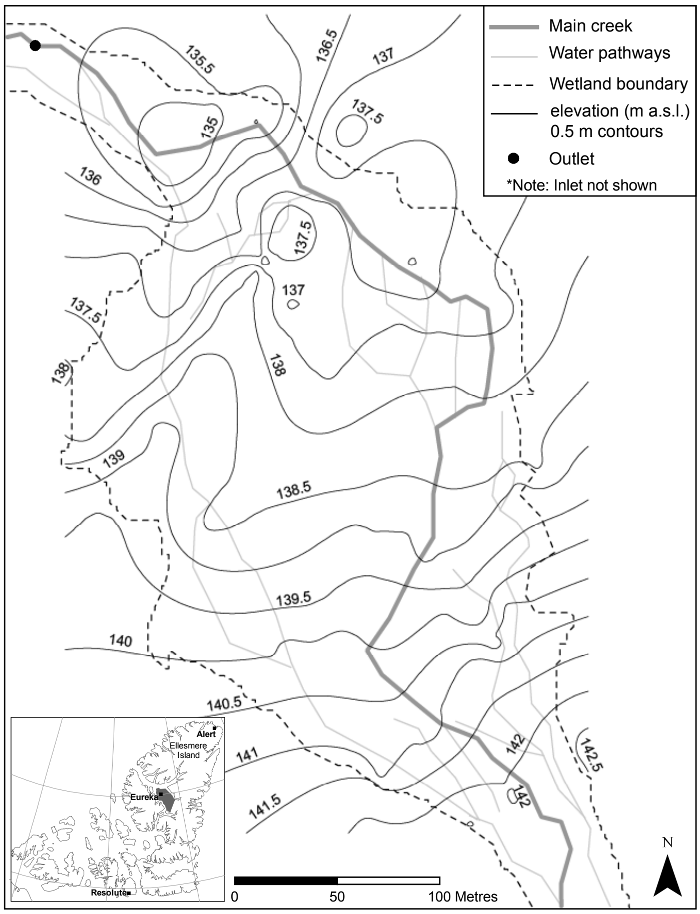

Figure 1. Topographic map of the riparian wetland (80°80'N, 85°35'W) located 20 km north of Eureka, Ellesmere Island, Nunavut, Canada (see inset map). Fosheim peninsula is shaded.

3. METHODOLOGY

3.1 Field

Five transects were laid out across the riparian wetland and a snow survey was conducted following after Woo (1998). Snow depth measurements were made every 10 m and snow density was determined at the beginning and end of each transect with an Environment Canada MSC snow tube. On occasion, snow depth was too deep for the snow rod, leading to an underestimate in snow water equivalent (mean SWE = 106±50 mm). Considering this error and the fact, that reasonable snow information for this site was needed to model melt elsewhere along the incised stream channel (see section 3.2), a decision was made to increase this initial value by 50% (new SWE=159 mm-see Table 1). Direct measurements of snowmelt followed after Heron and Woo (1978). In 2005, three permanent transects were established across the wetland (see Figure 2) and a series of perforated and screened water wells (3 to 4) per transect were installed. In the post-snowmelt period (2006), daily water levels were measured at wells and depth of thaw was measured weekly at 10-12 locations along each transect (see Figure 2). The approach by Cole and Brooks (2000) was followed to assess different moisture conditions within the wetland; here the 15 cm depth was set as the limit of the rooting zone. I defined inundation as occurring when water tables were >0 cm, saturation (0 to -15 cm) and dry conditions (< -15 cm). Soil moisture was also determined at two locations in the middle of the wetland using the gravimetric approach (Figure 2). These measurements were taken in association with others (e.g. wet meadow, tundra upland, mesic ground, pond rim), as part of a broader wetland study. An Automatic Weather Station (AWS) (elevation = 138 m) situated over a wet meadow provided hourly meteorological information (Q*, K↓, K↑, Ta, RH, U). Summer precipitation was measured with a recording tipping-bucket raingauge and verified with four manual raingauges, with one of them in the middle of the riparian wetland. A stilling-well was situated near the outlet of the riparian wetland in the stream channel and an Ecotone water level recorder measured stage here (±10 mm). Stage levels were corrected routinely with direct depth measurements. Current metering occurred at both the inlet and outlet locations (see Figure 1) usually 2 to 3 times per day during high flows and once per day in low flow conditions. This allowed rating curves to be determined for each site: inlet location-$Q = 4.98H^{2.23}$, r^2=0.93, n=38; and for the outlet- $Q= 4.98H^{2.14}$, r^2= 0.94, n=38. A continuous record of reliable discharge was determined for both locations from June 29 (JD 180) onwards. A topographic survey of the study site occurred in late July using a transit level and stadia rod. Elevations were tied to a known benchmark.

3.2 Snowmelt model

For this study I wanted to identify and understand the processes which were driving the stream flow pattern passing through this riparian wetland. An initial comparison of stream discharge to both air temperature and net radiation proved inadequate. A snowmelt model (Woo and Young 2004) was then employed to assess the processes (energy receipt vs. rain input) modifying sreamflow. The utility of this model was recently confirmed at another wetland site on Somerset Island (Young and Abnizova 2005). Inputs to the model include both climate and snow information. Hourly climate data came from the AWS (K↓, Ta, RH, U, and PPT) except for P (station pressure) which was obtained from the Eureka weather station, 20 km to the south. Initial snow information was limited to the study site. Given that most streamflow was likely generated from snow further upstream, snow information for this valley zone was required. Using a series of photos from 2005, obtained from students hiking up the creek to the top of Black Top Ridge on July 1 (JD 182), I dissected the stream channel into a series of sections (slope, aspect, elevation) and snow amount (i.e. I compared snow conditions in the photo to initial wetland snow to derive an estimated snow index) (see Table 1). Indices were kept to reasonable levels based on previous surveys of snow-filled valleys (Woo and Young 2004). Photographs taken during both 2005 and 2006 also indicated that most snow was constrained to the main stream valley and near-by slopes. This information helped to define areas for the different contributing zones (m^2). Here, a 1:50 000 topographic map of the Black Top Ridge area (340 B/3) was employed. Normally, extensive snow surveys should have been conducted along the stream channel but this was not logistically possible. Modelled streamflow was generated from both simulated melt and measured rainfall inputs obtained from the AWS. These data were areally weighted for each terrain unit.

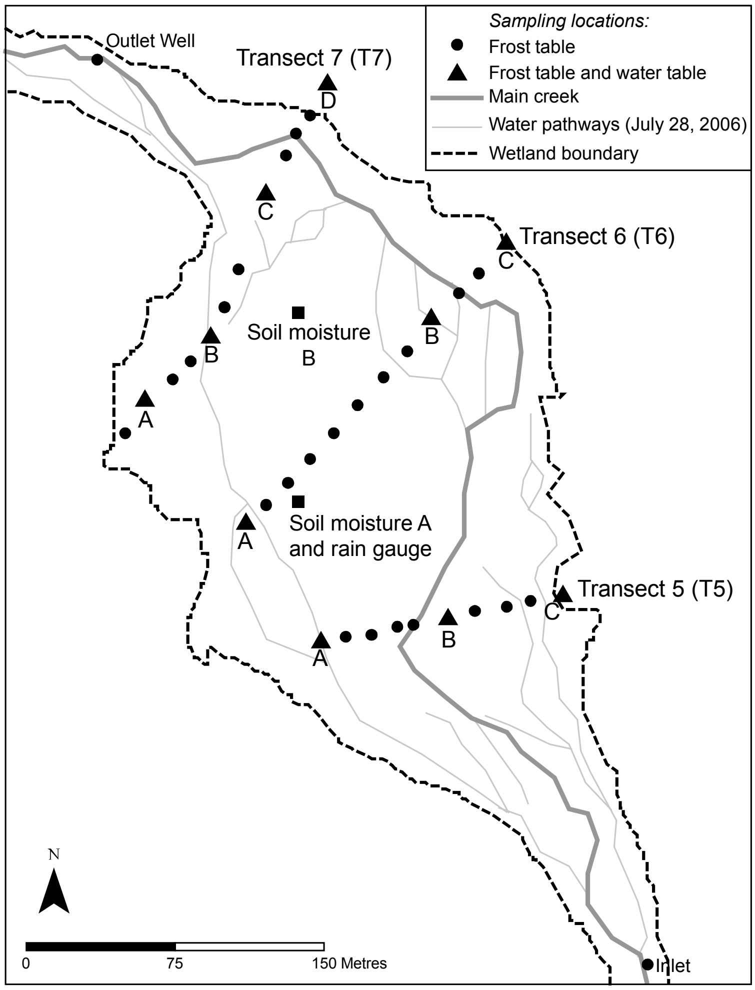

Figure 2. Series of transects across wetland indicating water wells and frost table locations. Stream gauging locations at the inlet and outlet are also indicated.

Table 1 provides the site conditions for the base and the series of valley terrain units. Isothermal conditions were assumed for the base station since the seasonal snow pack had largely disappeared from the low-land and only snow in the stream channel and valleys remained.

Table 1 Initial conditions for the snowmelt model (see Woo and Young 2004).

Terrain	Snow Index	Mean Elevation (m)	Aspect (degrees)	Slope Angle (degrees)	Area (m^2)
base (swe=159 mm)	1.00	138	–	–	
valley 1	1.00	134	315	0.01	97 656
valley 2	3.00	160	315	4	97 656
valley 3	4.5	220	315	19.7	317 383
valley 4	6.0	350	315	19.7	195 312
valley 5	6.0	500	315	19.7	67 139

4. Results and Discussion
4.1 Model results
A reasonable relationship between measured and modeled stream flow (see Figure 4b) at the outlet (within 5%) provides confidence in the initial conditions selected and the types of processes controlling stream

flow through the wetland (see below). Differences in results can be attributed to lags in the system, e.g. the snow dam in the channel delaying flow, a situation which cannot be reproduced by the model. Both over and under-estimates of measured stream flow also arise from errors in assessing initial snow amounts and areal coverage. Overall, this adequate performance is to be expected given the lack of snow information for this mountain stream.

4.2 Snow-dam period

Figure 3a indicates the saturation conditions of the wetland prior to the large flood event of July 9 (JD 190) (see Figure 4a). During this period the saturation levels are reduced with water tables falling below the ground surface and the absence of water in other wells (see Figure 5). Soil moisture levels while limited in extent confirm this drying pattern (i.e. θ_s < 100% vol. water content). Electrical conductivity values are also variable, especially for the wetland zone which had much higher and erratic values than channel water and minor flow paths (see Figure 6). Dall'O *et al.* 2001 indicates that dry intervals are common for riparian wetlands and are not considered critical (e.g. these episodes help to aerate the soil), yet Toner and Keddy (1997) indicate that saturated conditions are required for germination and infrequent flooding can lead to a change in plant structure. They discovered that for temperate wetlands, the duration of floods and the duration between initial and secondary floods were key factors in preventing woody substrates from succeeding herbaceous species. Drier conditions in the Athabaska Delta after a water diversion led to a shift in vegetation from herbaceous to woody plants (see Toner and Keddy 1997).

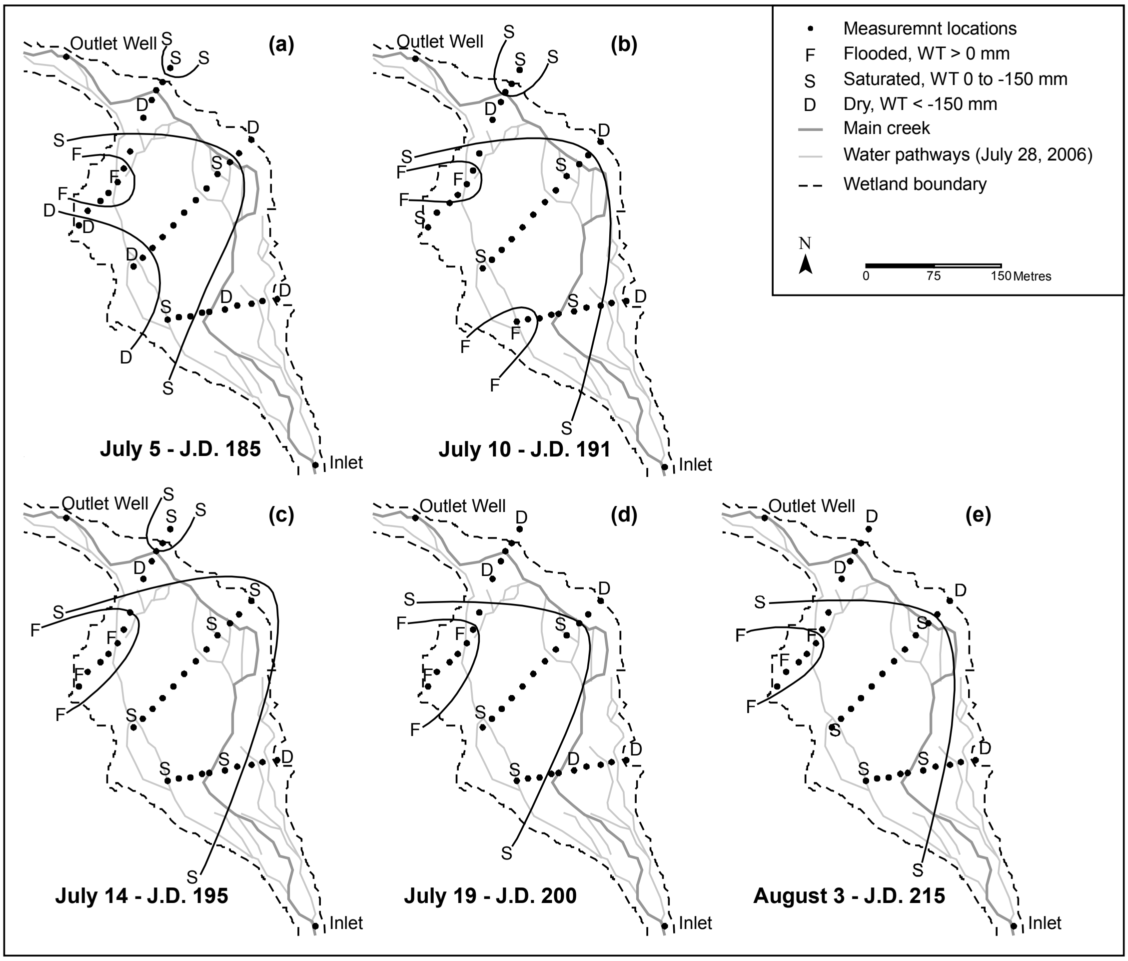

Figure 3. Water saturation patterns in the riparian wetland, 2006.

4.3 Flood period

A significant discharge event (see Figure 4a) did not occur until a snow dam diverting most seasonal snowmelt flow (**A**) from the riparian wetland was finally destroyed on July 9 (JD 190) (labeled here as, **B**). This large release of water was triggered by a stretch of sunny (□Q^*), warm and windy conditions (□Q_H fluxes), which enhanced melting after an unusually long and cool melt season. This pronounced flood event allowed water tables to rise (Figure 5) often above the ground surface, expand the saturated zone (Figures 3b, c) and dilute the wetland (see large drop in electrical conductivity, Figure 6a). This event which rapidly recharged the wetland occurred about three weeks later than in 2005. The occurrence of snow dams and snow-choked channels and their ability to delay and impound water levels is common in High Arctic environments (Woo and Sauriol 1980; Xia and Woo 1992). The surge of water after release followed by a dramatic drop in discharge can be described as a jökulhlaup (Blachut and McCann 1981).

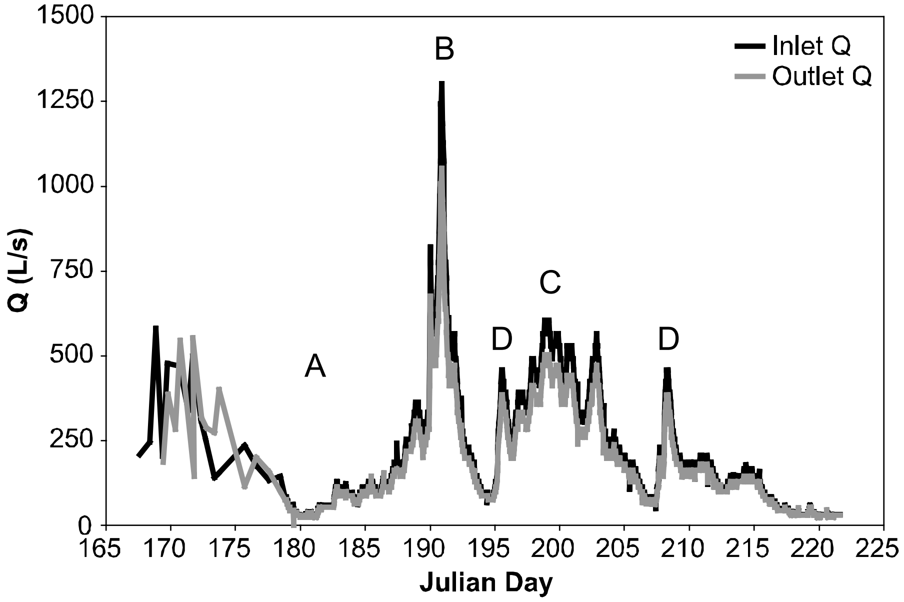

Figure 4a. Seasonal streamflow pattern of Black Top Ridge Creek (BTRC), 2006. Letters in the diagram are referred to in the text.

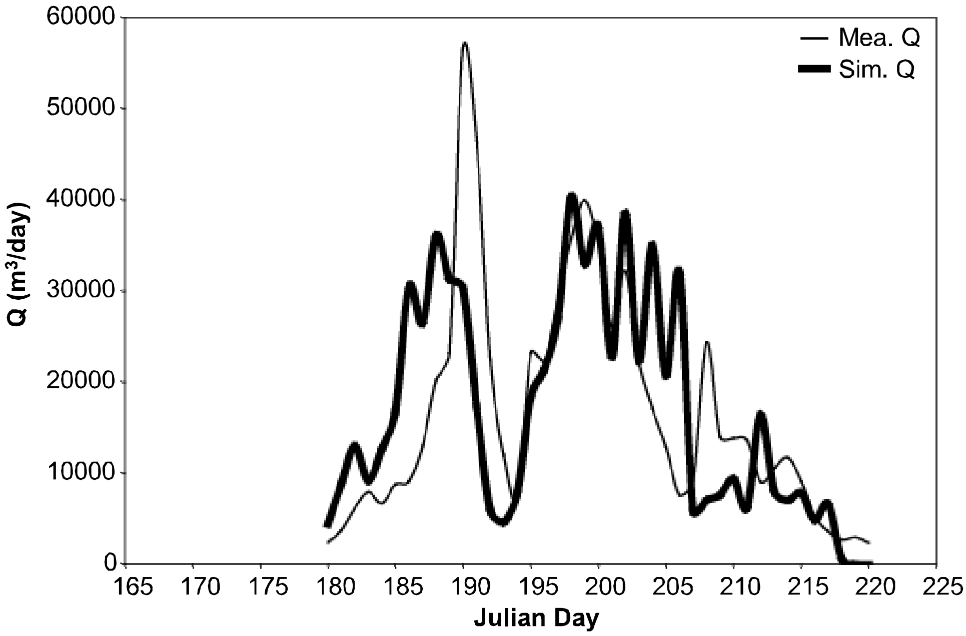

Figure 4b. Simulated and measured streamflow, Black Top Ridge Creek (BTRC), 2006.

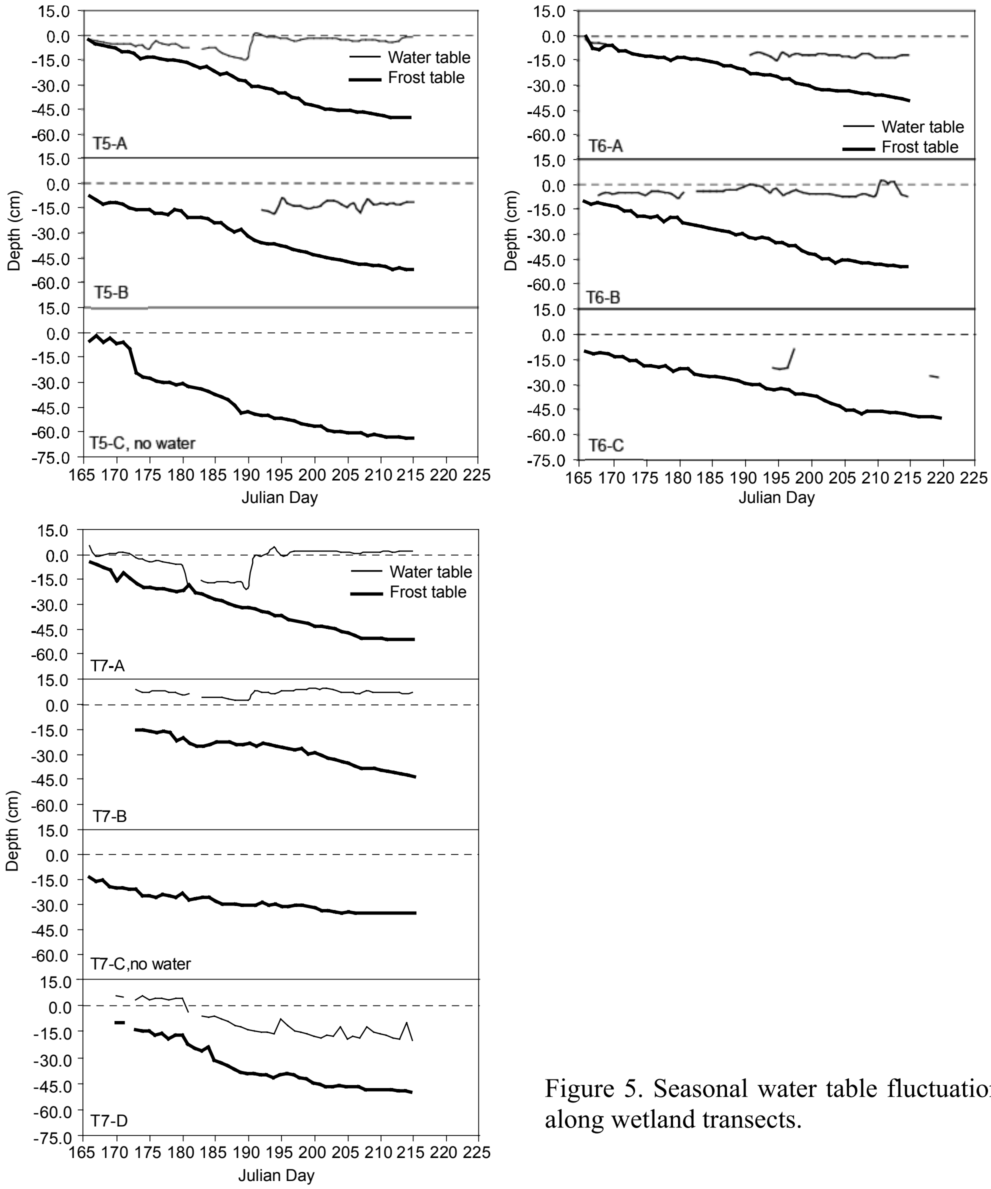

Figure 5. Seasonal water table fluctuations and frost table pattern along wetland transects.

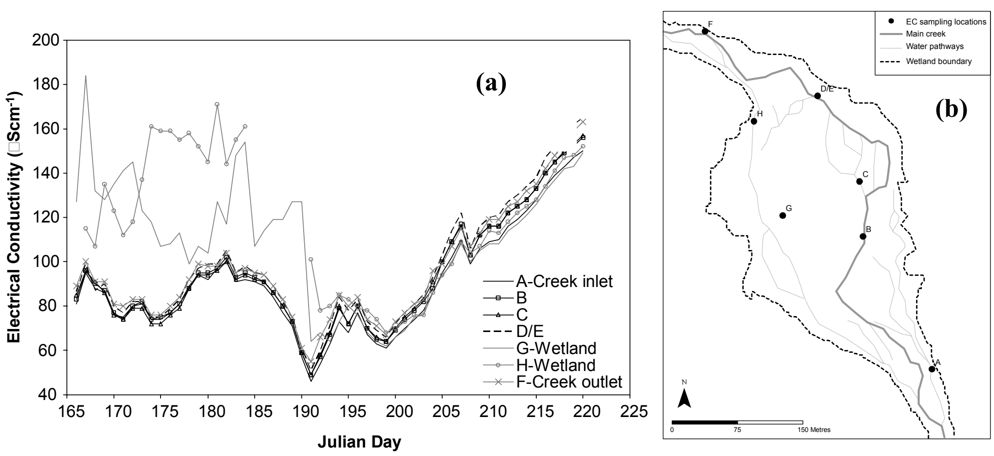

Figure 6. Seasonal pattern of electrical conductivity (a) at selected locations in the wetland (b).

4.2 Late-lying snowmelt period

Figure 4 (a) indicates that discharge levels were steady throughout July and did not drop off until early August when cooler and cloudy conditions became more frequent. The snowmelt model indicates that this period of enhanced flow (indicated by **C**) arises from the melting of channel snowbeds and lingering snow on steep slopes. The pulses or sharp increases are induced by sunny weather along with warm and windy conditions which enhance fluxes of Q_H. Young and Lewkowicz (1990) similarly found that Q* and Q_H dominated melt at a large perennial snowbank, near Ross Point, Melville Island and highest discharges occurred on clear, warm and windy days. Stream flow peaks labeled as **D**, are driven by rain and the melt generated by rain-on-snow (Q_P). Energy levels were low (cloudy, cool) for these days but rain helped to elevate the importance of Q_P and its ability to melt snow. These residual snowbeds and the meltwater that they produced were important for keeping the wetland saturated for the remainder of the summer. Figure 5 reveals that most water tables remain elevated and overall, the wetland continues to be saturated (see Figures 3d and e). The persistence of elevated soil moisture values (i.e. θ_s = 100% vol. water content) also confirms this pattern.

Comparable observations at this site in 2005, suggest that this period of "secondary flooding" is a regular event. Electrical conductivity values start rising during this post-peak period but increases are similar amongst sites suggesting stable moisture conditions throughout the wetland (Figure 6). Without these additional water inputs it is doubtful whether the wetland would have remained saturated given the potentially high losses of evaporation (ca. 4 mm/d) which can occur from wetland surfaces (see Woo and Guan 2006).

5. CONCLUSIONS

Dall'O *et al.* 2001 indicates that riparian wetlands are inherently complex, interface systems where different types of systems interact and where gradients can be high. They suggest that two main problems arise when dealing with riparian buffer zones: high temporal variation and extremely high spatial heterogeneity. For this riparian wetland which is found in a polar-oasis type climate snow plays a leading role in controlling this variable pattern. In summary,

1) The snow-choked channel initially deprives the wetland of much stream water, a delay of three weeks over the previous year. Delay in the arrival of these meltwaters results in the shrinkage of the saturated zone as the water table falls below the ground, often below the rooting zone. The water chemistry pattern also becomes altered (see Figure 6).

2) Contributions from flood waters and meltwater are important for these riparian wetlands. Water recharges the wetland and nutrients and matter (e.g. carbon), which are important for continued plant growth (Fellman and D'Amore 2007), are carried here in solution. During these events, water tables rise, often above the ground surface and some areas become inundated while saturated areas expand. Conductivity levels drop indicating diluted conditions.

3) A snowmelt model (Woo and Young 2004) was effective in helping to identify the reasons behind the stream discharge pattern. Much of the stream flow in the post-peak flow period is due to the melting of late-lying snowbeds either in the channel itself or on steep channel slopes. Net radiation (Q*) and sensible heat flux (Q_H) were the main drivers behind this melt, confirming what others have found (e.g. Young and Lewkowicz 1990). Rain was important in triggering stream flow by its control on the Q_p flux.

4) Considering that this is a one-time only study and its applicability to other riparian wetlands is limited, more attention should focus on channel snow and the role of this snow in steep catchments. Snow storage in these zones is important in providing meltwater to low-lying areas long after the seasonal snowpack has disappeared (Young 2006). Our study showed that this meltwater was essential for keeping a riparian wetland saturated for most of the summer. Loss of this snow and its ability to recharge the wetland on a regular basis might lead to drier conditions and eventually, a shift in vegetation-type (e.g. *Sedges* to *Salix arctica*) (Toner and Keddy 1997).

ACKOWLEDGEMENT

The author would like to acknowledge NSERC for funding, along with financial assistance from NSTP and York University. Thanks to PCSP for excellent logistical support and to May Guan and Kara Pul for their hard work and dedication in the field. May Guan also supplied photos from the 2005 field season and helped to clarify questions during the write-up of the study. Laura Brown's assistance in the production of maps and diagrams is gratefully acknowledged.

REFERENCES

Blachut, S.Pl. and McCann, S.B. (1981) The behavior of a polar ice-dammed lake, Ellesmere Island, Canada. *Arctic and Alpine Res.* **13**, 63-74.

Cole, C.A. and Brooks, R.P. (2000) Patterns of wetland hydrology in the Ridge and Valley Province, Pennsylvania, USA. *Wetlands* **20**, 438-447.

Dall'O. and Kluge, W. and Bartels, F. (2001) FEUWAnet: a multi-box water level and lateral exchange model for riparian wetlands. *J. of Hydrol.* **250**, 40-62.

Fellman, J.B. and D'Amore, D.V. (2007) Nitrogen and phosphorus mineralization in three wetland types in southeast Alaska, USA. *Wetlands* **27**, 44-53.

Hauer, F.R. and Smith, R. D. (1998) The hydrogeomorphic approach to functional assessment of riparian wetlands: evaluating impacts and mitigation on river floodplains in the USA. *Fresh. Bio.* **40**, 517-530.

Heron, R. And Woo, M.K. (1978). Snowmelt computations for a High Arctic site. Proc. *35th Eastern Snow Conference*, Hanover, New Hampshire. pp. 162-172.

Toner, M. and Keddy, P. (1997) River hydrology and riparian wetlands: A predictive model for ecological assembly. *Eco. Appli.* **7**, 236-246.

Van Hove, P., Belizile, C., Gibson, J.A.E. and Vincent, W.F. (2006) Coupled landscape-lake evolution in High Arctic Canada. *Can. J. of Earth Sci*. **43**, 533-546.

Vidon, P. And Hill, A.R. (2006) A landscape based approach to estimate riparian hydrological and nitrate removal functions. *J. of Amer. Water Resour. Assoc.* **42**, 1099-1112.

Woo, M.K. and Sauriol, J. (1980) Channel development in snow-filled valleys, Resolute, N.W.T., Canada. *Geog. Ann.* **62A**, 37-56.

Woo, M.K. (1998) Arctic snow cover information for hydrological investigations at various scales. *Nord. Hydrol.* **29**, 245-266.

Woo, M.K. and Young, K. (2003) Hydrogeomorphology of patchy wetlands in the High Arctic, polar desert environment. *Wetlands* **23**, 291-309.

Woo, M.K. and Young, K (2004) Modeling arctic snow distribution and melt at the 1-km grid scale. *Nord. Hydrol.* **35,** 295-307.

Xia, Z.J. and Woo, M.K. (1992) Theoretical analysis of snow dam decay. *J. of Glaciol*. **38**, 191-199.

Young, K.L. and Lewkowicz, A. (1990) Surface energy balance of a perennial snowbank, Melville Is., N.W.T. Canada. *Arctic and Alpine Res.* **22**, 290-301.

Young, K.L. and Woo, M.K. (2004a) Queen Elizabeth Islands: problems associated with water balance research. *IAHS Publ*. **290**, 237-248.

Young, K.L. and Woo, M.K. (2004b) Queen Elizabeth Islands: water balance investigations, *IAHS Publ*. **290**, 152-163.

Young, K. L. and Abnizova, A. (2005) High Arctic Ponds, Somerset Island, Nunavut: Spatial and temporal variations in snowcover and snowmelt. Proc. *62nd Eastern Snow Conference,* Waterloo, Ontario, June 7-10. pp. 69-92.

Young, K.L. (2006) Assessment of snow storage and ground ice melt in High Arctic environments. *Hydrol. Proc. Today*, **12***,* 2643-2645.

Proceedings of the

16th NORTHERN RESEARCH BASINS
INTERNATIONAL SYMPOSIUM AND WORKSHOP
27 August – 2 September, 2007
PETROZAVODSK, RUSSIA

Печатается по решению Ученого совета Института водных проблем Севера

Изд. лиц. № 00041 от 30.08.99 г. Сдано в печать 05.07.07. Формат $60 \times 84^1/_8$. Гарнитура Times.
Уч.-изд. л. 18,5. Усл. печ. л. 19,1. Тираж 70 экз. Изд. № 37. Заказ № 670.

Карельский научный центр РАН
Редакционно-издательский отдел
Петрозаводск, пр. А. Невского, 50